DESIGN AND EVALUATION OF PHOTOCATALYTIC REACTORS FOR WATER PURIFICATION

by

David de Villiers

Dissertation presented for the Degree of

Doctor of Philosophy (Chemistry)

at the

University of Stellenbosch

Promoter :   Prof. W.J. Engelbrecht
Co-Promoter :   Dr. G.F.S. Wessels

STELLENBOSCH
December   2001

DECLARATION

I, the undersigned, hereby declare that the work contained in this dissertation is my own original work and has not previously in its entirety or in part been submitted at any university for a degree.

David de Villiers

SUMMARY

The photo-mineralization of organic compounds (in the combined presence of a TiO_2 based semiconductor catalyst, UV radiation and molecular oxygen) represents an advanced oxidation technology with significant potential for environmental pollution abatement. This oxidation process (generally known as photocatalytic oxidation - PCO) is currently the subject of extensive global research, with the main objective being the oxidative removal of organic and inorganic pollutants from water, air and soil. Presently, many barriers still block the way to commercial implementation of this technology, hence a unique (and effective) configuration of catalyst, light source and reactor design needs to identified. In terms of the water treatment scenario (which is the emphasis of this work) the need exists to develop a practical and affordable PCO reactor for water treatment on a large scale.

The two laboratory-scale PCO reactors investigated in this work were based on a "falling film" flow reactor design and were constructed with commercially available materials and components. Degussa P-25 TiO_2 was used as semiconductor catalyst and two types of low-pressure mercury lamps as the UV light source. Three modes of operation were investigated in order to determine the practical feasibility of the reactors. These included the recirculation, single pass and sequential single pass modes. The reactors were operated either as a TiO_2 slurry-phase reactor (Reactor 1), or with TiO_2 immobilized on stationary fiber glass and fibrous activated carbon sheet modules (Reactors 2A and 2B respectively). Extensive parametric evaluations were done using conventional one-factor variation and statistical methods according to optimal experimental design principles. The PCO treatment of two model organic pollutants (*para*-Chlorophenol and cyanobacterial microcystin YA, YR, LR and RR) were investigated. These pollutants were spiked into various water matrices to the desired concentration level. The combined photocatalytic-carbon adsorption treatment of these two pollutants was also investigated in Reactor 2B.

The experimental results obtained through this work showed that both model pollutants were successfully degraded in several water matrices by means of treatment in the respective PCO reactors. Moreover, this research was the first ever demonstration of the TiO_2 photocatalytic degradation of microcystin toxins in the aqueous phase. The large number of parametric and optimization studies yielded the relative contributions of the various process parameters (in terms of the defined photocatalytic efficiency parameters as responses) very effectively. Furthermore, statistical evaluation of the experimental data provided valuable insight into the scientific phenomena associated with TiO_2 mediated PCO processes.

OPSOMMING

Die foto-mineralisasie van organiese verbindings (in die gekombineerde teenwoordigheid van 'n TiO$_2$ gebaseerde halfgeleier katalisator, UV straling en molekulêre suurstof) verteenwoordig 'n gevorderde oksidasie-tegnologie met beduidende potensiaal vir bekamping van omgewingsbesoedeling. Hierdie oksidasie-proses (algemeen bekend as fotokatalitiese oksidasie – FKO) is tans wêreldwyd die onderwerp van ekstensiewe navorsing, met hoofdoel die oksidatiewe verwydering van organiese en anorganiese besoedelingstowwe uit water, lug en grond. Huidiglik bestaan daar nog vele struikelblokke wat die weg na kommersiële implementering van hierdie tegnologie blokkeer, gevolglik moet 'n unieke (en effektiewe) konfigurasie van katalisator, ligbron en reaktor-ontwerp nog identifiseer word. In terme van die waterbehandeling situasie (wat die klem van hierdie werk is) bestaan die nodigheid om 'n praktiese en bekostigbare FKO reaktor te ontwikkel vir watersuiwering op 'n groot skaal.

Die twee laboratorium-skaal FKO reaktore in hierdie studie was gebaseer op 'n "vallende film" vloeireaktor ontwerp en is gekonstrueer met kommersieël beskikbare materiale en komponente. Degussa P-25 TiO$_2$ is aangewend as halfgeleier katalisator en twee tipes lae-druk kwik lampe as die UV ligbron. Drie bedryfsmodes is ondersoek met die doel om die praktiese haalbaarheid van die reaktore te bepaal. Hierdie het ingesluit die resirkulasie, enkeldeurvloei en enkeldeurvloei-sekwensie modes. Die reaktore is bedryf as óf 'n TiO$_2$ flodder-fase reaktor (Reaktor 1) óf met TiO$_2$ ge-immobiliseer op 'n stasionêre veselglas en veselagtige ge-aktiveerde koolstof blad-modules (Reaktor 2A en 2B onderskeidelik). Omvattende parametriese evaluasies is gedoen deur gebruik te maak van konvensionele een-faktor variasie en statistiese metodes na aanleiding van optimale eksperimentele ontwerp beginsels. Die FKO behandeling van twee model organiese besoedelingstowwe (*para*-Chlorofenol en siano-bakteriese mikrosistien YA, YR, LR en RR) is ondersoek. Hierdie besoedelingstowwe is ge-ent in verskeie watermatrikse tot die verlangde konsentrasievlak. The gekombineerde fotokatalitiese - aktiveerde koolstof behandeling van die twee besoedelingstowwe is ook ondersoek in Reaktor 2B.

Die eksperimentele resultate verkry deur hierdie werk het getoon dat beide die model-besoedelingstowwe suksesvol gedegradeer is in verskeie watermatrikse deur behandeling in die onderskeie FKO reaktore. Trouens, hierdie navorsing was die eerste demonstrasie ooit van die TiO$_2$ fotokatalitiese degradasie van mikrosistien toksiene in die waterige fase. Die groot aantal parametriese en optimiseringstudies het die bydraes van die verskeie proses-parameters (in terme van die gedefinieerde fotokatalitiese effektiwiteitsparameters as response) baie effektief verskaf. Verder, statistiese evaluasie van die eksperimentele data het waardevolle insig verskaf tot die wetenskaplike verskynsels te assosieer met TiO$_2$ gemedieërde FKO prosesse.

ACKNOWLEDGEMENTS

TABLE OF CONTENTS

PAGE NO.

CHAPTER 3 : EVALUATION OF REACTOR 1   80

LIST OF ABBREVIATIONS AND ACRONYMS

ANOVA	analysis of variance
AOT	advanced oxidation technology
AOTs	advanced oxidation technologies
AOX	adsorbable organic halogen
BDOC	biodegradable organic carbon
BTEX	benzene, toluene, ethylbenzene and xylenes
CCD	central composite design
CIL	catalyst impregnation loading
COD	chemical oxygen demand
CPI	controlled periodic illumination
CSL	catalyst suspension loading
CSTRs	continuously-stirred tank reactors
CWAO	catalytic wet air oxidation
DBPs	disinfection by-products
DCAA	dynamic contact angle analyzer
DMPO	5,5-dimethylpyrroline N-oxide
DOC	dissolved organic carbon
DRS	diffuse reflectance spectrometry
E-beam	electron beam
EDAX	energy dispersive analysis of X-rays
EED	energetic efficiency of degradation
EE/M	electrical energy per unit mass
EE/O	electrical energy per order
ESR	electron spin resonance spectroscopy
FAC	fibrous activated carbon
GPM	gallons per minute
HID	horizontal irradiation distance
HPLC	high-performance liquid chromatography
IMM	immobilized-bed reactor
LH	Langmuir-Hinshelwood
LOD	limit of detection
MGD	million gallon per day
MTBE	methyl $tert$-butyl ether
NA	not analyzed
NApp	not applicable
ND	not detected
NOM	natural organic matter
NTP	non-thermal plasma
NTPs	non-thermal plasmas
OA	orthogonal array
OED	optimal experimental design
OFV	one-factor variation
PBN	phenyl-$tert$-butyl nitrone
PCO	photocatalytic oxidation
p-CP	$para$-chlorophenol
PCR	photocatalytic reduction
PEPs	photocatalytic efficiency parameters
PROMEC	Programme on Mycotoxins and Experimental Carcinogenesis

PTEF	photochemical thermodynamic efficiency factor
PZC	point of zero charge
QSAR	quantitative structure-activity relationship
R	reaction rate
RSD	relative standard deviation
RSM	response surface methodology
SEM	scanning electron microscopy
SC	semiconductor catalyst
SCWO	supercritical water oxidation
SD	standard deviation
SLIMM	combined slurry-immobilized bed reactor
SP	semiconductor photocatalysis
SPE	solid phase extraction
THMs	trihalomethanes
TOC	total organic carbon
UV	ultraviolet
VFR	volumetric flow rate
VOCs	volatile organic compounds
VUV	vacuum ultraviolet
WAO	wet air oxidation
WRC	Water Research Commission

LIST OF SYMBOLS

E_b	band-gap energy
k_A	adsorption rate constant (in mins^{-1})
k_{obs}	observed first order rate constant (in mins^{-1} or sec^{-1})
k_P	rate constant for photocatalytic oxidation (in mins^{-1})
k_T	rate constant for total removal (in mins^{-1})
N	number of single passes through reactor (viz: single pass number)
P	null hypothesis probability
R	reaction rate
ε	molar absorption coefficient
κ	illuminated specific surface area (in m^2/m^3 or m^{-1})
η	spin adduct generation efficiency
ϕ	radiant flux (in W/m^2)

CHAPTER 1

INTRODUCTION AND OBJECTIVES

OVERVIEW

This introductory chapter contains a detailed literature survey of advanced oxidation technology (AOT) as potential remedial treatment of waste pollutants. Emphasis is placed on the fundamentals and applications of TiO_2 photocatalysis as it pertains to the purification of polluted water. Mechanistic, kinetic and parametric details are furnished to highlight the chemistry of photocatalytic oxidation (PCO) within the context of TiO_2 photocatalysis. Several technical aspects regarding photocatalytic reactor design are also highlighted. Optimization theory for parametric experimentation (with the main emphasis on optimal experimental design) is discussed briefly. The chapter is concluded with a thorough explanation of the project objectives.

RESEARCH OBJECTIVES

In order to render TiO_2 based PCO technologies competitive against conventional water treatment processes, the need exists to develop innovative reactor designs capable of being scaled-up successfully. Such an exercise is very complex due to its multi-disciplined nature. It ultimately entails four distinct phases of development, i.e. (1) statistical optimization of reactor and reaction parameters (2) comprehensive reactor modeling (3) real-life operational trials, and (4) commercialization.

- *It is the primary objective of this work is to develop and expand the current knowledge base of phase 1 by evaluating two novel designs of TiO_2 PCO reactors via the optimal experimental design route.*

The experimental reactors used in this work are based on the falling film principle and will be evaluated in three separate flow system modes for the photocatalytic removal of two model organic pollutants, i.e. *para*-Chlorophenol (a typical industrial water pollutant) and four variants of cyanobacterial microcystin toxins (a typical domestic water pollutant).

- *As secondary objective, it is envisaged to evaluate and furnish several key process and photocatalytic efficiency parameters (PEPs) associated with the reactors in question, so as to facilitate global rating of the designs.*

The treatment of raw drinking water containing industrial pollutants, cyanobacterial microcystin toxins and natural organic matter (NOM) is of considerable relevance to the South African context of the provision of safe drinking water. This work is intimately related to the quest for innovative technologies to combat the country's pollution problem in the long term.

1.1   GENERAL INTRODUCTION

"Environmental pollution is the unfavorable alteration of our surroundings as a byproduct of man's actions through changes in energy patterns, radiation levels, chemical and physical constitution and abundances of organisms. These changes will affect mankind strongly in the future."
(Krüger, 1991)

The twentieth century has witnessed a phenomenal expansion in human activity, particularly in the industrial sector of society. These developments have yielded a multitude of products and commodities, mainly aimed at facilitating everyday life for man and bringing him closer to self-sufficiency (Kriek, 1998). A major drawback to this fairytale story, however, has been the alarming growth in pollution of one of the most basic of human commodities, viz: *water*. Apart from nature providing her fair share of aquatic environmental pollution (Miyamoto, 1996; Gribble, 1996) many divisions of industry have also contributed significantly to the problem. The petroleum refining, synthetic chemicals, milling and coal conversion, textile processing, pulp and paper manufacturing and several other industries have been branded as "water polluters" (Ollis *et al*., 1989; Serpone, 1995).

Also noteworthy has been the pollution brought about by the consumers themselves, through the utilization of fuels for heating and transportation, and the agricultural and domestic use of pesticides, insecticides, fertilizers, detergents and pharmaceuticals. Other routes arise from the effluents of wastewater treatment plants, poorly chosen hazardous waste sites and accidental chemical spills. As a result, more than 700 potentially hazardous chemical compounds have been identified in sources of drinking water in the United States and across the world. As far back as 1989 it was already estimated that approximately 1000 new chemicals go into commercial production every year and will inevitably find their way into the environment's aquatic cycles (Ollis *et al*., 1989).

Water covers more than 70% of the earth's surface and is practically indispensable to all forms of life known to man (Krüger, 1992). Despite the apparent abundance it has been estimated that about 1.5 billion people currently lack access to clean water resources and that by the year 2025, more than two-thirds of the world's burgeoning population will have to cope with water stresses (Galal-Gorchev, 1996; Terblanche, 1999). In addition, many parts of the world are arid or semi-arid areas as a result of seasonal droughts, variable rainfall patterns and unexpected tropical storms causing flooding and erosion. The economic growth of developing countries, particularly in sub-Saharan Africa, is seriously affected by the lack of sufficient and safe drinking water resources. Approximately 80% of all diseases and one-third of all deaths in developing countries are caused by water-related diseases such as cholera and typhoid (Galal-Gorchev, 1996). These factors, in tandem with perpetuated industrial and natural pollution of the hydrosphere, have all contributed to the present fragile state of the earth's drinking water supplies. It has become a topic of immense global concern (Legrini *et al*., 1993). Ultimately the reclamation, remediation and recycling of used waters (contaminated by whatever means) presents the only viable solution for augmenting the existing scarce resources of natural waters destined for domestic, agricultural and industrial consumption and for sustaining the planet's sensitive ecosystem.

The chemical treatment of contaminated waters (viz: surface water, groundwater and wastewater) has formed an integral part of a long-term strategy to improve the quality of drinking water resources by preventing the release of toxic and non-biodegradable compounds into natural aquatic cycles (Legrini *et al.*, 1993). Conventional water treatment processes to date have mainly included the use of biological treatment, phase-transfer processes (such as activated carbon adsorption) and chemical treatment via chlorine, potassium permanganate and several other oxidants (Ray, 1999).

Biological treatment is a tried and tested method, but degradation rates have mostly been too slow to cope with the high demand on volume and organic load of waste to be treated (Legrini *et al.*, 1993). In some instances toxic compounds present in wastewater were found to be lethal for the bio-organisms intended to facilitate their degradation (Ray, 1999).

Phase-transfer technologies (viz: air stripping, carbon-adsorption, membrane filtration and extraction) are essentially non-destructive processes that are frequently used as benchmarks against which new technologies are measured prior to commercialization (Rajeshwar, 1996). Unfortunately, all these technologies exhibit one major weakness in that they consistently involve the transport of organic pollutants from one phase to another and hence, do not effectively eliminate the problem of pollution. Air stripping, for example, shifts pollutants to the atmosphere, which results in the spread of several hazardous volatile organic compounds (VOCs). Carbon-adsorption produces environmentally hazardous solids that have to be disposed of through landfill procedures (Mills *et al.*, 1993; Serpone, 1995). Liquid extraction requires use of expensive and hazardous organic solvents, while polymeric membranes used in various filtration processes, require periodic treatment with hazardous anti-fouling chemicals (Jacobs *et al.*, 1997). As a result, phase-transfer technologies are gradually being legislated in countries such as the United States. In certain states (e.g. California) landfill and air stripping activities have been banned (Serpone, 1995).

Chemical oxidation methods (such as chlorination and ozonation) have been reliable treatment strategies, particularly toward the disinfection of raw natural water and industrial wastewater. However, these technologies also exhibit one common drawback, viz: the formation and persistence of disinfection by-products (DBPs) in treated water. Chlorination of raw water, for example, produces several trihalomethanes (THMs) as DBPs. The presence of THMs in chlorinated drinking water can be problematic since it has been irrefutably linked to the occurrence of human cancer and, in some instances, attributed to pregnancy problems and spontaneous abortion (Morrow and Minear, 1987; Waller *et al.*, 1998).

Electrochemical technologies are also being developed and mainly involve charge-transfer processes in combination with chemical degradation of waste pollutants. Although generally branded as efficient and selective, the commercial development of electrochemical technologies is hampered by slow reaction rates and the use of expensive electrode materials, e.g., platinum, gold and silver (Hitchman *et al.*, 1995).

In the last 15 years, the development of alternative water treatment techniques has incorporated a distinct shift in emphasis by addressing the issue of chemical destruction of the pollutant as opposed to phase-transfer (Ollis *et al.*, 1989). In this regard, advanced oxidation technologies (AOTs) have become popular subjects of research for many environmental scientists and engineers across the world. These technologies are defined

3

as chemical destruction processes induced mainly by light or electrical means and involving the *in-situ* generation of highly reactive free radical species, most notably hydroxyl radicals (Bolton *et al.*, 1996; Hoigné, 1997).

Hydroxyl radicals are potent oxidants with high diffusion rates in water, effecting oxidative degradation (hence structural decomposition) of dissolved organic compounds with a subsequent formation of innocuous breakdown products such as carbon dioxide, water and inorganic ions. With the exception of certain photochemical electron-transfer processes, all AOTs rely exclusively on oxidative degradation mechanisms either through the generation of organic radicals (via substrate photolysis) or chemical reactions with reactive hydroxyl radicals (Legrini *et al.*, 1993).

This discussion will be limited to the subject of hydroxyl radicals within the AOTs domain.

1.2 ADVANCED OXIDATION TECHNOLOGIES

1.2.1 Hydroxyl Radicals

(a) General Reactivity

The hydroxyl radical is generally regarded as a very strong oxidizing agent in the field of oxidation chemistry (Legrini *et al.*, 1993; Hoigné, 1997; Matthews, 1986). Table 1.1 illustrates the superior oxidation potential of this radical compared to standard water treatment oxidants such as ozone, hydrogen peroxide, chlorine dioxide and chlorine. It is surpassed only by fluorine in terms of oxidation potential.

Table 1.1: Oxidation potentials for some well-known oxidants (Legrini *et al.*, 1993).

Species	Oxidation Potential (V)
Fluorine	3.03
Hydroxyl radical	2.80
Atomic oxygen	2.42
Ozone	2.07
Hydrogen peroxide	1.78
Perhydroxyl radical	1.70
Permanganate	1.68
Chlorine dioxide	1.57
Hypochlorous acid	1.49
Chlorine	1.36
Bromine	1.09

Aqueous hydroxyl radicals are predominantly non-selective and oxidize a variety of organic and inorganic solutes with relatively high reaction rates that approach diffusion controlled limits. It is estimated that these radicals are consumed in natural and most drinking waters at a rate of 10^5 sec^{-1}, equivalent to a mean lifetime of 10 microseconds. A series of organic reference compounds (including hexane, benzene and atrazine) have been used as probe molecules for compiling kinetic calibration data with respect to hydroxyl radical reactions (Hoigné, 1997). Comprehensive bibliographies containing useful

rate constants for radical mediated reactions (including hydroxyl radicals) are available in literature (Buxton et al., 1988).

Despite the highly reactive nature of hydroxyl radicals they are present in sufficiently high steady-state concentrations during a given advanced oxidation technology (AOT) reaction to effect chemical degradation of target organic molecules (Legrini et al., 1993). AOTs are tailored for efficient hydroxyl radical production, responding specifically to the chemical and physical characteristics of the target pollution system (Braun et al., 1993). Producing the radicals is the crucial step and is governed by various factors depending on the AOT under investigation.

(b)   Oxidative Degradation

Oxidative degradation reactions mediated by hydroxyl radicals are adequately described through three distinct mechanisms, i.e. *hydrogen abstraction, electron transfer and electrophilic addition* (Legrini et al., 1993; Jakob et al., 1993; Braun and Oliveros, 1997).

The oxidation of an organic compound (RH) by hydroxyl radicals is mainly effected through the process of *hydrogen abstraction* (eqn 1.1):

$$HO\bullet + RH \rightarrow R\bullet + H_2O \tag{1.1}$$

(where $HO\bullet$ = hydroxyl radical)

Organic radicals ($R\bullet$) are generated which subsequently react with molecular oxygen to yield peroxyl ($RO_2\bullet$) radicals (eqn 1.2). These radicals are mainly carbon-centered radicals, as remarked by Al-Ekabi (1999).

$$R\bullet + O_2 \rightarrow RO_2\bullet \tag{1.2}$$
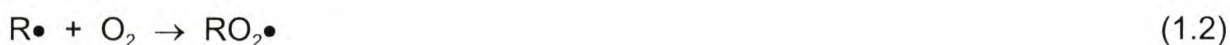
A chain of oxidative degradation reactions ensue, leading to the final breakdown products, i.e. carbon dioxide, water and inorganic salts (mineral acids). Degradation of peroxyl radicals is mainly effected via unimolecular and bimolecular decay, while the concomitant oxyl radicals ($RO\bullet$) degrade via reduction, rearrangement and β-cleavage mechanisms (Al-Ekabi, 1999; Von Sonntag et al., 1997) :

$$RO_2\bullet \rightarrow \rightarrow CO_2 + H_2O \ (+ HX) \tag{1.3}$$

$$RO\bullet \rightarrow \rightarrow CO_2 + H_2O \ (+ HX) \tag{1.4}$$

(where X = halides)

Electron transfer to the hydroxyl radical constitutes a second mechanism for oxidative degradation. This mechanism is favored in the case of protonated (RH) and halogenated substrates (RX) :

$$HO\bullet + RH \rightarrow RH^{\bullet+} + HO^- \tag{1.5}$$

$$HO\bullet + RX \rightarrow RX^{\bullet+} + HO^- \tag{1.6}$$

5

The hydroxyl radical is a known electrophilic agent and may consequently participate in *electrophilic addition* reactions, particularly when organic molecules contain π electron systems such as alkenes ($X_2C=CX_2$) and halogenated aromatic compounds (PhX) (eqns 1.7 and 1.8) :

$$HO\bullet \ + \ X_2C=CX_2 \ \rightarrow \ X_2C(OH)\text{-}C^{\bullet}\text{-}X_2 \qquad\qquad (1.7)$$

$$HO\bullet \ + \ PhX \qquad \rightarrow \qquad HOPhX^{\bullet} \qquad\qquad\qquad (1.8)$$
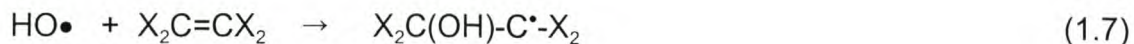
The rate and efficiency of oxidative degradation reactions are governed by the production and reactivity of radical intermediate species. Legrini *et al.* (1993) reported that the energy required to homolyze a given chemical bond and the concentration of dissolved molecular oxygen are parameters of paramount importance in these processes. Furthermore, it has been stated that carbon-chlorine (C-Cl) bonds are relatively stable toward potential substitution by hydroxyl radicals. Consequently the degradation of perchlorinated compounds with hydroxyl radicals as reactive intermediates have yielded very slow oxidation rates. As a result, the AOTs currently under development generally hinge on radical species (such as hydroxyl radicals) as *initiators* of oxidative degradation processes.

Hydroxyl radicals react very slowly with perfluorinated and perchlorinated compounds and are consequently unable to create carbon-centered radicals via halogen abstraction. In these circumstances, ultraviolet (UV)-photolysis of aqueous pollutants may be considered more relevant for initiating oxidation sequences, despite exhibiting lower efficiency than hydroxyl radical mediated reactions (eqn 1.9). Light sources emitting in the wavelength range between 210 and 230 nm may be applied for primary homolysis of C-Cl bonds in chlorinated organics via direct photolysis. Similarly, C-F bonds can be attacked using light souces in the vacuum-ultraviolet (VUV) range, viz: shorter than 190 nm (Legrini *et al.*, 1993; Braun *et al.*, 1993; Braun and Oliveros, 1997).

$$RX \ + \ h\nu \ \rightarrow \ R\bullet \ + \ X\bullet \qquad\qquad\qquad (1.9)$$

(where X = chlorine or fluorine)

(c)   Analytical Detection

Elucidating the mechanistic aspects of AOT reactions often require following the path of hydroxyl radicals in reaction with organic pollutants. Understandably, the detection of these radicals through analytical techniques is often a difficult task brought about by relatively high reaction rates. Hoigné (1997), for example, reported second order rate constants in the range of 10^9 $M^{-1}sec^{-1}$ for reactions of several organic probe compounds with hydroxyl radicals. Despite this seemingly limiting factor, direct monitoring of hydroxyl radicals has been reported using low temperature electron spin resonance spectroscopy (ESR), however these claims have been refuted elsewhere in public literature (Serpone *et al.*, 1993). Backa *et al.* (1997) reported that Symons (1978) achieved direct detection of the hydroxyl radical in ice by ESR.

A major complicating factor for the detection of hydroxyl radicals in aqueous phase has been their weak optical absorbance and emission properties in wavelength regions normally utilized for spectroscopic and chromatographic monitoring (Fox, 1993; Backa *et al.*, 1997). As a result, several indirect methods have been developed, primarily involving the reaction of hydroxyl radicals with organic molecules acting as spin trapping agents or spectroscopic probes. The spin trapping method yields stable free radicals known as "spin adducts" with ESR spectrums characteristic of the trapped hydroxyl radicals, while spectroscopic probes act as radical scavengers to produce hydroxylated reaction products which are easily detected and quantified by standard analytical means. A number of examples cited in literature are summarized in Table 1.2 :

Table 1.2: Indirect methods for the detection of hydroxyl radicals.

Spin trap / Probe	Reaction Product	Detection Method	Reference
Phthalic Hydrazide	3-Hydroxyphthalic Hydrazide	Chemiluminescence	Backa *et al.*, 1997
Salicylic Acid	2,3- and 2,5- Dihydroxybenzoic Acid	High-Performance Liquid Chromatography (HPLC)	Jen *et al.*, 1998
Dimethyl Sulphoxide	Methanesulphinic Acid	HPLC	Fukui *et al.*, 1993
Phenyl-tert-butyl Nitrone (PBN)	Hydroxylated PBN adduct	Oscillopolarography ; Cyclic Voltammetry	Ma *et al.*, 1999
5,5-Dimethylpyrroline N-oxide (DMPO)	Hydroxylated DMPO adduct	ESR Spectroscopy	Riegel and Bolton, 1995

Sun *et al.* (1996) defined a useful relationship for expressing the formation rate of hydroxyl radicals in AOT reactions in terms of hydroxylated DMPO spin adducts (DMPO-OH) (eqn 1.10) :

$$\eta \;=\; \{\, d/dt\ [DMPO\text{-}OH] \,\} \;/\; \{\, d/dt\ [HO\bullet] \,\} \tag{1.10}$$

(where η = spin adduct generation efficiency)

The generation efficiency can be calculated by independent determinations of the spin adduct and hydroxyl radical formation rates through ESR and indirect HPLC analyses, respectively.

Several other advanced analytical techniques are currently being used or developed for kinetic, mechanistic and structural studies of reactive species and product molecules in AOT reactions, viz: pulse radiolysis (Terzian, 1995), time-resolved diffuse reflectance spectroscopy (Fox, 1993; Fox and Dulay, 1993), time-resolved diffuse microwave conductivity and laser flash photolysis (Hoffmann *et al.*, 1995), laser-induced fluorescence (Zeng *et al.*, 1998) and solid-state nuclear magnetic resonance (Rice and Raftery, 1999).

1.2.2 AOT Chemistries

(a)   Fundamentals

AOTs constitute an important class of contemporary destruction technologies for environmental pollution abatement (Rajeshwar, 1996). Several distinct AOT processes are known, encompassing a wide array of activation mechanisms, mainly through electrical or light-driven means. Although hydroxyl radical chemistry is principally involved in some form or another (at least in part), several other oxy-radical species (such as superoxide, perhydroxyl, peroxyl and oxyl radicals) and highly reducing species (such as hydrated electrons and hydrogen atoms) may also be prevalent due to the utilization of water, ozone, hydrogen peroxide and heterogeneous catalysts as reagents (Bolton *et al.*, 1996). Both oxidation and reduction chemistry are at play.

The general chemistry associated with AOTs is elegantly summarized by Al-Ekabi (1999) using the following 5 discrete steps (see Table 1.3) :

Table 1.3: The chemistry of AOTs (Al-Ekabi, 1999).

Step	Event
1	Generation of Reactive Species (e.g. hydroxyl radicals, hydrated electrons and hydrogen atoms)
2	Reactions of Reactive Species with Organic Compounds (Generation of Carbon Centered Radicals)
3	Oxygen Addition to Carbon Centered Radicals (Formation of Peroxyl Radicals)
4	Degradation of Peroxyl Radicals (Formation of Oxyl Radicals)
5	Degradation of Oxyl Radicals (Formation of Alcohols, Ketones and Aldehydes)

In most instances, AOTs are used in an attempt to achieve full mineralization of aqueous and gaseous organic pollutants, yielding only carbon dioxide, water and inorganic ions as endproducts. Technical development has reached pilot and commercial scale in certain instances (Al-Ekabi, 1999). AOTs may be classified into the following broad groups :

- Chemical Oxidation Technologies
- Iron Based Oxidation Technologies
- UV, Ozone and Hydrogen Peroxide Technologies
- Vacuum UV Technologies
- Supercritical Water Oxidation
- Electron Beam and Gamma Irradiation
- Electrohydraulic Cavitation and Sonolysis
- Non-Thermal Plasma Technologies (for air treatment)
- Semiconductor Photocatalysis

These technologies involve several different methods of activation as well as oxidant generation. They can potentially use a number of different mechanisms for oxidative destruction of organic pollutants, however hydroxyl radical chemistry is mostly the common denominator (at least in part) among all groups (Bolton *et al.*, 1996).

8

(b)   Chemical Oxidation Technologies

Chemical oxidation methods are used to generate hydroxyl radicals via the hydroxyl-ion catalyzed decomposition of ozone in alkaline aqueous media (eqn 1.11) or the reaction of ozone with hydrogen peroxide (H_2O_2) in aqueous systems (eqn 1.12) (Hoigné and Bader, 1976; Al-Ekabi, 1999) :

$$2\,O_3 \;+\; H_2O \;\rightarrow\; HO\bullet \;+\; 2O_2 \;+ HO_2^{\bullet} \tag{1.11}$$

$$O_3 \;+\; H_2O_2 \;\rightarrow\; HO\bullet \;+\; O_2 \;+ HO_2^{\bullet} \tag{1.12}$$
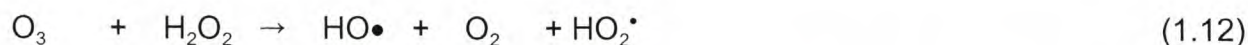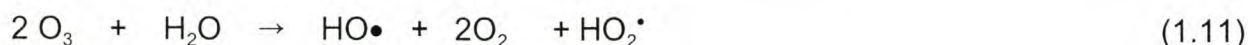
In both instances perhydroxyl ($HO_2^{\bullet}$) radicals (also known as hydroperoxyl radicals) are generated in addition to hydroxyl radicals. These processes have been applied for the oxidation of refractory organic compounds in groundwater (chloro-nitrobenzenes and pesticides) (Mokrini et al., 1997), removal of dissolved organic carbon (DOC) in simulated textile wastewater (Arslan et al., 1999) and the removal of THMs and geosmin from treated drinking water (Freese et al., 1997).

(c)   Iron Based Oxidation Technologies

Iron is the fourth most abundant metal found in the Earth's crust and has long been recognized for its importance in atmospheric photochemistry and the aquatic environment. Iron based oxidation can be described as the catalytic generation of hydroxyl radicals via the chain reaction between ferrous (Fe^{2+}) or ferric (Fe^{3+}) ions and H_2O_2 (Park et al., 1997). This reaction type was first reported by Fenton (in 1884) with the oxidation of maleic acid by Fe^{2+}/ H_2O_2, customarily known as "Fenton's reagent" or "Fenton oxidation" (Safarzadeh-Amiri et al., 1996). In addition, the Fe^{2+}/ H_2O_2 combination has also been referred to as the "classic Fenton reaction" (eqn 1.13) (Lei et al., 1998). Alternatively, the Fe^{2+} ion may be replaced with Fe^{3+} in which case perhydroxyl radicals can be generated via Fe^{3+}/ H_2O_2 processes, also known as "Fenton-like reactions" (eqn 1.14) :

$$Fe^{2+} \;+\; H_2O_2 \;\rightarrow\; HO\bullet \;+\; Fe^{3+} \;+ HO^{-} \tag{1.13}$$

$$Fe^{3+} \;+\; H_2O_2 \;\rightarrow\; HO_2^{\bullet} \;+\; Fe^{2+} \;+\; H^{+} \tag{1.14}$$
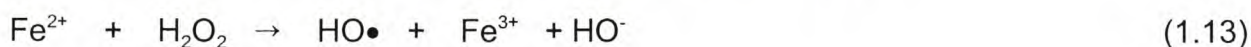
Fenton reactions have been widely used to oxidize phenols, chlorinated phenols and herbicides in water media, as well as reducing the chemical oxygen demand (COD) in municipal sewage water. Although the Fe^{2+}/ H_2O_2 molar ratio and solution pH are considered to be important factors in regulating the rate of oxidation, pronounced acceleration in rate is achieved by using photochemically enhanced Fenton reagents (Safarzadeh-Amiri et al., 1996; Lei et al., 1998). These "photo-Fenton" processes are based on the photoreduction of Fe^{3+} complexes, yielding Fe^{2+} ions (eqns 1.15 and 1.16) that can react with H_2O_2 in a classic Fenton reaction to produce hydroxyl radicals for oxidative degradation (eqn 1.13). Photo-Fenton processes are particularly effective when polluted water absorbs strongly in 200-300 nm range and pollutant concentrations are high (Bolton, 1999).

A solution pH in the vicinity of 3 and irradiation with wavelengths shorter than 580 nm are usually required to effect photoreduction of these complexes (Al-Ekabi, 1999; Spacek *et al.*, 1995).

$$Fe(OH)^{2+} \; + \; h\nu \; \rightarrow \; Fe^{2+} \; + HO\bullet \hspace{3cm} (1.15)$$

$$Fe(C_2O_4)_3^{3-} + \; h\nu \; \rightarrow \; Fe^{2+} \; + \; 2.5\,C_2O_4^{2-} \; + \; CO_2 \hspace{2cm} (1.16)$$
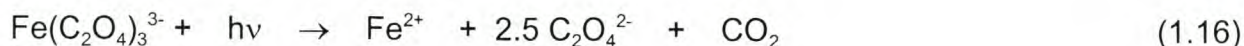
Photo-Fenton processes have been used for the oxidative degradation of polyvinyl alcohol (Lei *et al.*, 1998), phenol, cyclohexanol and 4-nitroanaline in aqueous solution (Spacek *et al.*, 1995). The decoloration and degradation of azo-dyes (e.g. Orange II) in dye wastewater have also been achieved (Morrison *et al.*, 1996; Bandara *et al.*, 1996). A novel electro-Fenton process, using the reaction of H_2O_2 with electrogenerated Fe^{2+} ions at a sacrificial iron anode, was applied for COD reduction within petrochemical wastewater (Huang *et al.*, 1997).

(d)   UV, Ozone & Hydrogen Peroxide Technologies

The UV-H_2O_2 process represents the most direct method for generation of hydroxyl radicals. The primary event comprises UV photolysis (photocleavage) of H_2O_2 to produce two hydroxyl radicals per quanta of light absorbed (eqn 1.17). As a result, the theoretical quantum yield is equal to two, however in practice, approximately 50% of all generated hydroxyl radicals undergo solvent cage recombination to form the original reactant, viz: H_2O_2 (eqn 1.18). The remaining hydroxyl radicals escape the cage and account for the observed quantum yield of one (Al-Ekabi, 1999; Bircher *et al.*, 1997).

$$H_2O_2 \; + \; h\nu \; \rightarrow \; HO\bullet \; + \; HO\bullet \hspace{3cm} (1.17)$$

$$(2\,HO\bullet)_{cage} \hspace{1cm} \rightarrow \; H_2O_2 \hspace{3.5cm} (1.18)$$

The UV photolysis of H_2O_2 is hampered by the inherent weak molar absorption coefficient of H_2O_2 in the 200 to 300 nm wavelength range, necessitating the use of elevated oxidant dosages (in excess of 100 mg/L) to ensure sufficient absorption of UV light (Al-Ekabi, 1999; Bolton, 1999). This phenomenon implies that treatment of turbid waters or waters containing strong UV absorbers may be highly impractical and expensive (Rajeshwar, 1996). Shock loading may be negated at high pH due to the decomposition of H_2O_2 via a dismutation reaction and competing absorption by the equivalent peroxide anion (HO_2^-). Despite this inhibiting effect, an increase in pH is generally associated with enhanced rates of H_2O_2 photolysis (Legrini *et al.*, 1993). This is ascribed to a markedly higher absorption coefficient for the anion, as opposed to H_2O_2 itself (Table 1.4). Powerful lamps (up to 30 kW), with strong spectral output in the 200 to 300 nm range, are used in UV-H_2O_2 systems (Bolton *et al.*, 1998).

A variety of refractory aqueous pollutants have been effectively oxidized by means of UV-H_2O_2 processes, i.e. halogenated aliphatics (dichloroethanes), aromatics (benzene, toluene, chlorobenzenes, phenol and chlorophenols) (Legrini *et al.*, 1993; Huang and Shu, 1995), organo-phosphorus pesticides (Doong and Chang, 1997) and azo-dyes (Ince *et al.*, 1997).

In addition, significant reduction of COD and adsorbable organic halogen (AOX) in pharmaceutical wastewater have been achieved (Höfl et al., 1997). The removal of natural organic matter (NOM) constituents from treated drinking water has been demonstrated, resulting in decolorization and total organic carbon (TOC) removal (Martin et al., 1999). Commercial UV-H_2O_2 systems are readily available for low cost water treatment, most notably for disinfection applications (Bolton, 1999a).

Ozone (O_3) in aqueous solution is capable of generating hydroxyl radicals under UV irradiation (Huang and Shu, 1995). The primary steps involve light-induced homolysis of ozone (eqn 1.19) and the subsequent production of hydroxyl radicals via the reaction of singlet-D oxygen (^1D) atoms with water molecules (eqn 1.20) (Legrini et al., 1993; Sigman et al., 1997). As in the case with the UV-H_2O_2 process, a portion of the generated hydroxyl radicals recombine in a solvent cage to yield H_2O_2 (eqn 1.18) (Al-Ekabi, 1999). The UV-O_3 process therefore provides a means to generate H_2O_2 in situ.

$$O_3 \quad + \quad h\nu \quad \rightarrow \quad O_2 \quad + \quad O(^1D) \quad\quad\quad\quad (1.19)$$

$$O(^1D) \quad + \quad H_2O \quad \rightarrow \quad HO\bullet \quad + \quad HO\bullet \quad\quad\quad\quad (1.20)$$

(where $O(^1D)$ = singlet-D oxygen)

An overall reaction equation is presented by Höfl et al. (1997) (eqn 1.21). Intermediates such as H_2O_2 and $O(^1D)$ are discarded :

$$3\,O_3 + H_2O + h\nu \rightarrow 4\,O_2 \quad + \quad 2\,HO\bullet \quad\quad\quad\quad (1.21)$$
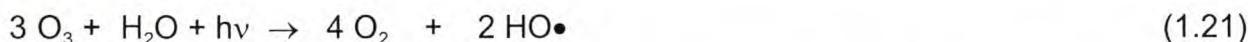
Although the process may appear to be an expensive method for generating H_2O_2 as primary oxidant, a complex series of photochemical reactions are involved that may generate additional reactive oxidants such as superoxide and perhydroxyl radical species (Sigman et al., 1997). Reactions involving O_3 are self-propagating, hence a stoigiometric amount of oxidant is not required. Moreover, direct reaction of the target organic pollutant with O_3 may be an added bonus in some cases (Rajeshwar, 1996). From a photochemical perspective, the absorption cross section at 254 nm are much higher for O_3 than H_2O_2, hence inner filter effects (caused by aromatic pollutants) may be less significant in the former case (Legrini et al., 1993) (see Table 1.4).

Table 1.4: Molar absorption coefficients (ε) for H_2O_2 species and O_3 at 253.7 nm (Legrini et al.,1993).

Oxidant	ε ($M^{-1}cm^{-1}$)
H_2O_2	18.6
HO_2^-	240
Ozone	3300

On the practical side, however, there are several restrictions concerning the UV-O_3 process. The yield for hydroxyl radicals is generally smaller compared to UV-H_2O_2 processes. Adequate transfer of O_3 into the liquid phase is a concern, which necessitates the development and implementation of efficient O_3/water contacting devices. Moreover, O_3 is an unstable gas and has to be generated on-site using fairly expensive equipment (Huang and Shu, 1995). Light scattering effects may also reduce photolysis rates in solution, although claims have been made to the contrary (Sigman et al., 1997). The strong pH dependence of O_3 decomposition in water is a further complicating factor in water treatment applications (Hoigné and Bader, 1976).

The UV-O_3 process has been widely used for the treatment of groundwater contaminants such as trichloroethylene and perchloroethylene (Bolton, 1999), trinitrotoluene (Peyton *et al.*, 1997) and other hazardous aromatic compounds such as phenol, xylene and lindane (Legrini *et al.*, 1993). THMs and NOM constituents (viz: humic substances) have been removed from treated drinking water (Takahashi *et al.*, 1999). The removal of COD and AOX from pharmaceutical wastewater (Höfl *et al.*, 1997) and the inactivation of micro-organisms in food-processing wastewater have also been demonstrated (Diaz and Law, 1999).

The triad combination of O_3, H_2O_2 and UV radiation presents a third option within the family of O_3 and H_2O_2 based AOTs. Under these conditions, hydroxyl radicals can be generated via anyone of the following routes (eqns 1.12 and 1.22 to 1.24) (Legrini *et al.*, 1993; Sigman *et al.*, 1997) :

$$O_3 \quad + \quad H_2O_2 \quad \rightarrow \quad HO\bullet \quad + \quad O_2 \quad + \quad HO_2^{\bullet} \tag{1.12}$$

$$O_3 \quad + \quad HO_2^- \quad \rightarrow \quad HO\bullet \quad + \quad O_2 \quad + \quad O_2^{-\bullet} \tag{1.22}$$

$$O_3 \quad + \quad O_2^{-\bullet} \quad \rightarrow \quad O_2 \quad + \quad O_3^{-\bullet} \tag{1.23}$$

$$O_3^{-\bullet} \quad + \quad H_2O \quad \rightarrow \quad HO\bullet \quad + \quad HO^- \quad + \quad O_2 \tag{1.24}$$
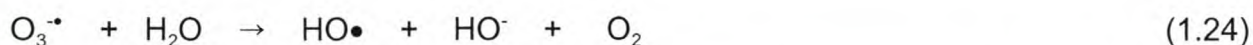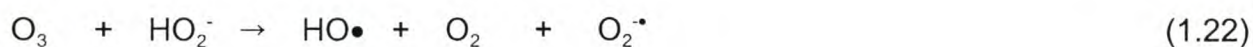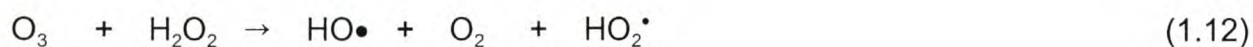
Hydroxyl radicals are again regarded as the primary intermediates that induce oxidative degradation of organic pollutants according to the mechanisms discussed earlier in 1.2.1. Rate constants in the order of 10^8 to 10^{10} $M^{-1}s^{-1}$ have mostly been reported. In several instances, the combination of UV, O_3 and H_2O_2 has been more efficient than treatment by anyone (or binary combination) of the three reactants alone (Legrini *et al.*, 1993; Mokrini *et al.*, 1997). A variety of refractory organic pollutants have been treated thus far and several pilot scale studies were conducted. The treatment of aqueous mixtures of aromatic compounds is noteworthy (Legrini *et al.*, 1993).

(e) Vacuum Ultraviolet Technologies

Photo-induced water treatment processes involving the use of vacuum ultraviolet (VUV) radiation represents an AOT with high efficiency for hydroxyl radical production without the need for supplementary oxidant (Hashem *et al.*, 1997). The VUV spectral domain comprises wavelengths shorter than 200 nm where air (oxygen) strongly exhibits absorption characteristics. As a result, spectroscopic work conducted at these and shorter wavelengths require the use of vacuum or non-absorbing gas molecules (Legrini *et al.*, 1993). Excitation in VUV processes predominantly leads to homolysis of chemical bonds and, as in the case of water molecules, leads to the production of reactice hydroxyl radicals and hydrogen atoms/molecules (eqn 1.25) (Jakob *et al.*, 1993).

$$H_2O \quad + \quad h\nu \quad \rightarrow \quad \tfrac{1}{2}H_2 \quad + \quad HO\bullet \tag{1.25}$$

The use of VUV processes in environmental applications are growing due to the development of excimer light sources for excitation of molecules at short wavelengths. Xe-excimers are popular choices for VUV excitation of water molecules at 172 nm. The high absorption cross-section of water at this wavelength facilitates homolysis and effects a high yield of radicals (Legrini *et al.*, 1993; Jakob *et al.*, 1993). Excimer sources can also be applied for the photochemical generation of ozone (Hashem *et al.*, 1997).

The technical development of VUV processes poses a definite challenge to other AOTs due to their inherent simplicity and absence of oxidant supplement. Practical concerns such as the dependence of process efficiency on pollutant concentration may be addressed through the development of efficient light sources and reactor geometries. The development of excimer light sources is still in its infancy and very few results are available on the use of VUV processes for water remediation. The degradation of a number of model pollutants (viz: 4-chlorophenol, xylidines and methyl-nitrobenzenes) have been reported (Legrini *et al.*, 1993; Jakob *et al.*, 1993). VUV radiation has been utilized to degrade 4-chlorophenol in water by means of two separate photochemical processes, viz: (1) the generation of O_3 from gaseous oxygen and (2) UV photolysis in water. It was found that combining the latter two processes yielded faster degradation rates in comparison to individual use of O_3 or VUV (Hashem *et al.*, 1997). The laser-assisted photochemical treatment of colored textile wastewater was studied using ArF excimer radiation at 193 nm (Unkroth *et al.*, 1997). In air treatment applications, VUV radiation (172 nm) has been used to enhance silent discharge plasma treatment of chlorinated VOCs in flue gases (Falkenstein, 1997). An alternative source of short wavelength VUV photons is currently being developed using microwave excitation of mercury and xenon gas in electrodeless lamps (Fassler *et al.*, 1999).

(f) Supercritical Water Oxidation

A supercritical fluid can be defined as a substance above its critical point, viz: the highest temperature and pressure at which vapor-liquid equilibrium can exist. The supercritical regions of many common gases and liquids are accessible, but are often very challenging to maintain in practice. Supercritical water, for example, requires temperatures and pressures above 374 $^\circ$C and 220 atmospheres, respectively (Brennecke, 1996). The process of supercritical water oxidation (SCWO) is of particular interest as an AOT, owing to the unique properties of water at these conditions. Supercritical water is a single-phase liquid which (1) is completely miscible with oxygen and most organic compounds (2) reduces interfacial diffusion (3) increases mass transfer rates (4) decreases solubility of inorganic salts and (5) undergoes thermal dissociation to yield hydroxyl radicals and hydrogen atoms (eqn 1.26) (Al-Ekabi, 1999). As a result, high degrees of carbon conversion can be attained within relatively short SCWO residence times. The desired degree of destruction may be achieved within seconds or minutes (Lin and Wang, 1999).

$$H_2O \ (T \geq 374\,^\circ C, \ P \geq 220 \ bar) \quad \rightarrow \quad HO\bullet \ + \ H\bullet \qquad\qquad (1.26)$$
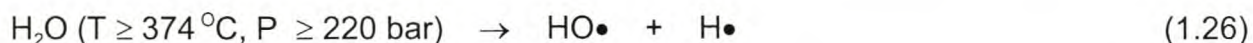
(where T = temperature and P = pressure)

Systems based on SCWO have been implemented on pilot scale for industrial wastewater remediation in the USA, Germany and Sweden. Wastewater generated by semiconductor manufacturing, paper and petroleum industries have been treated in this regard. SCWO is particularly useful in cleaning up highly explosive military wastes when no other viable method exists. Corrosion, high energy requirements, effective heat management, salt precipitation and safety aspects comprise the major technical challenges that need to be solved before SCWO reactors will be implemented commercially. Nevertheless, it remains an attractive oxidation method for hazardous and refractory pollutants (Rice *et al.*, 1999).

(g) Electron Beam Irradiation

Electron beam treatment is an AOT that involves the use of a high energy electron beam (E-beam) to irradiate polluted water. The ensuing interaction between electrons and water molecules results in the radiolysis of water with a concomitant generation of several oxidative and reducing species, including hydroxyl radicals, hydrogen atoms and hydrated electrons (eqn 1.27) (Bolton *et al.*, 1998; Cooper, 1999).

$$H_2O + E\text{-beam} \rightarrow e^-_{aq} + HO\bullet + H\bullet + H_2 + H_2O_2 + H^+ \qquad (1.27)$$
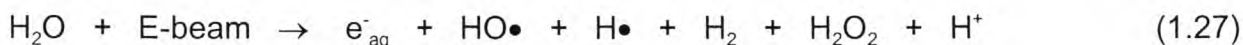
(where e^-_{aq} = hydrated electrons)

The oxygenated reactive species (i.e. hydroxyl radicals and H_2O_2) effect oxidative degradation of organic pollutants, leading to eventual mineralization. E-beams can be produced by electron accelerators in which a hot cathode emits a current of electrons in a vacuum. The kinetic energy of the electrons can be regulated by changing the voltage of the electrical field which is applied for accelerating the electrons. The number of electrons generated per unit time is proportional to the beam current, hence the beam power can be calculated from the beam current and accelerating voltage. A power requirement exists for operating E-beam instruments, even when the beam is off (Bolton *et al.*, 1998).

The amount of energy absorbed per unit mass of irradiated water is known as absorbed dose. Dose is an important design parameter for E-beam treatment processes and is expressed in Rads or Grays. 1 Megarad of absorbed energy corresponds to a temperature change of 2.39 $^{\circ}$C. Increasing the dose will increase the concentration of reactive species in solution. The increase is non-linear and may resemble steady state (equilibrium) kinetics as a result of mutual reaction (Cooper, 1999). E-beam processes have been demonstrated on pilot scale for water and air remediation (Al-Ekabi, 1999). Of particular interest was the treatment of aqueous chlorinated contaminants such as methyl *tert*-butyl ether (MTBE), carbon tetrachloride, trichloroethylene, THMs and dichloromethane - which are normally resistant to oxidation by AOT means. These compounds are often referred to as *refractory* compounds, for they resist oxidation appreciably (Blake, 2000; Ollis, 2000). The rate constants for reactions of these contaminants with E-beam generated species range from 10^7 to 10^{10} $M^{-1}s^{-1}$ with hydrated electrons being consistently more reactive than hydroxyl radicals and hydrogen atoms. Waters contaminated with aromatic compounds such as benzene, toluene, xylenes and phenol were also successfully treated (Cooper, 1999). In air treatment applications, E-beam technology has been used to oxidize sulfur dioxide (SO_2) in flue gases (Chmielewski *et al.*, 1996; Nichipor *et al.*, 1996)

14

Radiation-induced purification of water may also be achieved via gamma (γ) irradiation, most notably with ^{60}Co sources. In this regard, the destruction of petroleum products and groundwater contaminants have recently been reported (Pikaev *et al.*, 1999; Lee *et al.*, 1999).

(h) Electrohydraulic Cavitation & Sonolysis

The use of ultrasonic waves for the treatment of organic contaminants constitutes a relatively new AOT for water treatment. The main event in this process is known as "electrohydraulic cavitation" that is caused by irradiation of liquids with ultrasound at frequencies greater than 16 kHz. The cavitation entails formation, expansion and implosion of bubbles as a result of pressure variations within the liquid (Al-Ekabi, 1999; Schwikkard and Buckley, 1998). Compression of the bubbles causes pulsation and collapse, producing intense local heat and high pressure. Localized temperatures between 2273 K and 5000 K and pressures ranging from 101 MPa and 101300 MPa have been reported during collapse. In these conditions, water undergoes thermal dissociation to generate hydroxyl radicals and hydrogen atoms (eqn 1.28) (Al-Ekabi, 1999; Winship, 1999). The radicals initiate oxidative chemical reactions that may occur inside, at the interface, or some distance away from the cavitation bubbles. The chemical effects of sonolysis are similar to those observed in pyrolysis, radiolysis and supercritical fluids. These phenomena are the subject of much debate and several theories have been constructed thus far (Barbier and Petrier, 1996).

$$H_2O \ (T \geq 2000 \ K, P \geq 101 \ MPa) \quad \rightarrow \quad HO\bullet \ + \ H\bullet \qquad\qquad (1.28)$$

(where T = temperature and P = pressure)

In water treatment, a cavitation bubble may be regarded as a micro-reactor for the destruction of organic contaminants, since it produces hydroxyl radicals (Petrier and Francony, 1997). Examples of aqueous organic contaminants treated by these processes include 4-nitrophenol (Barbier and Petrier, 1996), phenol (Petrier and Francony, 1997), MTBE (Kang *et al.*, 1999), carbon tetrachloride, chloroform, dichloromethane (Hung *et al.*, 1999), TCE and ethylene dibromide (Peters *et al.*, 1999).

The efficiency of ultrasound oxidation processes is frequency dependent. In this regard, frequencies ranging from 20 kHz to 1078 kHz have been used throughout, however enhanced destruction rates were observed at higher frequencies (200-800 kHz). The addition of ozone to sonolytic systems often enhances oxidative destruction rates. This combination (known as sonozone) has been used to mineralize NOM in water (Barbier and Petrier, 1996).

(i)   Non-Thermal Plasma Technologies

Non-thermal plasmas (NTPs) are currently being applied for the AOT treatment of gas-phase pollutants. Chemical destruction is initiated by highly reactive oxidative and reductive species, e.g., $O(^3P)$, N, H, NH, CH, O_3, $O_2(^1\Delta_g)$, plasma electrons and hydroxyl radicals. NTPs are commonly created by electrical discharge or electron beam injection into a gas. Both methods generate highly energetic (*hot*) plasma electrons (viz: 1-10 eV), while ions and background gas species are at near-ambient temperatures (*cold*). For this reason NTPs are also referred to as cold plasmas (Rosocha, 1999).

Non-thermal plasma (NTP) technologies have been used for the treatment of flue-gas (SO_x and NO_x) and VOCs from waste incineration, motor-generators and jet engine test facilities. Several equipment designs have been investigated thus far, viz: pulsed corona plasma, dielectric-barrier discharge (silent discharge), electron-beam plasma, catalytic plasma systems and corona radical showers (Rosocha, 1999a). Systems based on NTP technology have been demonstrated on a pilot scale for treatment of contaminated air streams (Al-Ekabi, 1999).

(j)   Natural Sources of Hydroxyl Radicals

Hydroxyl radicals may be generated photochemically in natural aqueous systems. In this regard, the photolysis of nitrite and nitrate species is well known (eqns 1.29 to 1.31) (Faust, 1994; Vaughan and Blough, 1999).

$$NO_2^- \;+\; h\nu \;\rightarrow\; NO \;+\; O^- \tag{1.29}$$

$$NO_3^- \;+\; h\nu \;\rightarrow\; NO_2 \;+\; O^- \tag{1.30}$$

$$O^- \;+\; H_2O \rightarrow\; HO\bullet \;+\; HO^- \tag{1.31}$$

(where NO_2^- = nitrite and NO_3^- = nitrate)

Waters containing sufficiently high metal ion concentrations may also produce hydroxyl radicals via photo-Fenton chemistry and ligand-to-metal charge-transfer reactions. Moreover, it was recently shown that UV photolysis of NOM constituents (particularly fulvic acids) may induce hydroxyl radical formation in natural waters under both aerobic and anaerobic conditions (Vaughan and Blough, 1999).

16

(k)   Alternative Oxidation Technologies

Several alternative oxidation technologies are currently being used for water and wastewater treatment, but do not necessarily incorporate hydroxyl radical chemistry or AOT related reactions. These technologies include the use of ozone (Sarasa *et al.*, 1999; Liakou *et al.*, 1997), catalytic ozone (Cortés *et al.*, 1999; Logemann and Annee, 1997), potassium permanganate (Vella *et al.*, 1999), chlorine and chloramine (Nicholson *et al.*, 1994), chlorine dioxide and hypochlorite (Lopez *et al.*, 1997), and electrochemically generated oxidants such as cerium (IV) and silver (II) (Hitchman *et al.*, 1995).

Furthermore, molecular oxygen is a potent oxidant in the liquid phase when using high temperature and pressure conditions. This process is referred to as wet air oxidation (WAO) or catalytic wet air oxidation (CWAO) depending on the addition of suitable catalysts. WAO and CWAO have been used primarily for treatment of industrial wastewater with high COD (Debellefontaine *et al.*, 1997; Lei *et al.*, 1997; Yue, 1999).

Bio-oxidation, thermal oxidation, UV-disinfection and chemical disinfection technologies are noteworthy amongst a family of water treatment strategies either offered as alternatives or supplements to AOTs (Al-Ekabi, 2000).

(l)   Semiconductor Photocatalysis

The AOT discipline of *semiconductor photocatalysis* (SP) has been studied extensively in the last 15 to 20 years as a potential candidate for the treatment of contaminated water, air and soil. This discipline is mainly related to the area of heterogeneous catalysis and has consequently also been referred to as *heterogeneous photocatalysis*.

As in the case of conventional heterogeneous catalysis, the overall SP process comprises five distinctive steps, viz :

1. Transfer of liquid or gaseous phase reactants to the catalytic surface
2. Adsorption of at least one reactant
3. Reaction in the adsorbed phase
4. Desorption of product(s)
5. Removal of products from the interface region

The photocatalytic reaction occurs in the adsorbed phase (Step 3), hence in proximity of the catalytic surface. SP is mostly similar to conventional catalysis with the exception of the mode of activation. With SP, conventional thermal activation of catalyst is normally replaced by photonic activation (Herrmann, 1999), although combined thermal-photocatalytic activation has also been reported (Selvaggi *et al.*, 1999). The activation mode is primarily concerned with reaction in the adsorbed phase, although photoadsorption and photodesorption of reactants (mainly oxygen) do exist.

17

SP comprises a large variety of reactions and processes, e.g. photocatalytic oxidation (PCO), photocatalytic reduction (PCR), dehydrogenation, hydrogen transfer, O_2^{18}-O_2^{16} and deuterium-alkane isotopic exchange, metal deposition, water detoxification, gas-phase pollutants removal and a host of other environmental applications (Herrmann, 1999). PCO is most noteworthy within the family of SP reactions and usually involves the heterogeneous catalytic activation of a semiconductor via light irradiation of appropriate wavelength, depending on the band gap energy of the semiconductor under investigation. The generation of *hydroxyl radicals* and a few other highly reactive species (mostly oxygenated radicals) constitutes the central event in PCO related reactions. These reactive species may facilitate the breakdown (or removal) of various organic, inorganic and metallic pollutants via oxidative degradation mechanisms (as discussed earlier).

Various metal oxides (i.e. TiO_2, ZnO, MoO_3, CeO_2, ZrO_2, WO_3, α-Fe_2O_3, and SnO_2) and metal chalcogenides (i.e. ZnS, CdS, CdSe, WS_2 and MoS_2) are used as catalysts in SP reactions. In this regard, the sub-discipline of *TiO_2 photocatalysis* has been of particular interest due to recurrent use of anatase TiO_2 as heterogeneous photocatalyst.

TiO_2 photocatalysis (with specific reference to PCO) forms the cornerstone of this particular work and will be discussed in more detail. The PCO of aqueous pollutants will receive preference.

1.3 TiO_2 PHOTOCATALYSIS

1.3.1 TiO_2 as Semiconductor

The photocatalytic splitting of water on TiO_2 electrodes was discovered in 1972 by Fujishima and Honda. This event ushered in a new era for heterogeneous photocatalysis with the utilization of TiO_2 as semiconductor (Linsebigler *et al.*, 1995).

Titanium dioxide (TiO_2) exhibits three distinct polymorphs, viz: anatase, rutile and brookite (Mo and Ching, 1995). Of these three crystal forms only anatase is functional as a photocatalyst. This may be attributed to (1) the presence of crystal defects in the case of rutile (2) the fact that brookite is extremely difficult to synthesize and (3) the general scarcity of the latter (Kriek, 1998; Cloete, 1999). TiO_2 (anatase), being a semiconductor, requires a specified amount of energy to be an electrical conductor. This energy is equal to the band gap energy (E_b) separating the valence band and the conduction band (Figure 1.1). In the case of metals the valence bands are completely filled with electrons at zero Kelvin. Above absolute zero there is a free flow of electrons between the valence and conduction bands and no external energy is required to attain conductance. Insulators (on the other hand) exhibit very large band gap energy separations to the extent that that no amount of energy can render conductance (Kriek, 1998). TiO_2 (anatase) is typically a n-type semiconductor since the main charge carriers are electrons (Hand *et al.*, 1993).

E_b = Band gap Energy

Conduction Band

$E_b = 0$

Valence Band

Metals

Conduction Band

E_b = Small

Valence Band

Semiconductors

Conduction Band

E_b = Large

Valence Band
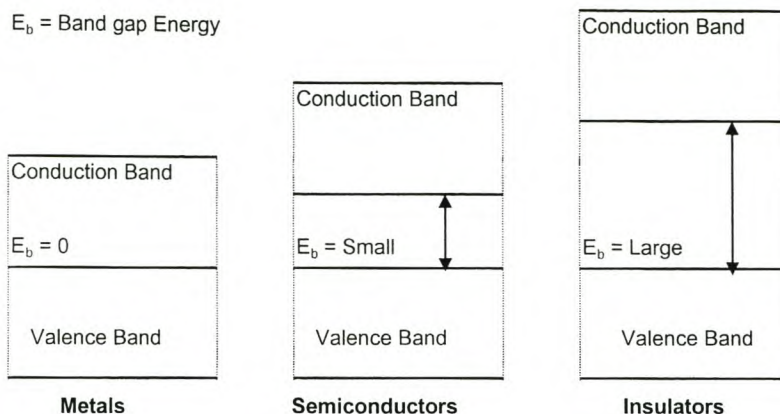
Insulators

Figure 1.1:   Band gap energies of metals, semiconductors and insulators.

For TiO_2 (anatase) the amount of energy separating the valence band and conduction
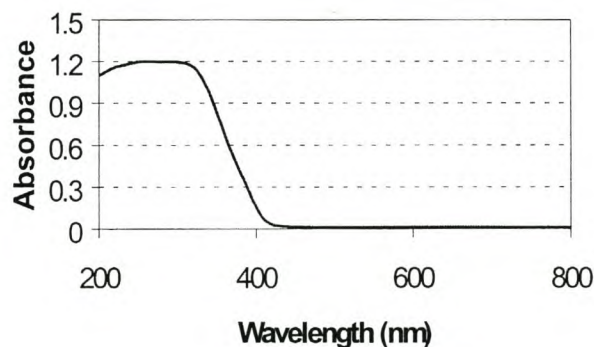
band is approximately 3.20 eV. It thus follows that light photons with wavelengths shorter than 380 nm (according to $E = hc/\lambda$) will be sufficient for the excitation of an electron from the valence band to the conduction band (Ray, 1999; Engelbrecht *et al.*, 2000). This phenomenon is adequately portrayed in the UV absorption spectra of anatase (Figure 1.2) (Hand *et al.*, 1993).

Figure 1.2: UV absorption spectrum of TiO_2 (anatase).

Anatase TiO_2 has constantly been the popular choice as semiconductor photocatalyst due to its non-toxicity, high photo-activity, high stability, low cost and favorable overlap with the UV portion of the solar spectrum, making it an attractive option for solar applications (Rajeshwar, 1996; Hoffmann *et al.*, 1995; Hand *et al.*, 1993).

Metal oxide particles often display amphoteric character when suspended in aqueous media. In the case of TiO_2, the principal amphoteric surface functionality is the "titanol" moiety (>TiOH). The adsorption of organic molecules onto the surface of TiO_2 in aqueous suspensions is therefore pH dependent.

The point of zero charge (PZC) for TiO_2 is around 6.3 and acts as a general demarcation for TiO_2 particles in terms of charge. For example, at elevated pH levels, the adsorption of molecules with electronegative functional groups (e.g. carboxylic functional groups of NOM) will be suppressed due to electrostatic repulsion in the vicinity of predominantly formed TiO^- species.

The charge variation of TiO_2 (hence its surface hydroxyl groups) is frequently depicted in terms of the acid-base equilibria and pH distribution curve presented in Figure 1.3 below (Fox and Dulay, 1996; Cloete, 1999; Hoffmann *et al.*, 1995):

$$>Ti\text{-}OH_2^+ \rightleftarrows >Ti\text{-}OH + H^+ \qquad (pK_a = 4.95)$$
$$>Ti\text{-}OH \rightleftarrows >Ti\text{-}O^- + H^+ \qquad (pK_a = 7.8)$$
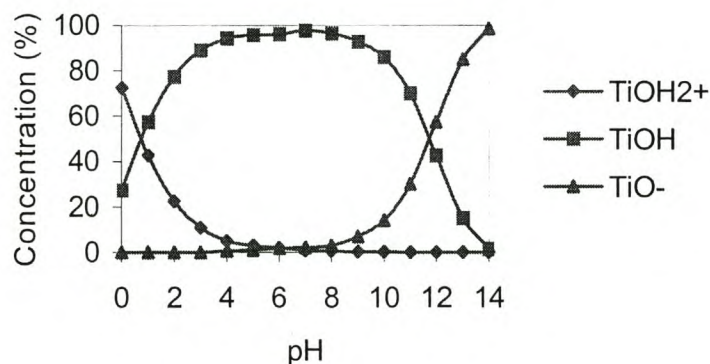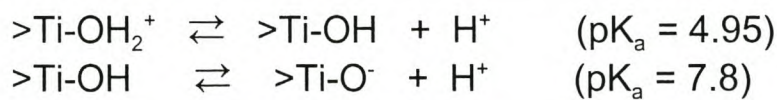
Figure 1.3: **Acid-base equilibria and pH distribution curve for aqueous TiO_2 species (Cloete, 1999)**

1.3.2 Principal Mechanistic Events

As stated earlier, TiO_2 mediated photocatalytic oxidation (PCO) of organic substrates in aqueous media involves the absorption of UV light quanta by the semiconductor catalyst (TiO_2) to produce hydroxyl radicals via adsorbed water molecules or hydroxyl ions on its surface in the presence of molecular oxygen. The formed hydroxyl radicals (and other oxygenated radical species) initiate and proceed with oxidative degradation of the target organic substrate molecules (Engelbrecht *et al.*, 2000).

The band-gap model is generally used to elucidate the mechanistic events for semiconductor catalyzed oxidative degradations of organic compounds in aqueous media (Legrini *et al.*, 1993). TiO_2 photocatalyzed oxidative degradations are no exception. Two oxidation mechanisms are presented here which have been adequately corroborated by experimental data (Braun *et al.*, 1993a).

(i) The *first mechanism* proposes the generation of hydroxyl radicals as intermediates for oxidation. When anatase TiO_2 is irradiated with UV quanta of an appropriate wavelength (< 380 nm), valence band electrons are promoted to the conduction band upon electronic excitation. The ensuing charge separation leads to the formation of charge deficient cavities (or positively charged holes) in the valence band.

$$TiO_2 \ + \ h\nu \ \rightarrow \ TiO_2 \, (e^- + h^+) \qquad\qquad (1.32)$$

The negative charge in the conduction band is readily transferred to dissolved molecular oxygen in aqueous media with the subsequent formation of a superoxide radical anion (eqn 1.33). The presence of oxygen is essential due to its function as an electron acceptor (scavenger) and consequently maintains the excited state of the process by preventing unwanted recombination of electrons and positive hole pairs (the reverse of eqn 1.32).

$$TiO_2 \, (e^- + h^+) \ + \ O_2 \ \rightarrow \ TiO_2 \, (h^+) \ + \ O_2^{-\bullet} \qquad\qquad (1.33)$$
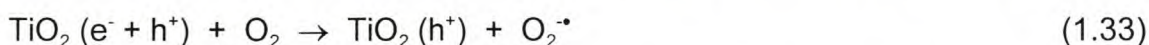
Depending on the pH of the aqueous media, the formed superoxide radical anion (and its protonated form) can dismutate rapidly to yield hydrogen peroxide (eqns 1.34 to 1.36) :

$$O_2^{-\bullet} \ + \ H_3O^+ \ \rightleftarrows \ HO_2^{\bullet} + \ H_2O \qquad\qquad (1.34)$$
$$O_2^{-\bullet} \ + \ HO_2^{\bullet} \ \rightarrow \ HO_2^- \ + \ O_2 \qquad\qquad (1.35)$$
$$HO_2^- \ + \ H_3O^+ \ \rightleftarrows \ H_2O_2 \ + \ H_2O \qquad\qquad (1.36)$$

The TiO_2 surface catalyzes the decomposition of the resultant hydrogen peroxide to yield hydroxyl radicals (eqn 1.37) :

$$HO_2^- \ + \ H_2O_2 \ \rightarrow \ O_2^{-\bullet} \ + \ HO\bullet \ + \ H_2O \qquad\qquad (1.37)$$

In addition (depending on water pH) water molecules and/or hydroxyl ions adsorbed onto the TiO_2 surface are oxidized by the charge deficient holes in the valence band to yield hydroxyl radicals (eqns 1.38 and 1.39):

$$TiO_2(h^+) \ + \ HO^- \ \rightarrow \ TiO_2 \ + \ HO\bullet \qquad\qquad (1.38)$$
$$TiO_2(h^+) \ + 2\,H_2O \ \rightarrow \ TiO_2 \ + \ HO\bullet \ + \ H_3O^+ \qquad\qquad (1.39)$$
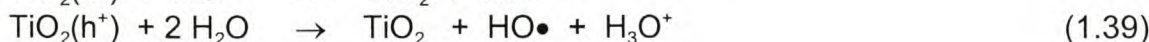
Sorbed on the TiO_2 surface, the hydroxyl radicals proceed to react with organic substrates via hydrogen abstraction, electron transfer or electrophilic addition (as explained in 1.2.1) and ultimately yielding CO_2 and H_2O as products (mineralization).

(ii) The *second mechanism* proposes a direct reaction between the positively charged holes (h^+) and the organic molecules adsorbed onto the TiO_2 surface via electron transfer (eqn 1.40) :

$$TiO_2(h^+) + RH_2 \rightarrow TiO_2 + RH_2^+ \hspace{3cm} (1.40)$$

Although this mechanism may apply to the treatment of halogenated (nucleophilic) compounds in cases where hydrogen abstraction is precluded, it exhibits very little practical value in terms of conventional water treatment scenarios. Electron transfer processes rely on sufficient high concentrations of the organic compound to be adsorbed onto the catalytic surface, however, this condition is rarely attained due to high dilution factors and preferential adsorption of water molecules or hydroxide ions (Braun *et al.*, 1993a).

It is generally believed that PCO is surface catalyzed in nature and not induced in bulk aqueous solution. An ongoing global debate still exists on whether surface hydroxyl radicals or positively charged holes are directly responsible for PCO (Serpone *et al.*, 1993). The two mechanisms cannot be differentiated by product analysis alone, since both pathways yield identical products (Terzian *et al.*, 1995). Still, the popular vote lies with hydroxyl radical pathway. Superoxide and several other oxygenated radical species (e.g. perhydroxyl, peroxyl and oxyl radicals) may also contribute to the complex series of surface catalyzed oxidative degradation reactions. A simplified mechanistic profile of TiO_2 mediated PCO is presented in Figure 1.4 below.
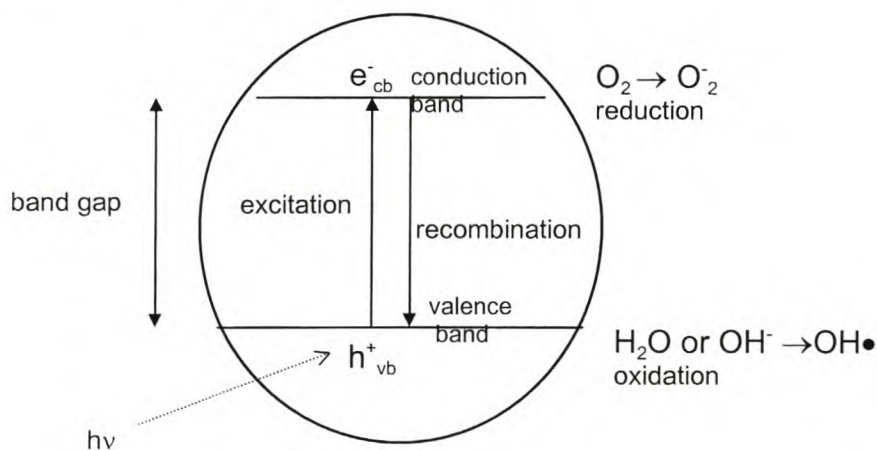
Figure 1.4: Hydroxyl radical formation via TiO$_2$ photocatalytic oxidation.

Mills and Le Hunte (1997) provides an efficient documentation of the primary photo-physical events (and corresponding time domains) associated with TiO_2 catalyzed photomineralization of organic pollutants (Table 1.5). This account represents a generalized mechanism for heterogeneous photocatalysis on TiO_2, as first proposed by Hoffmann *et al.* (1995).

Table 1.5: Primary processes and associated time domains for TiO_2 sensitized PCO.

Primary Process	Characteristic Time
(a) Charge carrier generation $TiO_2 + h\nu \rightarrow h^+ + e^-$	fs (very fast)
(b) Charge carrier trapping $h^+ + >Ti^{IV}OH \rightarrow \{>Ti^{IV}OH^{\bullet+}\}$ $e^- + >Ti^{IV}OH \leftarrow\rightarrow \{>Ti^{III}OH\}$ $e^- + >Ti^{IV} \rightarrow Ti^{III}$	100 ns (fast) 100 ps (shallow trap) 10 ns (deep trap)
(c) Charge carrier recombination $e^- + \{>Ti^{IV}OH^{\bullet+}\} \rightarrow >Ti^{IV}OH$ $h^+ + >Ti^{III}OH \rightarrow >Ti^{IV}OH$	100 ns(slow) 10 ns (fast)
(d) Interfacial charge transfer $\{>Ti^{IV}OH^{\bullet+}\}$ + organic pollutant $\rightarrow >Ti^{IV}OH$ + oxidized pollutant $\{>Ti^{III}OH\} + O_2 \rightarrow Ti^{IV}OH + O_2^{\bullet-}$	100 ns (slow) ms (very slow)

Key: $>TiOH$ = primary hydrated surface functionality of TiO_2
$\{>Ti^{IV}OH^{\bullet+}\}$ = surface-trapped valence band hole (= surface bound hydroxyl radical)
$\{>Ti^{III}OH\}$ = surface trapped conduction band electron

According to the mechanism summarized in Table 1.5, the overall quantum efficiency for interfacial charge transfer is determined by competition between (1) charge-carrier recombination and trapping (picoseconds to nanoseconds) and (2) trapped carrier recombination and interfacial charge transfer (microseconds to milliseconds). An increase in either interfacial electron-transfer rate constants or recombination lifetime of charge carriers will inevitably induce higher quantum efficiency (Hoffmann *et al.*, 1995).

Although rutile TiO_2 exhibits an energy bandgap of 3.02 eV it remains photocatalytically inactive due to intrinsic crystal defects attributing to a quick charge recombination. This reaction exerts an inhibitory effect on the photocatalytic efficiency of semiconductors and is usually associated with the dissipation of heat energy and/or light. The lifetime of the excited electron and the created positive hole should be long enough to enable their participation in reduction and oxidation reactions. Moreover, both charges must migrate to the surface of the TiO_2 particle to be available to the surrounding medium (Kriek, 1998).

The TiO_2 semiconductor particles will invariably strive to a state of lowest potential energy. The conduction band electrons and the valence band positive holes may follow a number of pathways in order to attain the required state of lower energy. These include (1) recombination with subsequent dissipation of input energy as heat (2) trapping in metastable surface states or (3) reaction with electron donors and electron acceptors that are adsorbed on the semiconductor surface or within the surrounding electrical double layer of the charged particles (Hoffmann *et al.*, 1995).

1.3.3 Reaction Kinetics

In general, TiO$_2$ sensitized photocatalytic degradation of organic substrates by oxygen fit a Langmuir-Hinshelwood kinetic regime under steady-state illumination conditions (Mills and Le Hunte, 1997; Mills and Morris, 1993). The rate of photochemical degradation can be expressed in terms of both the oxidant (e.g., O$_2$) and the reductant (organic pollutant) as indicated in eqn 1.41 (Hoffmann *et al.*, 1995):

$$- d[Red]/dt = - d[Ox]/dt = k_d\,\theta_{Red}\theta_{Ox} \tag{1.41}$$

(where Red = reductant, Ox = oxidant, k_d = PCO rate constant, θ = fraction of species sorbed to TiO$_2$)

The model is subject to the assumption that sorption of both oxidant and reductant is a rapid equilibrium process in both the forward and reverse directions. Moreover, the rate-determining step involves both species present in a monolayer at the liquid-solid interface.

The generalized Langmuir-Hinshelwood model for PCO related reactions is expressed as follows (Mills and le Hunte, 1997) (eqn 1.42) :

$$R_i = \ -d[S]_i/dt \qquad = \{\,k(S)K(S)[S]_i\,\}/\{1 + K(S)[S]_i\,\} \tag{1.42}$$

where : R_i = initial rate of substrate removal
$[S]_i$ = initial substrate concentration
$k(S)$ = intrinsic reactivity of TiO$_2$ with regard to substrate
$K(S)$ = Langmuir adsorption constant of species S sorbed on TiO$_2$

The proportionality constant, $k(S)$, is dependent on the rate of light absorption and the fraction of oxygen absorbed. It will also exhibit as dependence on flow rate in flow through irradiation systems, indicating a mass transfer dependence not found in batch systems. The Langmuir constant, $K(S)$, is not a true reflection of the dark Langmuir adsorption isotherm for substrate (S) sorbed on the catalyst, with the latter usually much smaller (Mills and Le Hunte, 1997).

TOC diminution rates in PCO reactions generally follows apparent zero-order kinetics where (1) saturation coverage of surface sites by organic substrate molecules occurred and (2) steady-state concentrations of hydroxyl radicals are generated at the irradiated TiO$_2$ surface. Pseudo first-order kinetic regimes may be observed in cases of substrate photolysis at very low initial concentrations of substrate. The PCO kinetics for model compounds are often apparent zero-order, however substrate concentrations may decrease rapidly by one or two orders of magnitude, leading to a first, second or mixed order regime at low concentration. Consequently, the kinetics of substrate degradation by PCO have been successfully modeled by Langmuir-Hinshelwood equation modified for competitive adsorption of both solvent and the organic substrate at the active sites of the TiO$_2$ photocatalyst (Legrini *et al.*, 1993).

In addition, Herrmann (1995) furnished the following generalized boundary conditions for photocatalytic reaction rates in terms of substrate concentrations:

- for concentrations lower than 10^{-3} M : the reaction is first order, and
- concentrations greater than 5×10^{-3} M : reaction rate is maximized at zero'th order.

Apart from initial substrate concentration, the following physical parameters influence photocatalytic reaction kinetics substantially, viz: (1) mass of TiO_2 catalyst in terms of reactor configuration (2) irradiation wavelength (3) temperature (4) radiant flux (5) quantum yield and (6) catalyst modification strategies (Herrmann, 1995). Kriek (1998) extended this list by incorporating a number of photo-physical and surface-chemistry related criteria, viz: (1) crystal structure (2) surface area and porosity of catalyst (3) density of surface hydroxyl groups (4) rate of recombination of positive holes and electrons upon absorbance of UV photons (5) pH (6) chemical nature of reactant species and (7) photocatalytic reactor design.

It is important to note that a myriad of processes and conditions may affect the kinetics and overall reaction efficiency of the PCO process. A few selected items will be discussed further, including several elements of photocatalytic reactor design.

1.3.4 Target Pollutants

To date, a multitude of dissolved organic, inorganic and organo-metallic compounds have been treated by PCO reactions. This has mainly been achieved at laboratory scale using small PCO reactors operating as batch or flow reactor systems (Engelbrecht *et al.*, 2000).

PCO of organic compounds is of considerable interest to the environmental sector and in particular for the control (and eventual destruction) of hazardous wastes. Complete mineralization of the parent molecule (viz: complete oxidation to yield CO_2, H_2O and associated inorganic components) has been reported for a variety of aliphatic and aromatic chlorinated hydrocarbons. The general classes of compounds treated by PCO (although not necessarily to the point of complete mineralization) include alkanes, halo-alkanes, aliphatic alcohols, carboxylic acids, alkenes, aromatics, halo-aromatics, polymers, surfactants, dyes, herbicides and pesticides wastes (Hoffmann *et al.*, 1995). Other noteworthy organic-related compounds and parameters treated by photocatalytic processes include amino acids, DNA nitrogen bases, color, COD, TOC, DBPs, fullerenes, geosmin, humic substances (NOM), oil and petroleum, PCBs and algal toxins (Blake, 1999; Eggins *et al.*, 1997; Bekbolet, 1996). On the bio-medical side, PCO technologies have used successfully for the treatment of bacteria, viruses, fungi, yeast, cancer cells, tumor cells and mouth microbes (dental application) (Blake *et al.*, 1999).

In addition to organic compounds, a number of inorganic and organo-metallic compounds have also displayed photochemical transformation on TiO_2 surfaces, albeit not necessarily via PCO. Selected examples include ammonia, chromium species, copper, cyanide, gold, halide ions, iron species, manganese species, mercury, nitrates and nitrites, nitrogen, platinum group metal species, silver and sulfur species, inorganic complexes such as EDTA, among others (Blake,1999; Hoffmann *et al.*, 1995).

1.3.5 Photocatalytic Reactor Design

(a) Literature Review

Research efforts pertaining to photocatalytic reactor design have mainly been directed towards slurry-phase and immobilized-bed (fixed-bed) reactors operating as batch or flow systems. Slurried reactor configurations comprise the dispersion of TiO_2 colloidal particles in aqueous slurry medium. Immobilized configurations comprise the impregnation of TiO_2 on stationary supports such as quartz, glass, fiber glass, sand, ceramics, polymers, activated carbon, zeolites and optical fibers. They are usually operated as annular or falling film-type systems, but are less effective than slurried models in terms of reaction rates and photocatalytic efficiency. This is mainly ascribed to inherent low catalytic surface-to-volume ratios. To their advantage is the fact that expensive secondary removal of catalyst is not required as is the case with slurried systems. Immobilized configurations are consequently favored when scaling-up of designs are considered. Several types of small-scale photocatalytic reactors have been developed in laboratory studies using a variety of artificial light sources or solar irradiation. A number of literature examples are presented below (Table 1.6 and Figures 1.5 to 1.12):

Table 1.6: TiO$_2$ photocatalytic reactors for water purification.

Configuration of TiO$_2$	Reactor Description	Operation Mode	Light Source	Reference
Immobilized (fiber glass)	Annular (Flow)	Recirculation	Low-pressure Mercury lamp	Ireland et al., 1993
Immobilized (quartz sand)	Fluidized Bed (Flow)	Recirculation	Medium-pressure Mercury lamp	Haarstrick et al., 1996
Immobilized (polyethylene)	Batch reactor	Not applicable	Solar irradiation	Naskar et al., 1998
Immobilized (optical fibers)	Batch reactor	Not applicable	Xenon Arc UV lamp	Peill et al., 1998
Immobilized (glass sheet)	Falling Film (Flow)	Recirculation	Fluorescent UV lamps	Sclafani et al., 1999
Slurry-phase	Immersion (Flow)	Recirculation	Medium pressure Mercury lamps	Braun et al., 1993
Slurry-phase	Parabolic Trough (flow)	Recirculation	Solar irradiation	Matthews, 1986
Slurry-phase	Laminar Falling Film (Flow)	Recirculation	UV-A and UV-C Mercury lamps	Puma et al., 1999
Slurry-phase	Batch reactor	Not applicable	High-pressure Mercury lamp	Crittenden et al., 1997
Slurry-phase	Annular (Taylor Vortex)	Single Pass & Recirculation	Fluorescent UV lamps	Sczechowski et al., 1995
Slurry-phase	Parabolic Trough (flow)	Recirculation	Solar irradiation	Zhang et al., 1994
Immobilized (glass sheet)	Laminar Falling Film (flow)	Single Pass & Recirculation	Solar irradiation	Freudenhammer et al., 1997
Slurry-phase (double skin sheet)	Turbulent Falling Film	Recirculation	Solar irradiation	Goslich et al., 1997
Slurry-phase	Immersion (batch)	Not applicable	Fluorescent UV lamps	Kuo and Lo, 1997
Immobilized (dune sand)	Batch (flow-through)	Recirculation	Solar irradiation	Matthews, 1991

26

Schematics of selected examples of PCO reactors:
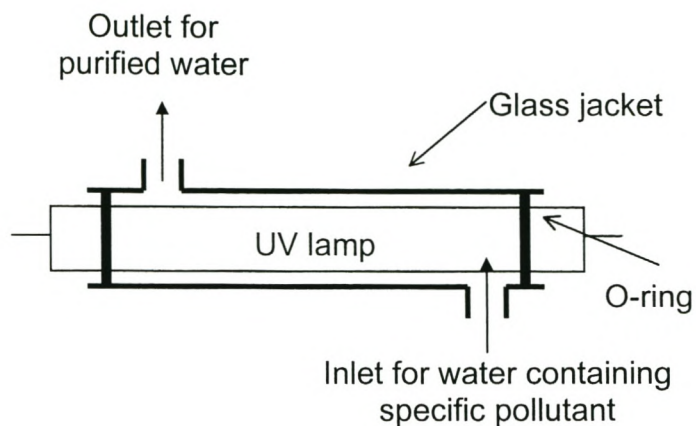
Figure 1.5: Conventional annular reactor (Matthews and McEvoy, 1992; Cloete, 1999)
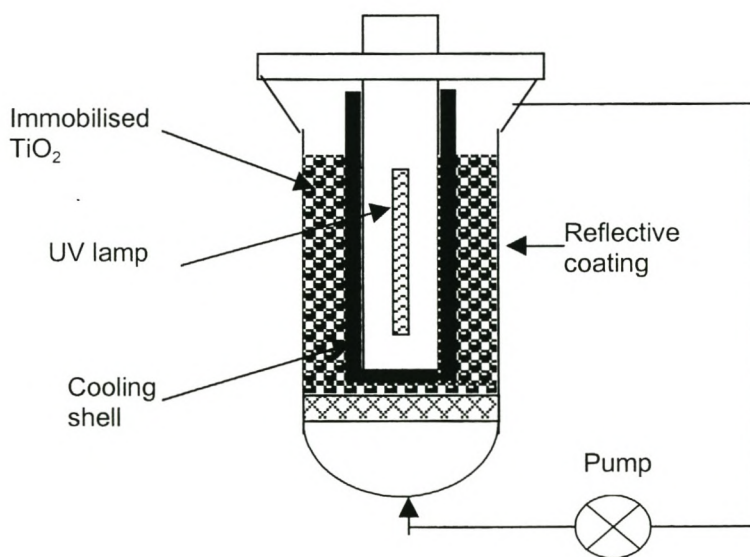
Figure 1.6: Immobilized-bed reactor (Haarstrick et al., 1996)

27
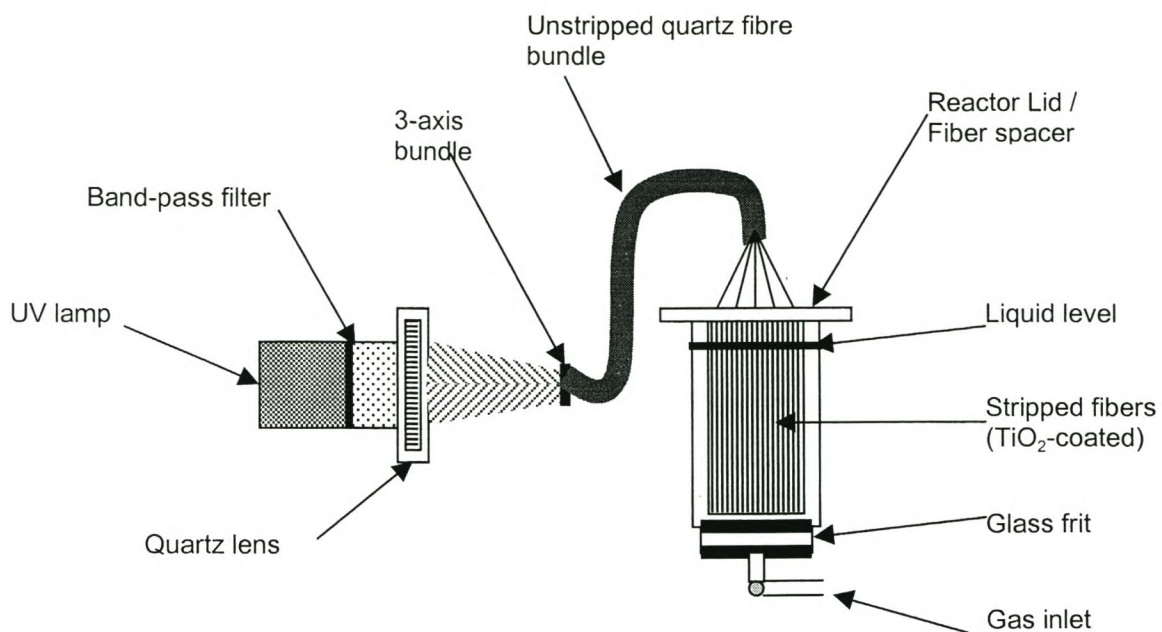
Figure 1.7: Fiber optic cable reactor (Peill and Hoffmann, 1998)
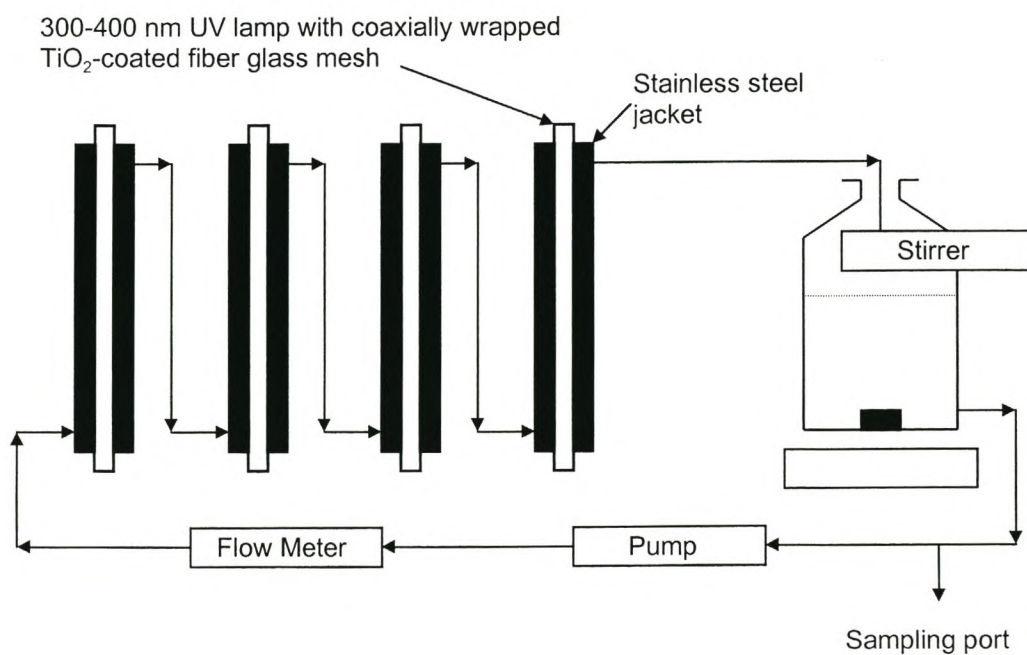
Figure 1.8: Direct contact flow-through reactor: Immobilized-bed and slurry-phase (Ireland et al., 1993)

28
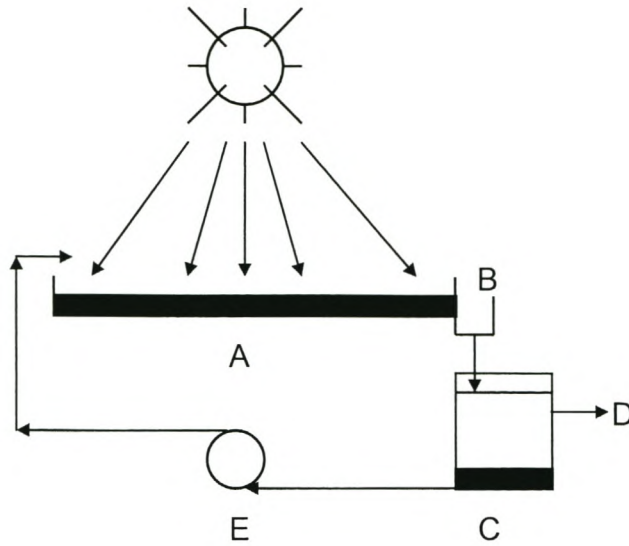
Figure 1.9: A solar-illuminated suspension pond reactor. (At sunset the suspension in lagoon A is dispensed via pumping-trough B into an underground settling tank C. The suspension settles overnight and the clear water phase is pumped off through D. The settled suspension is be pumped back to the lagoon near sunrise, via a pump E, together with untreated water.) (Matthews, 1993)
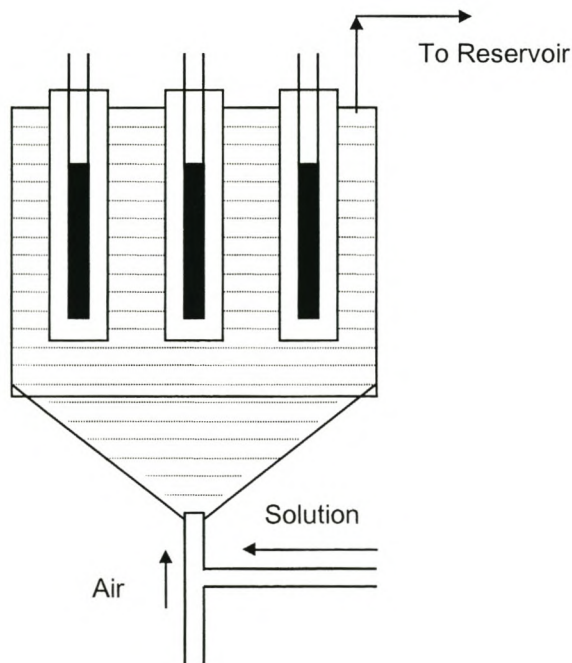
Figure 1.10: Multilamp immersion-type reactor (Braun *et al.*, 1993; Braun *et al.*, 1993a)

29
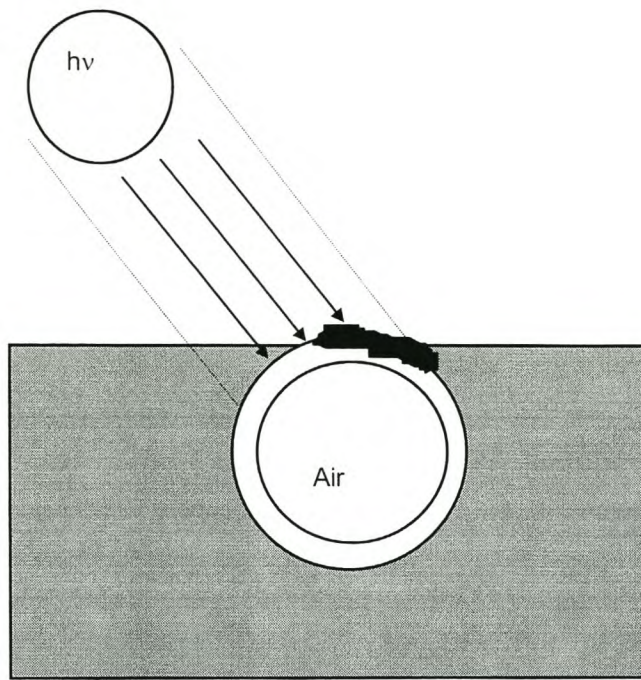
Figure 1.11: TiO$_2$ immobilized on glass micro beads (Jackson *et al.*, 1991)
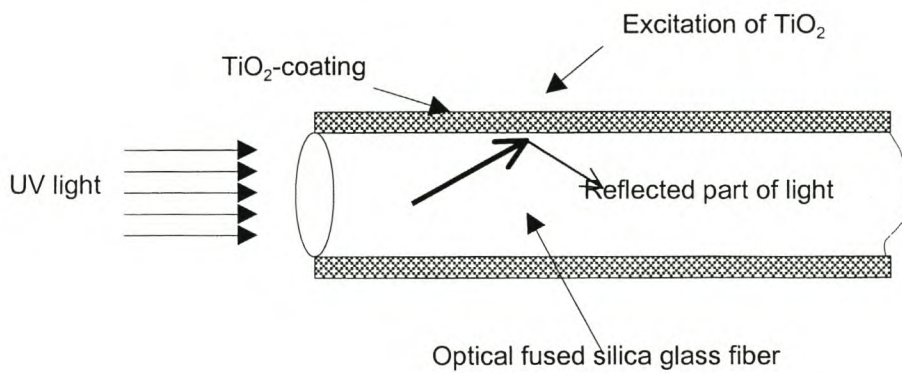
Figure 1.12: An optical fiber coated with TiO$_2$ (Hofstadler *et al.*, 1994)

(b)   Process Economics & Scale-up Potential

With respect to investigating the scaling-up of PCO reactors for treatment of polluted waters, a number of pilot-scale case studies have been completed, mostly in the United States, Canada and Germany. Cost calculations reported thus far have been variable and scaling-up projections were sensitive to the quality and volume of the untreated water. Comparisons are usually drawn with conventional treatments such as activated carbon adsorption and incineration. Rajeshwar (1996) projects a treatment cost of US$ 5.22 and 6.00 (per 1000 gallons) for UV photocatalysis and solar photocatalysis respectively. This amount compares favorably to granular activated carbon adsorption quoted at $ 6.20 (per 1000 gallons).

The cost to purify a small volume of highly contaminated water (e.g. 1000 L of wastewater containing 100 mg/L phenol) via UV photocatalysis has been projected to be in the vicinity of Aus$ 10. This calculation assumes 90 % mineralization of phenol and takes into account electrical power consumption (per kWh), lamp replacement and catalyst cost. Lamp maintenance and plant amortization were disregarded. If power were only to be consumed during off peak, costs would drop with approximately 50 %. The corresponding calculation when using granular activated carbon (GAC) amounted to Aus$ 6 taking disposal costs into account. The costs incurred in constructing a solar-based TiO_2 plant for treating 1 ML of water contaminated with 10 mg/L of phenol would amount to Aus$ 27500. Assuming 20 reuses of catalyst this amounts to Aus$ 1375/ML. Comparative GAC costs amounts to Aus$ 1000 (Matthews, 1993).

A more comprehensive calculation was conducted as part of an American Waterworks Association project on PCO (Hand *et al.*, 1993). Items such as catalyst cost, catalyst recovery, building materials, land and labour cost, lamp costs, lamp efficiency and life expectancy, electricity costs, contractor's profit, engineering administration costs and amortization periods were all incorporated. Solar PCO treatment proved to be the cheaper option, varying from US$ 0.48 per 1000 gallons for a 1 million-gallon per day (MGD) plant to US$ 0.25 for a 100 MGD plant. Corresponding costs for systems operated by artificial UV light amounted to a maximum of around US$ 1 per 1000 gallons for a 100 MGD plant with an average UV contact time of 60 minutes. GAC costs reported in their study ranged from US$ 0.14 to US$ 2.21 per 1000 gallons.

The National Renewable Energy Laboratory in the United States reported a cost of US$ 10.90 per 1000 gallons for a 100 000 gallons per day TiO_2 slurry PCO reactor operating as a solar trough system. Treatment costs are believed to be reduced considerably with the improvement in reactor designs and photocatalytic materials (Zhang *et al.*, 1994). Costs associated with the PCO degradation of benzene, toluene, ethylbenzene and xylenes (BTEX) in groundwater was reported to be around US$ 1.75 per 1000 gallons without pretreatment.

A British research group reported the following comparative costs (in US Dollars) for activated carbon, UV-ozone and PCO technologies in terms of various system sizes (Table 1.7) :

31

Table 1.7: Estimated process costs for different water purification technologies (Mills *et al.*, 1993a).

System size (MGD)	Carbon Adsorption	UV-Ozone Technology	UV-Photocatalytic Technology
0.029	$ 7.79	$13.00	$ 9.85
0.115	$ 4.25	$ 6.32	$ 4.36
0.23	$ 3.19	$ 4.92	$ 3.21
0.92	$ 2.21	$ 3.83	$ 2.32
2.44	$ 1.95	$ 3.10	$ 2.00

Trojan Technologies Inc., Matrix Photocatalytic Inc. and Purifics Environmental Technologies Inc. are three Canadian-based companies currently developing and marketing tailor-made UV and TiO_2 photocatalytic reactors for the treatment of contaminated groundwater, municipal wastewater and water for household purposes.

Trojan's reactors are mainly designed as multiple annular UV reactors assembled in modules or coupled in series. They have several systems on the market operating at a variety of flow rates ranging from 2-12 gallons per minute (GPM) for small point-of-use drinking water application, to several hundred MGD (for municipal wastewater disinfection). UV treatment in their systems occurs within 6-10 seconds in a flow-through channel in each segment of a module. Although Trojan specializes in disinfection of water by means of UV irradiation, they are also currently developing innovative PCO technology in collaboration with KSE Inc. in the United States.

Matrix Photocatalytic Inc. has commercialized and field-tested annular type PCO reactors as far back as 1992. Their system (reactor cell) comprises an outer stainless steel jacket containing an UV lamp covered with a multi-layered fiber glass sleeve coated with TiO_2. Modular systems have been developed for high flow rates with capacity increments of 5 GPM. Direct operating costs for raw effluent contaminated with organic compounds, mainly BTEX and MTBE, are reported to be between $1-2 per 1000 gallons, with an average treatment time of 60 seconds. Several other in-house treatability tests yielded operating costs around $0.5/m^3$ for aromatics in water and around $0.3/m^3$ for THMs in drinking water. Matrix Photocatalytic technology was also field-tested in the United States for groundwater remediation. A 60 GPM minute parallel mode reactor system was employed. Based on the results achieved, the PCO remediation costs were calculated to be much less compared to conventional groundwater remediation. For the treatment of 29 million gallons over a 2.5 year period at a flow rate of 24 GPM, the costs projected to US$ 50.76 per 1000 gallons. For the treatment of 341 million gallons over a 30 year period at the equivalent flow rate, the costs projected to US$ 28.41 per 1000 gallons (Al-Ekabi, 1999).

The reactors developed by Purifics Environmental Technologies Inc. are used to purify and detoxify a variety of waters ranging from ground water and surface waters to ultra-pure steam condensates. Claims are being made that their technology can remove BOD, COD and TOC to the desired level of purification, despite adverse conditions of turbidity, alkalinity or pH. A typical ground water treatment PCO reactor operate in excess of 10000 hours at flow rates of about 120 m^3/day, yielding operating costs of Can $ 0.37/m^3$.

PCO reactors are also currently being developed outside of North America, most notably in Japan, Germany, the Netherlands, Singapore, Italy, South Africa and Hong Kong, however it is not sure whether commercialization has been attained.

The task to develop and scale-up multi-phase photocatalytic reactors (particularly immobilized configurations) is significantly more complex than that of conventional homogeneous photochemical reactors. Factors to consider include (1) mixing (2) mass transfer (3) reaction kinetics (4) catalyst immobilization and (5) illuminated specific surface area. The latter is an engineering parameter describing the efficiency of immobilized PCO reactors in terms of the total illuminated surface area of catalyst within the reactor that is in contact with reaction liquid (Ray and Beenackers, 1998). PCO reactor engineering is a complicated discipline, involving multiple aspects. Most noteworthy are elements such as (1) photoreactor design (2) modeling of reaction kinetics and reactors (3) modeling of momentum, mass and thermal energy balances and (4) the determination of radiation field properties and emission models (Cassano *et al.*, 1995).

Other challenges relate to the practicality of reactor designs, optimal use of UV light sources and the development of efficient photocatalysts. The high degree of interaction between transport processes, reaction kinetics and light absorption leads to a strong coupling of physico-chemical phenomena, which complicates development via modeling (Ray and Beenackers, 1998). The notion of chemical reaction engineering is very much applicable to the entire field of PCO, ultimately spanning a development from atomic and molecular level (nanometer and femtosecond scale) to full-production level (Sapre and Katzer, 1995). Reactor modeling must be complemented by results obtained from statistical optimization of reactor and reaction parameters, starting at laboratory scale (Braun *et al.*, 1993a).

El-Akabi (1999) indicated that several barriers still hamper commercialization of PCO and AOTs. Scientific information gaps still exist to a large extent, together with a number of manufacturing, marketing and economic barriers.

A successful commercial reactor, in conclusion, would consist of a unique configuration of light source, photocatalyst and reactor material. Such an undertaking would inevitably require extensive collaboration between scientists, engineers and material specialists from a variety of backgrounds (Engelbrecht *et al.*, 2000).

1.3.6 Miscellaneous Aspects

(a)   PCO Light Sources

Most research in the PCO field is performed with commercially available light sources or by using solar illumination. The commercial lamps vary from monochromatic low-pressure mercury lamps (254 nm) to polychromatic irradiators such as medium pressure mercury arcs, Xe arc lamps, KrCl-excimer lasers and pulsed light sources (Mills and Le Hunte, 1997; Legrini *et al.*, 1993; Bolton, 1999; Bolton, 1999a; Unkroth *et al.*, 1997). In terms of the current state of light source technology, the nature and costs associated with these sources exerts little impact insofar as selecting a given AOT is concerned. This statement is based on the premise that the ability of the photochemical AOT to produce hydroxyl radicals should ideally not be influenced by pollutant's light absorption characteristics, which certainly holds true for TiO_2 based PCO processes.

The use of medium pressure Hg-arcs is advised for PCO work, and in some cases, the use of doped Hg-arcs may increase efficiency (Braun and Oliveros, 1997).

The measurement of light irradiance is based on the principle that the influent quanta be converted into a form that induces a change in a measuring device. In this regard, radiometers, semiconductor-based UV sensors and chemical actinometers are widely used to detect and quantify light (Bolton, 1999).

Radiant flux (ϕ) is an important parameter with respect to UV light sources and represents the light power invested as a function of the total light power emitted. PCO reaction rates normally exhibit a linear dependence on ϕ up to a threshold of approximately 250 W/m^2. A square root relationship ($\phi^{1/2}$) exists beyond this limit. Optimal light power utilization corresponds to the domain of linear dependence (Herrmann, 1995).

(b)   Photocatalytic Efficiency Parameters

Photocatalytic efficiency parameters (PEPs) constitute a group of response variables that are used as "figures-of-merit" for evaluating different photocatalytic reactions (and reactors) on equal footing. The need for PEPs arises from the fact that a standard framework of PCO conditions will be virtually impossible to construct, since each research group utilizes a unique combination of reaction conditions and photocatalytic reactor designs. For *AOTs (including PCO)* these parameters should be based on (1) electrical energy input (2) water volumes to be treated (3) volumetric flow rates (4) pollutant concentrations (5) level of purification required and (6) time of treatment.

To date, three useful electrical energy parameters have been devised for comparing the efficiency of AOTs in an industrial environment, i.e. (1) Electrical Energy per Order (EE/O) (2) Electrical Energy per unit Mass (EE/M) and (3) Energetic Efficiency of Degradation (EED)(Bolton *et al.*, 1996; Serpone, 1997).

EE/O is defined as the electrical energy in kWh required to effect the degradation of a pollutant by one order of magnitude in 1 m^3 (1000 L) of polluted water. EE/O values (in kWh per order per m^3) can be calculated according to eqn 1.43 (for batch systems) and eqn 1.44 (for flow systems). EE/O is best used in situations where pollutant concentrations are low, hence overall first order degradation kinetics apply.

EE/O (batch)   = P x t x 1000 / V x 60 x log (c_o / c_f)   (1.43)

EE/O (flow-through)   = P / F x log (c_o / c_f)   (1.44)

Where:
P = Lamp power (in kW)
V = Volume of water treated (in L)
t = Treatment time (in mins)
F = Volumetric water flow rate (in m^3/h)
c_o = Initial concentration
c_f = Final concentration
EE/O = kWh/order/m^3

Eqn 1.44 is designed for idealized plug-flow reactors, however reactor volumes and first order kinetics can be accounted for. EE/O can be calculated directly from kinetic rate constants, hence indirectly from UV contact times. In all cases, lower values of EE/O correspond to enhanced electrical efficiency and lower treatment costs. EE/O equations have also been suggested for idealized batch and continuously-stirred tank reactors (CSTRs) (Bolton *et al.*, 1996).

EE/M is defined as the electrical energy in kWh required to effect the degradation of a unit mass (one kilogram) of a pollutant suspended in contaminated water or air. EE/M is more useful when concentrations are high (viz: in zero order kinetic regimes). The general demarcation between "high" and "low" concentration varies considerably but is more often than not in the range of 100 mg/L (Bolton *et al.*, 1996).

$$EE/M = P \times t \times 1000 / V \times M \times 60 \times (c_o - c_f) \qquad (1.45)$$

Where:
P = Lamp power (in kW)
t = Treatment time (in mins)
V = Volume of water treated (in L)
M = Molecular weight of pollutant (in g/mole)
c_o = Initial concentration
c_f = Final concentration
EE/O = kWh/kg

EE/O and EE/M calculations can be directly related to electrical operating costs per unit volume or mass of pollutant, however a true estimation of the total costs will have to incorporate other factors such as (1) amortized investment (2) installation and maintenance costs and (3) chemicals.

In an environment where engineering efficiency is more useful, Braun and co-workers have suggested the use of the EED parameter (Serpone, 1997). EED relates to the concentration of organic carbon in a given solution volume irradiated per kWh of electrical energy utilized (ppm C.L.kWh^{-1}). More recently this parameter has been exchanged for its volume-corrected equivalent, viz: mgC per kWh. Conversely, Matthews and McEvoy (1992) utilized the amount of organic substrate (in ppm) per unit volume per kWh to express PCO reaction efficiency.

Apart from initial rate (r_0), rate constant (k) and normalized concentration (C/C_0) used as conventional kinetic parameters to evaluate PCO reactions, the following PEPs have also been suggested:

- Plots of substrate concentration (mol/L) versus energy consumed (kWh) (Braun and Oliveros, 1997)
- Plots of TOC and/or DOC (in ppm C) versus energy consumed (kWh) (Braun and Oliveros, 1997)
- Removal rate in terms of mass per area per time, e.g.: mmole/m^2/day (Dionysiou et al., 1999) and µmole/m^2/sec (Ray, 1999)
- Degradation rate in terms of percentage difference between initial and final substrate concentration (Castillo et al., 1997)
- Reduction rate constants (in mg/L/min) as a function of UV irradiance (in mW/cm^2) (Prairie et al., 1993)
- Expressing rates and concentrations as a function of UV dosages (Bolton, 1999a)
- PEP in terms of moles converted per unit time per unit reactor volume per unit electrical power consumed, viz: µmole/sec/m^3/W (Ray, 1999; Ray and Beenackers, 1998).

It is further suggested that published results should at least contain the following basic data (Braun and Oliveros, 1997):

- Results of analysis (in mg/L or equivalent units), including blank (control) experiments and equipment calibration data
- A detailed description of the light source (type, manufacturer, electrical power consumption)
- Total volume of water treated per experiment

The PEPs discussed herein are all useful in engineering and economical interpretations, however they do not afford a fundamental parameter that could establish photon efficiency (Serpone et al., 1996; Serpone, 1997). Serpone advised the use of "photonic efficiency" in heterogeneous photocatalysis, a term which is foreign to homogeneous photochemistry. This parameter is defined as the number of reactant molecules transformed (or product molecules created) divided by the number of photons, at a fixed wavelength, incident inside the front window of a reactor cell (flat parallel windows). In reporting such efficiencies, it is required to stipulate the reactor geometry and light source, as well as the properties of the photocatalyst. Recent developments in this area have seen the birth of a reactor-independent parameter, viz: "relative photonic efficiency". The photonic efficiency for the PCO of any unknown organic substrate can now be related to a set of standardized PCO conditions and reagents.

Furthermore, Serrano and De Lasa (1997) have used a "photochemical thermodynamic efficiency factor" (PTEF) to assess the energy efficiency with which photons may contribute to hydroxyl radical formation in TiO_2 mediated PCO reactions. PTEF is a dimensionless parameter and has to be calculated at high enough pollutant concentrations, viz: where zero-order kinetics prevail. The rationale behind this methodology is based on a gradual asymptotic increase of PTEF as a function of initial pollutant concentration. The upper limit of PTEF is a unique characteristic of the PCO reactor that blends together various reactor characteristics (e.g. illumination, catalyst light absorption, fluid dynamics and mass transfer) into a single thermodynamic efficiency factor.

It is important to note that PEPs (in general) may also apply to other AOTs.

(c)   Catalyst Modification Strategies

TiO_2 mediated PCO reactions often suffer from inherent low quantum efficiencies, viz: the amount of reactant molecules generated as a function of the amount of UV quanta absorbed by the catalyst are very small. Values ranging from 0.01 to 70% have been reported (Herrmann, 1995). TiO_2 particles can never absorb all the incident photon flux from a given source as the intensity of scattered light depends heavily on the ratio of the refractive indices of TiO_2 and the surrounding medium. The greater the difference in refractive indices, the greater the amount of scattering will be. Taking this fact into account, it seems likely that the number of photons adsorbable by TiO_2 could only reach a maximum of 60-65% in aqueous surroundings (Serpone et al., 1996).

One remedial strategy is to develop novel TiO_2 catalysts (superior in photo-efficiency) by applying surface pertubation methods. These methods inevitably modify the electronic nature of the catalyst. The primary objectives of this approach are to (1) increase energy ranges of excitation (2) inhibit electron and positive hole recombination (3) enhance interfacial electron transfer and (4) increase the spectral response of TiO_2 towards the visible light wavelength region (Fox and Dulay, 1993; Linsebigler et al., 1995). The application of these fundamental principles of photochemical transformation provides a rich area for both basic scientific research and technology development.

The main surface pertubation methods (with objectives achieved in parentheses) include:

- Chelation and covalent attachment, e.g. EDTA (objectives 1 and 3)
- Composite semiconductors, e.g. CdS-TiO_2 couples (objectives 1 and 2)
- Dye sensitization, e.g. erythrosin B and thionine (objectives 1 and 4)
- Transition metal doping, e.g. Fe^{3+} and Cu^{2+} (objectives 2 and 4)
- Co-deposition of PGMs or transition metals, e.g. Pt and Au (objective 3)

(d)   Electron Acceptors

The addition of electron acceptors presents another mechanism for increasing photocatalytic efficiency associated with TiO_2 mediated processes. These additives are generally required to (1) be effective scavengers of conduction band electrons (2) dissociate rapidly into innocuous products and (3) generate additional hydroxyl radicals (if possible).

Examples of electron acceptors include hydrogen peroxide, ammonium persulfate, potassium bromate and potassium peroxymonosulfate (oxone). Al-Ekabi et al. (1993) reported a marked improvement in the TiO_2 mediated PCO rate for 2,4-dichlorophenol by addition of ultra-low amounts of the above mentioned compounds. The reaction rates displayed the following trend : bromate > oxone > peroxide > persulfate > no additive. No co-dependence of additives was found. The examination also extended to the PCO of other organic substances where similar trends were observed.

(e) Controlled Periodic Illumination

Controlled periodic illumination (CPI) is a strategy that is believed to increase photo-efficiencies of PCO reactions markedly. The hypothesis states that CPI (a sequence of light-and-dark periods) counters the build-up of intermediates that may participate in unwanted redox side-reactions and electron-hole recombination during continuous illumination. Exposure of TiO_2 particles to UV light for short intervals generates a limited number of electron-hole pairs. When the particles are in the dark, the redox reactions leading to PCO of the target pollutants proceed until most of the radical intermediates are consumed. After the dark recovery period, illumination is resumed for a short interval and the cycle of light-and-dark periods continues (Sczechowski et al., 1993). Experimental validation of the CPI hypothesis has met with variable success depending on the phase of treatment and light intensity. Although a 500% increase in photoefficiency was reported for the PCO treatment of formate ions in aqueous media (Sczechowski et al., 1993), others have witnessed little to negligible effects (Buechler et al., 1999; Buechler et al., 1999a).

(f) Tandem Technologies

Apart from using PCO on its own for water purification, it has been suggested that the process be operated in tandem with other conventional treatment technologies in order to increase both capacity and efficiency. In this regard, conventional technologies such as granular activated carbon adsorption (Crittenden et al., 1997a), biological degradation (Li and Zhang, 1996) and WAO (Duffy et al., 1999) have been operated in tandem with PCO for the removal of organic compounds from water. The conventional treatment, in each case, functioned as the "workhorse", thus performing the bulk of the purification (viz: COD, color and TOC reduction). On the other hand, the PCO technology could also be introduced as a final polishing step or as a tool for the regeneration of spent adsorbents. It seems likely that successful commercial application of PCO related technologies may ultimately boil down to their utilization within tandem based systems.

(g) Photocatalytic Reduction

Photocatalytic reduction (PCR) reactions are less frequently encountered than PCO related ones. This is primarily ascribed to the fact that the reduction potential of the conduction band electron is significantly smaller in magnitude than the oxidation potential of the valence band hole (or equivalent hydroxyl radical). Moreover, most reducible substrates cannot compete kinetically with oxygen for trapping photogenerated conduction band electrons (Nieuwoudt, 1997). Many PCR reactions require the presence of a co-catalyst such as platinum and sacrificial reducing agents acting as a hole scavenger. PCR is mainly applied for the recovery of metal ions (such as PGMs) in their reduced metallic state through preferential deposition on catalytic surfaces (Kriek, 1998). It has also been used for the photochemical production of ammonia via nitrate (Li and Wasgestian, 1998) and methane via high pressure CO_2 (Kaneco et al., 1998).

(h)   General Applications

Although TiO_2 is primarily used as a PCO catalyst in environmental remediation strategies, the discipline of TiO_2 photocatalysis and TiO_2 (*per se*) have found application in several other academic, industrial and commercially related sectors, e.g. :

- Photo-electrocatalysis (Candal *et al.*, 1998)
- Organic photo-synthesis (Mills and Le Hunte, 1997)
- Oil spill clean-ups (Kriek, 1998; Grzechulska *et al.*, 2000)
- Self-cleaning devices and materials (Blake, 1999; Fujishima *et al.*, 1999)
- Super-hydrophilic materials (Fujishima *et al.*, 1999)
- TOC analysis (Bennett and Van der Merwe, 1995)
- Drinking-water disinfection (Richardson *et al.*, 1996; Hand *et al.*, 1995)
- Treatment of contaminated soils (Borrell-Damian and Ollis, 1999)
- Treatment of contaminated air from offices, military installations and hospitals (Blake 2000; Freihaut *et al.*, 1999)
- Deodorizing devices (Fujishima *et al.*, 1999)
- UV sunscreens using rutile TiO_2 (Kriek, 1998)
- Paint pigments (Kriek, 1998)
- Solar to chemical energy conversion (Bard, 1982; Kriek, 1998).

1.3.7   Global Research Needs

The economics and practical aspects of PCO technologies have been thoroughly addressed in 1.3.5. These elements generally extend to other AOT fields as well. Undoubtedly, future research and development (R&D) demands a multi-disciplined approach, spanning both fundamental and applied technology aspects. Al-Ekabi (1999) elegantly summarized the status quo of AOTs (including PCO) by listing a number of global research needs :

"Future R&D should aim at:

- *Understanding the radical and redox chemistry of AOTs*
- *Understanding, eliminating or inhibiting, to the greatest extent possible, the chemical and the physical processes that reduce the efficiencies of AOTs*
- *Optimizing operating parameters of AOTs*
- *Developing hybrid AOTs systems*
- *Conducting multi-discipline research projects involving engineers, chemists and biologists to improve AOTs performance*
- *Integrating AOTs with conventional treatment technologies*
- *Developing efficient, cheap and durable components for AOTs*
- *Modeling studies for scale-up and predicting AOTs performance*
- *Comparing the performance of various AOTs – Figures of Merit*
- *Identification of undesirable by-products*
- *Innovation in reactor design"*

39

In this work, a number of the above-mentioned R&D issues are addressed, as will be indicated in the project objectives (section 1.5).

1.4   OPTIMAL EXPERIMENTAL DESIGN

1.4.1 Key Rationale

One of the primary research needs in PCO and AOTs related processes is the parametric optimization of reaction and reactor experimental conditions (Al-Ekabi, 1999). The key rationale behind this is that, for any given photochemical process, the experimental conditions have to be optimized prior to deciding on a feasible route of technical development and up-scaling. Optimization should typically commence at laboratory scale and be repeated at pilot level where small-scale production activities may be implemented (Braun *et al.*, 1993a).

As discussed in this text, TiO_2 mediated PCO processes are very complex given the large number of experimental parameters that may possibly influence the efficiency. Moreover, it has been advised that the following parameters and methodologies be considered during optimization procedures, using a small group of well-chosen model substrates (Braun and Oliveros, 1997):

- Spectral distribution of emitted light sources
- Light source surface
- Temperature control of the light source
- Irradiation geometry
- Power supply and electrical power of light source
- Volume capacity of the reactor
- Total volume of water treated
- Water flow rates
- Mode of air or oxygen supply
- Temperature control of the reaction system
- Quantitative details on the elements of the reaction system
- Adsorption spectrum of the reaction mixture at zero time
- Detailed description of mode of catalyst addition
- Details of analytical methodologies used
- Results furnished in applicable concentration units
- Details on control experiments and equipment calibration

Certain parameters mentioned above may be fixed randomly based on commercial availability of equipment or economic motivations, however a multi-parameter optimization methodology constitutes the only feasible strategy for evaluating the effects of all parameters within a reasonable timeframe. In this regard, the methodology of optimal experimental design (OED) has been proposed as statistical optimization strategy for PCO related technologies (Braun *et al.*, 1993a; Jakob *et al.*, 1993a).

1.4.2 Fundamentals

Although comprehensive mechanistic, kinetic and radiation data may be available for PCO related technologies examined in laboratory-scale experiments, it remains essential to ascertain the individual and combined influences of the different experimental parameters in an effort to predict optimal processing conditions at technical levels (e.g. full production scale). The complexity of this exercise increases appreciably when (1) a large number of parameters may significantly affect the process and (2) parameters are not intrinsically independent (viz: display significant interaction effects) (Jakob *et al.*, 1993a).

The conventional method of experimentation, i.e. one-factor-variation (OFV), entails adjusting the treatment level of only one parameter at any given time, while maintaining all other parameters at fixed levels. OFV is often completely inappropriate for multi-parameter investigations due to the (1) unreasonable and unrealizable amount of experiments required (2) erroneous location of "bogus" optima and (3) random selection of experimental settings, thus spanning only localized portions of the experimental region. Probably the greatest drawback of OFV is its inability to detect mutual interaction effects, thereby failing to indicate the significance of each parameter in the presence of others (Braun *et al.*, 1993a).

In contrast, OED affords a series of strategically planned experiments at well-defined settings for each parameter, thereby facilitating the extraction of scientifically and statistically meaningful data in the minimum number of trials and at the minimum cost and effort. As an efficient experimental methodology, OED is expressly designed to (1) reach objectives promptly (2) eliminate meaningless experiments (3) provide the highest possible statistical accuracy (4) facilitate data analysis and (5) accommodate optimization and modeling. As prerequisite to constructing the OED program of choice, the following tasks need to executed (Braun *et al.*, 1993a):

1. Define the research objective(s)
2. Identify and define the response parameters of interest
3. List all experimental parameters (both quantitative and qualitative) that may potentially influence the responses
4. Define the experimental region of interest by locating all physical and instrumental boundary conditions for the listed parameters
5. Check system reproducibility.

The basic strategy for operating an OED comprises three distinct phases, viz: (1) screening (2) optimization and (3) verification. Screening experiments typically incorporate a large number of parameters in the early stages of the investigation when knowledge about the system is still imprecise. The primary objective is to narrow the focus of the problem by identifying and eliminating the parameters of inferior significance (often referred to as "noise factors"). Optimization is used at the end of an investigation to construct predictive mathematical models with the aid of statistical designs. This is done to acquire specific settings for the significant parameters in optimal experimental regions. Verification at the predicted optima concludes the OED function. A schematic portrayal of a typical OED is presented in Figure 1.13 (Ghosh, 1990).
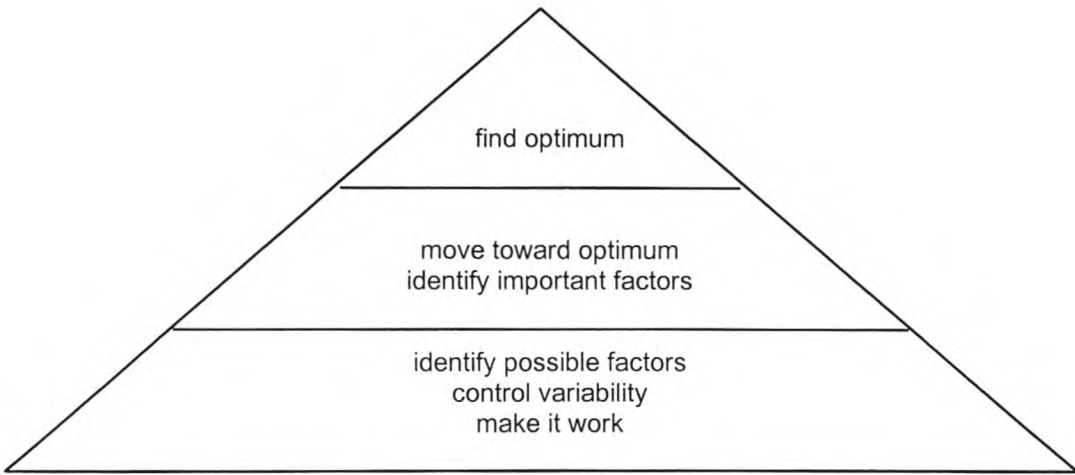
Figure 1.13: Typical OED pyramidal structure indicating the systematic acquisition of knowledge.

Mathematical modeling associated with OED studies is usually empirical due to the complex nature of the PCO process. The model is constructed and validated with the aid of conventional or user-specified statistical designs that indicate the response behavior of the experimental parameters in the region of interest. The associated response function (Y) is represented by a quadratic model (eqn 1.43) to compensate for interaction effects, or by a corresponding linear model (eqn 1.44) when parameter main effects dominate.

$$Y = b_0 + \sum_{i=1}^{k} b_i X_i + \sum_{i=1}^{k} b_{ii} X_i^2 + \sum_{i=1}^{k-1} \sum_{j=2}^{k} b_{ij} X_i X_j \qquad (1.43)$$

$$Y = b_0 + \sum_{i=1}^{k} b_i X_i \qquad (1.44)$$

Where: $j > i$, k is the number of parameters studied, b_0 is the average value of the experimental responses, b_i is the main effect of parameter X_i , b_{ii} is the quadratic effect of parameter X_i , and b_{ij} is the first order interaction between X_i and X_j (Braun *et al.*, 1993a; Benoit-Marquié *et al.*, 1997).

OED has witnessed a gradual development since the early 20th century. In this regard, a large number of conventional statistical designs are now available to assist mathematical modeling. These designs can also be adapted to address various types of problems, in which case they are referred to as user-specified designs (Montgomery, 2000).

OED research is invariably accompanied by graphic representation of results in two or three-dimensional format. The drawing of contour plots (lines or curves connecting areas of constant response) and response surfaces (depicting the behavior of responses in the presence of two parameters) have formed the basis of what is referred to as response surface methodology (RSM).

RSM offers a set of methods for quantifying the relationship between the experimental parameters and the responses presumed to be influenced by level-changes in these parameters. Although, response surface designs are primarily associated with optimization experiments, they could potentially act as screening designs in cases where a relatively small amount of parameters are investigated. In these circumstances (usually as a result of reduced design resolution) the screening design will only be able to evaluate parameter main effects accurately. It is important to note that the accuracy of predictions flowing from RSM does not depend on the experimental results *per se*, but is very much governed by both experimental error and the structure of the design matrix of choice (Braun *et al.*, 1993a). In this regard, the mathematical equations mentioned above (eqns 1.43 and 1.44) usually include an error function as final summation term. Fortunately, the statistical nature of OED ensures that systematic error (bias) is minimized through techniques such as randomization, replication and blocking (Chatfield, 1978).

In view of the fact that it is not the author's intention to arduously copy detailed OED theory into this text, the reader is referred to the following textbooks for comprehensive reading about the fundamentals and applications of OED, including all elements pertaining to RSM:

"Statistics for Experimenters" (Box *et al.*, 1978)
"Statistics for Analytical Chemistry" (Miller and Miller, 1984)
"Empirical Model-building and Response Surfaces" (Box and Draper, 1987)
"Statistical design and Analysis of Experiments" (Mason *et al.*, 1989)
"Statistical design and Analysis of Industrial Experiments" (Ghosh, 1990)
"Chemometrics: Experimental Design" (Morgan, 1991)
"Statistical Quality Design and Control" (De Vor *et al.*, 1992)

Table 1.8 provides a summary of the most notable screening and response surface designs used today. The demarcation between "screening" and "optimization" is not cast in stone, since several designs might be applicable to both instances.

Table 1.8: Common statistical designs used in RSM.

Screenings Designs	Response Surface Designs
2-level Factorial designs	Central Composite designs
3-level Factorial designs	Doehlert Arrays
Fractional Factorial designs	Box-Behnken designs
Plackett-Burmann (or Hadamard) matrices	Hybrid designs (e.g D-optimal)
Orthogonal Arrays	Designs for constrained surfaces
Block designs (e.g. Latin squares)	User specified designs
Square Matrices (n x n)	
User specified designs	

The use of statistical designs should be accompanied by appropriate significance tests contained within analysis of variance (ANOVA) techniques. Most contemporary OED software packages include standard ANOVA calculations as part of their function.

1.4.3 Applications

To date, very little effort has been made to approach TiO_2 based PCO research in statistical OED format. Researchers in Germany, France and South Africa are about the only ones known to have applied such methods (Braun *et al.*, 1993a; Jakob *et al.*, 1993a; Benoit-Marquié *et al.*, 1997; Cloete, 1999). Other AOTs (e.g. photo-Fenton) have also received limited attention in this regard (Oliveros *et al.*, 1997; Balanosky and Kiwi, 1998). Certainly, part of the problem lies with the fact that OED theory is not frequently taught at institutions of higher learning, especially in scientific courses. Hence, the existence of these techniques is often unknown to researchers (Montgomery, 2000).

OED and RSM have also found application in a diverse array of physical and industrial sciences. The most noteworthy fields of application include (1) analytical chemistry (chemometrics) (2) food, biological and clinical sciences and (3) social and economic sciences (Lavine, 1998; Myers *et al.*, 1989).

1.4.4 Complementary Methods

In addition to OED methods, a wide variety of mathematical and statistical methods exhibit potential for modeling and optimization of PCO processes. These methods mainly function as prediction tools and are fundamentally based on simulation strategies. Though not part of this study, it is important to make mention of their existence. Some selected examples include:

- Simplex optimization (Miller and Miller, 1984; Deming and Morgan, 1973)
- Gradient optimization, e.g. methods of steepest ascent/descent (Mason *et al.*, 1989)
- Artificial neural networks (Jakob *et al.*, 1993a)
- Monte Carlo simulations (simulated annealing) (Van Laarhoven and Aarts, 1987)
- Matrix algebra (Morgan, 1991)
- Multiple regression analysis (Mason *et al.*, 1989)
- Quantitative structure-activity relationships, or QSAR (Brasquet *et al.*, 1999)

As far as could be ascertained for TiO_2 based PCO processes, only artificial neural networks have been used as mathematical supplement to OED. (Braun *et al.*, 1993a). It has, however, been suggested that Monte Carlo simulations be used for modeling of absorption and scattering phenomena in typical heterogeneous TiO_2 PCO reactors (Yue, 1993).

1.5   PROJECT MOTIVATION & OBJECTIVES

In order to render TiO_2 based PCO technologies competitive against conventional water treatment processes, the need exists to develop innovative reactor designs capable of being scaled-up successfully. Such an exercise is very complex due to its multi-disciplined nature. It ultimately entails four distinct phases of development, i.e. (1) statistical optimization of reactor and reaction parameters (2) comprehensive reactor modeling (3) real-life operational trials, and (4) commercialization.

- *It is the primary objective of this work is to develop and expand the current knowledge base of phase 1 by evaluating two novel designs of TiO_2 PCO reactors via the optimal experimental design route. The intention is to identify and evaluate the significance magnitude of parameter main effects and interactions via OED screening designs, and to fine-tune optimum conditions via RSM designs. Moreover, the applicability of the Pareto Principle will be investigated in view of a large number of parameters at play.*

The experimental reactors used in this work are based on the falling film principle and will be evaluated in three separate flow system modes for the photocatalytic removal of two model organic pollutants, i.e. *para*-Chlorophenol (a typical industrial water pollutant) and four variants of cyanobacterial microcystin toxins (a typical domestic water pollutant).

- *As secondary objective, it is envisaged to evaluate and furnish several key process and photocatalytic efficiency parameters (PEPs) associated with the reactors in question, so as to facilitate global rating of the designs. These design parameters include e.g. catalyst loading (in suspension and immobilized), volumetric flow rate, horizontal distance of irradiation, reaction volume, solution and slurry pH, initial pollutant concentration, gas purge rate and UV irradiance.*

In terms of the *global requirements* for AOT related research (as mentioned earlier), this work will address (1) optimization of operating parameters (explained above) (2) development of hybrid systems and integrating AOTs with conventional treatment (through deposition of TiO_2 on sheets of fibrous activated carbon) (3) multi-disciplined research (in collaboration with Medical Research Council of South Africa) (4) development of cheap, efficient and durable components for AOTs (through the choice of reactor materials) (5) modeling and scale-up studies (through kinetic and statistical modeling, and choice of operational mode) (6) global rating via figures-of-merit (through use of PEPs e.g. EE/O and UV dosage response curves) (7) innovation in reactor design (through the unique choice of falling film designs).

The treatment of raw drinking water containing industrial pollutants, cyanobacterial microcystin toxins and natural organic matter (NOM) is of considerable relevance to the South African context of the provision of safe drinking water. This work is intimately related to the quest for innovative technologies to combat the country's pollution problem in the long term.

CHAPTER 1 - REFERENCES

AL-EKABI H (1999) Advanced oxidation technologies: Fundamentals and environmental applications. In: *Proceedings of Workshop on Advanced Oxidation Technologies*, Albuquerque, New Mexico, USA. 1-19.

AL-EKABI H (2000) Final programs of the AOTs-6 and TiO_2-5 conferences. Venue: London, Ontario, Canada. Conference date: June 25-30, 2000. *Internet page downloaded at* http://www.aotsconference.com/programs.htm (Download date: June 20th 2000)

AL-EKABI H, BUTTERS B, DELANY D, IRELAND J, LEWIS N, POWELL T and STORY J (1993) TiO_2 advanced photo-oxidation technology: Effect of electron acceptors. In: *Photocatalytic Purification and Treatment of Water and Air*, Ollis DF and Al-Ekabi H (eds.), Elsevier Science Publishers B.V., Amsterdam, The Netherlands. 321-336.

ARSLAN I, BALCIOGLU IA and TUHKANEN T (1999) Advanced oxidation of simulated dyehouse wastewater by UV/H_2O_2, UV/Fenton and O_3/H_2O_2 processes: Comparison of treatment performances and reaction kinetics. In: *Proceedings of The 5th International Conference on Advanced Oxidation Technologies for Water and Air Remediation*, Albuquerque, New Mexico, USA. 122.

BACKA S, JANSBO K and REITBERGER T (1997) Detection of hydroxyl radicals by a chemiluminescence method – A critical review. *Holzforschung* **51** 557-564.

BALANOSKY E and KIWI J (1998) Mathematical modeling of the photochemical reactor degradation of *p*-Nitrotoluenesulfonate. *Ind. Eng. Chem. Res.* **37** 347-356.

BANDARA J, MORRISON C, KIWI J, PULGARIN C and PERINGER P (1996) Degradation/decoloration of concentrated solutions of Orange II. Kinetics and quantum yield for sunlight induced reactions via Fenton type reagents. *J. Photochem. Photobiol. A: Chem.* **99** 57-66.

BARBIER PF and PETRIER C (1996) Study at 20 kHz and 500 kHz of the ultrasound-ozone advanced oxidation system: 4-Nitrophenol degradation. *J. Adv. Oxid. Technol.* **1** 154-159.

BARD AJ (1982) Design of semiconductor photoelectrochemical systems for solar energy conversion. *J. Phys. Chem.* **86** 172-177.

BEKBOLET M (1996) Destructive removal of humic acids in aqueous media by photocatalytic oxidation with illuminated titanium dioxide. *J. Environ. Sci. Health* **A31(4)** 845-858.

BENNETT PA and VAN DER MERWE J (1995) Photocatalytic oxidation – a safe and clean alternative in TOC analysis. *Water Sewage & Effluent* **15** 7-9.

BENOIT-MARQUIE F, PUECH-COSTES E, BRAUN AM, OLIVEROS E and MAURETTE MT (1997) Photocatalytic degradation of 2,4-dihydroxybenzoic acid in water: efficiency optimization and mechanistic investigations. *J. Photochem. Photobiol. A: Chem.* **108** 65-71.

BIRCHER KG, LEM W, SIMMS KM and DUSSERT BW (1997) Combination of UV oxidation with other treatment technologies for the remediation of contaminated water. *J. Adv. Oxid. Technol.* **2** 435-441.

BLAKE DM (1999) *Bibliography of work on the photocatalytic removal of hazardous compounds from water and air (update number 3 to January 1999).* NREL report no- NREL/TP-570-26797, National Renewable Energy Laboratory, Golden, CO, USA. Available from National Technical Information Service, Springfield, VA 22161, USA.

BLAKE DM (2000) *Personal Communication.* National Renewable Energy Laboratory, Golden, CO, USA.

BLAKE DM, MANESS PC, HUANG Z, WOLFRUM E, JACOBY WA and HUANG J (1999) Application of the photocatalytic chemistry of titanium dioxide to disinfection and the killing of cancer cells. *Separation and Purification Methods* **28** 1-50.

BOLTON JR (1999) *Ultraviolet Applications Handbook.* Available from Bolton Photosciences Inc., Ayr, Ontario, Canada (ISBN 0-9685432-0-0).

BOLTON JR (1999a) UV-disinfection of drinking water: Low-pressure, medium-pressure and pulse lamps. In: *Proceedings of Workshop on Advanced Oxidation Technologies*, Albuquerque, New Mexico, USA. 35-44.

BOLTON JR, BIRCHER KG, TUMAS W and TOLMAN CA (1996) Figures-of-merit for the technical development and application of advanced oxidation processes. *J. Adv. Oxid. Technol.* **1** 13-17.

BOLTON JR, VALLADARES JE, ZANIN JP, COOPER WJ, NICKELSON MG, KAJDI DC, WAITE TD and KURUCZ CN (1998) Figures-of-merit for advanced oxidation technologies: A comparison of homogeneous UV/H_2O_2, heterogeneous UV/TiO_2 and electron beam processes. *J. Adv. Oxid. Technol.* **3** 174-181.

BORRELL-DAMIAN L and OLLIS DF (1999) Sequential extraction and photocatalytic recovery of lead from model contaminated soils. In: *Proceedings of The 4th International Conference on TiO_2 Photocatalytic Purification and Treatment of Water and Air*, Albuquerque, New Mexico, USA. 89.

BOX GEP and DRAPER NR (eds.) (1987) *Empirical model-building and response surfaces.* Wiley, New York, USA.

BOX GEP, HUNTER WG and HUNTER JS (eds.) (1978) *Statistics for experimenters.* Wiley, New York, USA.

BRASQUET C, BOURGES B and LE CLOIREC P (1999) Quantitative structure-property relationship (QSPR) for the adsorption of organic compounds onto activated carbon cloth: Comparison between multiple linear regression and neural network. *Environ. Sci. Technol.* **33** 4226-4231.

BRAUN AM, JAKOB L and OLIVEROS E (1993) Advanced oxidation processes – concepts of reactor design. *Aqua* **42** 166-173.

BRAUN AM, JAKOB L, OLIVEROS E and DO NASCIMENTO CAO (1993a) Up-scaling photochemical reactions. In: *Advances in Photochemistry - Volume 18*, Volman DH, Hammond GS and Neckers DC (eds.), John Wiley & Sons Inc., New York, USA. 235-313.

BRAUN AM and OLIVEROS E (1997) How to evaluate photochemical methods for water treatment. *Wat. Sci. Tech.* **35** 17-23.

BRENNECKE JF (1996) New applications of supercritical fluids. *Chemistry & Industry* **4 November** 831-834.

BUECHLER KJ, NAM CH, ZAWISTOWSKI TM, NOBLE RD and KOVAL CA (1999) Design and evaluation of a novel controlled periodic illumination reactor to study photocatalysis. *Ind. Eng. Chem. Res.* **38** 1258-1263.

BUECHLER KJ, NOBLE RD, KOVAL CA and JACOBY WA (1999a) Investigation of the effects of controlled periodic illumination on the oxidation of gaseous trichloroethylene using a thin film of TiO_2. *Ind. Eng. Chem. Res.* **38** 892-896.

BUXTON GV, GREENSTOCK CL, HELMAN WP and ROSS AB (1988) Critical review of rate constants for reactions of hydrated electrons, hydrogen atoms and hydroxyl radicals in aqueous solution. *J. Physic. Chem. Ref. Data* **17** 513-886.

CANDAL RJ, ZELTNER WA and ANDERSON MA (1998) TiO_2-mediated photoelectrocatalytic purification of water. *J. Adv. Oxid. Technol.* **3** 270-276.

CASSANO AE, MARTIN CA, BRANDI RJ and ALFANO OM (1995) Photoreactor analysis and design: Fundamentals and applications. *Ind. Eng. Chem. Res.* **34** 2155-2201.

CASTILLO L, EL KHORASSANI H, TREBUCHON P and THOMAS O (1997) UV treatability test for chemical and petrochemical wastewater. In: *Proceedings of the International Association on Water Quality (IAWQ) Specialized Conference on Chemical Process Industries and Environmental Management*, Cape Town, South Africa, Paper P.1.4.

CHATFIELD C (1978) *Statistics for technology: A course in applied statistics* (2nd edition). John Wiley & Sons, New York USA. 225.

CHMIELEWSKI AG, ZIMEK Z, BULKA S, LICKI J, PIDERIT G, VILLANUEVA L and AHUMADA L (1996) Electron beam treatment of flue gas with high content of SO_2. *J. Adv. Oxid. Technol.* **1** 142-149.

CLOETE V (1999) Methods for establishing the efficiency of the photocatalytic destruction of humic substances in drinking water. *M.Sc. (Chemistry) Thesis, University of Stellenbosch, South Africa.*

COOPER W (1999) The electron beam process as an advanced oxidation process. In: *Proceedings of Workshop on Advanced Oxidation Technologies*, Albuquerque, New Mexico, USA. 45-67.

CORTES S, ORMAD P, SARASA J, GRACIA R and OVELLEIRO JL (1999) Study of the catalytic ozonation of organochloride compounds in water. In: *Proceedings of The 5th International Conference on Advanced Oxidation Technologies for Water and Air Remediation*, Albuquerque, New Mexico, USA. 106-107.

CRITTENDEN JC, LIU J, HAND DW and PERRAM DL (1997) Photocatalytic oxidation of chlorinated hydrocarbons in water. *Wat. Res.* **31** 429-438.

CRITTENDEN JC, SURI RPS, PERRAM DL and HAND DW (1997) Decontamination of water using adsorption and photocatalysis. *Wat. Res.* **31** 411-418.

DEBELLEFONTAINE H, CAMMAS FX, DEIBER G, FOUSSARD JN and REILHAC P (1997) Wet air oxidation: Kinetics of reaction, carbon dioxide equilibrium and reactor design – an overview. *Wat. Sci. Tech.* **35** 111-118.

DEMING SN and MORGAN SL (1973) Simplex optimization of variables in analytical chemistry. *Anal. Chem.* **45** 278A-283A.

DE VOR RE, CHANG T and SUTHERLAND JW (eds.) (1992) *Statistical quality design and control*. Maxwell Macmillan Publishers, New York, USA.

DIAZ ME and LAW SE (1999) UV-enhanced ozonation for treatment of food process wastewaters for recycling. In: *Proceedings of The 5th International Conference on Advanced Oxidation Technologies for Water and Air Remediation*, Albuquerque, New Mexico, USA. 51-52.

DIONYSIOU DD, KERN AM, KHODADOUST AP, SUIDAN MT, BAUDIN I and LAINE JM (1999) Rotating disk photocatalytic reactor (RDPR): Continuous flow operation for the degradation of phenol, chlorinated phenols and lindane in water. In: *Proceedings of The 4th International Conference on TiO₂ Photocatalytic Purification and Treatment of Water and Air*, Albuquerque, New Mexico, USA. 120-121.

DOONG RA and CHANG WH (1997) Photoassisted titanium dioxide mediated degradation of organophosphorus pesticides by hydrogen peroxide. *J. Photochem. Photobiol. A: Chem.* **107** 239-244.

DUFFY JE, ANDERSON MA, HILL CG and ZELTNER WA (1999) Photocatalytic oxidation as a secondary treatment method following wet air oxidation. In: *Proceedings of The 4th International Conference on TiO₂ Photocatalytic Purification and Treatment of Water and Air*, Albuquerque, New Mexico, USA. 128.

EGGINS BR, PALMER FL and BYRNE JA (1997) Photocatalytic treatment of humic substances in drinking water. *Wat. Res.* **31** 1223-1226.

ENGELBRECHT WJ, DE VILLIERS D, STOCKENSTROM S, SHEPHARD GS, CLOETE V and WESSELS GFS (2000) Photocatalytic purification of drinking water. *Final Report to the Water Research Commission of South Africa (Project K5/834)*.

FALKENSTEIN Z (1997) Processing of C_3H_7OH, C_2HCl_3 and CCl_4 in flue gases using silent discharge plasmas (SDPs), enhanced by (V)UV at 172 nm and 253.7 nm. *J. Adv. Oxid. Technol.* **2** 223-238.

FASSLER D, FRANKE U, GUENTHER K, AURICH J and MEYER A (1999) UV-oxidation techniques with microwave excitation. In: *Proceedings of The 5th International Conference on Advanced Oxidation Technologies for Water and Air Remediation*, Albuquerque, New Mexico, USA. 47.

FAUST BC (1994) Photochemistry of clouds, fogs and aerosols. *Environ. Sci. Technol.* **28** 217A-222A.

FOX MA (1993) The role of hydroxyl radicals in the photocatalyzed detoxification of organic pollutants: Pulse radiolysis and time-resolved diffuse reflectance measurements. In: *Photocatalytic Purification and Treatment of Water and Air*, Ollis DF and Al-Ekabi H (eds.), Elsevier Science Publishers B.V., Amsterdam, The Netherlands. 163-167.

FOX MA and DULAY MT (1993) Heterogeneous photocatalysis. *Chem. Rev.* **93** 341-357.

FOX MA and DULAY MT (1996) Acceleration of secondary dark reactions of intermediates derived from adsorbed dyes on irradiated TiO_2 powders. *J. Photochem. Photobiol. A: Chem.* **98** 91-101.

FREESE SD, NOZIAC D, PRYOR MJ, TROLLIP DL and SMITH RA (1997) Comparison of ozone and hydrogen peroxide/ozone for the treatment of eutrophic water. In: *Proceedings of the International Association on Water Quality (IAWQ) Specialized Conference on Chemical Process Industries and Environmental Management*, Cape Town, South Africa, Paper P.10.9.

FREIHAUT JD, HALL RJ, HAY SO, HOLLICK HH, OBEE TN and SANGIOVANNI JJ (1999) The application of UV photocatalytic technology to HVAC building systems. In: *Proceedings of The 4th International Conference on TiO_2 Photocatalytic Purification and Treatment of Water and Air*, Albuquerque, New Mexico, USA. 130.

FREUDENHAMMER H, BAHNEMANN D, BOUSSELMI L, GEISSEN SU, GHRABI A, SALEH F, SI-SALAH A, SIEMON U and VOGELPOHL A (1997) Detoxification and recycling of wastewater by solar-catalytic treatment. *Wat. Sci. Tech.* **35** 149-156.

FUJISHIMA A, HASHIMOTO K and WATANABE T (1999) *TiO_2 Photocatalysis: Fundamentals and Applications.* BKC Inc., Tokyo, Japan (ISBN4-939051-03-X).

FUKUI S, HANASAKI Y and OGAWA S (1993) High-performance liquid chromatographic determination of methanesulphinic acid as a method for the determination of hydroxyl radicals. *J. Chromatogr.* **630** 187-193.

GALAL-GORCHEV H (1996) Chlorine in water disinfection. *Pure & Appl. Chem.* **68** 1731-1735.

GHOSH S (ed.) (1990) *Statistical design and analysis of industrial experiments.* Marcel Dekker, New York, USA.

GOSLICH R, DILLERT R and BAHNEMANN D (1997) Solar water treatment : Principles and reactors. *Wat. Sci. Tech.* **35** 137-148.

GRIBBLE GW (1996) The diversity of natural organochlorines in living organisms. *Pure & Appl. Chem.* **68** 1699-1712.

GRZECHULSKA J, HAMERSKI M and MORAWSKI AW (2000) Photocatalytic decomposition of oil in water. *Wat. Res.* **34** 1638-1644.

HAARSTRICK A, KUT OM and HEINZLE E (1996) TiO_2 assisted degradation of environmentally relevant organic compounds in wastewater using a novel fluidized bed photoreactor. *Environ. Sci. Technol.* **30** 817-824.

HAND DW, PERRAM DL and CRITTENDEN JC (1995) Destruction of DBP precursors with catalytic oxidation. *J. Am. Water Works Assoc.* **87** 84-96.

HAND DW, CRITTENDEN JC and PERRAM DL (1993) Destruction of DBP precursors using photo-assisted heterogeneous catalytic oxidation. *Final report to the AWWA Research Foundation, USA*. (ISBN 0-89867-655-X).

HASHEM TM, ZIRLEWAGEN M and BRAUN AM (1997) Simultaneous photochemical generation of ozone in the gas phase and photolysis of aqueous reaction systems using one VUV light source. *Wat. Sci. Tech.* **35** 41-48.

HERRMANN JM (1999) Heterogeneous photocatalysis: fundamentals and applications to the removal of various types of aqueous pollutants. *Catalysis Today* **53** 115-129.

HERRMANN JM (1995) Heterogeneous photocatalysis: an emerging discipline involving multiphase systems. *Catalysis Today* **24** 157-164.

HITCHMAN ML, SPACKMAN RA, ROSS NC and AGRA C (1995) Disposal methods for chlorinated aromatic waste. *Chem. Soc. Rev.* **24** 423-430.

HOFFMANN MR, MARTIN ST, CHOI W and BAHNEMANN DW (1995) Environmental applications of semiconductor photocatalysis. *Chem. Rev.* **95** 69-96.

HOFL C, SIGL G, SPECHT O, WURDACK I and WABNER D (1997) Oxidative degradation of AOX and COD by different advanced oxidation processes: A comparative study with two samples of a pharmaceutical wastewater. *Wat. Sci. Tech.* **35** 257-264.

HOFSTADLER K, BAUER R, NOVALIC S and HEISLER G (1994) New reactor design for photocatalytic wastewater treatment with TiO_2 immobilized on fused-silica glass fibers: Photomineralization of 4-Chlorophenol. *Environ. Sci. Technol.* **28** 670-674.

HOIGNE J (1997) Inter-calibration of OH radical sources and water quality parameters. *Wat. Sci. Tech.* **35** 1-8.

HOIGNE J and BADER H (1976) The role of hydroxyl radical reactions in ozonation processes in aqueous solutions. *Wat. Res.* **10** 377-386.

HUANG YH, CHOU S, PENG MG, HUANG GH and CHENG SS (1997) Case study on the bioeffluent of petrochemical wastewater by electro-Fenton method. In: *Proceedings of the International Association on Water Quality (IAWQ) Specialized Conference on Chemical Process Industries and Environmental Management*, Cape Town, South Africa, Paper P.6.6.

51

HUANG CR and SHU HY (1995) The reaction kinetics, decomposition pathways and intermediate formations of phenol in ozonation, UV/O_3 and UV/H_2O_2 processes. *J. Hazard. Mater.* **41** 47-64.

HUNG HM, COLUSSI AJ and HOFFMANN MR (1999) Kinetics of halogenated organic compounds degradation by ultrasound. In: *Proceedings of The 5th International Conference on Advanced Oxidation Technologies for Water and Air Remediation*, Albuquerque, New Mexico, USA. 41.

INCE NH, STEFAN MI and BOLTON JR (1997) UV/H_2O_2 degradation and toxicity reduction of textile azo dyes: Remazol Black-B, a case study. *J. Adv. Oxid. Technol.* **2** 442-448.

IRELAND JC, KLOSTERMANN P, RICE EW and CLARK RM (1993) Inactivation of *Escherichia coli* by titanium dioxide photocatalytic oxidation. *Appl. Environ. Microbiol.* **59** 1668-1670.

JACOBS EP, BOTES JP, BRADSHAW SM and SAAYMAN HM (1997) Ultrafiltration in potable water production. *Water SA* **23** 1-6.

JACKSON NB, WANG CM, LUO Z, SCHWITZGEBEL J, EKERDT JG, BROCK JR and HELLER A (1991) Attachment of TiO_2 powders to hollow glass microbeads. *J. Electrochem. Soc.* **138** 3660-3664.

JAKOB L, HASHEM TM, BURKI S, GUINDY NM and BRAUN AM (1993) Vacuum-ultraviolet (VUV) photolysis of water: oxidative degradation of 4-chlorophenol. *J. Photochem. Photobiol. A: Chem.* **75** 97-103.

JAKOB L, OLIVEROS E, LEGRINI O and BRAUN AM (1993a) TiO_2 photocatalytic treatment of water. Reactor design and optimization experiments. In: *Photocatalytic Purification and Treatment of Water and Air*, Ollis DF and Al-Ekabi H (eds.), Elsevier Science Publishers B.V., Amsterdam, The Netherlands. 511-532.

JEN JF, LEU MF and YANG TC (1998) Determination of hydroxyl radicals in an advanced oxidation process with salicylic acid trapping and liquid chromatography. *J. Chromatogr. A* **796** 283-288.

KANECO S, SHIMIZU Y, OHTA K and MIZUNO T (1998) Photocatalytic reduction of high pressure carbon dioxide using TiO_2 powders with a positive hole scavenger. *J. Photochem. Photobiol. A: Chem.* **115** 223-226.

KANG JW, HUNG HM, LIN A and HOFFMANN MR (1999) Sonolytic destruction of methyl *tert*-butyl ether by ultrasonic irradiation: The role of O_3, H_2O_2, frequency, and power density. *Environ. Sci. Technol.* **33** 3199-3205.

KRIEK RJ (1998) Separation of platinum group metals: Photocatalytic reduction and complexation equilibria of Pt(IV), Pd(II) and Rh(III). *Ph.D. (Chemistry) Thesis, University of Stellenbosch, South Africa.*

KRÜGER H (1991) Chemistry and our endangered environment (Introduction: The environmental crisis). *Spectrum* **29**$_2$ 17-19.

KRÜGER H (1992) Chemistry and our endangered environment. *Spectrum* **30**₄ 59-62.

KUO CY and LO SL (1997) Adsorption of aqueous 4-chlorobiphenyl and treatment with UV-illuminated titanium dioxide. *J. Colloid Interface Sci.* **196** 199-206.

LAVINE BK (1998) Chemometrics. *Anal. Chem.* **70** 209R-228R.

LEE MJ, JEOUNG YD, OH YS and KANG JW (1999) A study on the decomposition of non-biodegradable substances by using γ-rays. In: *Proceedings of The 5ᵗʰ International Conference on Advanced Oxidation Technologies for Water and Air Remediation*, Albuquerque, New Mexico, USA. 28-29.

LEGRINI O, OLIVEROS E and BRAUN AM (1993) Photochemical processes for water treatment. *Chem. Rev.* **93** 671-698.

LEI L, HU X, CHU HP, CHEN G and YUE PL (1997) Catalytic wet air oxidation of dyeing and printing wastewater. *Wat. Sci. Tech.* **34** 311-319.

LEI L, HU X, YUE PL, BOSSMANN SH, GOB S and BRAUN AM (1998) Oxidative degradation of polyvinyl alcohol by the photochemically enhanced Fenton reaction. *J. Photochem. Photobiol. A: Chem.* **116** 159-166.

LI Y and WASGESTIAN F (1998) Photocatalytic reduction of nitrate ions on TiO_2 by oxalic acid. *J. Photochem. Photobiol. A: Chem.* **112** 255-259.

LI XZ and ZHANG M (1996) Decolorization and biodegradability of dyeing wastewater treated by a TiO_2 sensitized photooxidation process. *Wat. Sci. Tech.* **34** 49-55.

LIAKOU S, PAVLOU S and LYBERATOS G (1997) Ozonation of azo dyes. *Wat. Sci. Tech.* **34** 279-286.

LIN KS and WANG HP (1999) Rate enhancement by cations in supercritical water oxidation of 2-chlorophenol. *Environ. Sci. Technol.* **33** 3278-3280.

LINSEBIGLER AL, LU G and YATES JT (1995) Photocatalysis on TiO_2 surfaces: Principles, mechanisms, and selected results. *Chem. Rev.* **95** 735-758.

LOGEMANN FP and ANNEE JHJ (1997) Water treatment with a fixed bed catalytic ozonation process. *Wat. Sci. Tech.* **34** 353-360.

LONG DE (1969) Simplex optimization of the response from chemical systems. *Anal. Chim. Acta* **46** 193-206.

LOPEZ A, MASCOLO G, TIRAVANTI G and PASSINO R (1997) Degradation of herbicides (Ametryn and Isoproturon) during water disinfection by means of two oxidants (hypochlorite and chlorine dioxide). *Wat. Sci. Tech.* **34** 129-136.

MA Z, ZHAO B and YUAN Z (1999) Application of electrochemical and spin trapping techniques in the investigation of hydroxyl radicals. *Anal. Chim. Acta* **389** 213-218.

53

MARTIN CA, ALFANO OM and CASSANO AE (1999) UV radiation + hydrogen peroxide decolorization of waters for domestic supply. In: *Proceedings of The 5th International Conference on Advanced Oxidation Technologies for Water and Air Remediation*, Albuquerque, New Mexico, USA. 3-4.

MASON RL, GUNST RF and HESS JL (eds.) (1989) *Statistical design and analysis of experiments*. John Wiley and Sons, New York, USA.

MATTHEWS RW (1986) Photo-oxidation of organic material in aqueous suspensions of titanium dioxide. *Wat. Res.* **20** 569-578.

MATTHEWS RW (1991) Photooxidative degradation of coloured organics in water using supported catalysts: TiO_2 on sand. *Wat. Res.* **25** 1169-1176.

MATTHEWS RW (1993) Photocatalysis in water purification: Possibilities, problems and prospects. In: *Photocatalytic Purification and Treatment of Water and Air*, Ollis DF and Al-Ekabi H (eds.), Elsevier Science Publishers B.V., Amsterdam, The Netherlands. 121-138.

MATTHEWS RW and McEVOY SR (1992) A comparison of 254 nm and 350 nm excitation of TiO_2 in simple photocatalytic reactors. *J. Photochem. Photobiol. A: Chem.* **66** 355-366.

MILLER JC and MILLER JN (eds.) (1984) *Statistics for analytical chemistry*. Ellis Horwood Publishers, West Sussex, England.

MILLS A, DAVIES RH and WORSLEY D (1993a) Water purification by semiconductor photocatalysis. *Chem. Soc. Rev.* **22** 417-425.

MILLS A and MORRIS S (1993) Photomineralisation of 4-chlorophenol sensitised by titanium dioxide: a study of the initial kinetics of carbon dioxide photogeneration. *J. Photochem. Photobiol. A: Chem.* **71** 75-83.

MILLS A, MORRIS S and DAVIES R (1993) Photomineralisation of 4-chlorophenol sensitised by titanium dioxide: a study of the intermediates. *J. Photochem. Photobiol. A: Chem.* **70** 183-191.

MILLS A and LE HUNTE S (1997) An overview of semiconductor photocatalysis. *J. Photochem. Photobiol. A: Chem.* **108** 1-35.

MIYAMOTO J (1996) Environmental and health issues. *Pure & Appl. Chem.* **68** 1737-1748.

MO SD and CHING WY (1995) Electronic and optical properties of three phases of titanium dioxide: Rutile, anatase, and brookite. *Phys. Rev. B* **51** 13023-13032.

MOKRINI A, OUSSE D and ESPLUGAS S (1997) Oxidation of aromatic compounds with UV radiation/ozone/hydrogen peroxide. *Wat. Sci. Tech.* **35** 95-102.

MONTGOMERY DC (2000) *Personal communication*. Department of Industrial Engineering, Arizona State University, Tempe, AZ, USA.

MORGAN E (ed.) (1991) *Chemometrics: Experimental design*. John Wiley and Sons, New York, USA.

MORRISON C, BANDARA J and KIWI J (1996) Sunlight induced decoloration/degradation of non-biodegradable Orange II dye by advanced oxidation technologies in homogeneous and heterogeneous media. *J. Adv. Oxid. Technol.* **1** 160-169.

MORROW CM and MINEAR RA (1987) Use of regression models to link raw water characteristics to trihalomethane concentrations in drinking water. *Wat. Res.* **21** 41-48.

MYERS RH, KHURI AI and CARTER WH (1989) Response surface methodology: 1966-1988. *Technometrics* **31** 137-157.

NASKAR S, PILLAY SA and CHANDA M (1998) Photocatalytic degradation of organic dyes in aqueous solution with TiO_2 nanoparticles immobilized on foamed polyethylene sheet. *J. Photochem. Photobiol. A: Chem.* **113** 257-264.

NICHIPOR H, RADOUK E, CHMIELEWSKI AG and ZIMEK Z (1996) SO_2 oxidation by simultaneous application of electron beam and electric field in humid air. *J. Adv. Oxid. Technol.* **1** 150-153.

NICHOLSON BC, ROSITANO J and BURCH MD (1994) Destruction of cyanobacterial peptide hepatotoxins by chlorine and chloramine. *Wat. Res.* **28** 1297-1303.

NIEUWOUDT TW (1997) Application of the photocatalytic process to the treatment of tannery waste. *M.Sc. (Chemistry) Thesis, University of Stellenbosch, South Africa*.

OLIVEROS E, LEGRINI O, HOHL M, MULLER T and BRAUN AM (1997) Large scale development of a light-enhanced Fenton reaction by optimal experimental design. *Wat. Sci. Tech.* **35** 223-230.

OLLIS DF (2000) *Personal Communication*. Department of Chemical Engineering, North Carolina State University, Raleigh, NC 27695, USA (on sojourn in France).

OLLIS DF, PELIZZETTI E and SERPONE N (1989) Heterogeneous photocatalysis in the environment: Application to water purification. In: *Photocatalysis: Fundamentals and Applications*, Serpone N and Pelizzetti E (eds.), John Wiley & Sons, New York, USA. 603-637.

PARK TJ, LEE KH, JUNG EJ and KIM CW (1997) Removal of refractory organics and color in pigment wastewater with Fenton Oxidation. In: *Proceedings of the International Association on Water Quality (IAWQ) Specialized Conference on Chemical Process Industries and Environmental Management*, Cape Town, South Africa, Paper P.6.17.

PEILL NJ and HOFFMANN MR (1998) Mathematical model of a photocatalytic fiber-optic cable reactor for heterogeneous photocatalysis. *Environ. Sci. Technol.* **32** 398-404.

PETERS RW, WILKEY MR ONDER A and SPANN N (1999) In-well sonication/In-well vapor stripping treatment of trichloroethane (TCA) and tetrachloroethylene (PCE). In: *Proceedings of The 5th International Conference on Advanced Oxidation Technologies for Water and Air Remediation*, Albuquerque, New Mexico, USA. 42.

PETRIER C and FRANCONY A (1997) Incidence of wave-frequency on the reaction rates during ultrasonic wastewater treatment. *Wat. Sci. Tech.* **35** 175-180.

PEYTON GR, BELL OJ and LEFAIVRE MH (1997) Kinetic modeling for process optimization during the free-radical treatment of nitro compounds in aqueous solutions. *J. Adv. Oxid. Technol.* **2** 424-434.

PIKAEV AA, PODZOROVA EA and PIKAEV AK (1999) Radiation-chemical purification of water from petroleum products. In: *Proceedings of The 5ᵗʰ International Conference on Advanced Oxidation Technologies for Water and Air Remediation*, Albuquerque, New Mexico, USA. 25.

PRAIRIE MR, EVANS LR, STANGE BM and MARTINEZ SL (1993) An investigation of TiO_2 photocatalysis for the treatment of water contaminated with metals and organic chemicals. *Environ. Sci. Technol.* **27** 1776-1782.

PUMA GL and YUE PL (1999) Enhanced photocatalysis in a pilot laminar falling film slurry reactor. *Ind. Eng. Chem. Res.* **38** 3246-3254.

RAJESHWAR K (1996) Photochemical strategies for abating environmental pollution. *Chemistry & Industry* **17 June** 454-458.

RAY AK (1999) Design, modelling and experimentation of a new large-scale photocatalytic reactor for water treatment. *Chem. Eng. Sci.* **54** 3113-3125.

RAY AK and BEENACKERS AACM (1998) Novel photocatalytic reactor for water purification. *AIChE Journal* **44** 477-483.

RICE CV and RAFTERY D (1999) Photocatalytic oxidation of trichloroethylene using TiO_2 coated optical microfibers. *Chem. Commun.* 895-896.

RICE SF, HAROLDSEN BL and STODDARD MC (1999) Design considerations and recent advances in the application of supercritical water oxidation. In: *Proceedings of Workshop on Advanced Oxidation Technologies*, Albuquerque, New Mexico, USA. 93-113.

RICHARDSON SD, THRUSTON AD, COLLETTE TW, PATTERSON KS, LYKINS BW and IRELAND JC (1996) Identification of TiO_2/UV disinfection byproducts in drinking water. *Environ. Sci. Technol.* **30** 3327-3334.

RIEGEL G and BOLTON JR (1995) Photocatalytic efficiency variability in TiO_2 particles. *J. Phys. Chem.* **99** 4215-4224.

ROSOCHA LA (1999) Gas-phase pollutant decomposition with non-thermal plasmas (NTPs): Simple removal equations and figures-of-merit. In: *Proceedings of The 5ᵗʰ International Conference on Advanced Oxidation Technologies for Water and Air Remediation*, Albuquerque, New Mexico, USA. 75-76.

ROSOCHA LA (1999a) *Non-thermal plasma techniques for air treatment. In:* Proceedings of Workshop on Advanced Oxidation Technologies, *Albuquerque, New Mexico, USA. 69-91.*

SAFARZADEH-AMIRI A, BOLTON JR and CATER SR (1996) The use of Iron in advanced oxidation processes. *J. Adv. Oxid. Technol.* **1** 18-26.

SAPRE AV and KATZER JR (1995) Core of chemical reaction engineering: One industrial view. *Ind. Eng. Chem. Res*. **34** 2202-2225.

SARASA J, ORMAD P, CORTES S, GRACIA R and OVELLEIRO JL (1999) Study of the purification with ozone of dye manufacturing wastewaters. In: *Proceedings of The 5th International Conference on Advanced Oxidation Technologies for Water and Air Remediation*, Albuquerque, New Mexico, USA. 104-105.

SCHWIKKARD GW and BUCKLEY CA (1998) Ultrasound for water treatment. In: *Proceedings of WISA 98: Biennial Conference and Exhibition of the Water Institute of South Africa (WISA)*, Cape Town, South Africa. Paper P-52, 1-4.

SCLAFANI A, SCIASCIA A and RIZZUTI L (1999) Pollutants photocatalytic degradation in a falling film reactor. *J. Adv. Oxid. Technol.* **4** 91-96.

SCZECHOWSKI JG, KOVAL CA and NOBLE RD (1995) A Taylor vortex reactor for heterogeneous photocatalysis. *Chem. Eng. Sci.* **50** 3163-3173.

SCZECHOWSKI JG, KOVAL CA and NOBLE RD (1993) Evidence of critical illumination and dark recovery times for increasing the photoefficiency of aqueous heterogeneous photocatalysis. *J. Photochem. Photobiol. A: Chem.* **74** 273-278.

SELVAGGI A, DAVID A and ZAPPELLI P (1999) Thermophotocatalytic degradation of gaseous organic pollutants. In: *Proceedings of The 4th International Conference on TiO$_2$ Photocatalytic Purification and Treatment of Water and Air*, Albuquerque, New Mexico, USA. 79-80.

SERPONE N (1997) Relative photonic efficiencies and quantum yields in heterogeneous photocatalysis. *J. Adv. Oxid. Technol.* **2** 203-216.

SERPONE N (1995) Brief introductory remarks on heterogeneous photocatalysis. *Sol. Energy Mater. Sol. Cells* **38** 369-379.

SERPONE N, PELIZZETTI E and HIDAKA H (1993) Identifying primary events and the nature of intermediates formed during the photocatalyzed oxidation of organics mediated by irradiated semiconductors. In: *Photocatalytic Purification and Treatment of Water and Air*, Ollis DF and Al-Ekabi H (eds.), Elsevier Science Publishers B.V., Amsterdam, The Netherlands. 225-250.

SERPONE N, SAUVE G, KOCH R, TAHIRI H, PICHAT P, PICCININI P, PELIZZETTI E and HIDAKA H (1996) Standardization protocol of process efficiencies and activation parameters in heterogeneous photocatalysis: relative photonic efficiencies. *J. Photochem. Photobiol. A: Chem.* **94** 191-203.

SERRANO B and DE LASA H (1997) Photocatalytic degradation of water organic pollutants. Kinetic Modeling and energy efficiency. *Ind. Eng. Chem. Res*. **36** 4705-4711.

57

SIGMAN ME, BUCHANAN AC and SMITH SM (1997) Application of advanced oxidation process technologies to extremely high TOC containing aqueous solutions. *J. Adv. Oxid. Technol.* **2** 415-423.

SPACEK W, BAUER R and HEISLER G (1995) Heterogeneous and homogeneous wastewater treatment – comparison between photodegradation with TiO_2 and the photo-Fenton reaction. *Chemosphere* **30** 477-484.

SUN L, AITKEN RH and BOLTON JR (1996) Generation efficiency of the hydroxyl radical adduct of the DMPO spin trap in homogeneous and heterogeneous media. *J. Adv. Oxid. Technol.* **1** 44-52.

SYMONS M (1978) *Chemical and biochemical aspects of electron-spin resonance spectroscopy*. Van Nostrand Reinhold Co., New York, USA. 62.

TAKAHASHI Y, KOBAYASHI Y and SUZUKI T (1999) Removal of trihalomethanes and pesticides by ozone/UV oxidation process. In: *Proceedings of The 5th International Conference on Advanced Oxidation Technologies for Water and Air Remediation*, Albuquerque, New Mexico, USA. 120-121.

TERBLANCHE DE (1999) Bethlehem precipitation research project. *Internet page downloaded at* http://nprp0.ofs.gov.za/results.htm (Download date: October 4th 1999).

TERZIAN R, SERPONE N and FOX MA (1995) Primary radicals in the photo-oxidation of aromatics – reactions of xylenols with OH, N_3 and H radicals and formation and characterization of dimethylphenoxyl, dihydroxydimethylcyclohexadienyl and hydroxydimethylcyclohexadienyl radicals by pulse radiolysis. *J. Photochem. Photobiol. A: Chem.* **90** 125-135.

UNKROTH A, WAGNER V and SAUERBREY R (1997) Laser-assisted photochemical wastewater treatment. *Wat. Sci. Tech.* **35** 181-188.

VAN LAARHOVEN PJM and AARTS EHL (1987) *Simulated annealing: Theory and Applications*. D.Reidel, Dordrecht, The Netherlands.

VAUGHAN PP and BLOUGH NV (1999) Photochemical formation of hydroxyl radical by constituents of natural waters. *Environ. Sci. Technol.* **32** 2947-2953.

VELLA P, VERONDA B and VLASTNIK E (1999) Chemical oxidation of industrial pollutants by potassium permanganate. In: *Proceedings of The 5th International Conference on Advanced Oxidation Technologies for Water and Air Remediation*, Albuquerque, New Mexico, USA. 90-91.

VON SONNTAG C, DOWIDEIT P, FANG X, MERTENS R, PAN X, SCHUCHMANN MN and SCHUCHMANN HP (1997) The fate of peroxyl radicals in aqueous solution. *Wat. Sci. Tech.* **35** 9-15.

WALLER K, SWAN SH, DELORENZE G and HOPKINS B (1998) Trihalomethanes in drinking water and spontaneous abortion. *Epidemiol.* **9** 134-140.

WINSHIP S (1999) Evaluating hydrodynamic cavitation for the treatment of raw water and effluents. *SA Waterbulletin* **25 (5)** 12-14.

YUE PL (1999) A new reactor for catalytic wet air oxidation. In: *Proceedings of The 5ᵗʰ International Conference on Advanced Oxidation Technologies for Water and Air Remediation*, Albuquerque, New Mexico, USA. 61.

YUE PL (1993) Modeling, scale-up and design of multiphasic photoreactors. In: *Photocatalytic Purification and Treatment of Water and Air*, Ollis DF and Al-Ekabi H (eds.), Elsevier Science Publishers B.V., Amsterdam, The Netherlands. 495-510.

ZENG G, HEARD DE, PILLING MJ and ROBERTSON SH (1998) A master equation study of laser-generated interference in the detection of hydroxyl radicals using laser-induced fluorescence. *Geophys. Res. Lett.* **25** 4497-4500.

ZHANG Y, CRITTENDEN JC and HAND DW (1994) The solar photocatalytic decontamination of water. *Chemistry & Industry* **19 September** 714-717.

CHAPTER 2

MATERIALS AND METHODS

OVERVIEW

This chapter contains a summary of the experimental materials and methods used during the course of the investigation. The basic design parameters, operational details and general utilities are furnished for each of the prototype PCO reactors. In addition, some background details are provided with respect to the two model pollutants of choice, i.e. *para*-Chlorophenol and cyanobacterial microcystin toxins. The chapter is concluded with details of the analytical methodology used. The general experimental philosophy is also explained.

2.1   EXPERIMENTAL PHOTOCATALYTIC REACTORS

2.1.1 Design and Operation

Two types of experimental photocatalytic (PCO) reactors were designed, constructed and optimized for the removal of low concentrations of organic contaminants in water. These reactors were operated as flow systems based on a "falling film" principle. The first system (Reactor 1) was operated only as a slurry-phase reactor using aqueous suspensions of anatase TiO_2 catalyst. The second system (Reactors 2A and B) were operated either as immobilized-bed or combined slurry immobilized-bed reactors.

Reactor 1 consisted of a cylindrical Pyrex glass tube (140 cm long, e.d = 8.5 cm., i.d. = 7.0 cm) equipped at the top with a receiver cup with 1 L volume capacity. The tube was mounted vertically in a base reservoir and encircled by a set of eight 30 W germicidal UV lamps (90 cm long) connected to an external framework.

Reactor 2 consisted of a vertically suspended rectangular sheet module (40 $\times$110 cm) with six 15 W UV lamps (45 cm long) assembled uniformly on both sides of the sheet for maximum irradiation. Both reactors were covered with a protective UV shield to prevent loss of UV radiation and to ensure operator safety. Electrical power input per unit area of irradiated surface amounted to 954 and 204.5 W/m^2 for Reactors 1 and 2 respectively.

The reactors are schematically illustrated in Figure 2.1. Photographs and full dimensional details for these systems (and their interior components) are furnished in Appendices A to F.

Reactor 1   **Reactors 2A and B**
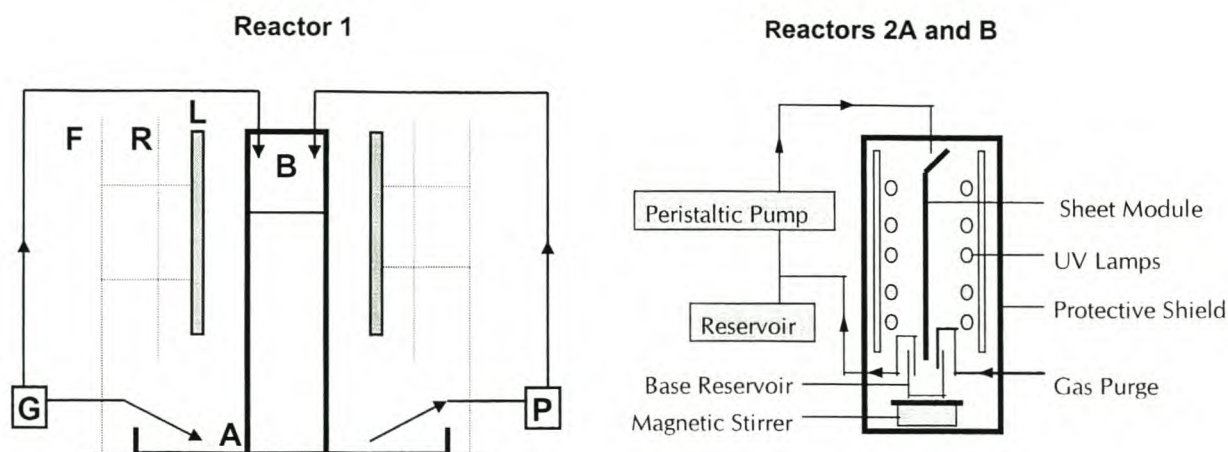
Figure 2.1: Schematics of experimental photocatalytic reactors.

Reactor 1 :   Cylindrical glass tube reactor (A: Base reservoir; B: Glass tube with cup; F: External frame; G: Gas purge; L: Germicidal UV lamps; P: Peristaltic Pump; R: Shield and reflector)
Reactor 2A: Fiber glass sheet module
Reactor 2B: Fibrous Activated Carbon (FAC) sheet module

The designs of the reactors were chosen to (1) facilitate the use of commercially available materials for the construction (2) avoid the use of components prone to fouling during operation and (3) accommodate future developments in photocatalysts. The falling film concept was selected to (1) support the objectives stated above (2) address the issue of attaining a favorable *irradiated catalyst surface-to-reaction volume ratio* for immobilzed-bed reactor configurations, and (3) facilitate the penetration of UV light through the water film, hence optimizing the UV catalyzed reaction.

Reactor 2 was essentially designed with its scaling-up potential and overall capacity in mind - i.e. in the vertical direction by increasing the length of the sheet and the number of parallel UV lamps, in the lateral direction by increasing the width of the sheet and the length of the UV lamps, and in the horizontal direction by increasing the number of sheets sharing a set of UV lamps. Optimization, however, could be performed at laboratory scale using one reactor consisting of a single sheet with a set of lamps on each side.

Three basic modes of operation were identified for the falling film flow reactors, i.e.:

- single pass mode
- sequential single pass mode
- recirculation mode

Aqueous TiO$_2$ suspensions (slurries) were prepared in 3 or 6 L batch containers by addition of the desired loading of catalyst to the water sample of choice. Magnetic stirring was conducted for 5 minutes prior to spiking the sample with the organic pollutant of choice. An additional 5 minutes of stirring were used to attain adsorption equilibrium prior to feeding the sample into the reactors.

Immobilization of TiO$_2$ on reactor sheet modules was achieved by applying suspension coating or droplet spraying methods. Suspension coating was selected as standard method due to reliable statistical reproducibility.

For this work, a typical UV photocatalytic irradiation experiment (test run) comprised of the spiked water sample (or slurry) of choice being introduced to the top section of the designated reactor from a batch reservoir using a peristaltic pump. A "falling film" was obtained from the top through (mostly) laminar gravitational flow along the *exterior surface* of the cylindrical tube (Reactor 1) or *both sides* of the sheet module (Reactors 2A and B) while UV irradiation proceeds. Catalyst slurries were kept in suspension by incorporating a gas purge (oxygen or compressed air) in the receiver cup of the slurry reactor and in the base reservoirs of both reactors. As mentioned earlier, the inclusion of oxygen is vital to the photocatalytic production of hydroxyl radicals. For all test runs, the ambient temperature was kept at approximately $25 \pm 2\ ^{\circ}C$.

During the course of any given experiment, fixed-volume aliquots of treated water were collected from the reactor base reservoir using peristaltic pumps. Where necessary, slurry aliquots were filtered in the dark to remove excess TiO_2 particles prior to analysis. Whatman 42 (Ashless, 110 mm ϕ, Catalogue number: 1442 110) and Whatman 44 (Ashless, 185 mm ϕ, Catalogue number: 1444 185) filter papers were used in *para*-Chlorophenol and microcystin studies, respectively.

Table 2.1: Summary of design parameters.

Parameter	Reactor 1	Reactor 2A	Reactor 2B
Photocatalyst	Degussa P-25 TiO_2	Degussa P-25 TiO_2	Degussa P-25 TiO_2
Catalyst Immobilization	Slurries only	Fiber glass sheets[c]	FAC sheets[d]
UV-C lamps (germicidal; 254 nm)	Yes	Yes	Yes
UV-A lamps (fluorescent; *ca* 360 nm)	No	Yes	No
Surface area irradiated (m^2)	0.252	0.880	0.880
Max. Lamp power per unit area (mW/cm^2)	95.40	20.45	20.45
UV residence time per single pass (secs)	2.1 ± 0.1	4.1 ± 0.1	11.5 ± 0.2
Vertical distance of Irradiation (cm)	90	110	110
Linear Flow Velocity (cm/sec)	42.9	26.8	9.6
Horizontal distance of irradiation (cm)	2 to 8	5 to 15	5 to 15
Volumetric flow rate (pumps) (L/min.)[b]	0.05 to 2	1 to 2	1 to 4
Surface Flow Rate per hour (L / hr / m^2)	12 to 475	70 to 135	70 to 270

Table 2.1: Summary of design parameters (continued).

Parameter	Reactor 1	Reactor 2A	Reactor 2B
Reaction Volumes (L)	3 to 6	3 to 6	3 to 12
Oxygen flow rate (L/min.)	5 and 20	5 and 20	5
Calculated film layer thickness (μm)	112 to 296	75 to 150	218 to 436
Illuminated specific surface area ($m^2/m^3 = m^{-1}$)	3380	6620	2300-2600

2.1.2 Film Layer Thickness

Calculation of film layer thickness for falling film reactors depends on water flow rates, UV residence times (contact times) and the catalyst surface area covered by liquid during irradiation (Freudenhammer *et al.*, 1997). These calculations imply that layer thickness varies inversely proportional to the illuminated specific surface area (κ) (Ray, 1999). Film thickness for reactor 1 was calculated between 112 and 296 μm depending on the flow rate used. For reactor 2A film thickness varied between 75 and 150 μm and for reactor 2B between 218 and 436 μm. Thickening effects caused by catalyst slurries, turbulent flow or surface roughening were not accounted for.

2.1.3 UV Dosage

UV dosages may be calculated using the residence time of irradiation within the reactor and the level of UV irradiance (in mW/cm^2 or W/m^2). These parameters will be determined by the reactor type and operation mode under investigation. The actual power output of commercial UV lamps are approximately one-third of the value specified as input power (Martin *et al.*, 1999). UV power output (levels of irradiance) is also referred to as "Radiant flux" and is normally determined with UV sensors, radiometers and actinometric analyses (as discussed in 1.3.6). Irradiance may vary markedly throughout a reactor, hence complex mathematical techniques such as multiple point source modeling is often required to calculate this parameter for a given design (Bolton, 1999; Bolton, 1999a). Moreover, UV lamps have a limited life-span (*ca* 5000 h for commercial low-pressure mercury arcs) which complicates the calculation.

For the purpose of this work, only theoretical UV dosages (in $mW\text{-}s/cm^2$) will be calculated in an effort to construct UV-dosage response curves. The determination of absolute UV dosages was precluded due to the (1) unavailability of radiometers and lack of actinometric studies (2) extended use of the original batch of UV lamps and (3) lack of modeling studies addressing the true magnitude and spatial variation of UV irradiance within the reactors.

2.1.4 Reactor Materials

(a) General Items

Germicidal and fluorescent (low-pressure Mercury) UV lamps (Product Code: TUV 15W G15T8 – UV LONG LIFE) and starters (Product Code: S2/CEBEC74/BS3772/4JKLM) were supplied by Phillips (The Netherlands). Power ballasts (Catalogue no. CS/2201230) were supplied by Harper Electrical Industries (Pty) (Cape Town, RSA). No lamp characterization data was available.

Variable-speed peristaltic pumps (Watson-Marlow 505S, Product Code: 050•4841•L0U) were supplied by Aeromix (Pty) Ltd (Cape Town, RSA).

Oxygen (99% pure), compressed air and argon were supplied in 100 bar cylinders by Afrox (RSA).

TiO_2 (Degussa P-25, FW 79.90 g/mole) was purchased in 10 kg batches from Degussa AG (Frankfurt, Germany) (CAS no. 13463-67-7) and used as received. Degussa's product consists of approximately 75% anatase and 25% rutile TiO_2. Further specifications for P-25 has been furnished elsewhere in open literature (Hand *et al.*, 1993).

(b) Sheet Materials

Sheets of fiber glass and fibrous activated carbon (FAC) were used as TiO_2 immobilizing matrices in this work. The use of fiber glass materials for this purpose is well-known (Hoffmann *et al.*, 1995; Blazkova *et al.*, 1998), however, for FAC this application is fairly virgin territory.

FAC is a relatively new formulation of activated carbon that has entered the marketplace in the mid-nineties. Apart from exhibiting several domestic applications, FAC has also demonstrated its potential in the field of water treatment (Barnardt, 1997). The adsorption of organic water pollutants by FAC has been reported in scientific literature (Brasquet *et al.*, 1996; Le Cloirec *et al.*, 1997; Brasquet *et al.*, 1999). FAC is manufactured from natural precursors (e.g. coconut) or synthetic precursors (phenolic resins or viscose). The raw material undergoes carbonization at 1000 °C to eliminate volatiles. This is followed up by steam or CO_2 activation at 800 °C that produces the FAC product with a large specific surface area and a significant volume of micropores. The average pore diameter for FAC ranges from 5 to 21 Å. As a result, the total surface area may vary from 700 to approximately 2500 m^2/g depending on the manufactured grade. To date, FAC has not been engineered in industrial processes but recent laboratory studies confirmed its superior adsorption potential for water pollutants (e.g. phenol) compared to GAC and PAC. The application of neural networks and statistical regression analysis to predict adsorbability of organic compounds onto FAC as a function of molecular structure is currently being addressed (Brasquet *et al.*, 1999).

In this work, a portion of the PCO experiments will be conducted in a reactor with TiO_2 catalyst immobilized on a sheet of FAC. This approach will simulate a tandem process.

Details pertaining to the reactor sheet materials used in this work are presented in Tables 2.2 and 2.3 below. The woven and micro-porous structure of the FAC used herein, are shown in Appendices G and H. TiO$_2$ coated FAC is depicted in Appendix I.

Table 2.2: Design details of reactor sheets.

Sheet	Supplier	Product Code / Catalogue No.	Approximate Weight (g/m^2)
Fiber glass (reinforced)	Foyntech Africa cc (Stellenbosch)	GLASS COAT 60	60
Fiber glass tissue (non-reinforced)	Freudenberg Nonwovens Pty (Ltd) (Parow Industria)	DIN 60001-T01	26
FAC (Kuractive 15)	Kuraray (Japan) via Enviro Services cc (RSA)	CH700-15 K81006-701	118
FAC (Kuractive 20)	ibid.	CH700-20 K80314-603	60

Table 2.3: Product details of Kuractive FAC sheet materials.

Property	Grade 10	Grade 15	Grade 20	Grade 25
Total Surface Area (m^2/g)	1000	1500	2000	2500
Pore Radius (angstr)	9	12	16	22
Pore Volume (mL/g)	0.22	0.50	0.75	1.20
Benzene Adsorption (wt%)	22	45	65	90
Iodine Adsorption (mg/g)	950	1550	2000	2400
Ash Content (%)	0.03	0.03	0.04	0.05
Ignition Point ($^{\circ}$C)	470	470	470	470

2.2 MODEL POLLUTANTS

2.2.1 *para*-Chlorophenol

Chlorophenols represent a family of organic water pollutants that are omnipresent in wastewater as a result of their extensive use in industrial processes (Ollis *et al.*, 1989). From this group of compounds, *para*-Chlorophenol (p-CP) was selected as *primary* representative pollutant to conduct a series of parametric and OED related experiments as part of the proposed *reactor development* strategy. The use of p-CP as universal model pollutant has also been advocated elsewhere in terms of creating a standard framework of conditions for figure-of-merit comparison (viz: global rating) of PCO technologies (Mills and Morris, 1993).

65

2.2.2 Cyanobacterial Microcystin Toxins

(a) Drinking Water Scenario

In order to evaluate the general utility of the proposed PCO reactors to drinking water treatment, a naturally occurring group of compounds was selected as *secondary* representative pollutant. Cyanobacterial microcystin toxins can potentially deteriorate drinking water quality. This could be due to inefficient removal of these compounds from raw waters by conventional processes such as coagulation/flocculation, filtration, carbon-adsorption and subsequent chlorination. The end-result is either (1) the presence of microcystin toxins or (2) high levels of disinfection by-products in treated waters (Pieterse, 1997).

(b) Origin

Cyanobacterial microcystins represent a major group of natural biotoxins produced by several species of blue-green algae (cyanobacteria) in aquatic environments (Carmichael, 1992; Lawton and Robertson, 1999). The cyanobacteria are microscopic inhabitants of surface waters and known as a group of bacteria in which the cells contain chlorophyll and consequently participate in photosynthesis reactions. Individual algal cells are not visible to the naked eye, but do become visible when in concentrated form as suspended colonies (e.g. *Microcystis aeruginosa*) or filaments (e.g. *Anabaena*). Overabundant growths of algae result in the formation of dense green blooms which may resemble pea-soup suspended on water surfaces (Carmichael, 1994) (see Appendix J). Excessive nutrient enrichment of natural waters (eutrophication) is known to cause profuse growth or blooms that may subsequently release microcystin toxins into water. The primary sources of nutrients (e.g phosphates and nitrates) are raw sewage spills, industrial effluents and run-offs from agricultural and urban regions. Warm summer conditions (high temperatures and light intensities) and calm, stable waters (low turbidity, no wind) also contribute to bloom formation. On windy days, blooms can easily spread from one side of a lake to another in relative short time.

(c) Classification & Chemical Structure

Cyanobacterial toxins are divided into two main groups, i.e. neurotoxins and hepatotoxins. Neurotoxins affect the nervous system and are fast-acting, small molecules. Examples include anatoxin and saxitoxin. Hepatotoxins, on the other hand, affect the liver and are cyclic peptide molecules acting more slowly compared to neurotoxins. Examples include the microcystins and nodularins. The microcystins are cyclic heptapeptides containing 5 invariant amino acids and 2 variable L-amino acids. These toxins are labelled using one-letter abbreviations to indicate the 2 variable amino acids. Microcystin-LR, for example, contains leucine (L) and arginine (R) in the variable positions (see Appendix K). Thus far, more than 60 structural analogues (also known as variants) have been discovered and the number continues to grow (Carmichael, 1994; Lawton and Robertson, 1999).

(d) Toxicity Issues

At least one of the cyanobacterial species (*M. aeruginosa*) has been shown to produce hepatotoxic microcystins in South African waters. Wicks and Thiel (1990) determined the seasonal occurrence and distribution of 6 microcystin variants (LA, LR, YA, YR, FR and LAba) isolated from this species found in the Hartebeespoort Dam, South Africa. Microcystins are capable of causing acute and chronic toxicosis in both humans and animals. Toxicological studies revealed LD_{50} values for the microcystins around 0.05 mg/kg in mice (by intra-peritoneal injection) compared to 4.3 mg/kg for sodium cyanide (Lam *et al.*, 1995). The microcystins have been responsible for a number of livestock poisonings and deaths in South Africa (Van Halderen *et al.*, 1995). They have also been linked to the high incidence of liver cancer in areas of China where populations are dependent on surface drinking water (Nishiwaki-Matsushima *et al.*, 1992). Moreover, the unfortunate death of approximately 60 hospital patients in Caruaru, Brazil (1996) have been unequivocally linked to microcystin contamination of the water supply to the kidney dialysis unit of the local hospital (Hitzfeld *et al.*, 2000). Not all cyanobacterial blooms are toxic, but a significant number are. Risk assessment studies are difficult to execute mainly due the variable toxicity of the blooms. Moreover, the actual exposure and resulting effects have still not been conclusively ascertained, particularly for the human scenario. The most likely route for human exposure is believed to be the oral route via (1) drinking water consumption (2) recreational use of lakes and rivers and (3) the consumption of algal food tablets. The dermal route may also be significant, e.g. during the recreational use of lakes (viz: swimming and canoeing). Due to a growing concern about the adverse health effects associated with cyanotoxins, particularly for drinking water, the World Health Organization has adopted a provisional guideline limit of 1.0 ug/L (ppb) for microcystin-LR in terms of a tolerable daily intake (Hitzfeld *et al.*, 2000; WHO, 1998).

(e) Analytical Detection

A validated method has been developed for the standard analytical determination of microcystins in water (Lawton *et al.*, 1994). The procedure comprises the following steps :

- Methanol extraction of the toxins from freeze-dried algal material
- Sample purification with solid phase extraction (SPE)
- Separation and identification using isocratic reversed-phase HPLC with UV diode-array detection at 240 nm.
- The limit of detection (LOD) is below 250 ng/L (ppb) depending on the nature of the water (raw or treated) analyzed.

Other sensitive techniques (e.g. capillary electrophoresis and tandem-Mass Spectrometry) have also been developed to reduce detection limits further within the ng/L range (Bateman *et al.*, 1995). In addition, liquid chromatographic methods, coupled with electrospray mass spectrometry, have been used to identify microcystin variants by means of molecular weight differentiation (Shephard, 1997).

(f) Treatment Options

Problems encountered with the treatment and subsequent removal of microcystins from drinking water sources have been related to the chemical stability of these toxins with regard to temperature and pH variation. Conventional water treatment (e.g. coagulation) has been ineffective due to the relative small size of the toxin molecules (ca 800-1000 Daltons). Other treatment techniques (e.g. chlorination, carbon adsorption and UV irradiation) have all met with variable success and were limited to the treatment of small laboratory scale water samples (Nicholson *et al.*, 1994; Donati *et al.*, 1994; Tsuji *et al.*, 1995).

Reverse osmosis retained the toxins successfully, however toxin enriched water had to be disposed of by other means. Chemical treatment methods such as ozonation and oxidation by hydrogen peroxide or permanganate have also been investigated, but it remains uncertain whether oxidant stability as a function of water quality will render these processes economically viable (Lawton and Robertson, 1999).

As part of the primary study objective of this work, it was proposed to investigate the use of TiO_2 mediated PCO as potential means for the complete oxidative destruction of microcystins in water. This was the first time ever that studies were to be initiated and subsequently reported in this regard (Stockenström *et al.*, 1996). To date, only two other research groups (from Scotland and Australia) have reported similar work on the TiO_2 PCO treatment of microcystin toxin molecules in aqueous matrices (Robertson *et al.*, 1997; Robertson *et al.*, 1999; Feitz *et al.*, 1999).

2.3   ANALYTICAL METHODOLOGY

2.3.1 *para*-Chlorophenol

(a)   UV Spectrometry

p-CP dissolves readily in water and exhibits sufficiently high molar absorption coefficients at two UV wavelengths (i.e. 225 and 280 nm) to render UV spectrometry a useful screening tool for quantitative measurement. The absorbance peak at 225 nm was chosen as primary detection element due the higher molar absorption (and sensitivity) in the concentration range of interest (0 to 50 mg/L) (ε_{225nm}: *ca* 8400 $cm^{-1}mole^{-1}dm^3$; ε_{280nm}: *ca* 1600 $cm^{-1}mole^{-1}dm^3$). In this work, a GBC-920 scanning-wavelength double-beam UV-Visible spectrometer was used with the following scanning parameters:

- Cuvettes :   Quartz, 1cm x 1cm
- Sample Volume :   *ca* 3 mL
- Measurement mode :   Absorbance
- Scan range :   200 – 400 nm
- Scan Speed :   1000 nm/min.
- Wavelength step :   1.25 nm
- Monochromator slit width :   2 nm

A representative example of a UV absorbance spectrum for 40 mg/L p-CP in water is shown in Figure 2.2. In addition, Figure 2.3 illustrates a typical decrease in absorbance that occurred for aqueous p-CP as a result of degradation or adsorptive removal.
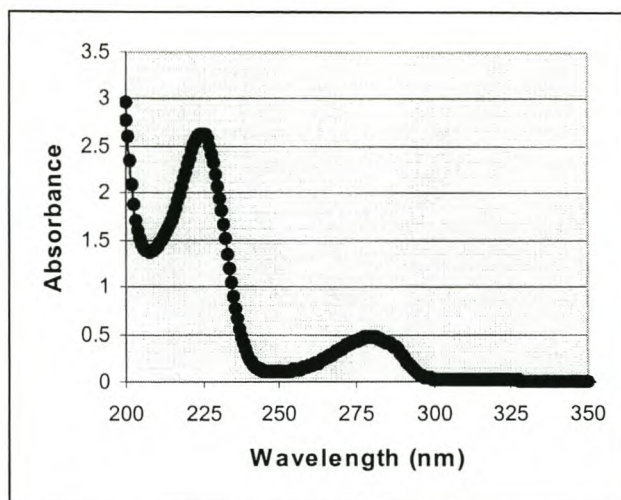
Figure 2.2: Typical UV absorbance spectrum for 40 mg/L p-CP in water (λ_{max} at 225 and 280 nm).
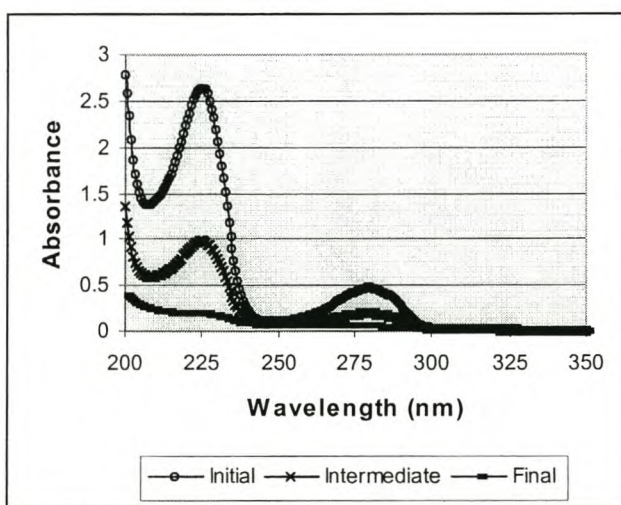
Figure 2.3: Typical degradation pattern for p-CP with initial > intermediate > final concentration.

A standard linear calibration curve was used to convert absorbance signals to the equivalent p-CP concentrations (Figure 2.4 and Table 2.4). In cases where constant initial concentration was assumed for different batches of p-CP stock solutions, the calibration curves were supplemented by statistical formulae as indicated in 2.4.1. The limit of detection (LOD) was set at 1 mg/L p-CP.

Table 2.4: UV calibration data for p-CP at 225 and 280 nm (in distilled water).

p-CP (mg/L)	Absorbance (225 nm)	Absorbance (280 nm)
1	0.101	0.070
5	0.379	0.113
10	0.696	0.172
20	1.330	0.278
30	1.979	0.387
40	2.612	0.499
50	3.135	0.592
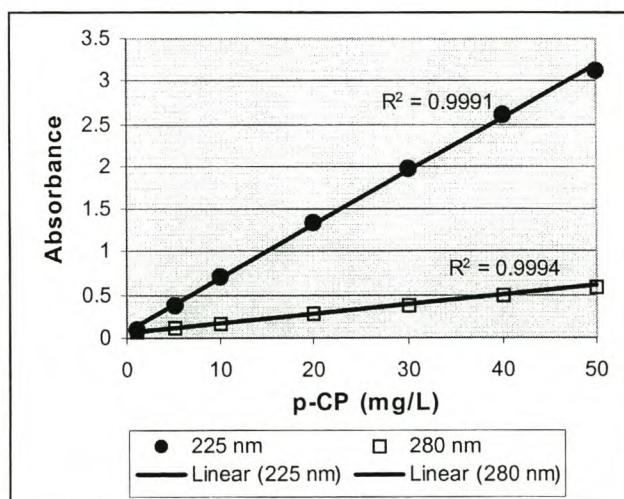
Figure 2.4: Linear calibration curves for UV detection of p-CP at 225 and 280 nm.

The UV absorbance measurement at fixed wavelength and p-CP concentration displayed no dependence on batch variations. As example, the detection of 40 mg/L p-CP (at 225 nm) from 10 different batch solutions of p-CP produced a relative standard deviation of less than 3 %(Table 2.5):

Table 2.5: UV absorbance variation as a function of p-CP batch number.

p-CP Batch Number	Absorbance (225 nm)
1	2.612
2	2.651
3	2.697
4	2.653
5	2.735
6	2.640
7	2.571
8	2.702
9	2.491
10	2.531
Mean	2.628
Standard deviation (SD)	0.078
Relative standard deviation (%)	2.96

(b)   Total Organic Carbon

UV spectrometry was used as primary screening tool for p-CP as part of a large number of OED and parametric studies. In addition, *one* representative p-CP sample (40 mg/L) was subjected to PCO treatment in Reactor 1 to determine the degree of mineralization in terms of total organic carbon (TOC) (see next Chapter for details). For this purpose a calibration curve, as constructed by Nieuwoudt (1997), was used to relate p-CP concentration to TOC values (Figure 2.5).
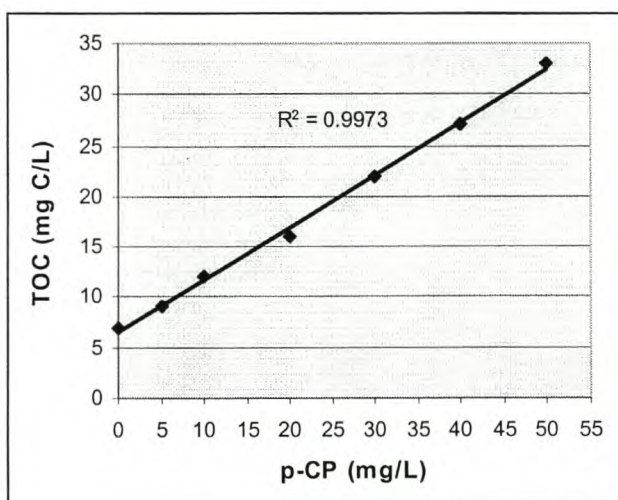
Figure 2.5: Linear calibration curves for TOC analysis of p-CP in distilled water (Nieuwoudt, 1997).

Continuous determination of TOC was discarded in this work due the following main reasons:

- Synthetic laboratory samples (i.e. distilled water spiked with pollutant) were prepared and used in the majority of the test work.
- A study of p-CP mineralization and the formation of intermediate products (contributing to TOC) were not required.
- No interfering intermediates resulting from the PCO treatment of p-CP were detected via UV spectrometry, hence the latter method could be used as a true measure of the rate and magnitude of p-CP concentration changes.
- The available TOC analyzer (i.e. ANATOC) required relatively long sample preparation and analysis times. Hence, in view of the large number of OED tests planned, a quicker analytical determination was paramount (Bennett and Van der Merwe, 1995).

(c)   Stock Material

p-CP (FW 128.56 g/mole, 99% purity, CAS no. 106-48-9, Catalogue No. 18578-7) was obtained from Aldrich Chemical Co. and used as received without further purification.

71

(d)   Water Sources

Distilled water (conductivity 2.4 uS/m) and deionized water (conductivity 1.5 uS/m) were prepared in-house using Aquatron (A8S) and Milli-Q (CDOF-01205, Millipore Corporation, Bedford, MA, USA) systems, respectively. Tap water experiments were conducted using Stellenbosch (RSA) tap water (conductivity 80 uS/m) treated by flocculation and chlorination processes. The total alkalinity in Stellenbosch tap water typically ranges from 10 to 16 mg/L (as $CaCO_3$) (Mansfield, 2000).

2.3.2 Microcystins

(a)   High-Performance Liquid Chromatography

In this work, 4 microcystin variants (i.e. YR, LR, YA and RR) were used to spike water samples meant for PCO experiments. For analytical purposes these toxins were separated and quantified by isocratic reversed-phase High-Performance Liquid Chromatography (HPLC) with UV detection at 240 nm. Sample preparation comprised purification on C_{18} Solid Phase Extraction (SPE) cartridges. Identity of the HPLC peaks was confirmed by spectral comparison (over the range 200-300 nm) with authentic standards using UV diode-array detection. The authenticity of the various analytes was unequivocally confirmed by electrospray Liquid Chromatography- Mass Spectrometry (LC-MS) operated in single ion recording mode at $^m/_z$ = 1045, 995, 959 and 1038 for the YR, LR, YA and RR variants, respectively.

The HPLC analytical method for microcystin determinations included the following conditions: mobile phase (46 % acetonitrile in 0.05 % trifluoroacetic acid, TFA), flow rate (1 mL/min.) and isocratic programming. The analytical column used was a Phenomenex Ultremex C_{18} , 3μ (100 × 4.6 mm).

Clean-up and preparation of aqueous microcystin samples prior to HPLC analysis involved the following steps:

* A 100 mL sample collected from the reactor for each determination was centrifuged at 3000 rpm for about 10 minutes to facilitate the separation of the water phase and any solid catalyst particles that might be present.
* The required amount of water sample was then added to an Erlenmeyer flask.
* The C_{18} end-capped SPE cartridges were then conditioned with methanol and water.
* The clear water sample was applied to the cartridge at a flow rate of 5 mL/min.
* The flask was rinsed with water.
* The column was washed with 10 mL each of 10%,20% and 30% methanol in water.
* The microcystins were then eluted with 3 mL of 0.1% TFA in methanol and dried under nitrogen.
* The microcystins were taken up in about 200 μL methanol, ready for HPLC analysis.

The concentrations of the microcystins were monitored and calculated using calibrated standards for each of the variants studied: YA, YR, LR and RR. Limit of detection in most instances was set as 10 ug/L (ppb) for all variants.

Appendix L illustrates a typical HPLC chromatogram for the analysis of microcystins YA, YR and LR, as generated from this work (i.e. before and after PCO treatment). Separation and detection occurs within 25 minutes.

(b)   Stock Material

Initial PCO experiments with cyanobacterial toxins were performed using an algal extract containing microcystins YR, LR and YA. These toxins were extracted with methanol from freeze-dried algal material provided by the Programme on Mycotoxins and Experimental Carcinogenesis (PROMEC) division of the Medical Research Council in Tygerberg, South Africa. The freeze-dried material originated from a toxic strain of *Microcystis aeruginosa*.

In order to circumvent the need to seek natural sources of toxic strains (given that not all isolated strains produce toxins) several batches of cyanobacterial culture material were obtained from abroad, cultured and analyzed for microcystin content, i.e :

* M. *aeruginosa* UV027
* *M. aeruginosa* PCC7820
* *M. aeruginosa* SAG 14.85
* *M. aeruginosa* PCC7806
* *M. aeruginosa* PCC7813

The initial culturing of these strains proved to be problematic, mainly due to problems related to the transportation and contamination. Some strains, however, were revived and successfully cultured with the aid of PROMEC. Eventually, a natural source of toxins was located at Wildevoël Vlei (Noordhoek, Cape Town, RSA) where an outbreak of cyanobacterial blooms yielded microcystins LR and RR in detectable amounts (viz. greater than 10 ug/L) in extracts from freeze-dried material. These extracts were used in the latter part of the microcystin studies (as reported in Chapter 5).

(c)   Water Sources

Deionized water (conductivity 1.5 uS/m) was prepared in-house using a Milli-Q (CDOF-01205, Millipore Corporation, Bedford, MA, USA) system. Raw lake water was obtained on a periodic basis from two hypertrophic lakes on the Cape Flats near Cape Town (RSA), i.e. *Zeekoevlei* and *Rondevlei*. The respective sampling areas were at Zeekoevlei Yacht Club and Rondevlei Nature Reserve. Table 2.6 summarizes the main water quality parameters of these waters during their periods of collection and subsequent use.

Table 2.6: Characterization of raw waters used in microcystin studies.

Reactor	1	2A	2B
Water Source (Sampling Date)	Zeekoevlei (8 Feb.1996)	Zeekoevlei (29 Aug.1999)	Rondevlei (25 Jan.1999)
Temperature ($^{\circ}$C)	23.7	14.2	23.8
Dissolved Oxygen (mg/L)	12.4	13.7	5.8
O_2 Saturation (%)	148	134	69
Total Suspended Solids (mg/L)	NA	43	64
pH	9.3	8.0**	8.1
Conductivity (mS/m)	124	87.7	143
Chemical Oxygen Demand (mg/L)	NA*	34	159
Total Persulphate Oxidizable Nitrogen (mg/L)	1.88	2.31	2.44
Ammonia (mg/L)	0.027	0.020	0.330
Nitrite + Nitrate (mg/L)	0.023	0.470	0.030
Total Phosphorous (mg/L)	0.539	0.752	0.293
Soluble Reactive Phosphorous (mg/L)	0.284	0.205	0.010
Chlorophyll-a (ug/L)	202.0	349.8	71.8
Phaeophytin (ug/L)	24.0	45.9	36.5

* NA = Not analyzed
** Determined in-house at the Department of Chemistry, University of Stellenbosch, South Africa.

2.3.3 Miscellaneous

In-house determination of water sample conductivity was done with a Metrohm 644 conductometer. The corresponding pH measurements were performed with a Metrohm E520 pH-meter. The use of a dynamic contact angle analyzer (DCAA), diffuse reflectance spectrometry (DRS) and scanning electron microscopy (SEM) will be explained in Chapters 4 and 5.

2.4 EXPERIMENTAL METHODOLOGY

2.4.1 Treatment of *para*-Chlorophenol

As stated before, p-CP was selected as model pollutant for a series of experimental runs aimed at evaluating the efficiency of the designed prototypes of PCO reactors. This was done in terms of defined system parameters and by using mainly OED approaches. Random parametric studies were also scheduled by using the conventional OFV method and by operating the reactor of choice in recirculation, single pass or sequential single pass mode. Screening and optimization studies were conducted using multi-parameter experimental designs in similar fashion.

- For the *recirculation mode* of operation, exponential first order kinetics were used to model reaction rates. The corresponding observed first order rate constants (in mins^{-1}) and half-lives (in mins) were obtained via normalization and logarithmic conversion of temporal concentration data. Initial reaction rates were obtained by the product of initial concentration and the observed rate constant (eqn 2.1) :

$$r_o = -dc(t)/dt = k_{obs} c_o \qquad (2.1)$$

where :
r_o = Initial rate (in concentration per time units)
$c(t)$ = Concentration as a function of time
c_o = Initial concentration
k_{obs} = Observed first order rate constant (in $mins^{-1}$)
t = Time (mins)

Naturally, eqn 2.1 also implies the standard first order exponential expression for concentration as function of time (eqn 2.2):

$$c(t) = c_o \exp(-k_{obs} t) \qquad (2.2)$$

The corresponding half-live ($t_{1/2}$) for 50 % removal of the initial concentration can be expressed as (eqn 2.3):

$$t_{1/2} = \ln 2 / k_{obs} \qquad (2.3)$$

In this work, the rate constants (k_{obs}) were constantly reported as "$10^2 k_{obs}$" values in order to facilitate their comparison and to circumvent exponential or decimal notation. For example, where a $10^2 k_{obs}$ value of 4.10 $mins^{-1}$ is reported, it actually refers to a k_{obs} of 4.10 x 10^{-2} or 0.0410 $mins^{-1}$.

- For the *single pass mode* of operation, a standard statistical response function (denoting the percentage of pollutant degradation) was adopted according to Castillo *et al.* (1997) (eqn 2.4):

$$\% D = 100 \times [(p\text{-}CP)_0 - (p\text{-}CP)_E] / (p\text{-}CP)_0 \qquad (2.4)$$

where:
$\% D$ = Percentage of degradation
$(p\text{-}CP)_0$ = Initial p-CP concentration
$(p\text{-}CP)_E$ = Final p-CP concentration (after one single pass)

- For *sequential single pass mode* of operation, a response was constructed to denote the first order decay in concentration as a function of the number of single passes (N) (eqn 2.5). This response is analogous to conventional first order decay as a function of time:

$$c(N) = c_o \exp(-k_{obs}N) \qquad\qquad (2.5)$$

where :

$c(N)$ = Concentration as a function of single pass number
c_o = Initial concentration
k_{obs} = Observed first order rate constant (in passes^{-1})
N = Single pass number

By incorporating the UV residence time (contact time) per single pass for each reactor, eqn 2.5 can be converted to the conventional first order kinetic regime with time as independent parameter.

In this work, the linear regression of X-Y data (for two-dimensional graphs) was done via standard least squares fitting, as afforded by MS Excel. Accuracy of fitting was typically reported in terms of the correlation coefficient (R^2). Generally, a R^2 value greater than 0.9 was assumed to be statistically acceptable.

Analysis of Variance (ANOVA) was used as statistical aid for OED. This included an assessment of significance probabilities of parameters according to the null-hypothesis theory. Pareto-charts, contour plots and three-dimensional surfaces (linear and quadratic) were used as tools to report the OED results. A commercial software package (Statistica ®, Version 5, 1997) was used to conduct all OED and ANOVA. Statistical precision were expressed in terms of standard deviation (SD) and relative standard deviation (RSD) using the known conventional formulae (Brewer, 1980) and the software mentioned above. Statistical process control (SPC) was also executed in certain studies. The corresponding SPC charts were also generated with Statistica ®.

PEPs, as defined the first and final chapter, were calculated and compared for each reactor in terms of the PCO treatment of p-CP.

2.4.2 Treatment of Microcystins

Experimental test runs conducted with microcystins as model pollutant were limited to the recirculation mode of operation with the exception of one run (conducted in sequential single pass mode). Therefore, the conventional first order kinetic model was applied in similar fashion as the p-CP scenario for the same mode. Normalization of data was executed in cases where batch-to-batch variations and matrix effects caused high SD for equivalent starting concentrations.

Microcystin spiking material was limited throughout the entire period of this work, hence comprehensive screening and optimization studies were discarded in favor of conventional OFV in a series of random parametric studies. Precision analyses were limited to SD and RSD as before.

PEPs, as defined the final chapter, were calculated and compared for each reactor in terms of the PCO treatment of microcystins.

CHAPTER 2 - REFERENCES

BARNARDT N (1997) *Personal communication*. Enviro Services cc, Weltevredenpark, Gauteng, RSA.

BATEMAN KP, THIBAULT P, DOUGLAS DJ and WHITE RL (1995) Mass spectral analyses of microcystins from toxic cyanobacteria using on-line chromatographic and electrophoretic separations. *J. Chromatogr. A* **712** 253-268.

BENNETT PA and VAN DER MERWE J (1995) Photocatalytic oxidation – a safe and clean alternative in TOC analysis. *Water Sewage & Effluent* **15** 7-9.

BLAZKOVA A, CSOLLEOVA I and BREZOVA V (1998) Effect of light sources on the phenol degradation using Pt/TiO$_2$ photocatalysts immobilized on glass fibres. *J. Photochem. Photobiol. A: Chem.* **113** 251-256.

BOLTON JR (1999) *Ultraviolet Applications Handbook*. Bolton Photosciences Inc., Ayr, Ontario, Canada (ISBN 0-9685432-0-0).

BOLTON JR (1999a) UV-disinfection of drinking water: Low-pressure, medium-pressure and pulse lamps. In: *Proceedings of Workshop on Advanced Oxidation Technologies*, Albuquerque, New Mexico, USA. 35-44.

BRASQUET C, BOURGES B and LE CLOIREC P (1999) Quantitative structure-property relationship (QSPR) for the adsorption of organic compounds onto activated carbon cloth: Comparison between multiple linear regression and neural network. *Environ. Sci. Technol.* **33** 4226-4231.

BRASQUET C, ROUSSY J, SUBRENAT E and LE CLOIREC P (1996) Adsorption and selectivity of activated carbon fibers application to organics. *Environ. Technol.* **17** 1245-1252.

BREWER S (1980) *Solving problems in analytical chemistry*. John Wiley & Sons, New York, USA. 8.

CARMICHAEL WW (1992) Cyanobacterial secondary metabolites-the cyanotoxins. *J. Appl. Bacteriol.* **72** 445-459.

CARMICHAEL WW (1994) The toxins of cyanobacteria. *Scientific American* **27** 64-72.

CASTILLO L, EL KHORASSANI H, TREBUCHON P and THOMAS O (1997) UV treatability test for chemical and petrochemical wastewater. In: *Proceedings of the International Association on Water Quality (IAWQ) Specialized Conference on Chemical Process Industries and Environmental Management*, Cape Town, South Africa, Paper P.1.4.

DONATI C, DRIKAS M, HAYES R and NEWCOMBE G (1994) Microcystin-LR adsorption by powdered activated carbon. *Wat. Res.* **28** 1735-1742.

FEITZ AJ, WAITE TD, JONES GJ, BOYDEN BH and ORR PT (1999) Photocatalytic degradation of the blue-green algal toxin microcystin-LR in a natural organic aqueous matrix. *Environ. Sci. Technol.* **33** 243-249.

FREUDENHAMMER H, BAHNEMANN D, BOUSSELMI L, GEISSEN SU, GHRABI A, SALEH F, SI-SALAH A, SIEMON U and VOGELPOHL A (1997) Detoxification and recycling of wastewater by solar-catalytic treatment. *Wat. Sci. Tech.* **35** 149-156.

HAND DW, CRITTENDEN JC and PERRAM DL (1993) Destruction of DBP precursors using photo-assisted heterogeneous catalytic oxidation. *Final report to the AWWA Research Foundation, USA*. (ISBN 0-89867-655-X).

HITZFELD BC, HOGER SJ and DIETRICH DR (2000) Cyanobacterial Toxins: Removal during water treatment and human risk assessment. *Environ. Health Perspect.* **108** 113-122.

HOFFMANN MR, MARTIN ST, CHOI W and BAHNEMANN DW (1995) Environmental applications of semiconductor photocatalysis. *Chem. Rev.* **95** 69-96.

LAM AKY, FEDORAK PM and PREPAS EE (1995) Biotransformation of the cyanobacterial hepatotoxins microcystin-LR, as determined by HPLC and protein phosphatase bioassay. *Environ. Sci. Technol.* **29** 242-246.

LAWTON LA, EDWARDS C and CODD GA (1994) Extraction and high-performance liquid chromatographic method for the determination of microcystins in raw and treated waters. *Analyst* **119** 1525-1530.

LAWTON LA and ROBERTSON PKJ (1999) Physico-chemical treatment methods for the removal of microcystins (cyanobacterial hepatotoxins) from potable waters. *Chem. Soc. Rev.* **28** 217-224.

LE CLOIREC P, BRASQUET C and SUBRENAT E (1997) Adsorption onto fibrous activated carbon: applications to water treatment. *Energy & Fuels* **11** 331-336.

MANSFIELD J (2000) *Personal communication*. Cape Water Programme, Environmentek, CSIR, Stellenbosch, South Africa.

MARTIN CA, ALFANO OM and CASSANO AE (1999) UV radiation + hydrogen peroxide decolorization of waters for domestic supply. In: *Proceedings of The 5th International Conference on Advanced Oxidation Technologies for Water and Air Remediation*, Albuquerque, New Mexico, USA. 3-4.

MILLS A and MORRIS S (1993) Photomineralisation of 4-chlorophenol sensitised by titanium dioxide: a study of the initial kinetics of carbon dioxide photogeneration. *J. Photochem. Photobiol. A: Chem.* **71** 75-83.

NICHOLSON BC, ROSITANO J and BURCH MD (1994) Destruction of cyanobacterial peptide hepatotoxins by chlorine and chloramine. *Wat. Res.* **28** 1297-1303.

NIEUWOUDT TW (1997) Application of the photocatalytic process to the treatment of tannery waste. *M.Sc. (Chemistry) Thesis, University of Stellenbosch, South Africa*.

NISHIWAKI-MATSUSHIMA R, OHTA T, NISHIWAKI S, SUGANUMA M, KOYAMA K, ISHIKAWA T, CARMICHAEL WW and FUJIKI H (1992) Liver tumor promotion by the cyanobacterial cyclic peptide toxin microcystin LR. *J. Cancer Res. Clin. Oncol.* **118** 420-424.

OLLIS DF, PELIZZETTI E and SERPONE N (1989) Heterogeneous photocatalysis in the environment: Application to water purification. In: *Photocatalysis: Fundamentals and Applications*, Serpone N and Pelizzetti E (eds.), John Wiley & Sons, New York, USA. 603-637.

PIETERSE SA (1997) *Personal communication*. Scientific Services Branch, Cape Town Metropolitan Council, Cape Town, RSA.

RAY AK (1999) Design, modelling and experimentation of a new large-scale photocatalytic reactor for water treatment. *Chem. Eng. Sci.* **54** 3113-3125.

ROBERTSON PKJ, LAWTON LA, MUNCH B and CORNISH B (1999) The destruction of cyanobacterial toxins by titanium dioxide photocatalysis. *J. Adv. Oxid. Technol.* **4** 20-26.

ROBERTSON PKJ, LAWTON LA, MUNCH B and ROUZADE J (1997) Destruction of cyanobacterial toxins by semiconductor photocatalysis. *Chem. Commun.* 393-394.

SHEPHARD GS (1997) *Personal communication*. Programme on Mycotoxins and Experimental Carcinogenesis, Medical Research Council, Tygerberg, RSA.

STOCKENSTROM S, DE VILLIERS D, ENGELBRECHT WJ, SHEPHARD GS, SYDENHAM EW, THIEL PG and WESSELS GFS (1996) Photocatalytic decomposition of microcystins in water. *Proceedings of IXth IUPAC International Symposium on Mycotoxins and Phycotoxins*, Rome, Italy. (ISBN-1-880293-09-9)

TSUJI K, WATANUKI T, KONDO F, WATANABE MF, SUZUKI S, NAKAZAWA H, SUZUKI M, UCHIDA H and HARADA K (1995) Stability of microcystins from cyanobacteria – Effect of UV light decomposition and isomerization. *Toxicon* **33** 1619-1631.

VAN HALDEREN A, HARDING WR, WESSELS JC, SCHNEIDER DJ, HEINE EWP, VAN DER MERWE J and FOURIE JM (1995) Cyanobacterial (blue-green algae) poisoning of livestock in the Western Cape province of South Africa. *J. S.Afr. Vet. Ass.* **66** 260-264.

WHO (1998) *Guidelines for drinking-water quality. Second edition, Addendum to Volume 2, Health criteria and other supporting information*. World Health Organization, Geneva, Switzerland.

WICKS RJ and THIEL PG (1990) Environmental factors affecting the production of peptide toxins in floating scums of the cyanobacterium *Microcystis aeruginosa* in a hypertrophic African reservoir. *Environ. Sci. Technol.* **24** 1413-1418.

CHAPTER 3

EVALUATION OF REACTOR 1

OVERVIEW

This chapter contains a comprehensive evaluation of Reactor 1 operated in three different modes and assessed for the PCO of two model pollutants in water, i.e. p-CP and cyanobacterial microcystin toxins. A number of system parameters are evaluated by the conventional OFV approach, however, basic screening en response surface OED are also utilized to monitor and optimize the responses associated with the PCO degradation of the primary model pollutant (p-CP).

3.1 TREATMENT OF *para*-CHLOROPHENOL

3.1.1 Recirculation Mode

(a) System Parameters

The photocatalytic oxidation (PCO) treatment of p-CP in water was investigated in a random parametric study using one-factor variation (OFV) for each experiment. The following system parameters were evaluated at discrete levels in terms of first order reaction kinetics and half-lives (see Table 3.1).

Note: The standard reference level for each parameter was used throughout unless stated otherwise by the study in question. This applies to all work reported further on.

Table 3.1: System parameters for p-CP study (Reactor 1; Recirculation Mode)

Parameter	Assigned Levels
Catalyst Suspension Loading (g/L)	0; 1*; 2.5; 5; 10; 20; 30
Volumetric Flow Rate (mL/min.)	225[a]; 750*[b]
Horizontal Irradiation Distance (cm)	2; 8*
p-CP Initial Concentration (mg/L)	5; 13; 40*; 70; 100
Reaction Volume (L)	3*; 6
Water Matrix	Distilled*; De-ionized; Tap
Initial Slurry pH	3; 5*; 7; 9; 11
Gas Purge	Oxygen*; Air; Argon
Oxygen Flow Rate (L/min.)	5*; 20
Number of UV-C lamps	2[c]; 8*[d]

* Denotes standard reference level of parameters
a Surface flow rate = 53.5 L/hr/m^2
b Surface flow rate = 178.5 L/hr/m^2
c UV irradiance   = 238 W/m^2 = 2 x 30W lamps (per 0.252 m^2)
d UV irradiance   = 954 W/m^2 = 8 x 30W lamps (per 0.252 m^2)

(b)   Catalyst Suspension Loading

Introduction and Objectives:

The effect of catalyst suspension loading was examined by comparing results for 7 different loadings of TiO_2 (0; 1; 2.5; 5; 10; 20 and 30 g/L). The objectives of this study were to (1) establish a region of maximum PCO treatment of p-CP and (2) assess the effect of UV photolysis.

81

Results and Discussion:

Table 3.2: p-CP concentration data (in mg/L) as a function of time and catalyst suspension loading.

Irradiation Time (mins)	Catalyst Suspension Loading (g/L TiO_2)						
	0	1*	2.5	5	10	20	30
0	40.0	40.0	40.0	40.0	40.0	40.0	40.0
5	37.1	34.2	26.9	24.0	21.8	20.5	24.4
10	35.5	29.0	22.5	15.5	15.0	10.5	16.1
15	32.9	22.2	18.2	11.0	9.8	7.6	11.9
30	30.0	12.3	4.5	3.9	2.1	0.9	4.1
45	27.2	6.5	ND	ND	ND	ND	ND
60	24.8	ND**					
10^2 k_{obs} (mins^{-1})	0.76	4.10	7.12	7.60	9.63	12.44	7.43
Half-life (mins)	91.2	16.9	9.7	9.1	7.2	5.6	9.3
R^2	0.98	0.99	0.97	0.99	0.99	0.99	0.99

* Denotes standard reference level of parameter
ND** = Not Detected; Limit of Detection (LOD) = 1 mg/L
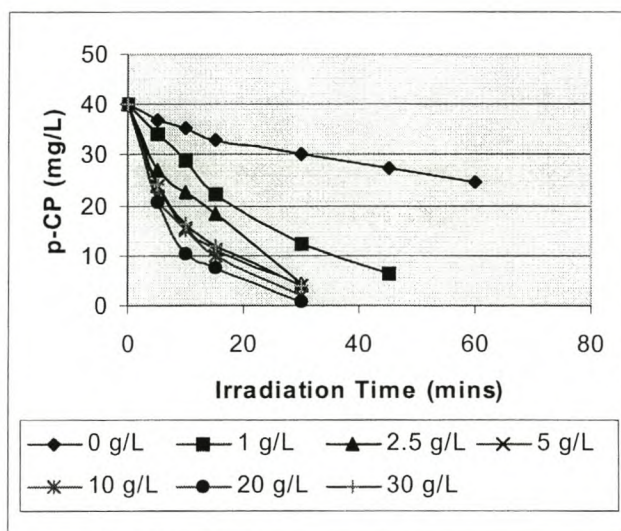
Figure 3.1: p-CP oxidation as a function of time and catalyst suspension loading (g/L TiO_2).
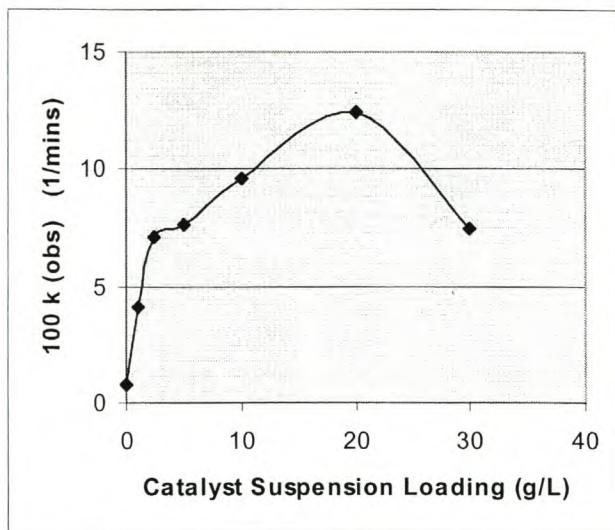
Figure 3.2: Reaction rate constant as a function of catalyst suspension loading (g/L TiO$_2$).
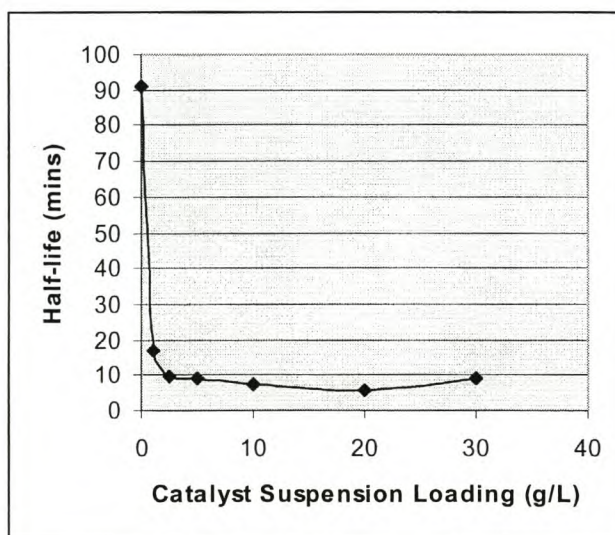
Figure 3.3: Half-life as a function of catalyst suspension loading (g/L TiO$_2$).

The results obtained from these experiments (Table 3.2; Figures 3.1 to 3.3) indicated that :

- first order exponential decay kinetics apply for the TiO$_2$ assisted PCO of p-CP;
- the observed first order rate constant (k$_{obs}$) increases with an increase in catalyst suspension loading, yielding a maximum rate around 20 g/L TiO$_2$;
- beyond a loading of 20 g/L TiO$_2$ a marked decrease in rate is observed. This is ascribed to pronounced UV shielding effects and problems related to maintaining catalyst particles in suspension;
- the half-lives for p-CP removal are significantly reduced (by one order of magnitude) when increasing the catalyst suspension loading from 0 to 2.5 g/L ;
- UV photolysis of p-CP (at 0 g/L TiO$_2$) is possible, but at a significantly slower rate compared to TiO$_2$ photocatalysis.

(c)   Volumetric Flow Rate

Introduction and Objectives:

The effect of volumetric flow rate was examined by comparing results for a reduced flow rate (225 mL/min) against the standard flow rate (750 mL/min) used. The objectives of this study were to (1) assess the positive effect of a higher number of recycles (obtained when using higher flow rate) and (2) assess the auxiliary effect of a thin falling film (obtained when using lower flow rates).

Results and Discussion:

Table 3.3: p-CP concentration data (in mg/L) as a function of time and volumetric flow rate.

Irradiation Time (mins)	Volumetric Flow Rate (mL/min.)	
	225	750*
0	40.0	40.0
5	32.7	34.2
10	26.1	29.0
15	25.0	22.2
30	19.8	12.3
45	16.3	6.5
60	11.8	ND**
$10^2 \, k_{obs}$ (mins^{-1})	1.83	4.10
Half-life (mins)	37.9	16.9
R^2	0.96	0.99

* Denotes standard reference level of parameter
ND** = Not Detected; LOD = 1 mg/L
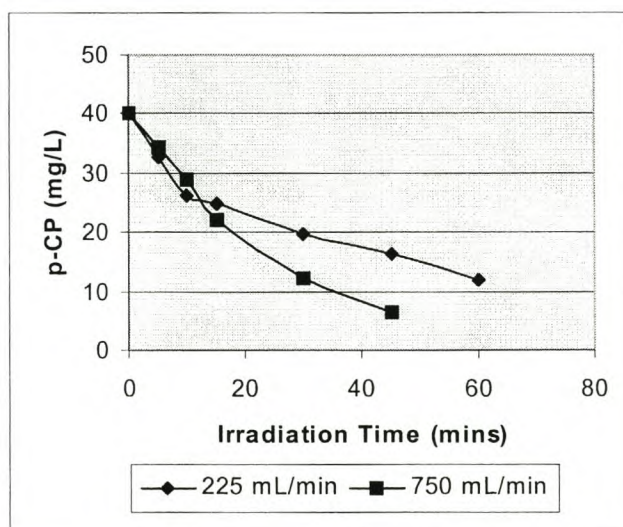
Figure 3.4: p-CP oxidation as a function of time and volumetric flow rate (mL/min).

84

The results obtained from these experiments (Table 3.3 and Figure 3.4) indicated that :

- the observed first order rate constant (k_{obs}) increases with an increase in volumetric flow rate. This is ascribed to a higher recirculation rate obtained at higher flow rate;
- the effect of a thin falling film will be more pronounced when using low flow rates for shorter periods of irradiation, e.g. in a single pass reactor with UV contact times in the order of seconds.

(d)   Horizontal Irradiation Distance

Introduction and Objectives:

Horizontal irradiation distance (HID) represents the mean distance between the circular configuration of UV lamps and the irradiated surface, viz. the cylindrical tube in Reactor 1 (see Appendices A and B). The effect of HID was examined by comparing results for a reduced distance (2 cm) against the standard distance (8 cm) used. The objective of this study was to determine whether it was beneficial for the PCO process to minimize HID by assembling the UV lamps at the closest distance possible.

Results and Discussion:

Table 3.4: p-CP concentration data (in mg/L) as a function of time and HID.

Irradiation Time (mins)	Horizontal Irradiation Distance (cm)	
	2	8*
0	40.0	40.0
5	35.8	34.2
10	33.0	29.0
15	28.7	22.2
30	21.2	12.3
45	15.8	6.5
60	12.1	ND**
$10^2 \, k_{obs}$ (mins^{-1})	2.01	4.10
Half-life (mins)	34.5	16.9
R^2	0.99	0.99

* Denotes standard reference level of parameter
ND** = Not Detected; LOD = 1 mg/L
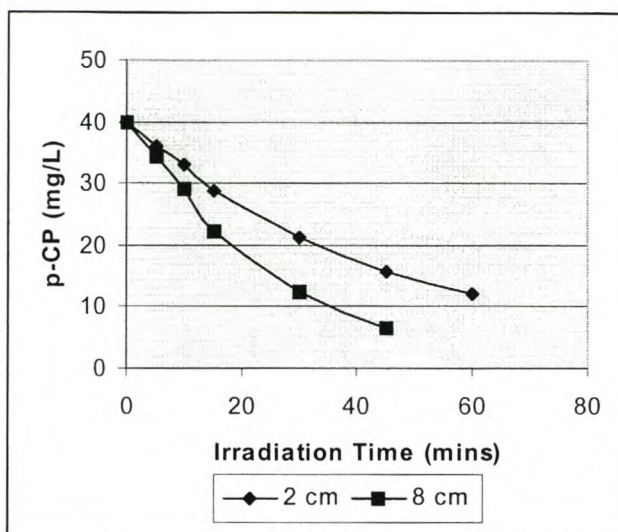
Figure 3.5: p-CP oxidation as a function of time and horizontal irradiation distance (cm).

The results obtained from these experiments (Table 3.4 and Figure 3.5) indicated that :

- the observed first order rate constant (k_{obs}) decreases with a decrease in horizontal irradiation distance from 8 to 2 cm. It is postulated that the inhibiting effect is due to localized irradiation and reduced reflection on isolated portions of the irradiated surface at 2 cm distance. Thus far, this effect has been unknown for the UV light source employed ;
- excess lamp contamination occurs at 2 cm distance with minute droplets of catalyst slurry settling on lamp envelopes, possibly contributing to reduced lamp efficiency.

(e)   p-CP Initial Concentration

Introduction and Objectives:

The effect of initial concentration was examined by comparing results for 5 different loadings of p-CP (5; 13; 40; 70 and 100 mg/L). The objectives of this study were to (1) locate a concentration region for maximum PCO of p-CP and (2) assess the validity of Langmuir-Hinshelwood kinetics in terms of the selected initial concentrations.

Results and Discussion:

Table 3.5: p-CP concentration data (in mg/L) as a function of time and initial p-CP concentration.

Irradiation Time (mins)	p-CP Initial Concentration (mg/L)				
	5	13	40*	70	100
0	5.0	13.0	40.0	70.0	100.0
5	1.9	8.1	34.2	59.1	85.1
10	0.9	5.8	29.0	53.5	79.9
15	ND**	4.5	22.2	47.2	72.2
30		1.0	12.3	37.5	60.2
45		ND	6.5	27.8	50.8
60			ND	20.8	43.1
75				13.5	38.9
90				8.5	34.5
120				ND	22.8
150					11.9
180					4.1
210					ND
$10^2 \, k_{obs}$ (mins^{-1})	17.15	8.38	4.10	2.19	1.51
Half-life (mins)	4.0	8.3	16.9	31.7	45.9
R^2	0.99	0.99	0.99	0.99	0.95

* Denotes standard reference level of parameter
ND** = Not Detected; Limit of Detection = 1 mg/L
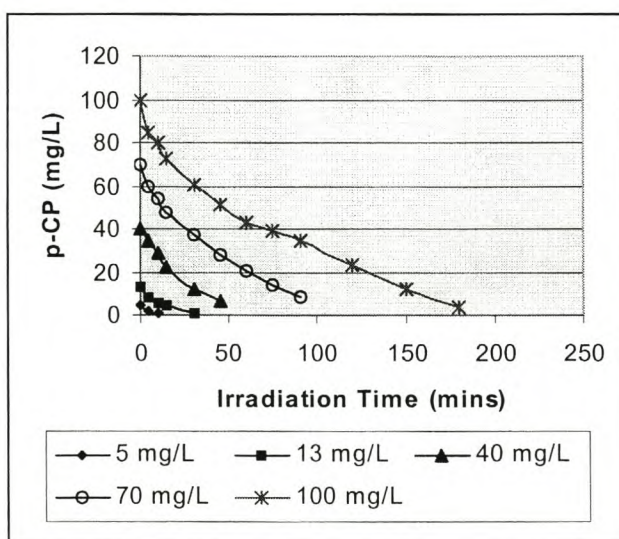
Figure 3.6: p-CP oxidation as a function of time and initial p-CP concentration (in mg/L).
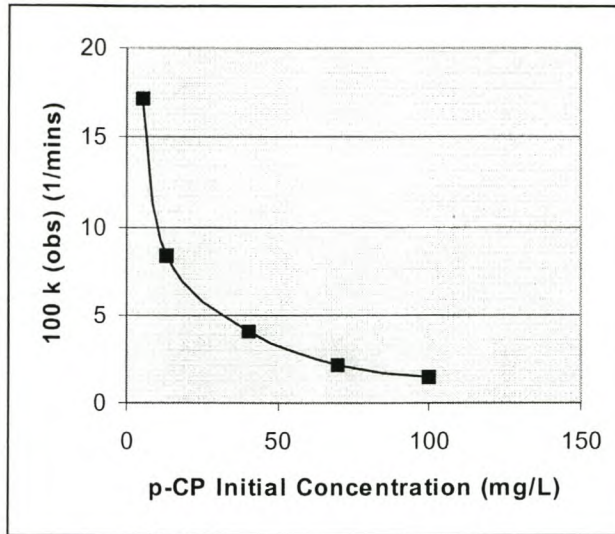
Figure 3.7: Reaction rate constant as a function of p-CP initial concentration (in mg/L).
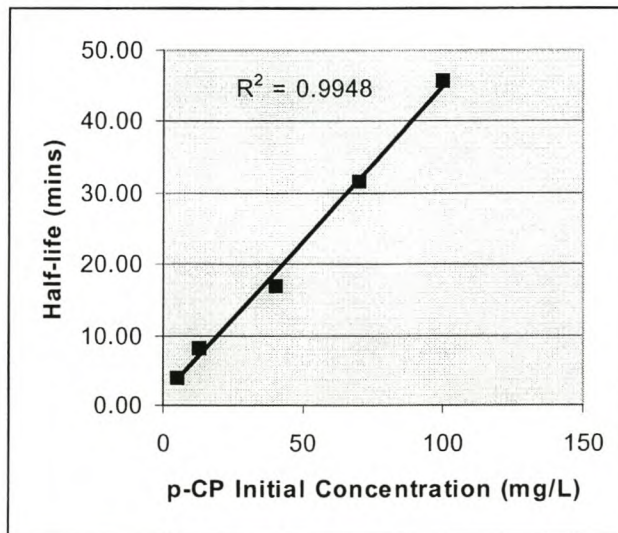
Figure 3.8: Half-life as a function of p-CP initial concentration (in mg/L).

The results obtained from the initial set of experiments (Table 3.5 and Figures 3.6 to 3.8) indicated that :

- the observed first order rate constants (k_{obs}) are inversely proportional to initial p-CP concentration. A hyperbolic dependence with increase in initial concentration from 5 to 100 mg/L is confirmed. The corresponding half-lives increased linearly as a function of initial concentration;
- the recirculation mode of operation is effective when treating low concentration levels of p-CP in water (viz: *ca* 5 to 40 mg/L).

In addition, the applicability of Langmuir-Hinshelwood (LH) kinetics was investigated by calculating the initial PCO reaction rates (R_o) for each initial concentration of p-CP from the product of initial concentration and the corresponding observed rate constant (Al-Sayyed et al., 1991; Herrmann, 1995; Herrmann, 1999) (Table 3.6).

A plot of R_o versus p-CP initial concentration ($[p-CP]_0$) yielded an asymptotic type relationship (Figure 3.9), thus confirming a change in reaction order as the concentration increased steadily. From 0 to 40 mg/L, the reaction rate increases linearly with increasing initial concentration, thus indicating apparent first order behavior. However, beyond 40 mg/L p-CP, the rate becomes independent of concentration, hence the PCO reaction probably becoming zero'th order (Herrmann, 1999).

The corresponding inverse plot of $1/R_o$ versus $1/([p-CP]_0$ yielded a linear trend with a slope of 0.327 min^{-1}, surprisingly similar to the sum of all the observed rate constants over the 5 to 100 mg/L range (0.333 min^{-1}) (see Table 3.6 and Figure 3.10). Adsorption constants and intrinsic reactivity constants were not calculated further.

Table 3.6: Langmuir-Hinshelwood kinetic calculations.

$[p-CP]_o$ (mg.L^{-1})	K_{obs} (min^{-1})	$R_o = k_{obs} \times [p-CP]_o$ (mg.L^{-1}.min^{-1})	$1/R_o$ (L.min.mg^{-1}).	$1/[p-CP]_o$ (L.mg^{-1})
5	0.1715	0.858	1.166	0.200
13	0.0838	1.089	0.918	0.077
40	0.0410	1.640	0.610	0.025
70	0.0219	1.533	0.652	0.014
100	0.0151	1.510	0.662	0.010
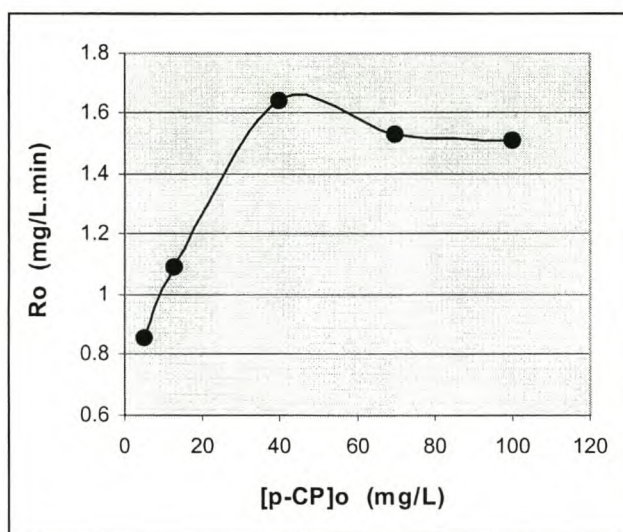
Figure 3.9: Initial PCO rate (R_o) as a function of initial p-CP concentration (in mg/L).
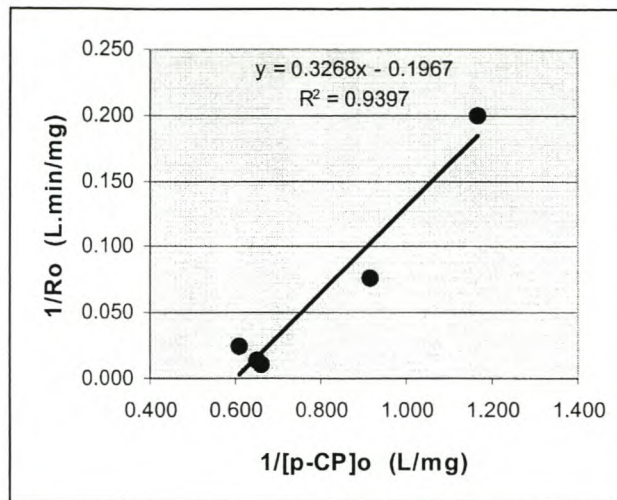
Figure 3.10: Inverse plot: Initial PCO rate ($1/R_o$) versus initial p-CP concentration ($1/[p\text{-}CP]_o$).

The observations stated above confirmed the heterogeneous surface catalyzed nature of the PCO process. Moreover, the PCO of p-CP achieved in this work were shown to display LH type kinetic behavior. The mass transferred adsorption of the p-CP substrate onto TiO_2, which contributed approximately 5-10% loss in initial concentration in the absence of UV irradiation, may be an important factor to take cognizance of. The latter effect, however, is dependent on several parameters and requires a more detailed study.

(f)   Reaction Volume

Introduction and Objectives:

The effect of reaction volume (viz: the total volume of water used per test run) was examined by comparing results for a 6 L volume against the standard volume of water used (3 L). The objective of this study was to determine whether an increase in reaction volume exerted an inhibitory effect on the PCO rate when operating Reactor 1 in recirculation mode.

Results and Discussion:

Table 3.7: p-CP concentration data in (mg/L) as a function of time and reaction volume.

Irradiation Time (mins)	Reaction Volume (L)	
	3*	6
0	40.0	40.0
5	34.2	36.5
10	29.0	32.5
15	22.2	29.1
30	12.3	23.3
45	6.5	18.6
60	ND**	14.4
$10^2 \ k_{obs}$ (mins^{-1})	4.10	1.67
Half-life (mins)	16.9	41.5
R^2	0.99	0.99

* Denotes standard reference level of parameter
ND** = Not Detected; LOD = 1 mg/L

Figure 3.11: p-CP oxidation as a function of time and reaction volume (in L).

The results obtained from these experiments (Table 3.7 and Figure 3.11) indicated that :

- the observed first order rate constant (k_{obs}) decreases markedly with a two-fold increase in reaction volume. This is ascribed to the larger amount of p-CP administered in the 6 L water sample and a lower recirculation rate achieved at constant volumetric flow rate;
- Reactor 1 is not suitable for treating large volumes of water in a recirculation mode of operation.

(g) Water Matrix Effects

Introduction and Objectives:

Water matrix effects were examined by comparing results for deionized and chlorine disinfected Stellenbosch tap water (see 2.3.1) against distilled water as standard water matrix. The objective of this study was to assess the effect of ionic strength and foreign ions (in terms of conductivity) on the PCO rate.

Results and Discussion:

Table 3.8: p-CP concentration data (in mg/L) as a function of time and water matrix.

Irradiation Time (mins)	Water Matrix		
	Distilled Water*	Deionized Water	Tap Water
0	40.0	40.0	40.0
5	34.2	29.8	35.2
10	29.0	24.8	32.5
15	22.2	21.4	30.2
30	12.3	11.4	22.8
45	6.5	4.9	20.1
60	ND**	ND	16.1
$10^2\ k_{obs}$ (mins^{-1})	4.10	4.49	1.47
Half-life (mins)	16.9	15.4	47.2
R^2	0.99	0.99	0.98

* Denotes standard reference level of parameter
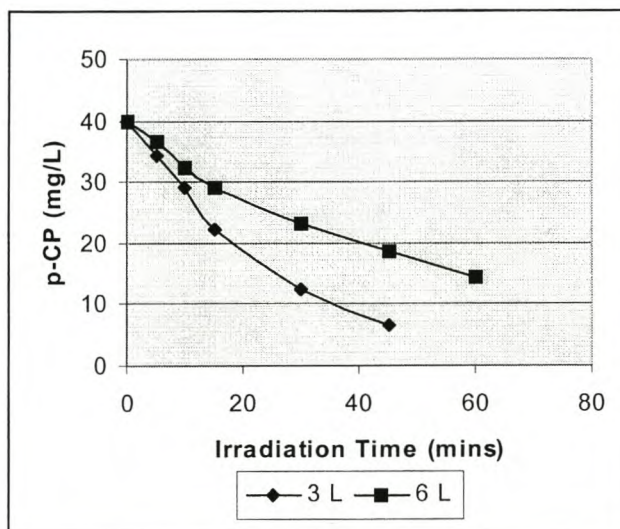**ND** = Not Detected; LOD = 1 mg/L**
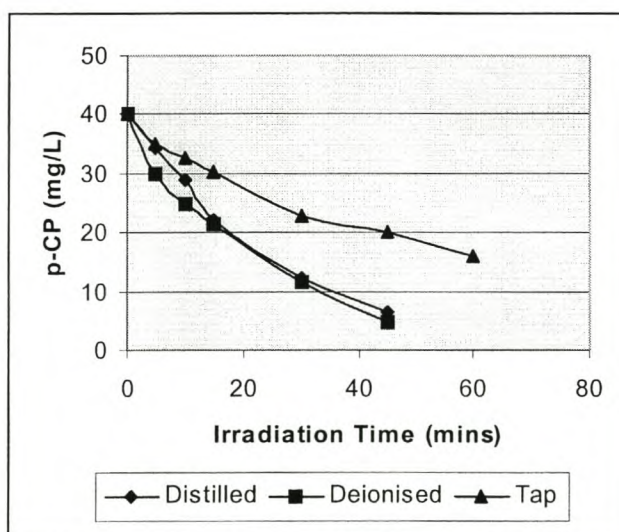
Figure 3.12: p-CP oxidation as a function of time and water matrix used.

92

The results obtained from these experiments (Table 3.8 and Figure 3.12) indicated that :

- the observed first order rate constants (k_{obs}) increases marginally when using de-ionized water as spiking matrix for p-CP as opposed to distilled water ;
- chloride ions (as end-product of p-CP oxidation) could be detrimental on the PCO rate *per se.* The chloride ions will compete with hydroxyl radicals, water molecules, p-CP and O_2 for adsorption sites on the TiO_2 surface. A reduction in reaction pH (as a result of HCl formation) is detrimental to PCO and needs to be addressed in detail;
- the PCO rate decreases markedly when using chlorine disinfected tap water. This could indicate the inhibiting effect of inorganic ions (e.g. HCO_3^- and CO_3^{2-}) and organic carbon (TOC) as potential hydroxyl radical scavenger agents (tap water conductivity: 80 uS/m; total alkalinity: *ca* 10-16 mg/L as $CaCO_3$). Further confirmation of NOM presence via UV analysis is required to confirm the observed result.

(h)   Initial pH

Introduction and Objectives:

The effect of pH was examined by comparing results for 4 different initial pH conditions against the standard pH of 5 (for a 1 g/L TiO_2 slurry). 1M NaOH and 1M HCl (and dilutions thereof) were used as additives to adjust the pH. The objective of this study was to investigate the behavior of the photocatalytic system under both acidic and alkaline slurry conditions.

Results and Discussion:

Table 3.9: p-CP concentration data (in mg/L) as a function of time and initial pH.

Irradiation Time (mins)	Initial Slurry pH				
	3	5*	7	9	11
0	40.0	40.0	40.0	40.0	40.0
5	35.1	34.2	34.9	37.2	36.5
10	30.3	29.0	29.9	34.3	34.1
15	23.5	22.2	22.5	29.4	32.5
30	14.5	12.3	13.3	21.8	28.5
45	7.2	6.5	6.8	16.8	25.6
60	ND**	ND	ND	12.6	22.5
$10^2 k_{obs}$ (mins^{-1})	3.81	4.10	3.98	1.96	0.91
Half-life (mins)	18.2	16.9	17.4	35.4	76.2
R^2	0.99	0.99	0.99	0.99	0.98

* Denotes standard reference level of parameter
ND = Not Detected; LOD = 1 mg/L**
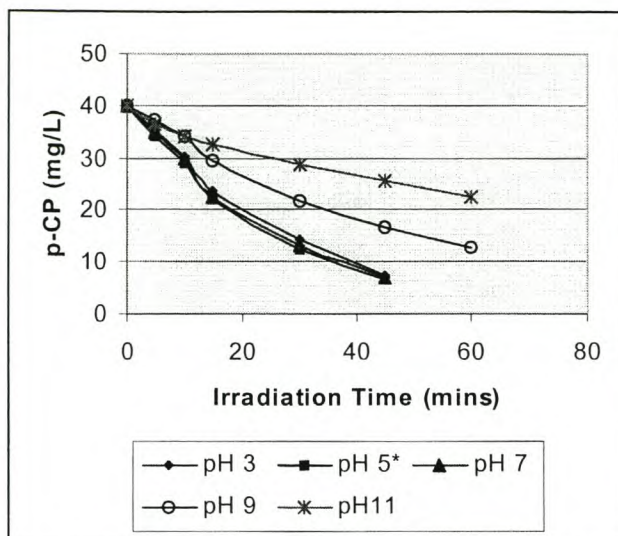
Figure 3.13: p-CP oxidation as a function of time and initial slurry pH.

Figure 3.14: Observed PCO rate constant as a function of initial slurry pH.

The results obtained from these experiments (Table 3.9 and Figures 3.13 to 3.14) indicated that :

- the observed first order rate constant (k_{obs}) is largely independent of pH in the range pH 3 to 7 (standard pH 5). This is ascribed to favorable adsorptive interaction of undissociated p-CP with TiO_2 (predominantly existing as TiOH species in this pH range);

- the PCO rate decreases markedly when increasing the slurry pH to 9 and 11 respectively. This is ascribed to electrostatic repulsion between dissociated p-CP (present as phenolate anions) and TiO_2 (present as TiO^- anions) (Hoffmann *et al.*, 1995; Cloete, 1999).

94

(i)   Gas Purge

Introduction and Objectives:

The effect of gas purge was examined by comparing results for compressed air and argon against pure oxygen used as standard gas purge. The objectives of this study were to (1) compare the rates of PCO when using pure oxygen and air and (2) investigate the behavior of the photocatalytic system in the absence of an oxygenated gas purge.

Results and Discussion:

Table 3.10: p-CP concentration data (in mg/L) as a function of time and gas purge used.

Irradiation Time (mins)	Gas Purge		
	Pure Oxygen*	Compressed Air	Argon
0	40.0	40.0	40.0
5	34.2	35.5	38.2
10	29.0	31.9	37.3
15	22.2	28.0	36.5
30	12.3	19.5	34.9
45	6.5	14.1	34.3
60	ND**	10.2	33.5
$10^2 \ k_{obs}$ (mins^{-1})	4.10	2.29	0.27
Half-life (mins)	16.9	30.3	256.7
R^2	0.99	0.99	0.90

* Denotes standard reference level of parameter
ND** = Not Detected; LOD = 1 mg/L
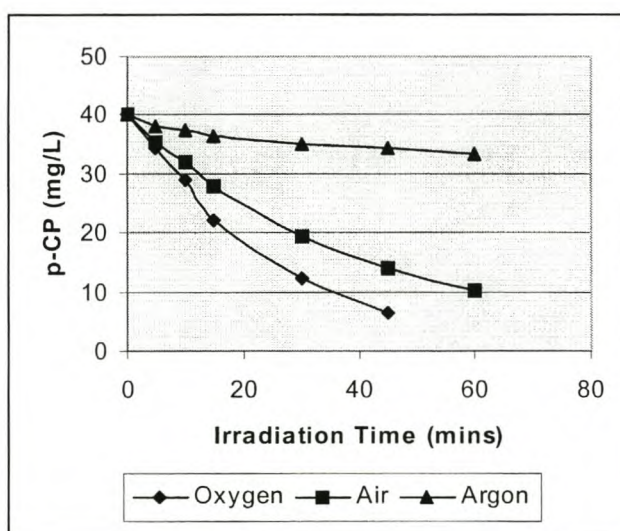
Figure 3.15: p-CP oxidation as a function of time and gas purge.

The results obtained from these experiments (Table 3.10 and Figure 3.15) indicated that :

- the observed first order rate constant (k_{obs}) for PCO decreases with approximately 50% when using compressed air at the standard gas flow rate of 5 L/min. This result is ascribed to the reduced oxygen content of air. Oxygen depletion may enhance charge recombination reactions and inhibit production of hydroxyl radicals;
- the PCO rate constant decreases further by one order of magnitude when using an argon purge. The net removal of a small amount of p-CP is ascribed to UV photolytic effects;
- use oxygen as gas purge is a prerequisite for efficient PCO.

(j)   Gas Flow Rate

Introduction and Objectives:

The effect of gas flow rate was examined by comparing results for 20 L/min O_2 against the standard gas flow rate of 5 L/min O_2. The objectives of this study were to (1) establish whether an increased oxygen flow rate will enhance oxidation and (2) assess the observed effect in terms of reaction time, mode of operation and reactor type.

Results and Discussion:

Table 3.11: p-CP concentration data (in mg/L) as a function of time and O_2 flow rate.

Irradiation Time (mins)	Oxygen Gas Flow Rate (L/min.)	
	5*	20
0	40.0	40.0
5	34.2	29.6
10	29.0	23.5
15	22.2	18.5
30	12.3	8.8
45	6.5	4.1
60	ND**	ND
$10^2 \, k_{obs}$ (mins^{-1})	4.10	5.00
Half-life (mins)	16.9	13.9
R^2	0.99	0.99

* Denotes standard reference level of parameter
ND** = Not Detected; LOD = 1 mg/L
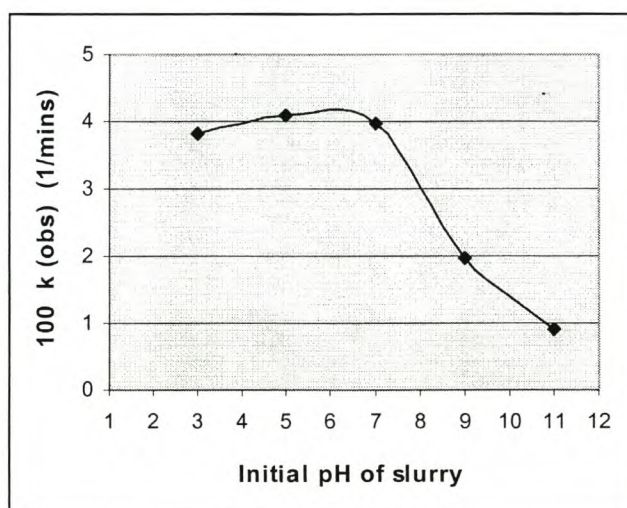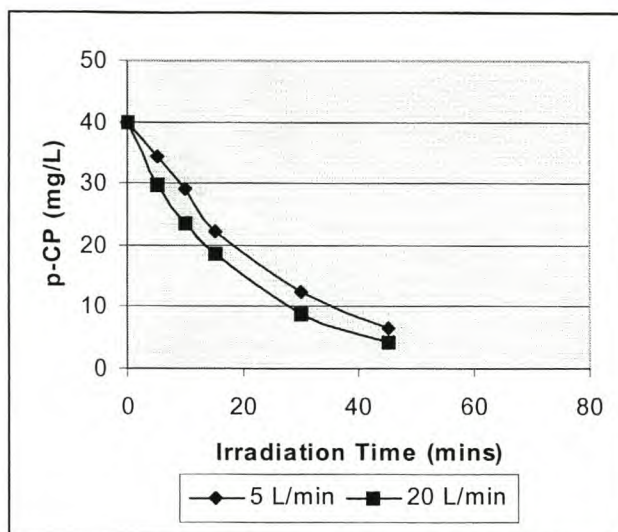
Figure 3.16: p-CP oxidation as a function of time and O_2 gas flow rate (L/min.).

The results obtained from these experiments (Table 3.11 and Figure 3.16) indicated that :

- the observed first order rate constant (k_{obs}) for PCO increases only marginally when increasing the oxygen gas flow rate from 5 of 20 L/min., hence dependence of reaction rate on oxygen flow rate are less important in this instance. Oxygen concentration, however, is considered significant (as shown in the previous section);
- aqueous TiO_2 suspensions used for PCO are sufficiently saturated with pure oxygen at low gas flow rates. This is possibly due to longer reaction times utilized in recirculation mode experiments;
- the positive auxiliary effect of increased oxygen flow rate may be more pronounced when using operation modes with shorter UV contact times (e.g. the single pass mode);
- a slurry-phased continuously stirred tank reactor (CSTR), such as Reactor 1, can be operated efficiently in recirculation mode using economical (low) oxygen flow rates;
- reduction in operational costs for slurried configurations (such as Reactor 1) can probably be achieved in recirculation mode by using high air flow rates (viz: lower O_2 concentrations, but longer reaction times).

(k)   UV Irradiance

Introduction and Objectives:

The effect of UV irradiance (radiant flux) was examined by comparing results for irradiation experiments conducted with two UV germicidal lamps against the standard (maximum) number of lamps used in Reactor 1 (eight). The irradiation experiment with two lamps comprised a 180° configuration, viz: using lamps assembled at directly opposite ends of the circular array (see Appendix A). The objectives of this study were to (1) determine whether a 75% reduction in UV irradiance (W/m^2) rendered a proportional reduction in PCO rate and (2) explain the observed deterioration or improvement in performance.

Results and Discussion:

Table 3.12: p-CP concentration data (in mg/L) as a function of time and UV irradiance.

Irradiation Time (mins)	Number of UV lamps used for Irradiation	
	2 lamps (238.4 W/m^2)	8* (953.6 W/m^2)
0	40.0	40.0
5	36.3	34.2
10	33.9	29.0
15	31.5	22.2
30	27.5	12.3
45	23.4	6.5
60	20.4	ND**
$10^2 k_{obs}$ (mins^{-1})	1.08	4.10
Half-life (mins)	64.2	16.9
R^2	0.99	0.99

* Denotes standard reference level of parameter
ND** = Not Detected; LOD = 1 mg/L
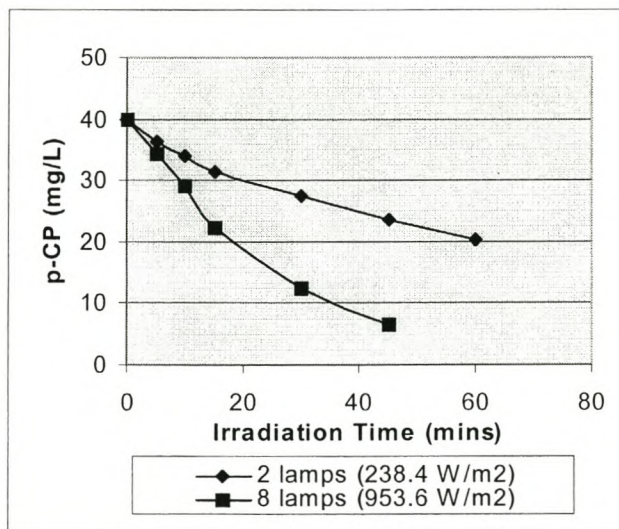
Figure 3.17: p-CP oxidation as a function of time and UV irradiance (in W/m^2).

98

The results obtained from these experiments (Table 3.12 and Figure 3.17) indicated that :

- the observed first order rate constant (k_{obs}) for PCO is reduced by approximately 75% when applying 2 UV lamps for irradiation (in a 180° configuration) as opposed to the standard number of 8 lamps. This result correlates with the 75% reduction in UV irradiance (radiant flux), i.e. from 953.6 W/m^2 (8 lamps) to 238.4 W/m^2 (2 lamps);
- the PCO rate *could be* linearly dependent on UV irradiance in the region examined (*ca* 240- 950 W/m^2), however more experimental data points at intermediate irradiances will be required to confirm this statement. A linear dependence indicates efficient utilization of UV light photons for oxidation (Herrmann, 1995; Herrmann, 1999). This may be attributed to (1) minimized loss of UV radiation (2) efficient reflection characteristics (3) high illuminated specific surface area (κ) and (4) efficient catalyst-analyte interaction in the slurry-phased Reactor 1.

(I)   Mineralization Test

Introduction and Objectives:

As mentioned in the previous chapter (2.3), UV spectrometry was primarily used as screening tool for p-CP in water. *One* representative p-CP sample, however, was subjected to PCO treatment in Reactor 1 to determine the degree of mineralization in terms of total organic carbon (TOC). For this purpose a calibration curve, as was shown in Figure 2.5, was used to relate p-CP concentration to TOC values (in mg C/L).

For this test, a low temperature TOC analyzer (ANATOC) was used (Bennett and Van der Merwe, 1995). ANATOC is operated on the principle of TiO_2 mediated PCO of the organic content of the target samples. A catalyst suspension of 0.2% $^w/_v$ Degussa P-25 TiO_2 (in combination with two 8 W blacklight fluorescent tubes) defines the photocatalytic system within the instrument. Organic carbon content is decomposed in aqueous medium to yield CO_2, H_2O and the acid, base or salt of any inorganic constituents. The CO_2 gas evolved through oxidation is captured in a conductivity cell. The corresponding conductivity signal is used to produce a reading in TOC units. $CO_2 – HCO_3^- - H_2CO_3$ equilibria as a function of pH is also taken into account.

Instrument calibration was done with a standard 200 mg C/L solution of benzoic acid. To ensure accurate and consistent TOC analyses, it was necessary to adjust the pH of each sample to a value below pH 5 to render a maximum yield of CO_2 from oxidation of TOC within each sample. Suggested pH levels were between 3.5 and 4.0. pH adjustments were done with 0.1 M solutions of perchloric acid and NaOH to obtain the required pH 3.5. A standard sample injection volume of 1000µL was used throughout.

The preceding PCO test run was conducted at the standard reference levels of each system parameter (see Table 3.1). The initial p-CP concentration was 40 mg/L.

Results and Discussion:

Table 3.13: p-CP concentration data (in mg/L) and TOC (in mgC/L) as a function of time.

Irradiation Time (mins)	TOC and p-CP parameters	
	TOC (mgC/L)	[p-CP] (mg/L)
0	26.5	40.0
5	23.3	34.2
10	20.3	29.0
15	16.5	22.2
30	11.0	12.3
45	7.7	6.5
60	3.9	ND**

ND = Not Detected; LOD for UV analysis = 1 mg/L**
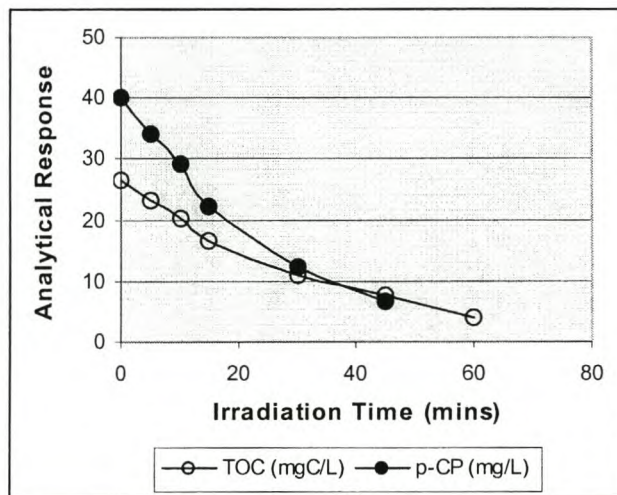
Figure 3.18: Comparison of TOC and p-CP analyses for the temporal diminution of p-CP via PCO.

The results obtained from this experiment (Table 3.13 and Figure 3.18) indicated that :

- the PCO of p-CP is accompanied by a diminution in TOC, hence a degree of mineralization does occur;
- at 60 minutes reaction time a residual TOC still exists in the water despite a non-detection of p-CP via UV analysis. This could be attributed to either (1) incomplete mineralization and the formation of refractory intermediates such as carboxylic acids (2) TOC generated from the TiO_2 itself (Siemon et al., 1999) (3) incomplete removal of CO_2 generated from the PCO reactor prior to TOC analysis (Offringa, 2000), or (4) substantial error variation as a result of combined UV and TOC analyses.

The continuous determination of TOC was discarded in this work for reasons already explained in 2.3.1.

3.1.2 Single Pass Mode

(a)   System Parameters

The PCO treatment of p-CP in water was investigated using (1) one-factor variation for random parametric studies (2) two-level experimental designs for screening studies and (3) response surface designs for optimization studies. A global statistical formula was adopted as response function to denote the percentage of pollutant degradation (%D) (see Section 2.4.1). The following system parameters were evaluated as discrete levels in terms of the percentage degradation (Table 3.14):

Table 3.14: System parameters for p-CP study (Reactor 1; Single Pass Mode)

Parameter	Assigned Levels
Catalyst Suspension Loading (g/L)	0; 1; 5; 10; 20; 30
Volumetric Flow Rate (mL/min.)	50; 225[a]; 400; 575; 750[*b]
Horizontal Irradiation Distance (cm)	2; 8*
p-CP Initial Concentration (mg/L)	3; 5; 13; 27; 40*; 70; 100
Reaction Volume (L)	3*; 6
Water Matrix Effects	Distilled*
Solution pH	3; 5*; 7; 9; 11
Gas Purge	Oxygen*; Air
Gas Flow Rate (L/min.)	5*; 20
Number of UV-C lamps	0; 1; 2[c]; 4; 8[*d]

* Denotes standard reference level of parameters
a Surface flow rate = 53.5 L/hr/m^2
b Surface flow rate = 178.5 L/hr/m^2
c UV irradiance   = 238 W/m^2 = 2 x 30W lamps (per 0.252 m^2)
d UV irradiance   = 954 W/m^2 = 8 x 30W lamps (per 0.252 m^2)

(b)   Screening Study

Introduction and Objectives:

Seven parameters were identified for an initial screening study (Tables 3.14 and 3.15). The objectives were to (1) obtain a rough estimate of the effects of the various parameters on the response function (2) eliminate insignificant parameters in accordance with the Pareto Principle (3) identify important parameters for optimization purposes and (4) evaluate the application of a highly fractionated (1/16th) two-level factorial design in a screening study (i.e. an orthogonal array). The result for each degradation response (%D) was reported as the mean from a triplicate set of runs (SD = 1 %). Responses outside the SD limit were discarded.

Results and Discussion:

Table 3.15: Design matrix for screening study (orthogonal array : OA 8.7.2.2).

Run	Catalyst Suspension Loading (g/L)	Volumetric Flow Rate (mL/min.)	Gas Purge	Gas Flow Rate (L/min.)	Initial p-CP Conc. (mg/L)	Reaction Volume (L)	HID (cm)	D** (%)
1	1	225	Air	5	13	3	2	41.4
2	30	225	Oxygen	5	40	3	8	63.2
3	1	750	Oxygen	5	13	6	8	45.3
4	30	750	Air	5	40	6	2	35.5
5	1	225	Air	20	40	6	8	28.7
6*	30	225	Oxygen	20	13	6	2	68.9
7	1	750	Oxygen	20	40	3	2	36.1
8	30	750	Air	20	13	3	8	42.2

a HID = Horizontal Irradiation Distance
* Best result in terms of degradation constant (run 6)
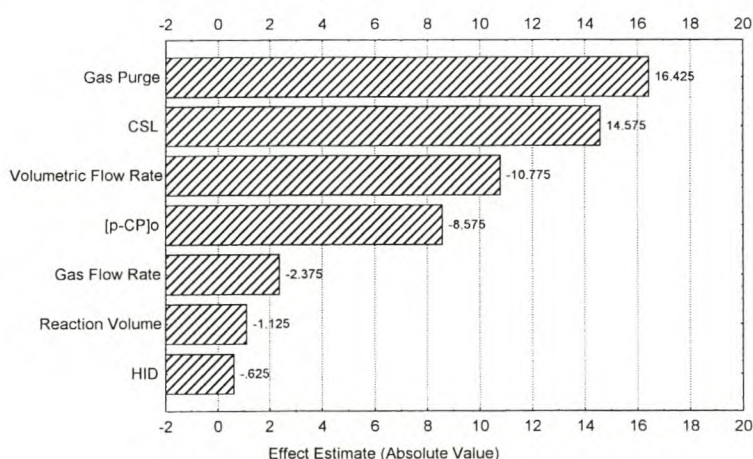** D = Degradation of p-CP (%); SD = ± 1 %.

Figure 3.19: Pareto chart illustrating parameter effects with respect to % D response function. (CSL = Catalyst Suspension Loading; [p-CP]o = p-CP Initial Concentration in mg/L; HID = Horizontal Irradiation Distance in cm)

The results obtained from these experiments (Table 3.15 and Figure 3.19) indicated that :

- gas purge with oxygen has a highly beneficial effect on PCO efficiency, while a higher gas purge flow rate does not have such a highly beneficial effect. More economical lower flow rates could be considered;
- a higher catalyst suspension loading has a highly beneficial effect on PCO efficiency. An optimum loading would be necessary;
- a higher volumetric flow rate has a substantial negative effect on PCO efficiency for single pass mode of operation. This is ascribed to limited penetration of UV photons through a denser falling film when applying a higher flow rate;
- p-CP initial concentration has an intermediate negative effect on the PCO efficiency for the single pass mode of operation. This observation confirms the utility of Reactor 1 for the treatment of low concentrations of pollutant ;
- the volume of polluted water passed through the reactor has a negligible effect. This observation confirms the utility of Reactor 1 for treating large volumes of water when operated in single pass mode;
- the horizontal distance of the lamps has a negligible effect. Although this observation is in contrast with the result obtained for the analogous experiment in recirculation mode, it can be explained in terms of the physical constraints of the reactor design and the complex interaction that exists between parameters when conducting a multi-parameter experiment;
- parameter main effects are calculated successfully when using highly fractionated factorial designs in tandem with linear mathematical models. This observation indicates the utility of the selected *orthogonal array* design in terms of multi-parameter screening. ANOVA significance probabilities, however, are not calculated due to an insufficient number of degrees of freedom;
- parameter effects are confounded with each other when applying quadratic (polynomial) modeling. The calculation of parameter interactions is therefore precluded.

Based on the results obtained above, it was decided to (1) assess the effects of catalyst suspension loading, volumetric flow rate and initial p-CP concentration individually through OFV (2) keep the remainder of the parameters fixed at standard reference levels (Table 3.14) that were considered to be economical or suitable for further experimentation.

(c)   Catalyst Suspension Loading & Volumetric Flow Rate

Introduction and Objectives:

The effects of catalyst suspension loading and volumetric flow rate were examined in a series of OFV experiments resembling a 5 x 4 matrix design. Five different loadings of TiO_2 were selected (1; 5; 10; 20 and 30 g/L) and treatment results thereof compared at four different volumetric flow rates (225; 400; 575 and 750 mL/min) for a p-CP initial concentration of 40 mg/L. The remainder of the system parameters was fixed at their standard reference levels. The objectives of this study were to (1) assess the individual effects of the two parameters on the response function over their respective ranges and (2) view the combined effect via a 3-dimensional representation without mathematical modeling.

Results and Discussion:

Table 3.16: Matrix design for catalyst suspension loading and volumetric flow rate study. %D responses are shown in the last four rows of the last five columns to the right.

Volumetric Flow Rate (mL/min.)	Catalyst Suspension Loading (g/L TiO_2)				
	1	5	10	20	30
225	44.9	55.1	64.2	68.4	63.2
400	35.3	46.2	54.3	54.5	55.0
575	30.1	37.8	43.8	44.2	44.3
750	30.2	33.1	35.2	35.9	40.3
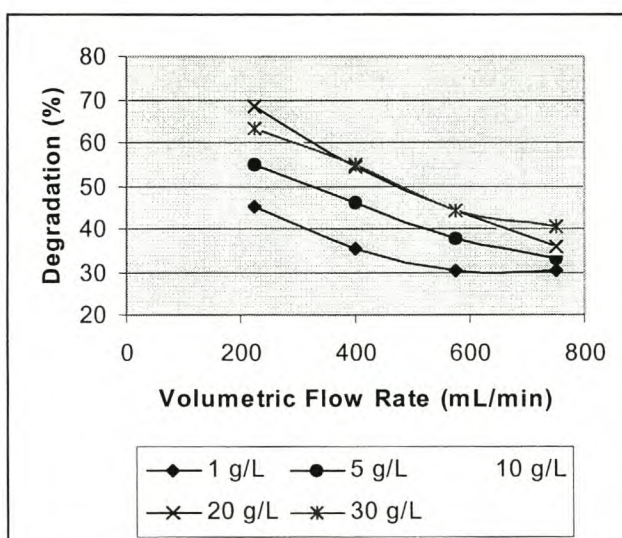
Figure 3.20: Degradation (%) as a function of volumetric flow rate for various catalyst suspension loadings (g/L TiO_2).
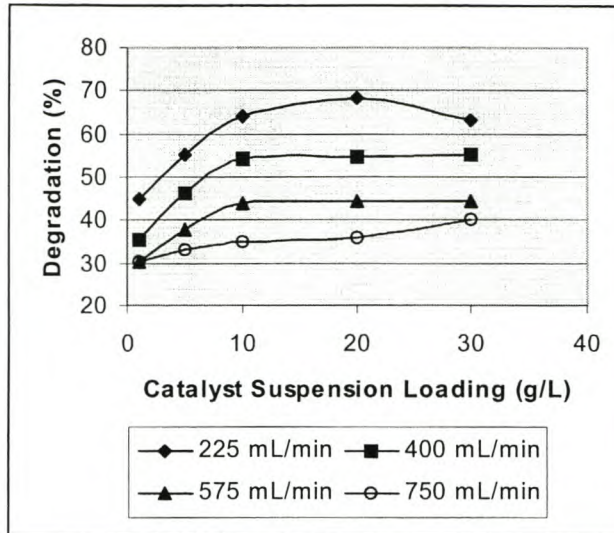
Figure 3.21: Degradation (%) as a function catalyst suspension loading for various volumetric flow rates (mL/min).
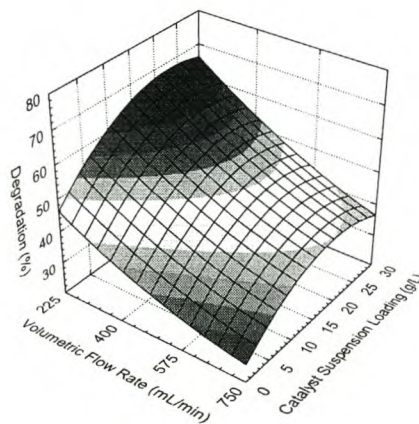
Figure 3.22: Three-dimensional representation illustrating the combined effects of volumetric flow rate and catalyst suspension loading on the % degradation of 40 mg/L p-CP.

The results obtained from these experiments (Table 3.16 and Figures 3.20 to 3.22) indicated that:

- an increase in catalyst suspension loading generally enhances PCO. This is in accordance with earlier results obtained in recirculation mode. The positive effect increases significantly with a reduction in volumetric flow rate;
- a decrease in volumetric flow rate generally enhances PCO. This is explained in terms of a thinner falling film attained at lower flow rate, which facilitates the penetration of UV light. The effect of flow rate is enhanced by increasing the catalyst suspension loading;
- the effect of catalyst suspension loading on the response is dependent on the magnitude of volumetric flow rate viz: (1) for a relatively low flow rate (225 mL/minute)

an optimum catalyst suspension loading (20 g/L) is attained from a quadratic type response curve (2) for intermediate flow rates (400-575 mL/min) a plateau value (10 g/L) is attained from an asymptotic curve and (3) for a high flow rate (750 mL/min) the response curve is linear, indicating a steady increase in catalyst suspension loading. The latter result naturally implies that responses (viz: the PCO efficiency) could be further increased at higher flow rate when applying loadings beyond 30 g/L TiO_2. This is an advantageous result in terms of practical application at high flow rate;

- the combined effect of the two parameters produces a saddle-like "rising ridge" surface when plotted in 3 dimensions against the response function (% Degradation). In this instance, no mathematical modeling was used. This demonstrates the utility of the matrix design to generate a true three-dimensional image of the combined influence exerted by the parameters on the response function.

(d)   UV Photolysis

Introduction and Objectives:

The effect of UV photolysis (in the absence of TiO_2 catalyst) was examined for various volumetric flow rates. The objectives of this study were to (1) assess and compare the efficiency of UV photolysis to TiO_2 photocatalysis and (2) obtain information regarding the falling film effect as a function of volumetric flow rate under UV photolytic conditions.

Results and Discussion:

Table 3.17: UV photolytic efficiencies as a function of volumetric flow rate.

Volumetric Flow Rate (mL/min.)	Degradation (%)
225	40.5
400	30.9
575	25.6
750	20.2
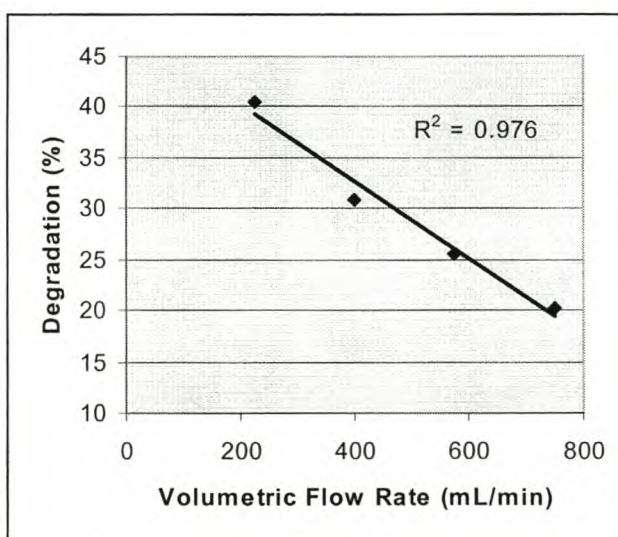
Figure 3.23: Degradation (%) as a function of volumetric flow rate under UV photolytic conditions.

106

The results obtained from these experiments (Table 3.17 and Figure 3.23) indicated that :

- UV photolysis of p-CP in water is feasible ;
- UV photolytic degradation efficiency increases linearly with a decrease in volumetric flow rate. This observation is attributed to a thinner falling film obtained at low flow rate;
- TiO_2 mediated PCO is superior to UV photolysis under identical conditions, although the disparity is less pronounced at low flow rate as a result of the thin film effect.

(e)   UV Irradiance

Introduction and Objectives:

The effect of UV irradiance (radiant flux) was examined by varying the number of UV lamps used for irradiation during a single pass experiment. A catalyst suspension loading of 10 g/L TiO_2 and a volumetric flow rate of 750 mL/minute were used. The objectives of this study were to (1) determine PCO efficiency as a function of UV irradiance and (2) to assess the efficiency of the reactor in terms of the nature of the UV irradiance response curve.

Results and Discussion:

Table 3.18: p-CP concentration data (in mg/L) for UV irradiance study.

Number of UV lamps used for irradiation	Theoretical UV irradiance (W/m^2)	Initial p-CP Concentration (mg/L)	Final p-CP Concentration (mg/L)	Degradation (%)
0	0	40.0	38.5	3.8
1	119.2	40.0	37.1	7.3
2	238.4	40.0	36.0	10.0
4	476.8	40.0	33.4	16.5
8	953.6	40.0	25.9	35.3

Figure 3.24: Degradation (%) as a function of UV irradiance (in W/m^2).

107

The results obtained from these experiments (Table 3.18 and Figure 3.24) indicated that :

- PCO degradation efficiency increases linearly with an increase in UV irradiance;
- less than 4% p-CP is lost due to mass transfer effects (in the absence of UV irradiation);
- based on the linear nature of the UV irradiance response curve, Reactor 1 represents an efficient photocatalytic design in terms of radiation characteristics.

(f)   p-CP Initial Concentration

Introduction and Objectives:

The effect of initial concentration was examined by comparing results for 7 different loadings of p-CP (3; 5; 13; 27; 40; 70 and 100 mg/L). A catalyst suspension loading of 1 g/L TiO_2 and a volumetric flow rate of 750 mL/min were used. The objectives of this study were to (1) determine the PCO efficiency of the single pass reactor for ultra-low and shock loadings respectively and (2) locate a region of maximum PCO degradation efficiency, if possible.

Results and Discussion:

Table 3.19: p-CP concentration data (in mg/L) for initial concentration study.

Initial p-CP Concentration (mg/L)	Final p-CP Concentration (mg/L)	Degradation (%)
3.0	2.1	30.0
5.0	3.4	32.0
13.0	6.9	46.9
27.0	18.5	31.5
40.0	27.9	30.2
70.0	56.8	18.9
100.0	85.7	14.3

Figure 3.25: Degradation (%) as a function of initial concentration of p-CP (in mg/L).

The results obtained from these experiments (Table 3.19 and Figure 3.25) indicated that :

- Reactor 1 is mostly suited for the removal of low concentrations of p-CP when operated in single pass mode. This is in accordance with results achieved earlier using the recirculation mode of operation;
- an optimum region of degradation exists when using an initial concentration of approximately 13 mg/L p-CP. This concentration is equivalent to 10^{-4} M.

(g)   Initial pH

Introduction and Objectives:

The effect of pH was examined by comparing results for a range of initial pH conditions (pH 2.3-11.9) against the standard pH of 5 (for a 1 g/L TiO_2 slurry). 1M NaOH and 1M HCl (and dilutions thereof) were used as additives to adjust pH. The experiments were conducted with the standard volumetric flow rate (750 mL/minute). The objective of this study was to investigate the behavior of the photocatalytic system under both acidic and alkaline slurry conditions.

Results and Discussion:

Table 3.20: p-CP concentration data (in mg/L) for pH study.

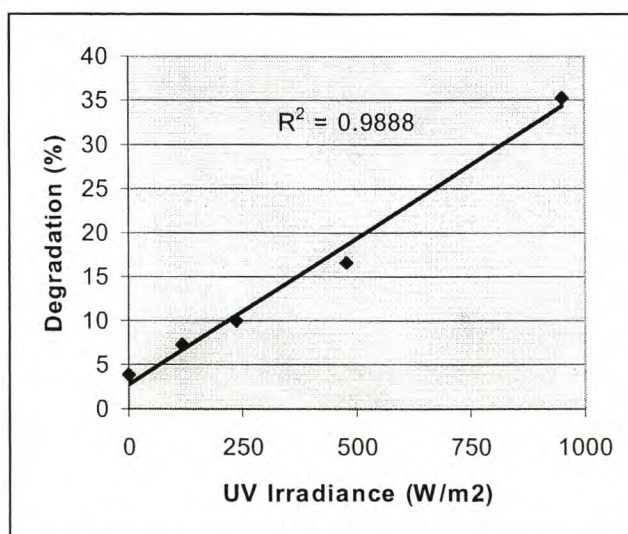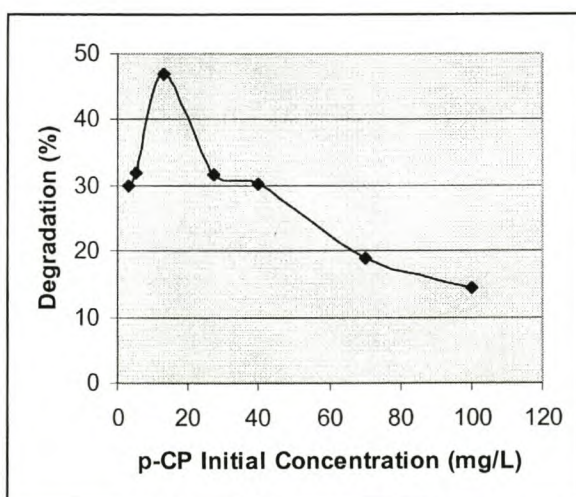| 10^5 [HCl] (M)	10^5 [NaOH] (M)	Initial slurry pH	Degradation (%)
1000	NApp*	2.3	15.0
100	NApp	3.0	23.3
50	NApp	3.4	24.3
10	NApp	4.2	26.9
5	NApp	4.4	27.9
1	NApp	4.7	28.2
0	0	5.0	33.0
NApp*	1	5.2	30.2
NApp	5	6.4	27.7
NApp	10	7.3	27.1
NApp	50	9.8	25.8
NApp	100	10.5	17.8
NApp	1000	11.9	14.8

NApp* = Not applicable.
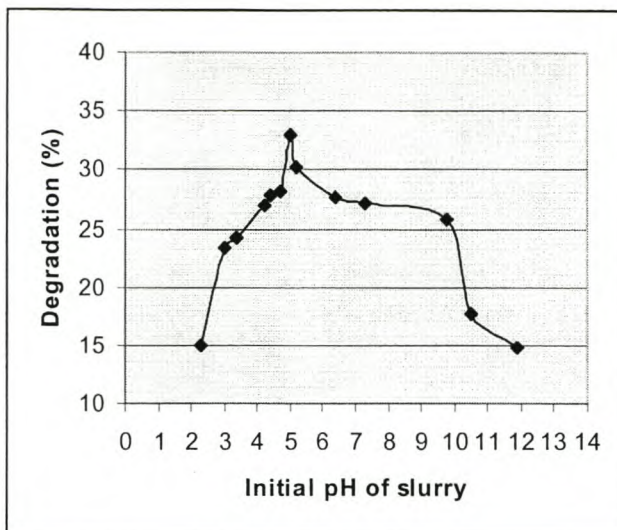
Figure 3.26: Degradation (%) as a function of initial slurry pH.

The results obtained from these experiments (Table 3.20 and Figure 3.26) indicated that :

- PCO degradation efficiency is marginally affected by pH in the region pH 4 to 10. This is ascribed to favorable adsorptive interaction of undissociated p-CP with TiO_2 (predominantly existing as TiOH species in this pH range);
- maximum efficiency is obtained at the natural pH of 5 for a 1 g/L TiO_2 slurry. It is concluded that the photocatalytic system is sensitive to the presence of inorganic ions in the reaction medium. This is possibly due to the fact that these species are blocking surface sites on the catalyst and thus hampering surface catalyzed PCO of p-CP;
- increasing the concentration of HCl or NaOH additive, thus moving further away from the natural slurry pH of 5, affects PCO degradation more substantially. The poor PCO degradation efficiency around pH 2 is ascribed to pronounced blocking of surface sites due by excess chloride ions, while a similar result around pH 12 is ascribed to weak electrostatic repulsion between dissociated p-CP (present as phenolate anions) and TiO_2 (present as TiO^- anions) ;
- no drastic change in PCO efficiency occurs around the point of zero charge (PZC) of TiO_2 (i.e. at pH 6.2).

(h)   Optimization Example

Introduction and Objectives:

Based on all previous results, two parameters (i.e. catalyst suspension loading and volumetric flow rate) were identified for an optimization study using a response surface design in conjunction with a polynomial mathematical model (Table 3.21). The initial concentration of p-CP was 40 mg/L, while the remainder of the system parameters were fixed at their standard reference levels (as listed in Table 3.14). The objectives of this study were to (1) monitor the behavior of the response function in the optimal region (2) fine-tune the optimum conditions for catalyst suspension loading and volumetric flow rate and (3) assess the utility of a Doehlert uniform array as potential experimental design in response surface optimization procedures.

Results and Discussion:

Table 3.21: Design matrix for optimization study (Doehlert uniform array).

Run	Catalyst Suspension Loading (g/L)	Volumetric Flow Rate (mL/min.)	Degradation (%)
1	20	225.0	68.4
2	21	242.5	61.1
3	22	225.0	65.5
4	21	207.5	63.0
5	19	207.5	67.4
6	18	225.0	65.3
7	19	242.5	64.1
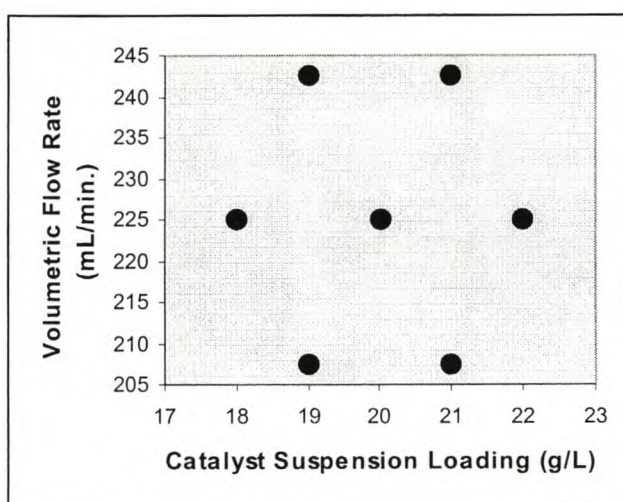
Figure 3.27: Graphic illustration of the uniform Doehlert array with experimental treatments (●).

111
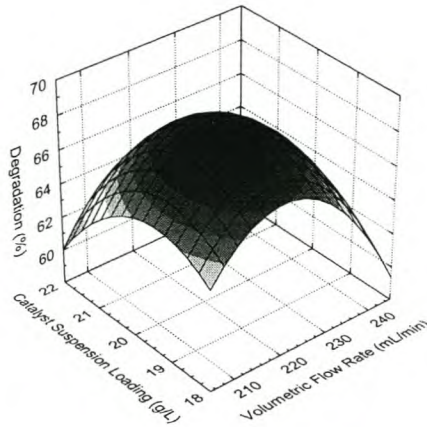
Figure 3.28: Three-dimensional response surface illustrating the combined effects of volumetric flow rate and catalyst suspension loading on the % degradation of 40 mg/L p-CP.
Quadratic model : $Z = -733.117 + 5.036\,X + 24.917\,Y - 0.012\,X^2 + 0.02\,XY - 0.75\,Y^2$
(Z = % Degradation; X = Volumetric flow rate; Y = Catalyst suspension loading)
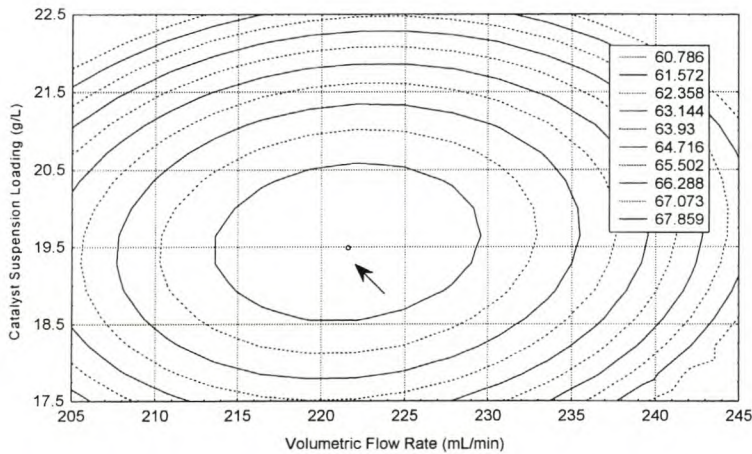
Figure 3.29: Two dimensional contour plot illustrating the existence of optimum conditions for catalyst suspension loading (*ca* 19.5 g/L TiO$_2$) and volumetric flow rate (*ca* 221.5 mL/min).

The results obtained from these experiments (Table 3.21 and Figures 3.27 to 3.29) indicated that:

- a parabolic response surface (denoting the existence of optimum conditions) is successfully generated with the aid of a Doehlert uniform array ;
- the optimum conditions (Figure 3.28) for catalyst suspension loading and volumetric flow rate are *ca* 19.5 g/L TiO$_2$ and *ca* 221.5 mL/minute for the single pass mode of operation ;
- despite the relative small variation in response values, the technique of Response Surface Methodology remains an efficient means for establishing optimum conditions via mathematical modeling.

3.1.3 Sequential Single Pass Mode

(a)   System Parameters

The PCO treatment of p-CP in water was investigated in terms of the defined first order kinetic responses for sequential single pass mode of operation (see Section 2.4.1). The following system parameters were evaluated at discrete levels (Table 3.22):

Table 3.22: System parameters for p-CP study
(Reactor 1; Sequential Single Pass Mode)

Parameter	Assigned Levels
Catalyst Suspension Loading (g/L)	1*; 20
Volumetric Flow Rate (mL/min.)	225[a]; 750*[b]
Horizontal Irradiation Distance (cm)	8*
p-CP Initial Concentration (mg/L)	40*
Reaction Volume (L)	3*
Water Matrix Effects	Distilled*
Gas Purge	Oxygen*
Gas Flow Rate (L/min.)	5*
Number of UV-C lamps	8*[c]

* Denotes standard reference level of parameters
a Surface flow rate = 53.5 L/hr/m^2
b Surface flow rate = 178.5 L/hr/m^2
c UV irradiance   = 954 W/m^2 = 8 x 30W lamps (per 0.252 m^2)

(b)   Representative Example

Introduction and Objectives:

The sequential single pass operation of Reactor 1 corresponds with a UV residence time (contact time) of 2.1 sec per single pass (N). Test runs were conducted by preparing fresh batches of catalyst for each single pass, thus eliminating catalyst deactivation effects as a function of pH. System parameters were fixed at the levels specified in Table 3.22. A catalyst suspension loading of 20 mg/L TiO_2 and a volumetric flow rate of 225 mL/min. were used. The objectives of this study were to (1) determine the theoretical number of passes required to reduce 40 mg/L of p-CP to below the limit of detection (1 mg/L) at near optimized conditions for catalyst suspension loading and volumetric flow rate and (2) compare the kinetic results with those obtained when operating the reactor in recirculation mode.

Results and Discussion:

Table 3.23: Kinetic analysis of sequential single pass experiment.

Number of Single Passes (N)	Cumulative Contact Time of Irradiation (sec)	p-CP Concentration (mg/L)	Cumulative Degradation (%)
0	0.0	40.0	0.0
1	2.1	12.8	68.0
2	4.2	4.1	89.8
3	6.3	1.5	96.3
4	8.4	ND*	>97.5
5	10.5	ND	>97.5
6	12.6	ND	>97.5
Independent Parameter	$10^2 k_{obs}$	Half-Life	R^2
Single Pass Number (N)	ca 110 passes⁻¹	ca 0.6 passes	0.99
Irradiation Time (sec)	ca 53.3 sec⁻¹	ca 1.3 secs	0.99
Irradiation Time (mins)	ca 3200 mins⁻¹	ca 0.02 mins	0.99

ND*= Not detected; LOD = 1 mg/L
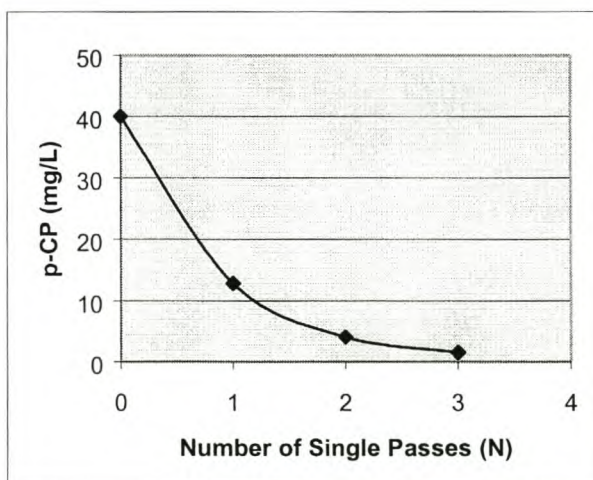
Figure 3.30: p-CP oxidation as a function of single pass number (N) where N = 2.1 sec for *each* pass.

114
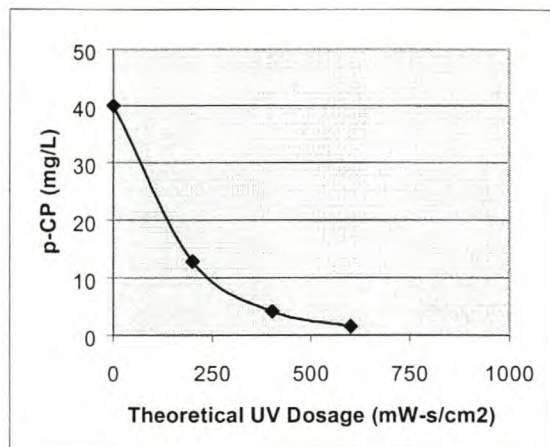
Figure 3.31: p-CP oxidation as a function of theoretical UV dosage (in mW-sec/cm^2).

The results obtained from this experiment (Table 3.23 and Figures 3.30 to 3.31) indicated that:

- first order exponential decay kinetics apply to the PCO of p-CP when operating Reactor 1 in sequential single pass mode ;
- the initial p-CP concentration of 40 mg/L decreases to below the detection limit (1 mg/L) within 4 single passes of the reactor ;
- a theoretical UV dosage in the order of 800 mW-s/cm^2 was required to achieve the result. This dosage is equivalent to approximately 8.5 seconds of UV exposure in the reactor ;
- the first order rate constants (in mins^{-1}) are generally 3 orders of magnitude greater than the analogous rate constants in recirculation mode, hence the sequential single pass mode of operation is significantly more efficient in terms of UV dosages (viz: irradiation times).

(c)   Scaling-up Potential

Introduction:

The sequential single pass mode can be utilized for scaling-up of the reactor system. The appropriate approach would be to use an array of reactors and split streams (branched networks) in order to make provision for high and low settings of volumetric flow rate (VFR) and possibly catalyst suspension loading (CSL).

The exponential decay of p-CP in the sequential single-pass mode was followed through a branched network defined in terms of CSL, with VFR as stream divisions. The corresponding series of experiments entailed the PCO treatment of each sample at constant CSL (either 1 or 20 g/L) by using two different VFR settings (i.e. 225 and 750 mL/min.) and the residual p-CP concentration brought over from the previous PCO treatment. Each experimental observation involved the use of fresh batches of TiO$_2$ (in distilled water) spiked with the designated p-CP concentration, as derived from the previous layer of the network. This was done to eliminate the effects of catalyst deactivation through residual pH variation. Two networks were generated, i.e. for a CSL of 1 and 20 g/L respectively. The network results are depicted in Figure 3.32:

Results and Discussion:
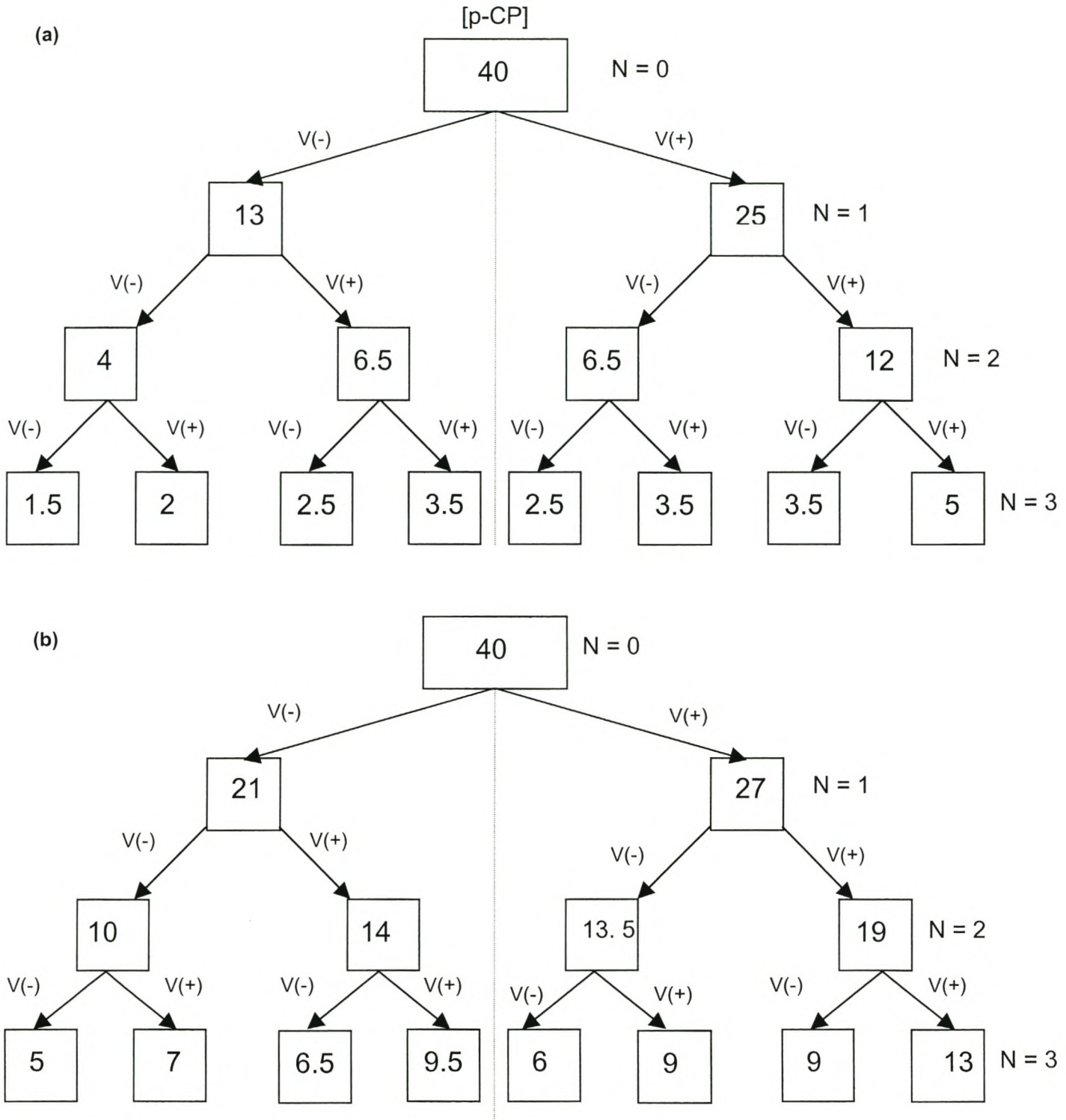
Figure 3.32: Branched networks indicating residual p-CP concentrations (in mg/L) after 3 sequential single pass treatments. Network (a) CSL = 20 g/L ; Network (b) CSL = 1 g/L. V(-) = 225 mL/min. ; V(+) = 750 mL/min. ; N = single pass number.

The results obtained from these experiments (Figures 3.32) indicated that:

- the PCO efficiency in the network reaches a maximum when using the higher catalyst suspension loading at the lower volumetric flow rate;
- the intermediate routes in the network display *commutative* behavior. This implies that, for a given concentration of p-CP, two consecutive treatments using opposite VFR settings produce the same end-result in terms of residual p-CP concentration. This phenomenon simplifies the branched networks appreciably to render binomial-type networks according to Pascal's triangle (Figure 3.33).
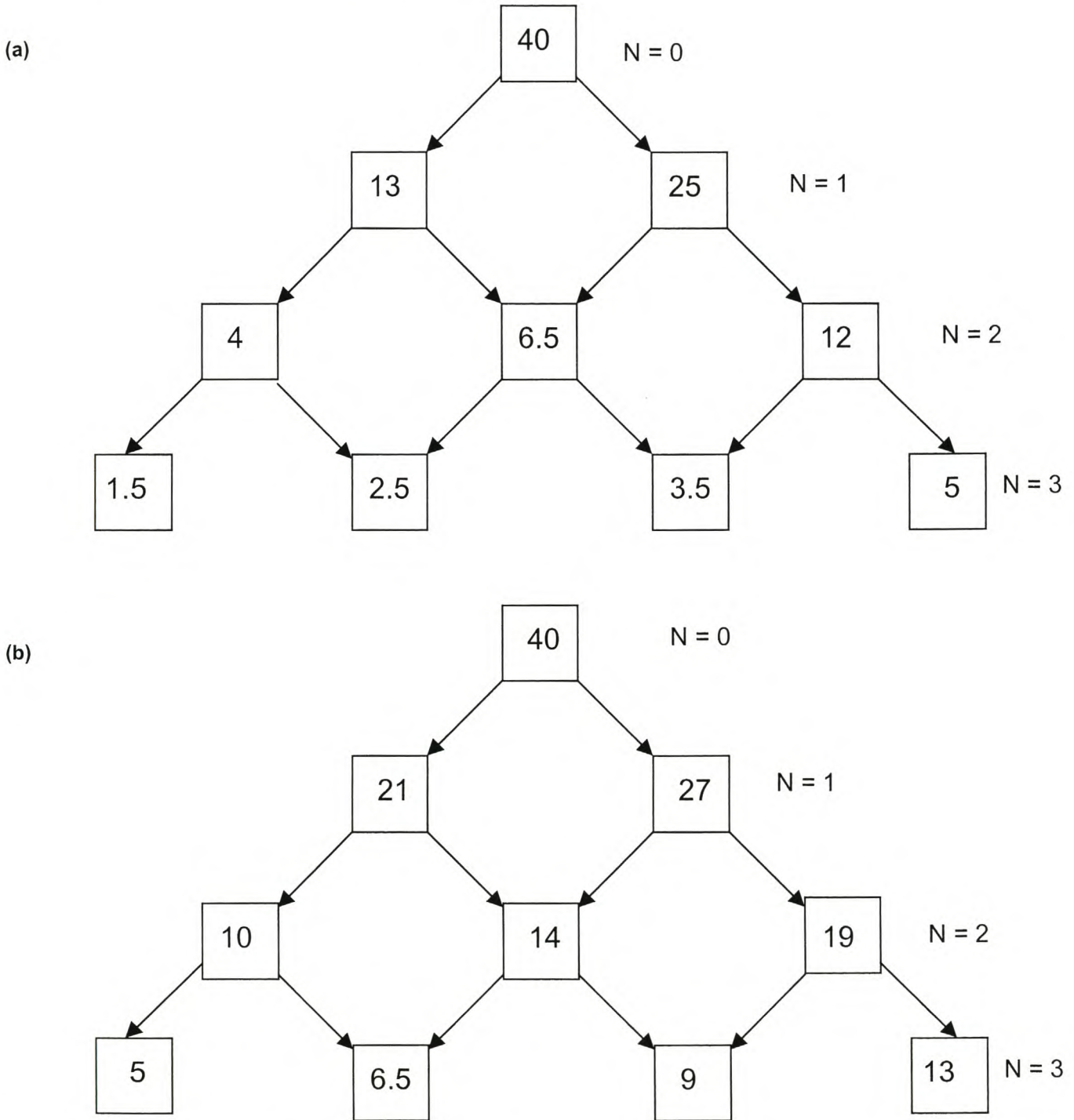
Figure 3.33: Simplified branched networks for (a) CSL = 20 g/L and (b) CSL = 1 g/L. Left and right legs indicate minimum and maximum VFR, respectively. Initial p-CP concentration (N=0) = 40 mg/L.

(d)   Relative Effects of N, CSL and VFR with respect to Scaling-up Potential

Introduction and Objectives:

The relative effects of single pass number (N), catalyst suspension loading (CSL) and volumetric flow rate (VFR), with respect to scaling-up potential, were investigated for the sequential single pass PCO treatment of p-CP. N, together with CSL and VFR, were chosen as parameters for a full two-level 2^3 factorial design. Cumulative degradation rate (%D) was selected as response parameter. Other system parameters were fixed at their standard reference levels as indicated in Table 3.22. The main objective of this study was elucidate the role of CSL and VFR at *high* N, thus evaluating the general scaling-up potential of the reactor when a large number sequential passes are utilized.

Results and Discussion:

Table 3.24: Design matrix for factorial study (2^3 two-level full factorial).

Run	Catalyst Suspension Loading (g/L)	Volumetric Flow Rate (mL/min.)	Number of Single Passes (N)	Cumulative Degradation (%)
1	1	225	1	44.9
2	20	225	1	68.4
3	1	750	1	30.2
4	20	750	1	35.9
5	1	225	3	88.0
6	20	225	3	96.3
7	1	750	3	68.1
8	20	750	3	88.1
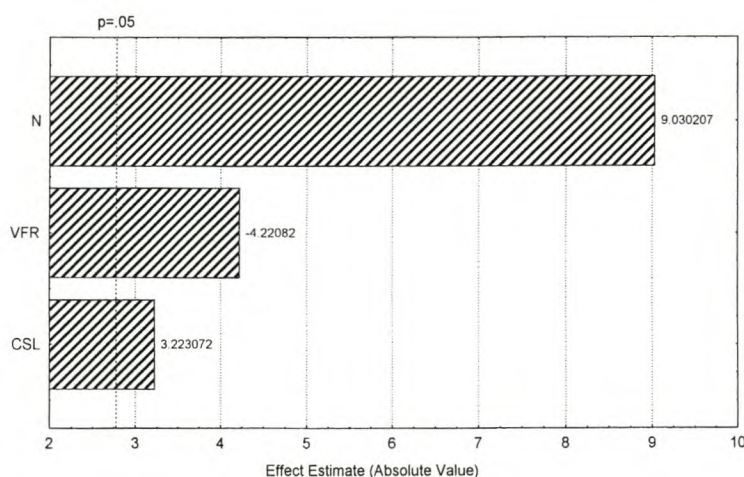
Figure 3.34: Pareto chart illustrating parameter main effects with respect to cumulative degradation. (CSL = Catalyst Suspension Loading; VFR = Volumetric Flow Rate; N = Single Pass Number)

The results obtained from these experiments (Table 3.24 and Figure 3.34) indicated that:

- the positive main effect for N, the number of single passes, overshadowed the effects of catalyst suspension loading and volumetric flow rate. This observation indicates that the relative effects of the latter two parameters can be negated when Reactor 1 is operated at large N. Thus, convenient (economical) settings for these parameters can be chosen without substantial deterioration in PCO performance ;
- linear modeling renders the main effects of all three parameters statistically significant within the 95% confidence level chosen. The quadratic determination of interaction effects was thus discarded. The ANOVA probabilities for the parameter main effects were calculated as 0.0322, 0.0135 and 0.0008, for catalyst suspension loading, volumetric flow rate and N, respectively (Statistica, 1997). These calculations imply that the null hypothesis can be discarded with a 95% assurance (P= 0.05).

(e)   Cost Calculation

A preliminary cost calculation was made for the PCO treatment of p-CP in distilled water, based on the operation of Reactor 1 as a slurried system in the sequential single pass mode. The calculation was done in view of assuming (1) first order kinetics (2) idealized plug-flow reactor conditions and (3) a constant electrical energy per order (EE/O).

Bolton's formula for EE/O in idealized plug-flow reactors has been defined earlier (in Section 1.3.6) :

$$EE/O = P / F \times \log (c_o / c_f) \qquad (1.44)$$

Where: P = Lamp power (in kW)
F = Volumetric water flow rate (in m^3/h)
c_o = Initial concentration
c_f = Final concentration
EE/O = kWh/order/m^3

Thus, taking the treatment result from *3.1.3(b)* as example (Table 3.23), the EE/O and cost (per m^3) for the PCO of an initial p-CP concentration of 40 mg/L to below the limit of detection (1 mg/L) can be calculated as follows :

- orders of removal = log (40/1) = 1.602
- P = 8 x 30 W = 240 W = 0.24 kW
- F = 0.225 L/minute = 13.5 L/h = 0.0135 m^3/h

EE/O amounts to: (0.24)/(0.0135 x 1.602) = 11.1 kWh/order/m^3. At a unit price of 11.8 c/kWh in the Stellenbosch (RSA) area during May 2000, the cost to reduce 40 mg/L p-CP with one order of magnitude (4 mg/L) amounts to 131c / m^3 of water. A further order of magnitude reduction (to 0.4 mg/L) will double the cost, since EE/O is a constant per order. When applying a volumetric flow rate of 750 mL/minute, EE/O amounts to: (0.24)/(0.045 x 1.602) = 3.33 kWh/order/m^3, hence the cost changes to 39c / m^3. This demonstrates that a higher volumetric throughput reduces EE/O costs if the sequential single pass reactor is treated as an idealized plug-flow system. It is noteworthy that UV treatment time (per single pass) has not been accounted for in these EE/O calculations. Thus, the higher number of passes (required at higher flow rates) do not negate cost-effectiveness.

3.2   TREATMENT OF MICROCYSTINS

3.2.1 Recirculation Mode

(a)   System Parameters

The PCO treatment of three variants of microcystins in water was investigated in a random parametric study using OFV for each experiment. The following system parameters were evaluated at discrete levels in terms of first order reaction kinetics (see Table 3.25):

Table 3.25: System parameters for microcystin study (Reactor 1; Recirculation Mode)

Parameter	Assigned Levels
Catalyst Suspension Loading (g/L)	0; 0.2; 1; 5
Volumetric Flow Rate (L/min.)	1.5^{*a}; 2.0^b
Horizontal Irradiation Distance (cm)	8*
Microcystin Variants	YR, LR and YA
Reaction Volume (L)	5*
Water Matrix Effects	Distilled; Deionized*; Lake water
Gas Purge	Oxygen*; Air
Oxygen Flow Rate (L/min.)	5*
Number of UV-C lamps for Irradiation	8^{*c}
Irradiation Time (mins.)	20^*; 60^d and 180^d

* Denotes standard reference level of parameters
a Surface flow rate = 357 L/hr/m^2
b Surface flow rate = 475 L/hr/m^2
c UV Irradiance   = 954 W/m^2
d For initial screening studies

(b)   Screening Study

Introduction and Objectives:

Three initial screening test runs were conducted to determine whether (1) PCO destruction of microcystin toxins in water was feasible (2) surface adsorption (mass transfer) of microcystin molecules onto TiO_2 slurry particles occurred in the absence of UV irradiation and (3) first order exponential decay kinetics could be applied using a minimized standard time of irradiation.

Results and Discussion:

For the first test run an irradiation period of 3 hours was selected. System parameters included a catalyst suspension loading of 1 g/L TiO_2, a volumetric flow rate of 1500 mL/minute (using a double-headed peristaltic pump) and a distilled water matrix. The remainder of the system parameters was fixed at their reference levels (listed in Table 3.25). Aliquots of a 100 mL were collected from the reactor for each sampling time (specified in Table 3.26) and consequently analyzed for microcystin content.

Table 3.26: Microcystin concentration data (in ug/L) as a function of time and variant.

Irradiation Time (mins)	Microcystins (ug/L)		
	YA	YR	LR
0	ND*	92	46
30		10	ND
60		ND	
180			

ND* = Not Detected; Limit of Detection (LOD) = 10 ug/L

The results obtained from the first experiment (Table 3.26) indicated that:

- the concentration of microcystin YA is already below the 10 ug/L detection limit prior to commencement of the reaction. This observation proves that YA may be sensitive to catalyst adsorption;
- the initial concentration of microcystin YR (92 ug/L) decreases to 10 ug/L within 30 minutes of UV exposure and is not detected after 1 hour;
- the initial concentration of microcystin LR (46 ug/L) decreases to below the 10 ug/L limit within the first 30 minutes of reaction;
- no intermediate or final breakdown products are detected via HPLC analysis.

Although the first screening test run confirmed microcystin removal from the water sample, it was not clear whether the observed reduction in concentration levels could be attributed to the PCO of microcystins or merely mass transferred removal thereof from the aqueous phase via surface adsorption onto slurried TiO_2 catalyst. A "dark" adsorption experiment (in the absence of UV light) was conducted by recirculating 5 L of distilled water (spiked with algal extract) through the reactor for a period of 60 minutes. 100 mL aliquots were collected from the reactor at 0 and 60 minutes of reaction time. The remainder of the system parameters was fixed at their reference levels (Table 3.25). An oxygen gas purge (at 5 L/minute flow rate) was applied to ensure suspension of TiO_2 particles.

Table 3.27: Microcystin concentration data (in ug/L) as a function of time and variant.

Recirculation Time (mins)	Microcystins (ug/L)		
	YA	YR	LR
0	22	102	52
60	21	93	41
Net Removal (%)	4.5	8.8	21.2

The results obtained from the second experiment (Table 3.27) indicated that:

- microcystin YA decreases from 22 to 21 ug/L (net removal of 4.5%);
- microcystin YR decreases from 102 to 93 ug/L (net removal of 8.8%);
- microcystin LR decreases from 52 to 41 ug/L (net removal of 21.2 %)
- the observed mean reduction of 11% (due to surface adsorption and partial oxidation via oxygen purging) is relative small compared to the reduction obtained by applying PCO.

The effect of surface adsorption on the PCO of microcystins is a complex function of several system parameters and is a topic that should be addressed in more detail.

The third screening test run was conducted to establish a minimum standard irradiation period for reducing all microcystin levels below 10 ug/L (detection limit) and to assess the application of first order kinetics in this regard. System parameters were identical in comparison to the first test run (Table 4.22). Deionized water was used as spiking matrix.

Table 3.28: Microcystin concentration data (in ug/L) as a function of time and variant.

Irradiation Time (mins)	Microcystins (ug/L)		
	YA	YR	LR
0	15	112	55
5	ND*	47	31
10		21	16
15		10	9
20		ND	ND
$10^2 \ k_{obs}$ (mins^{-1})	NC**	16.11	12.18
Half-life (mins)	-	4.3	5.7
R^2	-	0.99	0.99

ND* = Not Detected; LOD = 10 ug/L
NC = Not calculated**
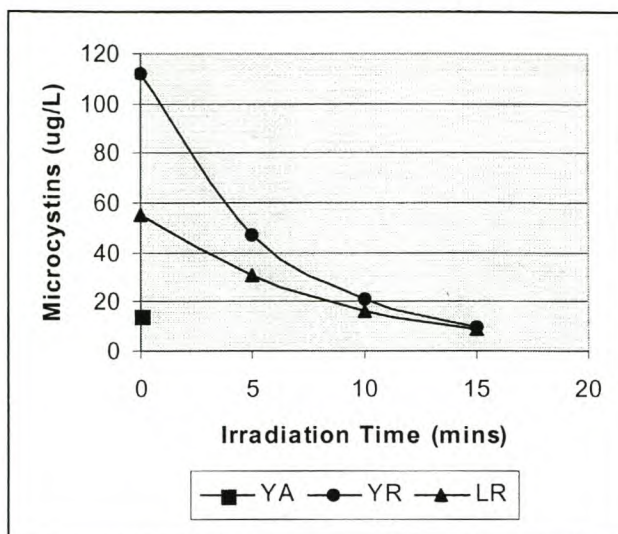
Figure 3.35: Microcystin oxidation as a function of time and microcystin variant.

The results obtained from the third experiment (Table 3.28 and Figure 3.35) indicated that:

- the decrease in microcystin levels adheres to first order exponential decay kinetics;
- the initial concentration of microcystin YA (15 ug/L) is reduced to below the detection limit within the first 5 minutes of PCO treatment;
- microcystins YR and LR require approximately 20 minutes to achieve the same result. This result is attributed to higher initial concentrations;
- microcystin LR (with initial reaction rate of 6.7 $ug.L^{-1}.min^{-1}$) is more resistant to PCO than YR (reaction rate of 18 $ug.L^{-1}.min^{-1}$), despite the disparity in initial concentration levels.

(c)   Catalyst Suspension Loading (Deionized Water)

Introduction and Objectives:

The effect of catalyst suspension loading was examined in deionized water by comparing results for 3 different loadings of TiO_2 (0; 0.2 and 1 g/L). System parameters were evaluated at standard reference levels (see Table 3.25). The objectives of this study were to (1) establish whether an increase in catalyst suspension loading promotes the PCO of microcystins and (2) assess and compare the effects of UV photolysis against TiO_2 mediated PCO.

Results and Discussion:

Table 3.29: Microcystin concentration data (in ug/L) as a function of time, catalyst loading and variant.

Irradiation Time (mins)	Microcystins (ug/L)								
	YA			YR			LR		
	Catalyst Suspension Loading (g/L)			Catalyst Suspension Loading (g/L)			Catalyst Suspension Loading (g/L)		
	0	0.2	1	0	0.2	1	0	0.2	1
0	14	17	ND	82	63	58	28	26	26
2	46	21		63	46	43	26	22	23
4	43	13		50	41	10	24	16	12
6	38	13		56	36	ND	23	15	ND
8	37	ND*		46	16		18	11	
10	35	12		44	12		19	15	
12	31	14		39	ND		17	10	
14	25	ND		28			14	ND	
16	32	ND		33			14		
18	NA***	12		NA			NA		
20	26	NA		26			17		
10^2 k_{obs} (mins^{-1})	NC**	NC	NC	6.25	16.56	43.95	4.72	7.16	19.33
Half-life (mins)	-	-	-	11.1	4.2	1.6	14.7	9.7	3.6
R^2	-	-	-	0.90	0.92	0.87	0.95	0.82	0.87

ND* = Not detected; LOD = 10 ug/L
NC** = Not calculated
NA*** = Not analyzed
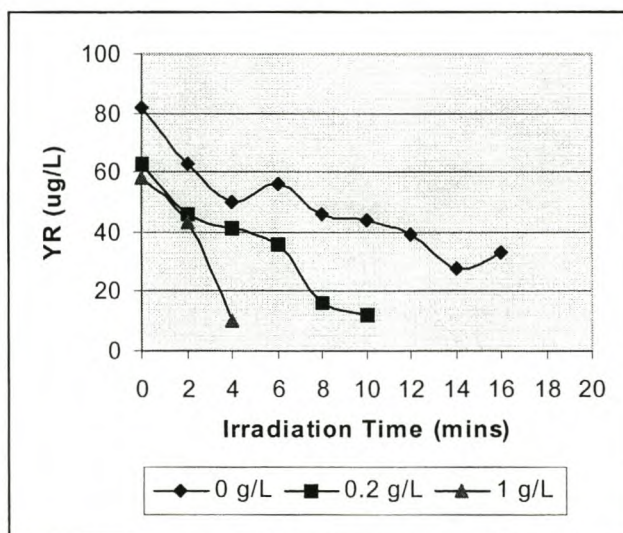
Figure 3.36: Microcystin YR oxidation as a function of time and catalyst suspension loading.

124
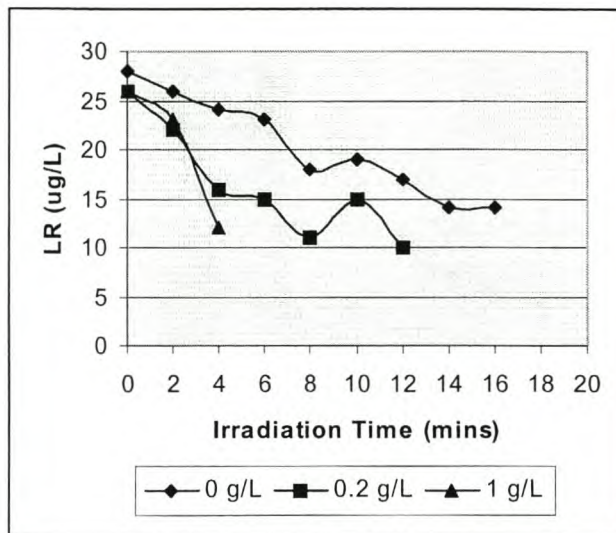
Figure 3.37: Microcystin LR oxidation as a function of time and catalyst suspension loading.

The results obtained from these experiments (Table 3.29 and Figures 3.36 to 3.37) indicated that:

- the rate constant for the PCO of microcystins increases by increasing the catalyst suspension loading;
- when using a deionized water matrix, the effect of catalyst suspension loading is amplified due to an absence of inorganic ions acting as oxidant scavengers;
- a catalyst suspension loading of 1 g/L TiO_2 reduces the microcystin YR and LR concentrations to a non-detectable level (ND) within 6 minutes of UV exposure. This observation is anticipated in terms of reduced starting concentrations used (e.g. 58 ug/L for YR) compared to earlier runs (test run 3 : 112 ug/L for YR);
- the addition TiO_2 catalyst significantly enhanced degradation of microcystin YR, compared to UV photolysis;
- microcystin LR is considerably more resistant to PCO than YR;
- surface adsorption of microcystin YA is favored by an increase in catalyst suspension loading.

(d)   Gas Purge

Introduction and Objectives:

The effect of gas purge was examined by comparing results for compressed air against pure oxygen used as standard gas purge. The economic implications of such an experiment would become significant in a scaling-up situation. Catalyst suspension loading was set at 0.2 g/L TiO_2. The remainder of the system parameters was evaluated at standard reference levels (see Table 3.25). The objective of this study was to compare rates of PCO for the two gas purges used.

Results and Discussion:

Table 3.30: Microcystin concentration data (in ug/L) as a function of time, gas purge and variant.

Irradiation Time (mins)	Microcystins (ug/L)					
	YA		YR		LR	
	Oxygen	Air	Oxygen	Air	Oxygen	Air
0	17	15	63	53	26	19
2	21	ND	46	52	22	18
4	13		41	31	16	10
6	13		36	32	15	ND
8	ND*		16	23	11	10
10	12		12	17	15	ND
12	14		ND	14	10	
14	ND			11	ND	
16	ND			ND		
18	12			ND		
20	NA***			ND		
$10^2 \ k_{obs}$ (mins^{-1})	NC**	NC	16.56	11.73	7.16	8.94
Half-life (mins)	-	-	4.2	5.9	9.7	7.8
R^2	-	-	0.92	0.97	0.82	0.74

ND* = Not detected; LOD = 10 ug/L
**NC**** = Not calculated
NA*** = Not analyzed

Figure 3.38: Microcystin YR oxidation as a function of time and gas purge used.

126

The results obtained from these experiments (Table 3.30 and Figure 3.38) indicated that:

- the PCO rate constant for microcystin LR removal is largely unaffected by switching the gas purge from oxygen to compressed air. This observation is coupled to high resistance of LR towards PCO in general;
- the PCO rate constant for microcystin YR removal is marginally reduced when switching gas purge to air. This observation is coupled to the greater susceptibility of YR towards PCO;
- the utilization of air as gas purge in PCO treatment is to be considered when treating recalcitrant organic pollutants in water.

(e)   Water Matrix Effects

Introduction and Objectives:

Water matrix effects were examined by comparing results for the treatment of microcystins in deionized water and natural lake water. Lake water was sampled at Zeekoevlei (a hypertrophic coastal lake on the Cape Flats, Cape Town, RSA). This lake has experienced seasonal outbreaks of cyanobacterial blooms. Catalyst suspension loading was set at 0.2 g/L TiO_2. The remainder of the system parameters was evaluated at standard reference levels (see Table 3.25). The objectives of this study were to (1) compare PCO efficieny for the two water matrices used and (2) assess the effect of inorganic ions on the PCO of microcystins in untreated natural water.

127

Results and Discussion:

Table 3.31: Microcystin concentration data (in ug/L) as a function of time, water matrix and variant.

| Irradiation Time (mins) | Microcystins (ug/L) | | | | | |
| | YA | | YR | | LR | |
	Deionised Water	Lake Water	Deionised Water	Lake Water	Deionised Water	Lake Water
0	17	21	63	64	26	35
2	21	17	46	58	22	30
4	13	15	41	50	16	31
6	13	12	36	41	15	26
8	ND*	11	16	38	11	25
10	12	11	12	41	15	32
12	14	ND	ND	32	10	22
14	ND			35	ND	22
16	ND			34		25
18	12			31		22
20	NA***			34		26
$10^2 k_{obs}$ (mins^{-1})	NC**	6.80	16.56	4.68	7.16	1.74
Half-life (mins)	-	10.2	4.2	14.8	9.7	39.8
R^2	-	0.93	0.92	0.88	0.82	0.51

ND* = Not detected; LOD = 10 ug/L
NC** = Not calculated
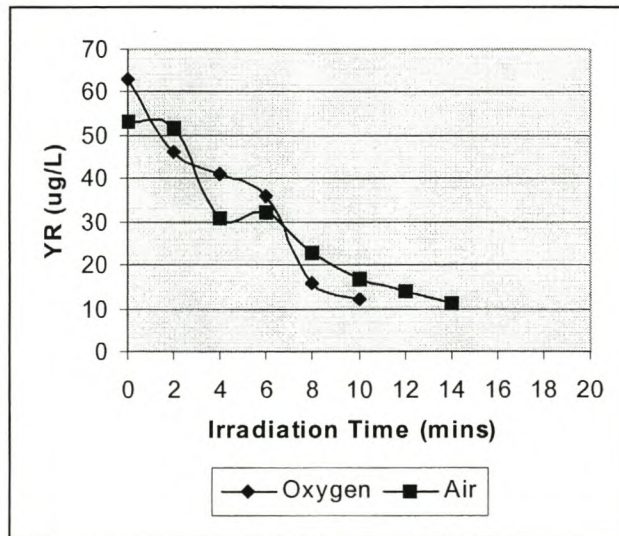NA*** = Not analyzed
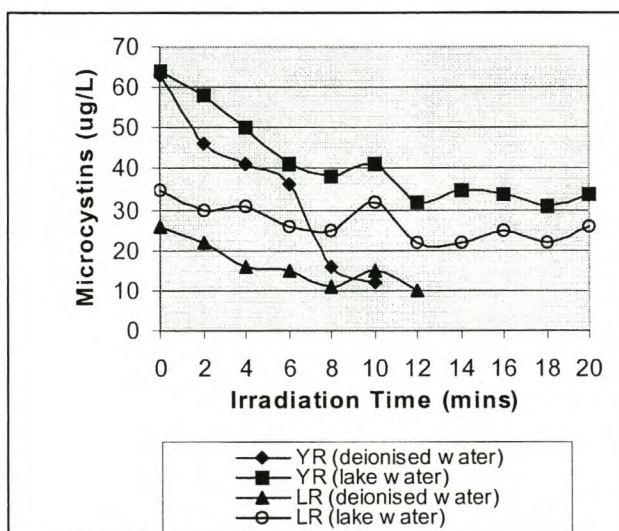
Figure 3.39: Microcystin oxidation as a function of time, variant and water matrix.

The results obtained from these experiments (Table 3.31 and Figure 3.39) indicated that:

- the utilization of untreated lake water (as opposed to deionized water) results in significantly slower PCO of microcystins. This result is attributed to the presence of pigments and inorganic ions (e.g. nitrates and phosphates) that can act as hydroxyl radical scavengers during PCO processes;
- the conductivity is approximately 5 orders of magnitude greater for the lake water used in this study compared to deionized water (124 mS/m versus 1.4 uS/m). This result confirms the higher concentration of inorganic species in the former water matrix ;
- the PCO susceptibilities of microcystins YR and LR are dissimilar, despite observed first order rate constants decreasing with more than 70% for both variants when using lake water as spiking matrix.

(f)   Catalyst Suspension Loading (Lake Water)

Introduction and Objectives:

The effect of catalyst suspension loading was examined in lake water by comparing results for 3 different loadings of TiO_2 (0.2; 2 and 5 g/L). System parameters were evaluated at standard reference levels according to Table 3.25. The objectives of this study were to (1) establish whether an increase in catalyst suspension loading promoted the PCO of microcystins in lake water and (2) monitor whether PCO efficiency could be enhanced to a level comparative with the rate achieved in a deionized water matrix.

Results and Discussion:

Table 3.32: Microcystin concentration data (in ug/L) as a function of time, catalyst loading and variant.

Irradiation Time (mins)	Microcystins (ug/L)								
	YA			YR			LR		
	Catalyst Suspension Loading (g/L)			Catalyst Suspension Loading (g/L)			Catalyst Suspension Loading (g/L)		
	0.2	2	5	0.2	2	5	0.2	2	5
0	21	14	18	64	44	66	35	22	37
2	17	15	16	58	49	54	30	22	30
4	15	ND	13	50	26	45	31	13	30
6	12	10	12	41	31	39	26	15	17
8	11	ND	10	38	36	33	25	27	17
10	11		ND	41	27	29	32	29	15
12	ND*			32	30	26	22	24	12
14				35	24	21	22	21	12
16				34	23	21	25	19	13
18				31	22	18	22	14	11
20				34	18	15	26	19	ND
10^2 k_{obs} (mins^{-1})	6.80	6.01	7.32	4.68	4.33	7.83	1.74	NC**	6.82
Half-life (mins)	10.2	11.5	9.5	14.8	16.0	8.9	39.8	-	10.2
R^2	0.93	0.89	0.99	0.88	0.97	0.99	0.51	-	0.88

ND* = Not detected; LOD = 10 ug/L
NC** = Not calculated
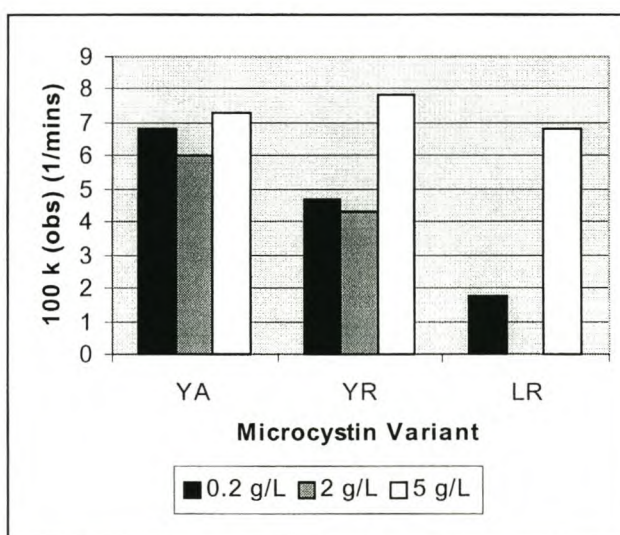

Figure 3.40: First order rate constants as a function microcystin variant and catalyst suspension loading (in g/L TiO$_2$).

The results obtained from these experiments (Table 3.32 and Figure 3.40) indicated that :

- an increase in catalyst suspension loading from 0.2 to 5 g/L does not significantly promote the PCO of microcystins YA and YR;
- an increase in catalyst loading from 0.2 to 5 g/L enhances the PCO of microcystin LR considerably;
- PCO performed at elevated catalyst loading is advised when treating recalcitrant organic compounds in the presence of inorganic ions (radical scavengers).

(g)   Volumetric Flow Rate

Introduction and Objectives:

The effect of volumetric flow rate was examined by comparing results for 2 different rates (i.e. the standard reference rate of 1.5 L/minute and 2 L/minute). The corresponding surface flow rates are presented below Table 3.25. Catalyst suspension loading was fixed at 5 g/L TiO_2 and the experiments were conducted in lake water. The remainder of the system parameters was evaluated at standard reference levels. The objectives of this study were to (1) assess the falling film effect at high flow rates and (2) determine whether the application of high flow rates is beneficial for PCO when applying a recirculation mode of operation.

Results and Discussion:

Table 3.33: Microcystin concentration data (in ug/L) as a function of time, flow rate and variant.

Irradiation Time (mins)	Microcystins (ug/L)					
	YA		YR		LR	
	Flow Rate 1.5 L/min.	Flow Rate 2 L/min.	Flow Rate 1.5 L/min.	Flow Rate 2 L/min.	Flow Rate 1.5 L/min.	Flow Rate 2 L/min.
0	18	18	66	69	37	30
2	16	18	54	60	30	25
4	13	17	45	56	30	22
6	12	14	39	50	17	21
8	10	11	33	47	17	21
10	ND*	11	29	45	15	20
12		ND	26	36	12	19
14			21	30	12	13
16			21	31	13	14
18			18	27	11	13
20			15	26	ND	15
10^2 k_{obs} (mins^{-1})	7.32	5.91	7.83	5.42	6.82	3.86
Half-life (mins)	9.5	11.7	8.9	12.8	10.2	18.0
R^2	0.99	0.90	0.99	0.96	0.88	0.86

Figure 3.41: First order rate constant as a function of microcystin variant and volumetric flow rate.

The results obtained from these experiments (Table 3.33 and Figure 3.41) indicated that :

- the PCO efficiency of microcystins YA and YR is marginally reduced when applying the higher volumetric flow rate;
- the PCO efficiency of microcystin LR is reduced by approximately 50% when applying the higher volumetric flow rate;
- the falling film effect is detrimental to PCO at high flow rates, particulary in the case of recalcitrant organic compounds;
- a higher rate of recirculation is not necessarily sufficient to compensate for the inhibiting effect of a denser falling film.

(h)   Reproducibility Study

Introduction and Objectives:

The statistical reproducibility of PCO efficiency was examined for a fixed set of experimental conditions. Experiments were conducted in triplicate using a catalyst suspension loading of 5 g/L TiO_2 and a volumetric flow rate of 2 L/minute. Lake water (spiked with microcystin algal extract) was used. The remainder of the system parameters was evaluated at their standard reference levels (Table 3.25). The objective of this study was to evaluate the reproducibility of the observed rate constants in terms of (1) standard deviation (SD) (2) relative standard deviation (RSD) and (3) microcystin variant.

Results and Discussion:

Table 3.34: Microcystin concentration data (in ug/L) as a function of time, replicate number and variant.

Irradiation Time (mins)	Microcystins (ug/L)								
	YA			YR			LR		
	Replicate Run Number			Replicate Run Number			Replicate Run Number		
	1	2	3	1	2	3	1	2	3
0	18	18	22	69	71	76	30	31	32
2	18	16	16	60	61	62	25	23	26
4	17	14	15	56	50	55	22	22	24
6	14	15	15	50	55	56	21	26	23
8	11	13	14	47	46	48	21	20	19
10	11	10	10	45	41	41	20	19	17
12	ND*	ND	10	36	38	41	19	18	19
14			ND	30	35	36	13	16	16
16				31	32	35	14	17	15
18				27	27	31	13	14	14
20				26	24	28	15	15	16
$10^2 \, k_{obs}$ (mins^{-1})	5.91	4.99	6.03	5.42	4.82	4.96	3.86	3.39	3.67
Half-life (mins)	11.7	13.9	11.5	12.8	14.4	14.0	18.0	20.4	18.9
R^2	0.90	0.85	0.89	0.96	0.95	0.96	0.86	0.87	0.88

ND* = Not detected; LOD = 10 ug/L)

Table 3.35: Statistical analysis of reproducibility for the 3 replicates.

Microcystin Variant	Measured Response	Mean	Standard Deviation	Relative Standard Deviation (%)
YA	10^2 k (obs)*	5.6	0.6*	10.7
YA	Half-life**	12.4	1.3**	10.5
YR	10^2 k (obs)	5.1	0.3	5.9
YR	Half-life	13.7	0.8	5.8
LR	10^2 k (obs)	3.6	0.2	5.6
LR	Half-life	19.1	1.2	6.3

* expressed in mins^{-1} ; ** expressed in mins.

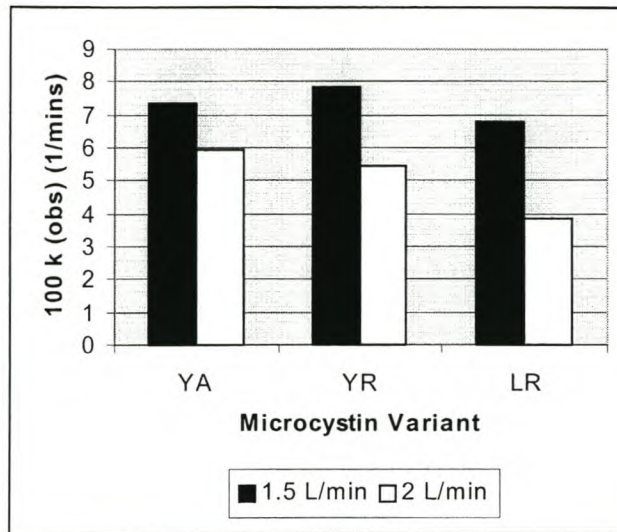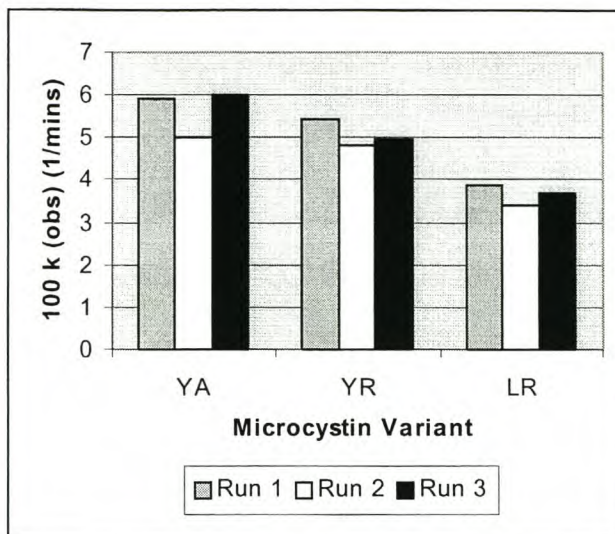**Figure 3.42: Reproducibility of observed first order rate constants as a function of microcystin variant.**

The results obtained from these experiments (Tables 3.34 to 3.35 and Figure 3.42) indicated that:

- the mean observed first order rate constants for PCO of microcystins YA and YR are largely similar;
- the PCO rate constants for LR are slightly smaller compared to YA and YR. This result demonstrates the more resistant nature of LR towards PCO treatment ;
- the relative standard deviation (RSD) of results is equal to or below 10% for all 3 variants, which is considered acceptable taking into account possible error variations resulting from (1) sample preparation (2) reactor efficiency and (3) analytical methodology ;
- RSD is slightly worse for the PCO of microcystin YA. This result is explained in terms of (1) an earlier observation related to the mass transfer adsorption of YA at higher catalyst suspension loadings and (2) practical problems related to the HPLC analysis of this variant.

Based on the results obtained above, it was considered to investigate the effect of slurry pH and solution pH on the PCO efficiency of microcystins. These studies were executed for Reactor 2A where immobilized TiO_2 configurations were used throughout (see Section 4.2).

3.2.2 Single Pass Modes

The application of Reactor 1 for studying the PCO treatment of microcystin toxins was limited to the recirculation mode of operation.

CHAPTER 3 – REFERENCES

AL-SAYYED G, D'OLIVEIRA JC and PICHAT P (1991) Semiconductor-sensitized photodegradation of 4-chlorophenol in water. *J. Photochem. Photobiol. A: Chem.* **58** 99-114.

BENNETT PA and VAN DER MERWE J (1995) Photocatalytic oxidation – a safe and clean alternative in TOC analysis. *Water Sewage & Effluent* **15** 7-9.

CLOETE V (1999) Methods for establishing the efficiency of the photocatalytic destruction of humic substances in drinking water. *M.Sc. (Chemistry) Thesis, University of Stellenbosch, South Africa.*

HERRMANN JM (1999) Heterogeneous photocatalysis: fundamentals and applications to the removal of various types of aqueous pollutants. *Catalysis Today* **53** 115-129.

HERRMANN JM (1995) Heterogeneous photocatalysis: an emerging discipline involving multiphase systems. *Catalysis Today* **24** 157-164.

HOFFMANN MR, MARTIN ST, CHOI W and BAHNEMANN DW (1995) Environmental applications of semiconductor photocatalysis. *Chem. Rev.* **95** 69-96.

OFFRINGA G (2000) *Personal communication.* Water Research Commission of South Africa, Pretoria, RSA.

SIEMON U, RAUER S, DILLERT R and BAHNEMANN D (1999) Comparing the photocatalytic activity of commercially available titanium dioxide materials. In: *Proceedings of The 4th International Conference on TiO2 Photocatalytic Purification and Treatment of Water and Air*, Albuquerque, New Mexico, USA. 18.

CHAPTER 4

EVALUATION OF REACTOR 2A

OVERVIEW

This chapter contains a comprehensive evaluation of Reactor 2A operated in three different modes and assessed for the PCO of two model pollutants in water, i.e. p-CP and cyanobacterial microcystin toxins. A number of system parameters are evaluated by the conventional OFV approach, however, basic OED screening studies are also utilized to monitor the responses associated with the PCO degradation of the primary model pollutant (p-CP). Detailed studies pertaining to the TiO_2 impregnation of the reactor sheet module are also reported.

4.1   TREATMENT OF *para*-CHLOROPHENOL

4.1.1 Recirculation Mode

(a)   System Parameters

The PCO treatment of p-CP in water was investigated by operating Reactor 2A as (1) immobilized-bed (IMM) and (2) combined slurry-immobilized bed (SLIMM) reactors. One-factor variation (for random parametric studies) and two-level experimental designs (for screening studies) were employed as before. The following system parameters were evaluated at discrete levels in terms of first order reaction kinetics (see Table 4.1).

Note: The standard reference level for each parameter was used throughout unless stated otherwise by the study in question. This applies to all work reported further on.

For the purpose of brevity, IMM and SLIMM will be used to denote the "immobilized-bed" and "combined slurry-immobilized bed" reactors, respectively.

Table 4.1: System parameters for p-CP study (Reactor 2A; Recirculation Mode)

Parameter	Assigned Levels
Catalyst Loading for Impregnation (g/L)	1; 5*; 10; 20; 30
Volumetric Flow Rate (L/min.)	1^a; 2^{*b}
Horizontal Irradiation Distance (cm)	5; 15*
p-CP Initial Concentration (mg/L)	13; 40*
Reaction Volume (L)	3*; 6
Water Matrix	Distilled
Initial Solution pH	3; 5; 6.2; 7.5*; 9; 11
Gas Purge	Oxygen
Gas Flow Rate (L/min. O_2)	5*; 20
UV lamps^c	Blacklight (UV-A); Germicidal (UV-C)*

* Denotes standard reference level of parameters
a Surface flow rate = 70 L/hr/m^2
b Surface flow rate = 135 L/hr/m^2
c UV irradiance   = 204.5 W/m^2 = 12 x 15W lamps (per 0.88 m^2)

(b)   Fiber Glass Examination

Introduction and Objectives:

Two types of locally available fiber glass sheet materials were examined for maximum impregnation of TiO_2 photocatalyst and their photochemical stability. Mechanical strength and fineness of the individual fibers were of primary concern in the selection of the sheets. The first sheet type (obtained from Foyntech Africa cc, Stellenbosch, RSA) was reinforced with a grid-like mesh on the surface. The second sheet type (obtained from Freudenberg Nonwovens Pty. Ltd., Parow Industria, Parow, RSA) was a glass tissue and resembled the Foyntech product without a reinforced mesh (see Section 2.1.4 for design details).

A dynamic contact angle analyzer (DCAA) was used to conduct a preliminary study of the TiO_2 impregnation properties of the two types of fiber glass materials (Engelbrecht *et al.*, 1998). The procedure entailed dipping square samples of each (impregnation area: 5.6 cm^2) in 30 mLs of TiO_2 suspension for a fixed period of time. The objectives of this study were to ascertain conditions for maximum catalyst impregnation as a function of (1) catalyst suspension loading (2) fiber glass type (3) impregnation time and (4) pH treatment of sheets. Standard one-factor variation and 2^3 factorial experiments were used for this purpose. These parameters will ultimately influence the optimized performance of the IMM reactor in terms of its PCO destruction efficiency.

Results and Discussion :

Table 4.2: DCAA results for TiO_2 impregnation study of two types of glass fiber.

Catalyst suspension loading (g/L)	Catalyst impregnation loading*** (in mg/cm^2)	
	Type 1 (reinforced)	Type 2 (non-reinforced)
0	0*	0**
1	0.6	0.5
5	0.8	0.7
10	0.9	0.8
20	1.1	1.0
30	1.2	1.2
50	1.3	1.2
75	1.4	1.3
100	1.5	1.3

* Water adsorption (at 0 g/L TiO_2) = 13.2 mg/cm^2
** Water adsorption (at 0 g/L TiO_2) = 11.2 mg/cm^2
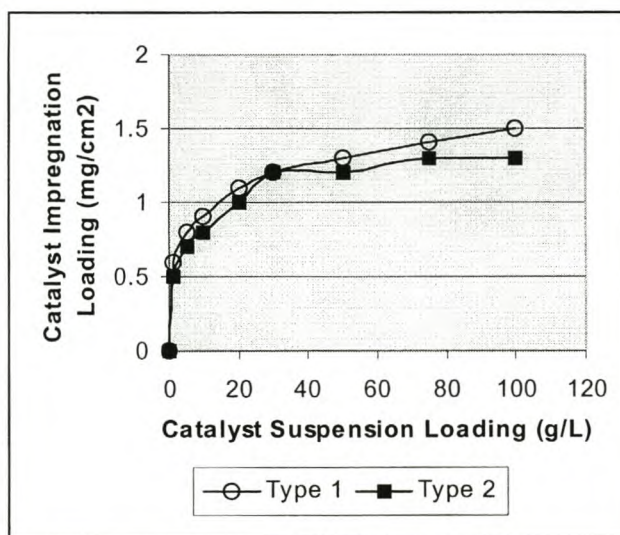*** Results corrected in terms of net uptake of water

Figure 4.1: Catalyst impregnation loading as a function of catalyst suspension loading.

The results obtained from these experiments (Table 4.2 and Figure 4.1) indicated that :

- the catalyst impregnation loading (CIL, in mg/cm^2) increases steadily with increasing catalyst suspension loading (CSL, in g/L) and reaches a plateau value of approximately 1.5 mg/cm^2 beyond 40 g/L TiO_2 used. This impregnation loading corresponds to a theoretical sheet module loading of 15 g/m^2 ;
- the two types of fiber glass materials display similar wetting properties with respect to TiO_2 suspension coating and wetting with clear water. Perfect wetting is observed for all analyses (advancing and receding contact angles are 0° throughout) ;
- CIL is not significantly affected by increasing the time of impregnation (Engelbrecht *et al.*, 1998) ;
- treating the sheets with acidic media (pH 4) marginally improves catalyst impregnation of TiO_2 (Engelbrecht *et al.*, 1998) ;
- treating the sheets with alkaline media (pH 9.5) results in a significant decrease of CIL. This is ascribed to the adverse effects of electrostatic repulsion between fiber glass surface hydroxyl ions and TiO^- species at high pH ;
- the mechanical stability of the reinforced fiber glass (Type 1) is significantly greater under wetting conditions, compared to Type 2. This observation is ascribed to the presence of the grid-like mesh.

Based on the results obtained above, it was envisaged that most of Reactor 2A's studies would probably have to be conducted with fiber glass sheet materials that are (1) mechanically very stable under wetting conditions or (2) reinforced by some structural means. As a result, the TiO_2 suspension coating and impregnation properties of the *reinforced fiber glass sheet module* (Type 1) was investigated in an effort to assess its utility as stationary support in Reactor 2A.

(c) TiO_2 Impregnation of Sheet Modules

Introduction and Objectives:

Suspension coating of the reinforced fiber glass sheet module (coating surface area: 0.88 m^2) was performed in triplicate. The coating procedure entailed the "dark" recirculation of suspensions of TiO_2 (in 3 L of *distilled* water) through the system (across the sheet module) using (1) a 2 L/min. volumetric flow rate (2) the natural suspension pH (4-5) and (3) magnetic stirring for a period of 30 minutes. Sheet modules were weighed before and after coating. Coated sheets were air-dried at room temperature for 24 hrs prior to determining the net increase in weight. The objective of this study was to assess the reproducibility of catalyst impregnation loading as a function of suspension loading when using this particular procedure for sheet coating.

139

The results obtained from these experiments (Tables 4.3 to 4.4 and Figure 4.2) indicated that :

- the average dry weight of the non-coated sheet modules is 28.9 ± 0.9 g (RSD = 3.2%);
- increasing the loading of catalyst used for suspension coating steadily increases the mass of TiO_2 impregnated onto the sheet module, albeit striving towards a saturation value (viz: maximum impregnation capacity) ;
- the mass transfer (%) of catalyst from the aqueous coating suspension to the sheet module decreases with an increase in catalyst suspension loading. This result is anticipated in view of the maximum impregnation capacity of the module;
- the reproducibility of the coating procedure improves with elevation in catalyst suspension loading. Acceptable RSD (*ca* 10 % or less) is attained when using loadings equal to or greater than 5 g/L ;
- the sheet module maintains mechanical stability, even at high catalyst suspension loading ;
- catalyst suspension loading in excess of 30 g/L TiO_2 are unsuited for suspension coating. Problems are encountered with maintaining TiO_2 in suspension, hence the recirculation thereof through the reactor becomes problematical ;
- suspension coating cannot be scaled-up linearly as a function of catalyst suspension loading and impregnation area (compare results from Tables 4.2 and 4.4).

Based on the results obtained above, it was decided to adopt a *standard suspension coating procedure* for further work. This procedure entailed the use of (1) a catalyst suspension loading of 5 g/L TiO_2 in 3 L of distilled water and (2) identical system parameters as specified in the introductory paragraph of this study. The equivalent catalyst impregnation loading amounts to 8.3 g/m^2 (i.e. 0.83 mg/cm^2) which is in the optimum range reported for immobilized-bed PCO reactors (Herrmann, 1995).

Droplet spraying was also assessed as potential coating procedure. This study, however, was limited to the TiO_2 impregnation of a fibrous activated carbon (FAC) sheet module, as explained in the next chapter (see Reactor 2B in Chapter 5).

(d)   Sheet Modifications

Introduction and Objectives:

Two compounded sheet modules were prepared in-house from the two types of fiber glass materials purchased originally. The first compounded module comprised the reinforced fiber glass sheet (Type 1) modified with a number of additional rectangular strips of the same material which were attached at intermittent positions (10 cm apart) as depicted below (Figure 4.3). The second compounded module comprised the non-reinforced sheet (Type 2) altered similarly using the reinforced material as intermittent strips.

The compounded modules were prepared in an effort to (1) enhance the coating ability of the existing sheet modules (2) create a turbulence (stirring) effect during the falling film irradiation procedure and (3) increase the water residence time on the sheet module, thereby prolonging contact with UV irradiation.

The main objective of this study was to compare the utility of the 4 sheet modules (i.e. the two original and two compounded modules) in terms of the PCO of p-CP in water by using (1) immobilized-bed (IMM) and (2) combined slurry-immobilized (SLIMM) reactor configurations. System parameters were evaluated at standard reference levels (Table 4.1) and an irradiation period of 30 minutes was selected. The standard suspension coating procedure was applied to all sheet modules (i.e. using a catalyst suspension loading of 5 g/L TiO_2).
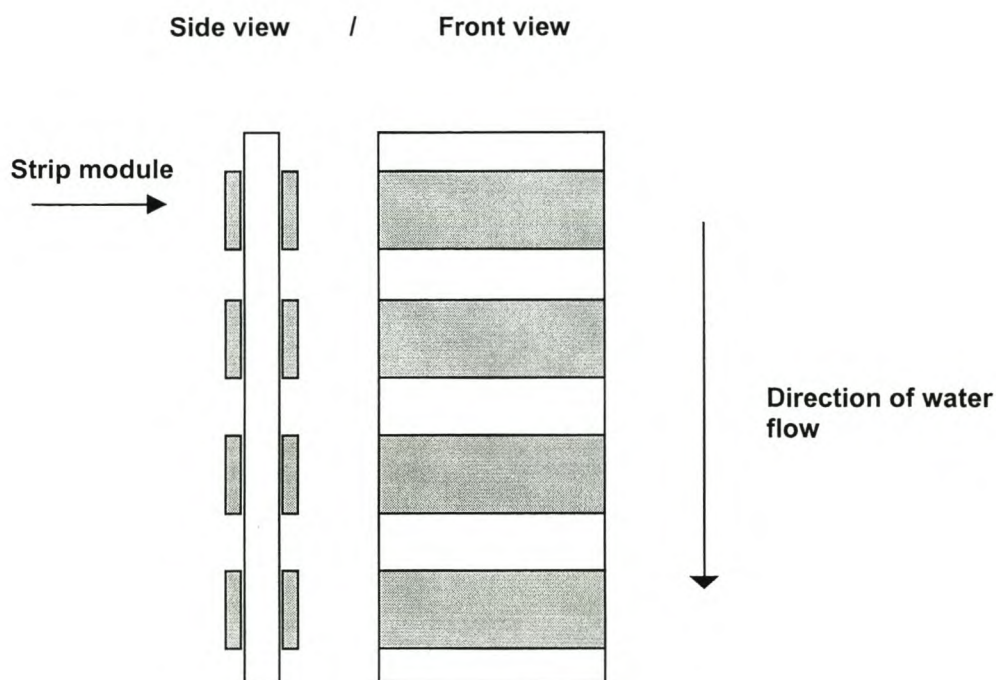
Figure 4.3: Schematic of the compounded sheet module design.

Results and Discussion:

Table 4.5: p-CP concentration data (in mg/L) as a function of time, sheet module and reactor configuration.

Irradiation Time (mins)	Fiber Glass 1 (reinforced sheet)		Compound 1 (reinforced + reinforced strips)		Fiber Glass 2 (non-reinforced tissue sheet)		Compound 2 (non-reinforced + reinforced strips)	
	IMM** Reactor	SLIMM*** Reactor	IMM Reactor	SLIMM Reactor	IMM Reactor	SLIMM Reactor	IMM Reactor	SLIMM Reactor
0	40.0	40.0	40.0	40.0	40.0	40.0	40.0	40.0
5	26.2	25.3	25.0	24.8	32.5	30.2	27.4	26.1
10	17.1	16.9	17.9	15.5	25.4	22.5	21.2	19.2
15	11.5	11.0	13.2	10.3	21.6	18.3	16.0	13.5
20	8.9	6.9	8.9	6.7	17.9	14.4	12.9	10.0
25	6.8	3.2	6.2	3.1	13.1	9.7	10.3	7.8
30	ND*	ND	ND	ND	9.7	5.1	7.5	4.0
$10^2 \, k_{obs}$ (mins^{-1})	7.14	9.69	7.27	9.78	4.58	6.35	5.34	7.13
Half-life (mins)	9.7	7.2	9.5	7.1	15.1	10.9	13.0	9.7
R^2	0.99	0.99	0.99	0.99	0.99	0.96	0.99	0.98

ND*   = Not Detected; Limit of Detection = 1 mg/L
IMM**   = Immobilized-Bed Reactor (no suspended TiO_2 after coating)
SLIMM** = Combined Slurry-Immobilized Reactor (suspension loading of 1 g/L TiO_2 after coating)
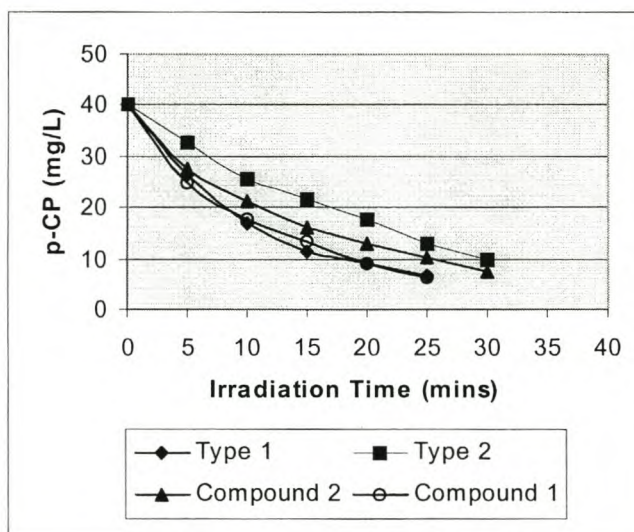
Figure 4.4: p-CP oxidation as a function of time and sheet module used (IMM reactor).
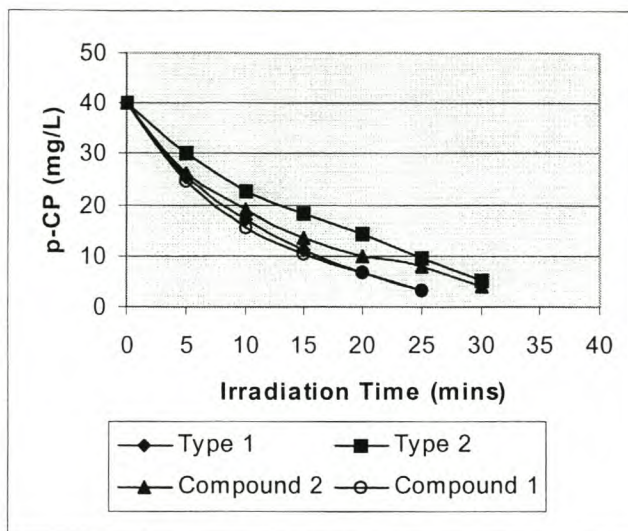
Figure 4.5: p-CP oxidation as a function of time and sheet module used (SLIMM reactor).
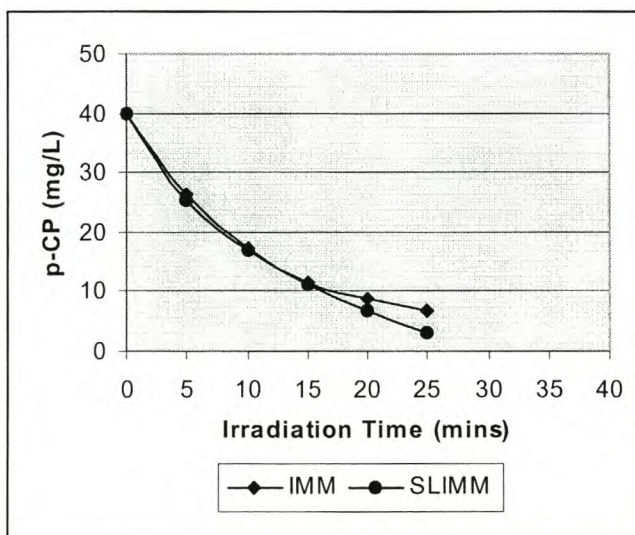
Figure 4.6: p-CP oxidation as a function of time and reactor configuration (IMM and SLIMM reactor results when using *Fibre Glass Type 1* as sheet module).

The results obtained from these experiments (Table 4.5 and Figures 4.4 to 4.6) indicated that :

- first order exponential decay kinetics apply for the PCO of p-CP in Reactor 2A ;
- the first order rate constants are higher for the modules which incorporate reinforced mesh (i.e. fiber glass Type 1 and Compound 1). This result is independent of reactor configuration and can be attributed to the positive auxiliary effect created by turbulence and additional mixing as a function of the surface roughness;
- the first order rate constant (for each sheet module used) increases marginally when switching from IMM to SLIMM reactor configuration. This result implies that additional suspended catalyst (i.e. 1 g/L TiO_2 in this study) do not significantly enhance p-CP oxidation in the presence of immobilized catalyst ;

- the UV residence time of the falling film (*ca* 4.1 sec) is not increased through modification of the original sheets, hence vertical elongation of the existing modules (1.1 m) presents the only alternative for increasing this critical design parameter.

Based on the results obtained above, it was decided to discard sheet modification and to conduct all further experimentation of Reactor 2A with the original fiber glass material (Type 1) as stationary support for TiO_2.

(e)   Screening Study (Immobilized-Bed Reactor)

Introduction and Objectives:

Seven parameters were identified for an initial screening study of Reactor 2A operated as an IMM reactor (see Tables 4.1 and 4.6). The objectives were to (1) obtain a rough estimate of the effects of the various parameters on the defined response functions (2) eliminate insignificant parameters in accordance with the Pareto Principle (3) identify important parameters for optimization purposes and (4) evaluate the application of a highly fractionated (1/16th) two-level factorial design in a screening study (i.e. an orthogonal array).

Results and Discussion:

Table 4.6: Design matrix for IMM screening study (orthogonal array : OA 8.7.2.2).

Run	CSL[a] (g/L)	Volumetric Flow Rate[b] (L/min.)	Gas Flow Rate[b] (L/min.)	[p-CP]$_o$[c] (mg/L)	UV[d] Source	HID[e] (cm)	Reaction Volume (L)	$10^2 k_{obs}$ (mins^{-1})	Half-life (mins)	R^2
1	1	1	5	13	1	5	3	1.22	56.8	0.98
2	20	1	20	13	2	5	6	2.76	25.1	0.99
3	1	2	20	13	1	15	6	0.86	80.6	0.98
4*	20	2	5	13	2	15	3	4.22	16.4	0.99
5	1	1	5	40	2	15	6	1.35	51.3	0.98
6	20	1	20	40	1	15	3	1.18	58.7	0.99
7	1	2	20	40	2	5	3	2.51	27.6	0.98
8	20	2	5	40	1	5	6	0.50	138.6	0.97

a CSL = Catalyst suspension loading *used for impregnation* (see Table 4.4 for conversion factors)
b Oxygen gas purge only
c [p-CP]$_o$ = Initial concentration of p-CP
d UV source : 1 = Fluorescent Blacklight (UV-C); 2 = Germicidal (UV-A)
e HID = Horizontal irradiation distance
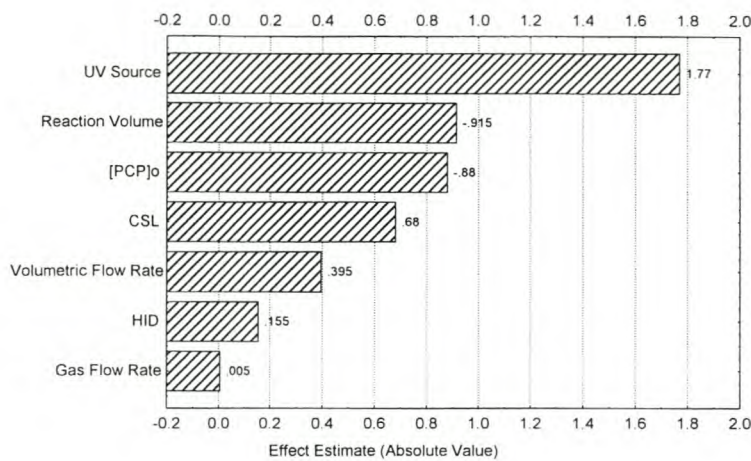* Best result in terms of reaction rate constant (run 4)

145

Figure 4.7: Pareto chart illustrating parameter effects with respect to first order rate constant (k_{obs}) as response function. (CSL = Catalyst Suspension Loading *used for impregnation of sheet*; [p-CP]o = p-CP Initial Concentration in mg/L; HID = Horizontal Irradiation Distance in cm)

The results obtained from these experiments (Table 4.6 and Figure 4.7) indicated that :

- first order exponential decay kinetics apply for the PCO of p-CP;
- operating the IMM reactor with germicidal UV-C lamps has a highly beneficial effect on the PCO efficiency of p-CP. This observation is attributed to the shorter wavelength (and thus higher energy) of UV-C radiation (254 nm) compared to fluorescent UV-A radiation (*ca* 315-400 nm). Theoretical power input in terms of radiant flux is identical for both types of lamps used (i.e. 15 W per lamp);
- an increase in reaction volume reduces the PCO rate constant. This result confirms the limitation of the Reactor 2A in terms of volume of water treated in recirculation mode;
- p-CP initial concentration has an intermediate negative effect on the PCO rate constant. This observation confirms the utility of Reactor 2A for the treatment of low concentrations of pollutant ;
- the PCO rate constant is marginally influenced by the amount of TiO_2 immobilized on the reactor sheet module. This result proves the utility of the reactor for economical operation using small amounts of catalyst ;
- the effects of volumetric flow rate, horizontal irradiation distance and oxygen flow rate are negligible within the framework of the selected experimental design ;
- parameter main effects are calculated successfully when using highly fractionated factorial designs in tandem with linear mathematical models. This observation indicates the utility of the selected design in terms of multi-parameter screening. ANOVA significance probabilities, however, could not be specified due to an insufficient number of degrees of freedom;
- parameter effects are confounded with each other when applying quadratic (polynomial) modeling. The calculation of parameter interactions is therefore precluded.

Based on the results obtained above, it became evident that the Pareto Principle applied, viz: (1) one or two parameters exerted predominant effects on the response and (2) several parameters are insignificant and could therefore be kept constant at convenient experimental levels. It remained to be seen what the absolute effect of catalyst impregnation loading is when applying a standard set of conditions to the operation of Reactor 2A as an IMM reactor.

(f)   Catalyst Impregnation Loading (Immobilized-Bed Reactor)

Introduction and Objectives:

The effect of catalyst impregnation loading was examined by comparing results for 5 different suspension loadings of TiO_2 (1; 5; 10; 20 and 30). The corresponding impregnation loadings amounted to 1.0, 8.1, 14.1, 21.6 and 24.8 g TiO_2 per sheet module (0.88 m^2). The remainder of the system parameters was evaluated at standard reference levels (Table 4.1). The objectives of this study were to (1) assess the effect of catalyst impregnation loading on the rate of oxidation of 40 mg/L p-CP in the recirculation mode and (2) to determine an optimum or plateau value for this parameter in terms of first order rate constants.

Results and Discussion:

Table 4.7: Kinetic results for impregnation loading study.

Catalyst Suspension Loading (g/L TiO_2) (used for sheet coating)	Catalyst Impregnation Loading (g TiO_2 per sheet*)	Catalyst Impregnation Loading (g TiO_2 per m^2)	Observed first order rate constant (k_{obs} in $mins^{-1}$)
1	1.0	1.1	2.55
5	8.1	9.2	7.14
10	14.1	16.0	5.75
20	21.6	24.5	3.90
30	24.8	28.2	3.80

* Sheet coating area = 0.88 m^2
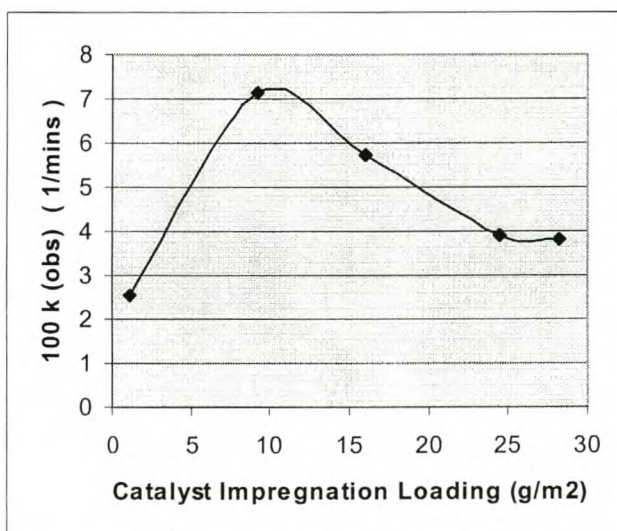
Figure 4.8: First order rate constant as a function of catalyst impregnation loading.

147

The results obtained from these experiments (Table 4.7 and Figure 4.8) indicated that :

- an optimum catalyst impregnation loading exists for the PCO of 40 mg/L of p-CP using Reactor 2A in recirculation mode. This observation is in contrast to literature examples which state that an asymptotic dependence of rate on catalyst mass exists for immobilized photocatalytic reactors (Herrmann, 1995). This result can probably be ascribed to the novel configuration of Reactor 2A. It is however an acceptable price to pay in order to circumvent the filtration problem associated with slurry phase reactors ;
- the optimum loading of 9.2 g/m^2 is obtained by applying a suspension loading of 5 g/L TiO$_2$ according to the specified standard suspension coating procedure. This value (equivalent to 0.92 mg/cm^2) is in good agreement with Herrmann's optimum value of 1.3 mg/cm^2 ;
- higher catalyst impregnation loadings are detrimental to the efficiency of the IMM reactor. This effect could possibly be ascribed to a change in mass transfer characteristics of the system as a function of the amount of immobilized catalyst ;
- the catalytic activity of TiO$_2$ is suppressed when operating Reactor 2A as an IMM reactor in recirculation mode.

Based on the results obtained above, it was evident that the surface-catalyzed nature of PCO processes should be addressed through comprehensive kinetic studies. Moreover, the contributing effect of mass transfer is dependent on several parameters such as (1) the initial concentration of p-CP (2) the amount of immobilized catalyst (3) byproduct interference and (4) pH variations.

(g)   pH Effects (Immobilized-Bed Reactor)

Introduction and Objectives:

The effect of pH was examined by operating Reactor 2A as an IMM reactor in recirculation mode. Results were compared for 5 different initial pH conditions against the standard (neutral) pH of 7.5 for distilled water spiked with p-CP. 1M NaOH and 1M HCl (and dilutions thereof) were used as additives to adjust the initial pH. The catalyst suspension loading used for coating was 20 g/L TiO$_2$ (equivalent impregnation loading of approximately 24.4 g/m^2). The remainder of the system parameters was evaluated at their standard reference levels (Table 4.1). These levels (in combination with an initial p-CP concentration of 13 mg/L) were selected to ensure the *highest* PCO efficiency possible. An equivalent "dark adsorption" experiment was conducted in tandem with each PCO reaction by employing identical parametric conditions and merely excluding the use of the UV light source.

The objectives of this study were to (1) assess the PCO efficiency of the IMM reactor as a function of initial pH and (2) determine variations in p-CP mass transfer at high impregnation loading, low initial concentration (13 mg/L) and in the absence of UV irradiation.

Results and Discussion:

Table 4.8: Kinetic results for pH study.

Initial solution pH	$10^2 \, k_{obs}$ (mins^{-1})	Dark adsorption (%)**
3.0	2.82	10.1
5.0	4.15	10.6
6.2*	4.18	10.2
7.5 (neutral)	4.22	9.5
9.0	3.99	5.2
11.0	2.49	3.1

*pH 6.2 is the point of zero charge (PZC) for TiO$_2$
** Dark adsorption = mass transfer
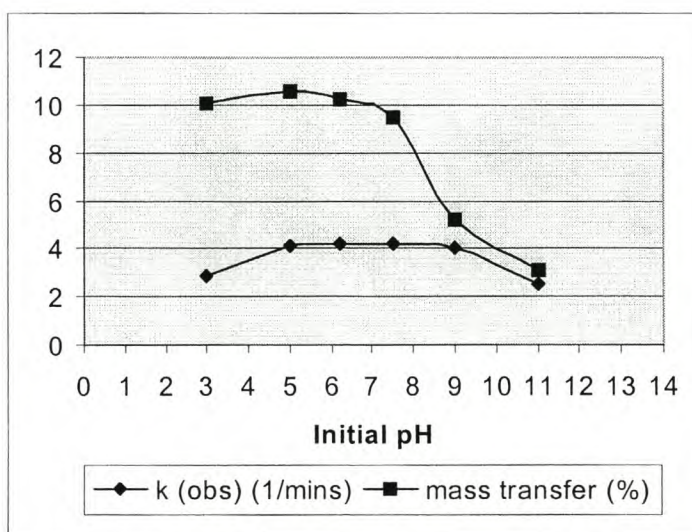
Figure 4.9: First order rate constant (k_{obs}) and mass transfer (%) as a function of initial pH.

The results obtained from these experiments (Table 4.8 and Figure 4.9) indicated that :

- the observed first order rate constant is largely independent of initial solution pH in the range pH 5 to 9. This result is ascribed to favorable adsorption kinetics attained for p-CP and TiO$_2$ in this region ;
- the degree of p-CP mass transfer to immobilized TiO$_2$ is generally in the order 10% (w/w) ;
- the rate constant for the PCO of p-CP is markedly suppressed at an initial pH of 3. The additive in this instance (HCl) is probably responsible for providing an excess of chloride ions in solution that could potentially block active sites on the surface of the TiO$_2$ particles. As stated before, this will hamper surface adsorption of p-CP, water and O$_2$ molecules, and will consequently inhibit p-CP's surface catalyzed oxidation ;
- the PCO efficiency is markedly suppressed at an initial pH of 11. This result is ascribed to reduced mass transfer of p-CP caused by electrostatic repulsion between dissociated p-CP (present as phenolate anions) and TiO$_2$ (present as TiO$^-$ anions) (pK$_a$ = 9.4 for p-CP) (Hoffmann et al., 1995);

149

- p-CP mass transfer in the order of 10% (w/w) is a good measure for efficient PCO in IMM type reactors.

Based on the results obtained above, it is clear that the phenomenon of mass transfer is a very complex one with regard to the efficiency and rate kinetics of surface catalyzed photocatalytic reactions. These aspects require more detailed investigation.

(h)   Screening Study (Combined Slurry-Immobilized Reactor)

Introduction and Objectives:

Eight parameters were identified for an initial screening study of Reactor 2A operated as a SLIMM reactor (see Tables 4.1 and 4.9). The objectives were to (1) obtain a rough estimate of the effects of the various parameters on the response functions (2) eliminate insignificant parameters in accordance with the Pareto Principle (3) identify important parameters for optimization purposes and (4) evaluate the utility of a highly fractionated $(1/16^{th})$ two-level factorial design in a screening study (i.e. an orthogonal array).

Results and Discussion:

Table 4.9: Design matrix for SLIMM screening study (orthogonal array : OA 16.8.2.3).

Run	CIL[a] (g/L)	CSL[b] (g/L)	VFR[c] (L/min.)	Gas[d] Flow Rate (L/min.)	[p-CP]$_o$[e] (mg/L)	UV[f] Source	HID[g] (cm)	Reaction Volume (L)	$10^2 k_{obs}$ (mins^{-1})	Half-life (mins)	R^2
1	1	1	1	5	13	1	5	3	2.14	32.4	0.98
2	1	20	1	20	13	2	5	6	3.58	19.4	0.99
3	1	1	2	20	13	1	15	6	2.38	29.1	0.97
4	1	20	2	5	13	2	15	3	7.24	9.60	0.98
5	1	1	1	5	40	2	15	6	1.88	36.9	0.99
6	1	20	1	20	40	1	15	3	1.42	48.8	0.99
7	1	1	2	20	40	2	5	3	6.84	10.1	0.97
8	1	20	2	5	40	1	5	6	1.87	37.1	0.98
9	20	20	2	20	40	2	15	6	3.91	17.7	0.99
10	20	1	2	5	40	1	15	3	2.08	33.3	0.98
11*	20	20	1	5	40	2	5	3	7.90	8.80	0.96
12	20	1	1	20	40	1	5	6	0.94	73.7	0.92
13	20	20	2	20	13	1	5	3	3.87	17.9	0.99
14	20	1	2	5	13	2	5	6	4.57	15.2	0.99
15	20	20	1	5	13	1	15	6	2.08	33.3	0.99
16	20	1	1	20	13	2	15	3	6.93	10.0	0.97

a CIL = Catalyst impregnation loading (expressed as suspension loading used for coating)
b CSL = True Catalyst suspension loading (in addition to immobilized catalyst)
c VFR = Volumetric Flow Rate
d Oxygen gas purge only
e [p-CP]$_o$ = Initial concentration of p-CP
f UV source : 1 = Fluorescent Blacklight (UV-C); 2 = Germicidal (UV-A)
g HID = Horizontal irradiation distance
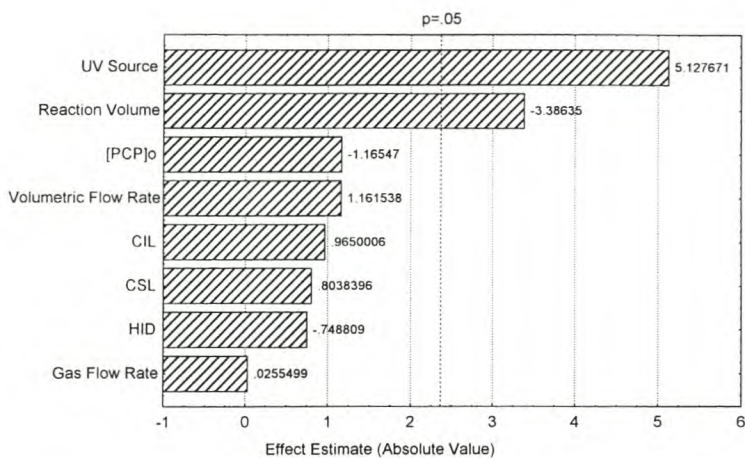* Best result in terms of reaction rate constant (run 11)

Figure 4.10: Pareto chart illustrating standardized parameter effects (AVOVA probability = 0.05) for first order rate (k$_{obs}$) as response function. (CIL = Catalyst Suspension Loading *used for impregnation of sheet*; CSL = True Catalyst Suspension Loading in addition to CIL; [p-CP]o = p-CP Initial Concentration in mg/L; HID = Horizontal Irradiation Distance in cm)

The results obtained from these experiments (Table 4.9 and Figure 4.10) indicated that :

• first order exponential decay kinetics apply for the PCO of p-CP;

• operating the SLIMM reactor with germicidal UV-C lamps has a highly beneficial effect on the PCO of p-CP. This result was also obtained with the IMM reactor and the same reasoning applies ;

• increase in reaction volume inhibits PCO significantly. This result confirms the limitation of the Reactor 2A in terms of treating TiO$_2$ suspensions of polluted water in recirculation mode (SLIMM) ;

• the relative contributions of the remainder of the parameters (i.e. p-CP initial concentration, volumetric flow rate, both catalyst loading parameters, horizontal irradiation distance and oxygen flow rate) are statistically insignificant with respect to the constraints of the chosen experimental design. They can be discarded with a 95 % confidence level ;

• parameter main effects are calculated successfully when using highly fractionated factorial designs in tandem with linear mathematical models. This observation indicates the utility of the selected design in terms of multi-parameter screening ;

• ANOVA significance probabilities are successfully calculated due to a sufficient number of degrees of freedom. The main effects for UV source and reaction volume are statistically significant (with null hypothesis confirmation probability of less than 5%) ;

• second order parameter interactions are not confounded with other effects and are successfully calculated by applying a quadratic polynomial model. The results show a similar trend to that obtained with linear modeling, however an interesting interaction between volumetric flow rate and catalyst impregnation loading is noted. This result confirms the importance of efficient contact between the falling film layer and the immobilized PCO catalyst (i.e. TiO$_2$) ;

• the Pareto Principle applies for the operation of Reactor 2A as a SLIMM reactor.

151

(i)   Reproducibility Tests

A number of tests were conducted to assess the reproducibility of results for the PCO of p-CP through the operation of Reactor 2A as SLIMM or IMM reactors in recirculation mode. Only the Type 1 fiber glass sheet module was used in these investigations. The main results for these tests (Table 4.10) showed that :

- reproducible rate constants (RSM < 10%) are achieved for the PCO of 40 mg/L p-CP when using *different* sheet modules from the same product batch (coated under identical conditions according to the *standard* coating procedure). This result is observed for both reactor configurations (IMM and SLIMM) using triplicate trial runs (studies A and B) ;
- a *single* TiO_2 coated fiber glass sheet maintains catalytic activity (hence statistical reproducibility) for at least 5 consecutive recirculation treatments of 40 mg/L p-CP (at the standard reference levels for the system parameters) and using fresh solutions for each run. This result is also observed for both configurations (studies C and D) ;
- catalytic activity is markedly suppressed when reusing the original aqueous solution or slurry matrix (spiked with fresh p-CP to a level of 40 mg/L) (studies E and F);
- recirculation of a sample of clean distilled water over the sheet module (between successive PCO runs) assists the retention of catalytic activity during operation of the IMM reactor (compare test G with E) ;
- virtually no impregnated catalyst is lost from sheet modules during or after the execution of a falling film experiment.

Table 4.10: Reproducibility study for Reactor 2A operated in recirculation mode.

Reactor Configuration	$10^2\ k_{obs}\ (mins^{-1})$ - for the PCO of 40 mg/L p-CP						
	Study	Run 1	Run 2	Run 3	Run 4	Run 5	RSD (%)
IMM	A	7.14	7.01	7.83	-	-	6.0
SLIMM	B	9.69	9.92	9.02	-	-	4.9
IMM	C	7.22	7.04	7.33	7.91	7.35	4.4
SLIMM	D	9.23	9.75	9.38	9.03	9.89	3.8
IMM	E	7.33	3.13	2.47	-	-	-
SLIMM	F	9.15	3.39	2.79	-	-	-
IMM	G	7.10	5.02	3.36	-	-	-

The results mentioned above are preliminary, hence a more detailed study is required to monitor and improve (where necessary) the catalytic activity of TiO_2 immobilized on the fiber glass sheet modules. Catalyst reactivation procedures such as (1) controlled periodic illumination (2) physical-chemical treatment of sheet modules and (3) pH correction of TiO_2 slurries, should be addressed in future.

(b)   Representative Example

Introduction and Objectives:

The effects of reactor configuration and fiber glass module type were examined by operating Reactor 2A as (1) IMM and (2) SLIMM reactors. System parameters were evaluated at standard reference levels (Table 4.11). A sequence of 10 consecutive single pass irradiations was used, thus N=0 to N=10 applied. The *standard* suspension coating procedure was applied to all sheet modules (i.e. using a catalyst suspension loading of 5 g/L TiO_2).

The objectives of this study were to (1) compare the utility of the 2 original sheet modules (i.e. the reinforced and tissue-like fiber glass modules) for the PCO of p-CP in single pass modes (2) assess the auxiliary effect of additional suspended TiO_2 when switching from IMM to SLIMM reactor configuration and (3) investigate the utility of 2^2 factorial designs for determining main effects and interactions with respect to the defined response functions.

Results and Discussion:

Table 4.12: p-CP concentration data (in mg/L) as a function of single pass number (N), sheet type and reactor configuration.

Single Pass Number (N)	Fiber Glass Type 1 (reinforced sheet)		Fiber Glass Type 2 (non-reinforced tissue sheet)	
	IMM Reactor	SLIMM*** Reactor	IMM Reactor	SLIMM Reactor
0	40.0	40.0	40.0	40.0
1	32.1	31.5	32.5	32.1
2	25.9	24.5	27.5	26.3
3	20.2	18.9	22.2	20.8
4	15.2	13.4	19.1	16.6
5	11.9	10.1	16.2	12.9
6	8.9	6.9	14.5	10.8
7	6.8	4.8	12.5	8.0
8	5.0	ND	12.4	6.9
9	2.9		11.9	4.9
10**	ND*		10.4	ND

* = Not detected; Limit of Detection = 1 mg/L
**   Cumulative UV irradiation time = 41.0 secs (theoretical UV dosage = *ca* 838 mW-s/cm^2)
*** Additional suspended catalyst = 1 g/L TiO_2 (for SLIMM)

154
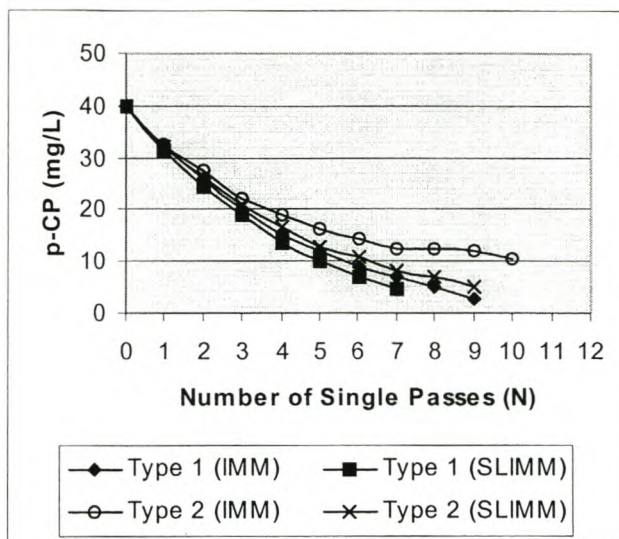
Figure 4.11: p-CP oxidation as a function of sheet module, reactor configuration and single pass number (N) - where each N equals 4.1 seconds of UV irradiation.

Table 4.13: Summary of kinetic analysis.

Kinetic Response Function	Fiber Glass Type 1 (reinforced sheet)		Fiber Glass Type 2 (non-reinforced tissue sheet)	
	IMM Reactor	SLIMM Reactor	IMM Reactor	SLIMM Reactor
10^2 k_{obs} (N)* (pass^{-1})	27.9	30.3	13.2	22.9
Half-life (passes)	2.5	2.3	5.3	3.0
10^2 k_{obs} (t)** (sec^{-1})	6.73	7.37	3.19	5.64
Half-life (secs)	10.3	9.4	21.7	12.3
10^2 k_{obs} (t) (mins^{-1})	403.8	442.4	191.4	338.1
Half-life (mins)	0.17	0.15	0.36	0.21
R^2	0.99	0.99	0.96	0.99

k_{obs} (N)* = Observed first order rate constant as a function of single pass number (N)
(each single pass is equivalent to a UV contact time of 4.1 secs)
k_{obs} (t)** = Observed first order rate constant as a function of irradiation time
(in sec or mins)

155
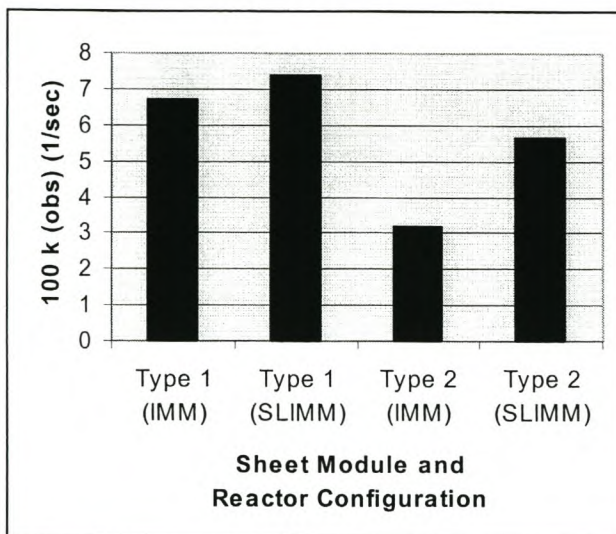
Figure 4.12: First order rate constants as a function of sheet module and reactor configuration.

Table 4.14: Design matrix for factorial study.

Sheet Module Type	Reactor Configuration	$10^2 \, k_{obs}$ (sec^{-1})
1	IMM	6.73
2	IMM	3.19
1	SLIMM	7.37
2	SLIMM	5.64

Figure 4.13: Pareto chart illustrating parameter main effects and second order interaction effect with respect to first order rate (k_{obs}) as response function.

Figure 4.14: Second order response surface illustrating parameter effects and second order interaction effect with respect to first order rate (k_{obs}). (Reactor configurations: 1 = IMM and 2 = SLIMM).

The results obtained from these experiments (Tables 4.12 to 4.14 and Figures 4.11 to 4.14) indicated that :

- first order decay kinetics apply for the PCO of p-CP when operating Reactor 2A in sequential single pass mode ;
- PCO efficiency is substantially greater when using the original reinforced fiber glass sheet module (Type 1) as stationary support for TiO_2. This result is attributed to the surface roughness of the Type 1 material, which may result in beneficial mixing and turbulence effects during falling film flow. The effect of sheet type used is also fairly independent of reactor configuration, which means that both IMM and SLIMM reactors will benefit from surface roughened supports ;
- for fiber glass Type 1 as sheet module, the oxidation rate increases marginally when switching from the IMM to SLIMM reactor configuration. This result demonstrates that the auxiliary effect of slurried catalyst (1 g/L in this study) is insignificant when surface roughness of the support is pronounced ;
- for the fiber glass Type 2 sheet module, PCO efficiency increases considerably when switching from IMM to SLIMM configuration. This result demonstrates that additional suspended TiO_2 is beneficial for oxidation when using a relatively smooth support (under laminar flow conditions) ;
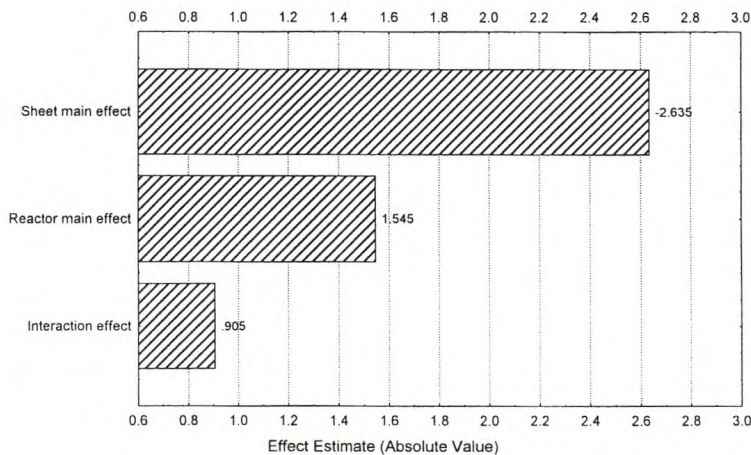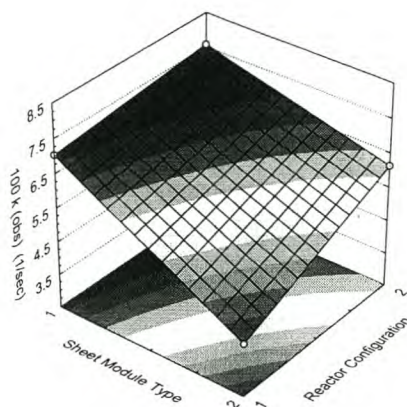- parameter main effects and interactions are calculated successfully using a quadratic (2nd order) model in conjunction with a 2 x 2 factorial design ;
- the interaction effect between reactor sheet type and configuration is insignificant compared to the individual main effects.

Based on the results obtained above, it is evident that the physical characteristics of the TiO_2 support is of critical importance when evaluating IMM reactor configurations and combinations thereof with slurried systems (SLIMM). The operation of Reactor 2A as IMM reactor for efficient PCO removal of p-CP is justified. Full characterization of the fiber glass materials is required (e.g. porosity, surface area and micro-structure analyses).

(c)   Screening Study (Immobilized-Bed Reactor)

Introduction and Objectives:

Seven parameters were identified for an initial screening study of Reactor 2A operated as an IMM reactor (Tables 4.11 and 4.15). The objectives were to (1) obtain a rough estimate of the effects of the various parameters on the response functions (2) eliminate insignificant parameters in accordance with the Pareto Principle (3) identify important parameters for optimization purposes and (4) evaluate the application of a highly fractionated (1/16th) two-level factorial design in a screening study (i.e. an orthogonal array).

Results and Discussion:

Table 4.15: Design matrix for IMM screening study (orthogonal array : OA 8.7.2.2).

Run	CSL (g/L)	Volumetric Flow Rate (L/min.)	Gas Flow Rate[b] (L/min.)	$[p\text{-CP}]_o{}^c$ (mg/L)	UV[d] Source	HID[e] (cm)	Reaction Volume (L)	D* (%)	$10^2 k_{obs}(N)$** (pass^{-1})
1	1	1	5	13	1	5	3	10.6	6.42
2***	20	1	20	13	2	5	6	23.8	25.74
3	1	2	20	13	1	15	6	6.0	5.66
4	20	2	5	13	2	15	3	22.9	18.40
5	1	1	5	40	2	15	6	13.8	12.02
6	20	1	20	40	1	15	3	4.3	4.88
7	1	2	20	40	2	5	3	15.7	11.66
8	20	2	5	40	1	5	6	3.3	3.28

a CSL = Catalyst suspension loading *used for impregnation* (see Table 4.4 for conversion factors)
b Oxygen gas purge only
c $[p\text{-CP}]_o$ = Initial concentration of p-CP
d UV source : 1 = Fluorescent Blacklight (UV-C); 2 = Germicidal (UV-A)
e HID = Horizontal irradiation distance
*   D = Degradation of p-CP (%)
** $k_{obs}(N)$ = First order rate constant as a function of single pass number
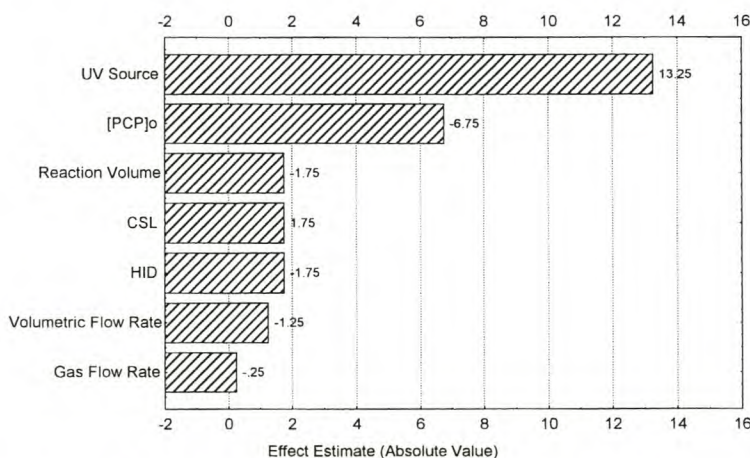*** Best result in terms of reaction rate constant (run 2)

Figure 4.15: Pareto chart illustrating parameter main effects with respect to p-CP degradation (%) as response function. (CSL = Catalyst Suspension Loading *used for impregnation of sheet*; [p-CP]o = p-CP Initial Concentration in mg/L; HID = Horizontal Irradiation Distance in cm)
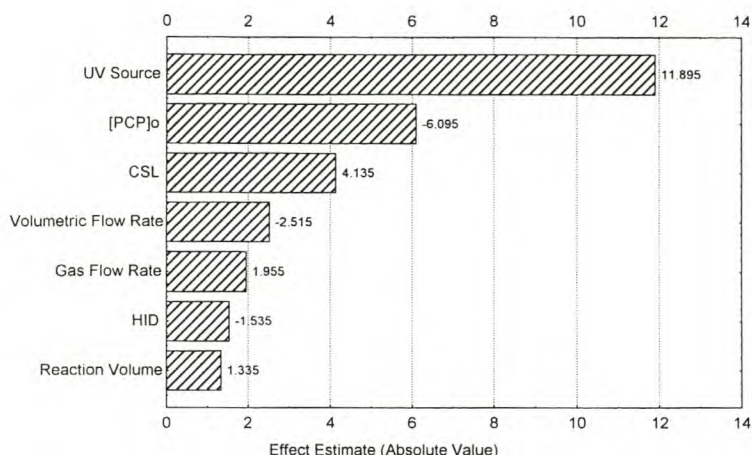
Figure 4.16: Pareto chart illustrating parameter main effects with respect to the first order rate constant (k_{obs}) as a function of sequential single pass number. (CSL = Catalyst Suspension Loading *used for impregnation of sheet*; [p-CP]o = p-CP Initial Concentration in mg/L; HID = Horizontal Irradiation Distance in cm)

The results obtained from these experiments (Table 4.15 and Figures 4.15 to 4.16) indicated that :

- first order exponential decay kinetics apply for the PCO of p-CP when operating Reactor 2A as IMM reactor in sequential single pass mode ;
- operating the IMM reactor with germicidal UV-C lamps has a highly beneficial effect on the PCO efficiency in both single pass modes ;
- p-CP initial concentration has an intermediate negative effect on the PCO efficiency for *both* modes. This observation confirms the utility of Reactor 2A for the treatment of low concentrations of pollutant ;
- the effect of volumetric flow rate is negligible in single pass mode and diminishes further for the sequential mode. These observations confirm the potential use of the reactor for treating large volumes of polluted water efficiently ;
- the effects of horizontal irradiation distance and oxygen flow rate are negligible within the framework of the selected experimental design. These results demonstrate the practical benefits of Reactor 2A ;
- the effect of immobilized catalyst (expressed in terms of the suspension loading used for coating) becomes more significant when switching from single pass to sequential single pass mode. This result confirms the importance of attaining optimized conditions for the *first* single pass in a network of sequential single pass reactors ;
- parameter main effects are calculated successfully when using highly fractionated factorial designs in tandem with linear mathematical models ;
- the Pareto Principle applies, viz: (1) one or two parameters exert predominant effects on the response and (2) several parameters are insignificant and could therefore be kept constant at convenient experimental levels.

Based on the results obtained above, it remained to be seen how significantly the degradation efficiency of the single pass reactor (2A) depended on the amount of immobilized catalyst.

159

(d)   Catalyst Impregnation Loading (Immobilized-Bed Reactor)

Introduction and Objectives:

The effect of catalyst impregnation loading was examined by comparing results for 5 different suspension loadings of TiO_2 (1; 5; 10; 20 and 30). The corresponding impregnation loadings amounted to 1.0, 8.1, 14.1, 21.6 and 24.8 g TiO_2 per sheet module (0.88 m^2). This specific batch of sheet modules were also used for the equivalent study in recirculation mode (see Section 4.1.1(f)). The remainder of the system parameters was evaluated at standard reference levels (Table 4.11). The objectives of this study were to (1) assess the effect of catalyst impregnation loading on the PCO of 40 mg/L p-CP in the single pass mode and (2) to determine an optimum or plateau value for this parameter in terms of the defined response function (i.e. percentage of p-CP degradation).

Results and Discussion:

Table 4.16: Kinetic results for impregnation loading study.

Catalyst Suspension Loading (g/L TiO_2) (*used for sheet coating*)	Catalyst Impregnation Loading (g TiO_2 per sheet*)	Catalyst Impregnation Loading (g TiO_2 per m^2)	p-CP Degradation (%)
1	1.0	1.1	11.3
5	8.1	9.2	19.1
10	14.1	16.0	19.6
20	21.6	24.5	19.7
30	24.8	28.2	19.8

* Sheet coating area = 0.88 m^2
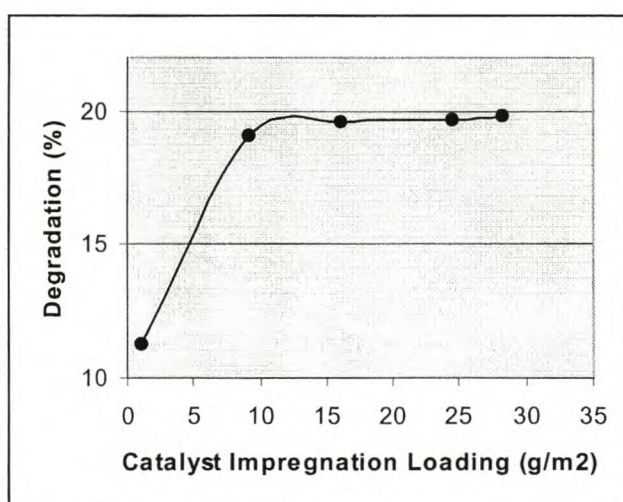
Figure 4.17: Degradation (%) of p-CP as a function of catalyst impregnation loading.

160

The results obtained from these experiments (Table 4.16 and Figure 4.17) indicated that :

- the PCO degradation efficiency increases with approximately 10% when increasing the impregnation loading from *ca* 1 to 9 g TiO_2 /m^2 ;
- beyond loadings of 10 g/m^2 a plateau value exists for the amount of p-CP oxidized as a function of catalyst impregnation loading (p-CP initial concentration: 40 mg/L). This result implies that PCO efficiency becomes independent of the mass of immobilized TiO_2 when operating Reactor 2A in single pass mode ;
- maximum degradation (*ca* 19%) is attained for a catalyst impregnation loading of between 9 and 16 g/m^2 TiO_2 (i.e. between 0.9 and 1.6 mg/cm^2). This value is in good agreement with literature values for typical immobilized-bed photoreactors (Herrmann, 1995; Herrmann, 1999).

Based on the results obtained above, it is evident that the existence of a plateau in the catalyst impregnation loading would facilitate the optimization of other configurations of immobilized PCO reactors (e.g. a single pass horizontal flow system).

(e)   pH Effects (Immobilized-Bed Reactor)

Introduction and Objectives:

The effect of pH was examined by operating Reactor 2A as an IMM reactor in the single pass mode and comparing results for 5 different initial pH conditions against the standard (neutral) pH of 7.5 for distilled water spiked with p-CP. 1M NaOH and 1M HCl (and dilutions thereof) were used as additives to adjust the initial pH. The catalyst suspension loading used for coating was 20 g/L TiO_2 (equivalent impregnation loading of approximately 24.4 g/m^2). The remainder of the system parameters was evaluated at their standard reference levels (Table 4.11). These levels (in combination with an initial p-CP concentration of 13 mg/L) were selected to complement the analogous study using the recirculation mode of operation. An equivalent "dark adsorption" experiment was conducted in tandem with each PCO reaction by employing identical parametric conditions and merely excluding the use of the UV light source.

The objectives of this study were to (1) assess the PCO efficiency of the IMM reactor as a function of initial pH and (2) determine variations in p-CP mass transfer at high impregnation loading, low initial concentration (13 mg/L) and in the absence of UV irradiation.

Results and Discussion:

Table 4.17: Degradation results for pH study.

Initial solution pH	Degradation (%)	Dark adsorption (%)
3.0	8.5	10.1
5.0	22.7	10.2
6.2	22.2	9.8
7.5 (neutral)	22.9	9.9
9.0	17.8	5.6
11.0	10.4	3.0

*pH 6.2 is the point of zero charge (PZC) for TiO_2
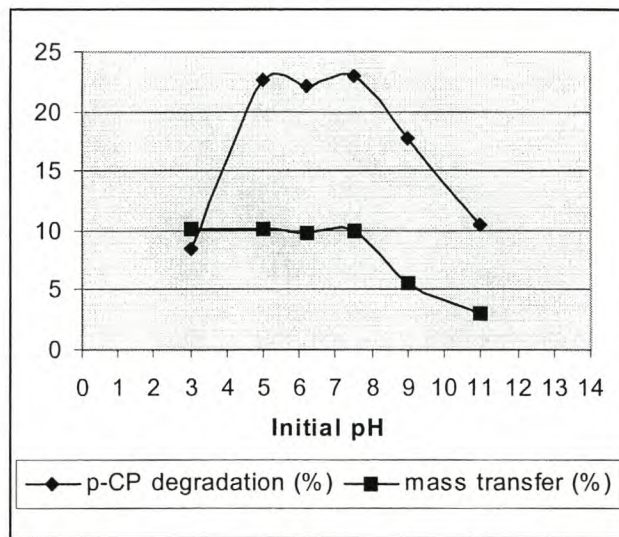
Figure 4.18: Degradation (%) of p-CP and mass transfer (%) as a function of initial pH.

The results obtained from these experiments (Table 4.17 and Figure 4.18) indicated that :

- the PCO degradation of p-CP is largely independent of initial solution pH in the range pH 5 to 7.5 when utilizing the single pass mode of operation. This result is ascribed to favorable adsorption kinetics attained for p-CP and TiO_2 in this region. The degree of p-CP mass transfer to immobilized TiO_2 is generally in the order 10% (w/w) ;
- the PCO efficiency is markedly suppressed at an initial pH of 3. The additive in this instance (HCl) is probably responsible for interfering with the PCO process (as explained before) although mass transfer of p-CP remains constant ;
- the PCO efficiency is suppressed when increasing the initial pH to 9 and 11, respectively. This result is ascribed to reduced mass transfer of p-CP as explained earlier ;
- p-CP mass transfer in the order of 10% (w/w) is a good measure for efficient PCO in single pass immobilized-bed reactors ;
- the superior PCO degradation efficiency of Reactor 2A operated in *single pass mode* (compared to recirculation mode) is clearly demonstrated (compare Figures 4.9 and 4.18).

162

(f)   Screening Study (Combined Slurry-Immobilized Reactor)

Introduction and Objectives:

Eight parameters were identified for an initial screening study of Reactor 2A operated as a SLIMM reactor (see Tables 4.11 and 4.18). The objectives were to (1) obtain a rough estimate of the effects of the various parameters on the response functions (2) eliminate insignificant parameters in accordance with the Pareto Principle (3) identify important parameters for optimization purposes and (4) evaluate the application of a highly fractionated (1/16th) two-level factorial design in a screening study (i.e. an orthogonal array).

Results and Discussion:

Table 4.18: Design matrix for SLIMM screening study (orthogonal array : OA 16.8.2.3).

Run	CIL[a] (g/L)	CSL[b] (g/L)	VFR[c] (L/min.)	Gas[d] Flow Rate (L/min.)	$[p\text{-}CP]_o$[e] (mg/L)	UV[f] Source	HID[g] (cm)	Reaction Volume (L)	D* (%)	10^2 k (N)** (pass^{-1})
1	1	1	1	5	13	1	5	3	8.1	7.4
2***	1	20	1	20	13	2	5	6	46.2	35.14
3	1	1	2	20	13	1	15	6	6.2	6.84
4	1	20	2	5	13	2	15	3	40.0	27.5
5	1	1	1	5	40	2	15	6	30.3	21.47
6	1	20	1	20	40	1	15	3	9.9	14.16
7	1	1	2	20	40	2	5	3	17.8	12.64
8	1	20	2	5	40	1	5	6	13.2	11.68
9	20	20	2	20	40	2	15	6	18.0	21.91
10	20	1	2	5	40	1	15	3	11.9	8.36
11	20	20	1	5	40	2	5	3	38.8	33.68
12	20	1	1	20	40	1	5	6	6.1	7.31
13	20	20	2	20	13	1	5	3	20.5	12.15
14	20	1	2	5	13	2	5	6	18.5	28.26
15	20	20	1	5	13	1	15	6	18.6	17.17
16	20	1	1	20	13	2	15	3	42.7	28.4

a CIL = Catalyst impregnation loading (expressed as suspension loading used for coating)
b CSL = True Catalyst suspension loading (in addition to immobilized catalyst)
c VFR = Volumetric Flow Rate
d Oxygen gas purge only
e $[p\text{-}CP]_o$ = Initial concentration of p-CP
f UV source : 1 = Fluorescent Blacklight (UV-C); 2 = Germicidal (UV-A)
g HID = Horizontal irradiation distance
* D = Degradation of p-CP (%)
** k_{obs} (N) = First order rate constant as a function of single pass number
*** Best result in terms of reaction rate constant (run 2)
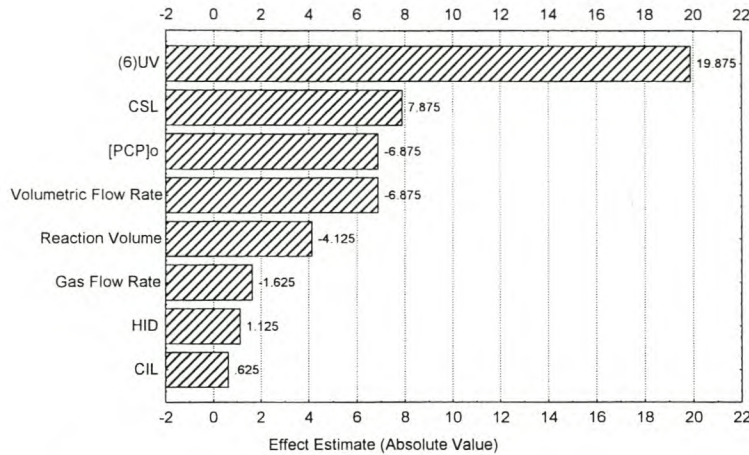
Figure 4.19: Pareto chart illustrating parameter main effects with respect to p-CP degradation (%) as response function. (CIL = Catalyst Suspension Loading *used for impregnation of sheet*; CSL = True catalyst suspension loading in addition to CIL; [p-CP]o = p-CP Initial Concentration in mg/L; HID = Horizontal Irradiation Distance in cm)
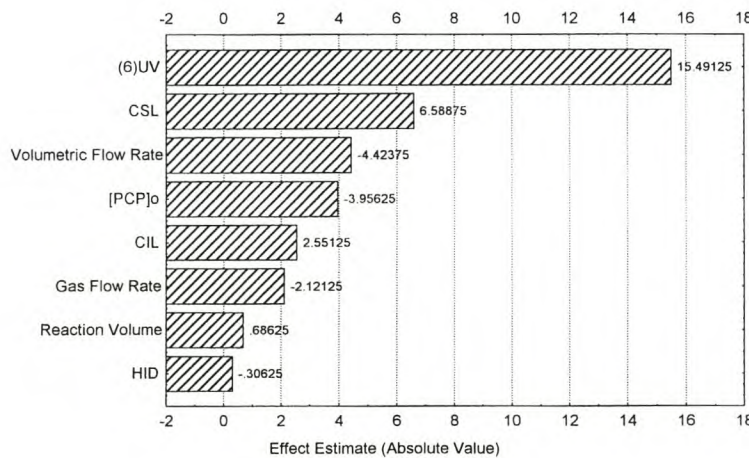
Figure 4.20: Pareto chart illustrating parameter main effects with respect to the first order rate constant (k_{obs}) as a function of sequential single pass number. (CIL = Catalyst Suspension Loading *used for impregnation of sheet*; CSL = True catalyst suspension loading in addition to CIL; [p-CP]o = p-CP Initial Concentration in mg/L; HID = Horizontal Irradiation Distance in cm)

The results obtained from these experiments (Table 4.18 and Figures 4.19 to 4.20) indicated that :

- first order exponential decay kinetics apply for the PCO of p-CP when operating Reactor 2A as a SLIMM reactor in sequential single pass mode ;
- operating the SLIMM reactor with germicidal UV-C lamps has a highly beneficial effect on the PCO treatment of p-CP in *both* single pass modes, i.e. *single pass* and *sequential single pass* ;

164

- p-CP initial concentration has an intermediate negative effect on PCO efficiency for *both* modes. This observation confirms the utility of Reactor 2A for the treatment of low concentrations of pollutant in single pass mode ;
- the intermediate negative effect of volumetric flow rate is applicable to both single pass modes. This observation implies that penetration of UV light through suspension films may be problematical when operating SLIMM reactors at high flow rate ;
- the effects of horizontal irradiation distance, oxygen flow rate and reaction volume are negligible for both modes within the framework of the selected experimental design. These results demonstrate the practical benefits of Reactor 2A (apart from filtration problems) operated as a SLIMM reactor ;
- the effect of immobilized catalyst (expressed in terms of the suspension loading used for coating) is negligible for the single pass mode, with marginal elevation in significance when switching to sequential single pass mode ;
- the effect of true catalyst suspension loading (in addition to immobilized catalyst) remains positive throughout and remains considerably more significant than the effect of immobilized catalyst. This observation is expected for a slurried system in terms of limited UV penetration ;
- parameter main effects are calculated successfully when using highly fractionated factorial designs (such as the selected orthogonal array) in tandem with linear mathematical models. Moreover, the experimental design approach affords multi-response evaluation ;
- standardized effects (with ANOVA probability specification) can also be generated as a result of a sufficient number of degrees of freedom, although this route was not chosen for the study in question ;
- the Pareto Principle applies, viz: (1) one or two parameters exert predominant effects on the response and (2) several parameters are insignificant and could therefore be kept constant at convenient experimental levels.

Based on the results obtained above and knowledge of the insurmountable problems associated with the filtration of TiO_2 slurries , it is clear that (1) the operation of Reactor 2A should be limited to the IMM reactor configuration and (2) optimized single pass conditions for IMM will render comparative PCO efficiencies to the SLIMM reactor.

(g)   Reproducibility Tests

A number of tests were conducted to assess the reproducibility of results for the PCO of p-CP through the operation of Reactor 2A as SLIMM or IMM reactors in the single pass mode. Only the Type 1 fiber glass sheet module was used in these investigations. The main results for these tests (Table 4.19) showed that :

- reproducible degradation efficiencies (%D) (RSM < 10%) are achieved for the PCO of 40 mg/L p-CP when using *different* sheet modules from the same product batch (coated under identical conditions according to the *standard* coating procedure). This result is observed for both reactor configurations (IMM and SLIMM) using triplicate trial runs (studies A and B) ;
- a *single* TiO_2 coated fiber glass sheet maintains catalytic activity (hence statistical reproducibility) for at least 15 consecutive single passes of 40 mg/L p-CP (at standard

reference levels for the system parameters) and using fresh solutions for each run. These results are observed for both configurations (studies C and D) and are illustrated in the corresponding statistical process control charts (Figures 4.21 and 4.22). All degradation efficiency readings are well within the ±1.5 process sigma limits, thus cannot be treated as outliers (suspect values) ;

- catalytic activity is mildly suppressed when reusing the original aqueous solution spiked with fresh p-CP to a level of 40 mg/L (IMM). The corresponding suppressing effect for the SLIMM reactor is more pronounced (studies E and F) ;
- recirculation of a sample of clean distilled water over the sheet module (between successive PCO runs) assists the retention of catalytic activity during operation of the IMM reactor (test G) ;
- virtually no impregnated catalyst was lost from sheet modules during or after the execution of a falling film experiment.

Table 4.19: Reproducibility study for Reactor 2A operated in single pass mode.

Reactor Configuration	Degradation (%) - for the PCO of 40 mg/L p-CP					
	Study	Run 1	Run 2	Run 3	Run 4	Run 5	RSD (%)
IMM	A	19.8	18.2	19.9	-	-	4.9
SLIMM	B	21.3	23.0	20.5	-	-	5.9
IMM	E	19.0	13.3	8.7	6.5	6.0	-
SLIMM	F	22.3	9.0	5.3	4.9	4.5	-
IMM	G	19.3	16.8	13.8	10.3	9.9	-

Figure 4.21: Statistical process control chart depicting the stability in catalytic activity for one sheet module coated with TiO$_2$. (IMM reactor, Study C).

166

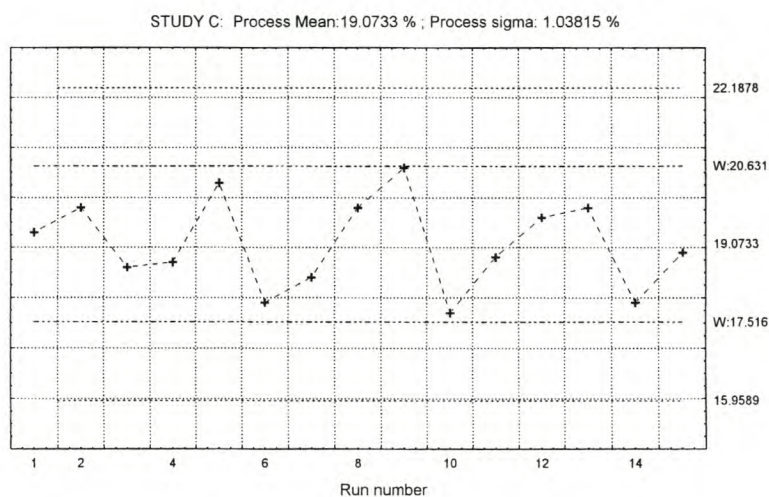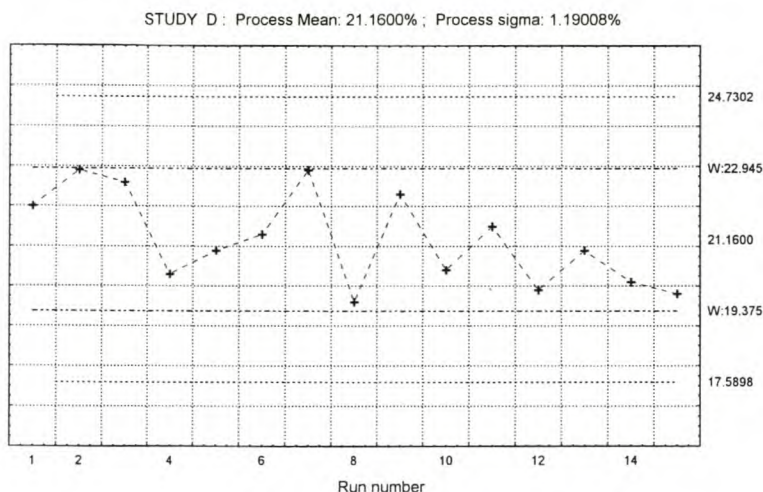STUDY D : Process Mean: 21.1600% ; Process sigma: 1.19008%

Figure 4.22: Statistical process control chart depicting the stability in catalytic activity for one sheet module coated with TiO$_2$. (SLIMM reactor, Study D).

The results mentioned above are preliminary, hence a more detailed study is required to monitor and improve (where necessary) the catalytic activity of TiO$_2$ immobilized on the fiber glass sheet modules. As mentioned before, catalyst reactivation procedures such as (1) controlled periodic illumination (2) physical-chemical treatment of sheet modules, and (3) pH correction of TiO$_2$ slurries, should be addressed in future.

(h)   Cost Calculation

A preliminary cost calculation was made for the PCO treatment of p-CP in distilled water, based on the operation of Reactor 2A as IMM reactor in the sequential single pass mode. The calculation was done in view of the same assumptions made previously (in Section 3.1.3). Bolton's formula for EE/O was used again. Thus, taking the above mentioned p-CP result as example, the EE/O and cost (per m^3) for the PCO of an initial concentration of 40 mg/L to below the limit of detection (1 mg/L) can be calculated as follows :

- orders of removal = log (40/1) = 1.602
- P = 12 x 15 W = 180 W = 0.18 kW
- F = 2 L/minute = 120 L/h = 0.12 m^3/h

EE/O amounts to: (0.18)/(0.12 x 1.602) = 0.94 kWh/order/m^3. At a unit price of 11.8 c/kWh in the Stellenbosch (RSA) area during May 2000, the cost to reduce 40 mg/L p-CP with one order of magnitude (4 mg/L) amounts to 11c / m^3 of water. A further order of magnitude reduction (to 0.4 mg/L) will double the cost, since EE/O is a constant per order. When applying a volumetric flow rate of 1 L/minute, the cost changes to 22c / m^3, which demonstrates that a low volumetric throughput increases EE/O costs in the single pass (plug-flow) reactor. The premise of this argument is similar to what has been explained earlier in Section 3.1.3 (e).

4.2   TREATMENT OF MICROCYSTINS

4.2.1 Recirculation Mode

(a)   System Parameters

The PCO treatment of four variants of microcystins in water was investigated by operating Reactor 2A as (1) immobilized-bed (IMM) and (2) combined slurry-immobilized (SLIMM) reactor. One-factor variation methods were mainly employed to conduct random parametric studies. The following system parameters were evaluated at discrete levels in terms of first order reaction kinetics (Table 4.20):

Table 4.20: System parameters for microcystin study (Reactor 2A; Recirculation Mode)

Parameter	Assigned Levels
Catalyst Suspension Loading (g/L)	0; 1[a]; 5*[a]
Catalyst Loading for Impregnation (g/L)	5*; 20
Volumetric Flow Rate (L/min.)	2.0*[b]
Horizontal Irradiation Distance (cm)	15*
Microcystin Variants	YA, YR, LR and RR
Reaction Volume (L)	5*
Water Matrix	De-ionized water; Lake water*
Gas Purge	Oxygen*
Gas Flow Rate (L/min. O_2)	5*; 20
Number of UV-C lamps for Irradiation	12*[c]
Irradiation Time (mins.)	20*

* Denotes standard reference level of parameters
a For SLIMM reactor configuration
b Surface flow rate = 136 L/hr/m^2
c UV irradiance = 204.5 W/m^2

(b)   TiO$_2$ Impregnation of Sheet Modules

Based on coating and impregnation results obtained earlier (see Section 4.1.1), the reinforced fiber glass material (Type 1) was used as stationary support for TiO$_2$ in the evaluation of Reactor 2A for the PCO of microcystins. The *standard coating procedure* was followed as explained before. This entailed "dark" recirculation of suspensions of TiO$_2$ (in 3 L of distilled water) through the system (across the sheet module) using (1) a 2 L/min. volumetric flow rate (2) a natural suspension pH (4-5) and (3) magnetic stirring for a period of 30 minutes. Sheet modules were weighed before and after coating. Coated sheets were air-dried at room temperature for 24 hrs prior to determining the net increase in weight. A suspension loading of 5 g/L TiO$_2$ was used as *standard reference level* and yielded an impregnation loading of about 7.5 g TiO$_2$ per sheet (i.e. 8.5 g/m^2). The effect of increased impregnation loading was assessed during experimentation (see Table 4.20).

(c)   Catalyst Suspension Loading (Lake Water)

Introduction and Objectives:

The effect of catalyst suspension loading was examined in natural water (Zeekoevlei, Cape Flats, RSA) by comparing results for 3 different loadings of TiO$_2$ (0; 1 and 5 g/L). System parameters were evaluated at standard reference levels (Table 4.20). The objectives of this study were to (1) establish whether an increase in catalyst suspension loading promotes the PCO of microcystins and (2) assess PCO efficiency as a function of reactor configuration (viz: operating Reactor 2A as an IMM or a SLIMM reactor).

Results and Discussion:

Table 4.21: Microcystin concentration data (in ug/L) as a function of time, catalyst loading and variant.

Irradiation Time (mins)	Microcystins (ug/L)								
	YA			YR			LR		
	Catalyst Suspension Loading (g/L)			Catalyst Suspension Loading (g/L)			Catalyst Suspension Loading (g/L)		
	0	1	5	0	1	5	0	1	5
0	18	21	21	53	66	71	23	31	30
2	16	17	12	48	62	55	19	39	27
4	15	13	11	44	48	47	18	26	23
6	13	ND*	ND	39	NA***	32	14	10	19
8	10			29	NA	25	11	10	15
10	ND			25	29	19	11	10	14
12				20	23	16	ND	11	11
14				21	15	ND		12	ND
16				17	14			ND	
18				14	13				
20				11	11				
10^2 k_{obs} (mins^{-1})	6.92	11.99	16.17	7.65	10.15	12.91	7.97	NC**	8.48
Half-life (mins)	10.0	5.8	4.3	9.1	6.8	5.4	8.7	NC	8.2
R^2	0.94	0.99	0.85	0.96	0.97	0.99	0.96	NC	0.99

Note: ND* = Not detected; Limit of Detection (LOD) = 10 ug/L
       NC** = Not calculated
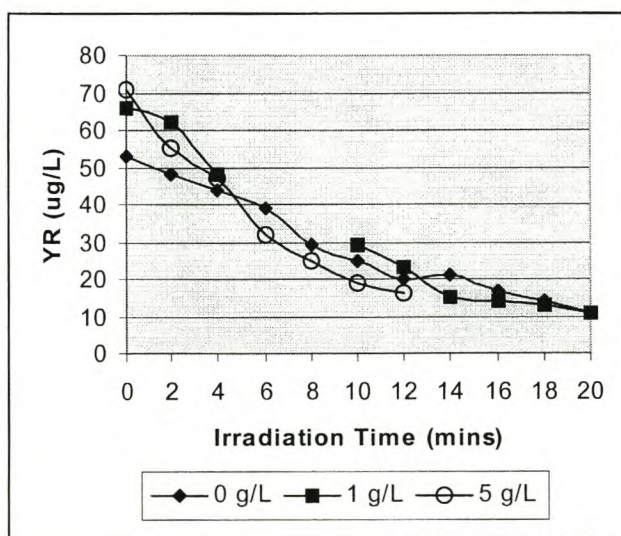   NA*** = Not analyzed

Figure 4.23: Microcystin YR oxidation as a function of time and catalyst suspension loading.
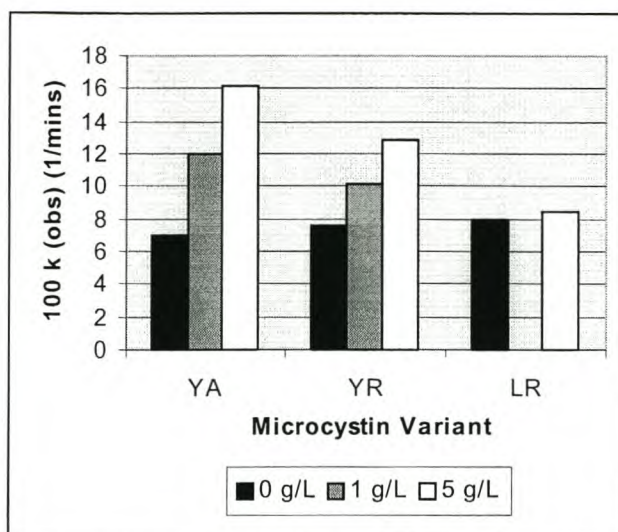
Figure 4.24: First order rate constants as a function microcystin variant and catalyst suspension loading (in g/L TiO$_2$).

The results obtained from these experiments (Table 4.21 and Figures 4.23 to 4.24) indicated that :

- an increase in catalyst suspension loading from 0 to 5 g/L promotes the PCO of microcystins YA and YR. This result confirms the (1) superior PCO efficiency of the SLIMM reactor for these variants (2) auxiliary PCO effect of slurried catalyst in the presence of immobilized catalyst and low starting concentrations (viz: *ca* 20 ug/L) ;
- an increase in catalyst loading from 0 to 5 g/L does not enhance PCO of microcystin LR significantly. This result demonstrates the (1) higher resistance of LR towards PCO and (2) utility of the IMM reactor for treatment of LR ;
- the high RSD for initial concentration data can be remedied by normalization (viz: expressing data as fraction percentages of the observed initial concentration) ;
- the use of IMM reactor configurations is suitable when treating recalcitrant organic compounds in natural lake water (viz: in the presence of inorganic ions and NOM as radical scavengers).

(d)   Reproducibility Study (Slurry-Immobilized Reactor)

Introduction and Objectives:

The statistical reproducibility of PCO was examined by operating Reactor 2A as SLIMM reactor at the standard reference levels for all parameters (Table 4.20). Test runs were conducted in triplicate using a catalyst suspension loading of 5 g/L TiO$_2$ *after* sheet coating (according to the standard procedure). Lake water (spiked with microcystin algal extract) was used in this instance. The objective of this study was to evaluate the reproducibility of the observed PCO rate constants in terms of (1) standard deviation (SD) (2) relative standard deviation (RSD) and (3) microcystin variant.

Results and Discussion:

Table 4.22: Microcystin concentration data (in ug/L) as a function of time, replicate number and variant.

Irradiation Time (mins)	Microcystins (ug/L)								
	YA			YR			LR		
	Replicate Run Number			Replicate Run Number			Replicate Run Number		
	1	2	3	1	2	3	1	2	3
0	24	22	21	77	72	71	32	25	30
2	17	15	12	61	56	55	26	24	27
4	14	14	11	49	48	47	23	21	23
6	12	ND	ND	47	33	32	23	21	19
8	10			34	25	25	19	17	15
10	11			26	20	19	15	14	14
12	10			19	16	16	14	13	11
14	ND*			11	ND	ND	10	ND	ND
16				12			10		
18				ND			11		
20							ND		
$10^2 k_{obs}$ (mins^{-1})	6.85	11.30	16.17	12.90	12.90	12.91	6.72	5.81	8.48
Half-life (mins)	10.1	6.1	4.3	5.4	5.4	5.4	10.3	11.9	8.2
R^2	0.85	0.86	0.85	0.95	0.99	0.99	0.94	0.95	0.99

ND* = Not detected; LOD = 10 ug/L

Table 4.23: Statistical analysis of reproducibility for 3 replicates.

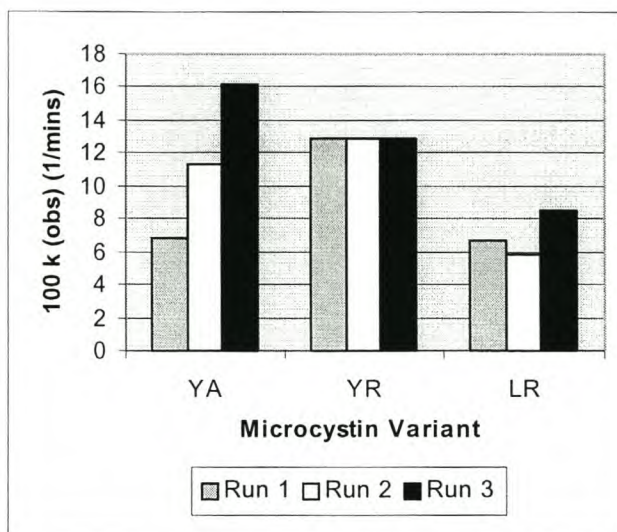| Microcystin Variant	Measured Response	Mean	Standard Deviation	Relative Standard Deviation (%)
YA	10^2 k (obs)*	11.4	4.7*	41.2
YA	Half-life**	6.8	3.0**	44.1
YR	10^2 k (obs)	12.9	0.0	0.0
YR	Half-life	5.4	0.0	0.0
LR	10^2 k (obs)	7.0	1.4	20.0
LR	Half-life	10.1	1.9	18.8

* in mins^{-1} ; ** in mins

172

Figure 4.25: Reproducibility of observed first order rate constants as a function of microcystin variant.

The results obtained from these experiments (Tables 4.22 to 4.22 and Figure 4.25) indicated that:

- the mean observed first order rate constants for PCO of microcystins YA and YR are largely similar. This result suggests that YA is more resistant to PCO than YR due to first order kinetics prescribing higher rate constants for lower initial concentrations (see Section 3.1) ;
- the rate constants for LR are slightly smaller compared to YA and YR. This result demonstrates the more resistant nature of LR towards PCO treatment ;
- the relative standard deviation (RSD) for the first order rate constant is close to 0% for the YR variant. This is considered a good result taking into account possible error variations in sample preparation, reactor efficiency and analytical methodology ;
- RSD is very high for the PCO of microcystins YA and LR. This result is explained in terms of (1) variable mass transfered adsorption as a function of catalyst suspension loading and (2) practical problems related to the HPLC analysis of these variants ;
- the overall PCO susceptibility of the three variants is in the order: YR>YA>LR.

Based on the results obtained above, a more detailed study would be required to link the organic structure of microcystin toxins to their respective photocatalytic reactivities. The application of quantitative-structure-activity relationships (QSAR) may be potential route to follow in this regard. Another possibility is quantum mechanical modeling.

(e)   Mass Transfer Effects

Introduction and Objectives:

A dark control experiment was performed by operating Reactor 2A as an IMM reactor at the standard reference levels for all system parameters (Table 4.20). Lake water from Zeekoevlei (spiked with microcystin algal extract) was used in this experiment. The objective of this study was to determine the extent of adsorptive mass transfer of microcystin YR and LR molecules to TiO_2 immobilized on the fiber glass support of the reactor.

Results and Discussion:

Table 4.24: Microcystin concentration data (in ug/L) as a function of time and variant.

Recirculation Time (mins)	Microcystins (ug/L)	
	YR	LR
0	84	46
20	83	42
Mass Transfer (%)	1.2	8.7

The results obtained from this experiment (Table 4.24) indicated that:

- less than 10% mass transfer (via adsorption) of microcystins YR and LR occurs to immobilized TiO_2 on the fiber glass sheet module ;
- PCO is most probably responsible for the bulk of the removal of microcystin toxins from water treated in this experimental reactor.

Based on the result obtained above, it is evident that although the effect of mass transfer is very small (*ca* 10% or less), the surface-catalyzed nature of PCO reactions still require a degree of mass transfer of the target pollutant. This reasoning is based on Langmuir-Hinshelwood kinetics for PCO (Legrini *et al.*, 1993).

(f)   Stability Study

Introduction and Objectives:

Two batches of blue-green algal extracts were used during the evaluation of Reactor 2A. Initial photocatalytic experiments were performed using an algal extract containing microcystins YA, YR and LR in detectable amounts (i.e. greater than 10 ug/L). These toxin variants were extracted with methanol from freeze-dried algal material stored at PROMEC (Tygerberg, RSA) from previous studies. The freeze-dried material originated from a toxic strain of *Microcystis aeruginosa*. The second extract (containing LR and RR in detectable amounts) was prepared from a natural bloom obtained at Wildevoëlvlei near Noordhoek (Cape Town, RSA).

A stability study was conducted on these extracts by spiking 10 mLs of each in 5 L of natural lake water in a continuously stirred reservoir. Lake water from Zeekoevlei and Rondevlei was used for this purpose (see Section 2.3.2). The experiments were conducted in the dark to eliminate UV effects. A 100 mL aliquot of water was collected at fixed sampling intervals and analyzed for microcystin content. The objectives of this study were to (1) confirm the stability of the toxins in natural water (2) show that the removal of microcystins from water treated by the reactor is mainly due to PCO effects.

Results and Discussion:

Table 4.25: Stability study for first extract spiked in natural water (from Zeekoevlei, Cape Town, RSA).

Sampling Time (mins)	Microcystins (ug/L)		
	YA	YR	LR
0 (not spiked)	ND*	ND	ND
0 (spiked)	42	107	43
5	42	107	44
10	44	117	48
15	45	111	46
20	45	114	52
30	44	111	52
60	31	102	43
1440 (24hrs)	41	106	46
8640 (6 days)	42	108	45

ND* = Not detected ; LOD = 10 ug/L

Table 4.26: Stability study for second extract (Wildevoëlvlei, Cape Town, RSA) spiked in natural water (from Rondevlei, RSA).

Sampling Time (mins)	Microcystins (ug/L)	
	LR	RR
0	80	NC*
10	86	NC
20	77	NC
60	78	NC
1440 (24hrs)	79	NC
2880 (48 hrs)	80	NC

NC* = Not calculated

The results obtained from this experiment (Tables 4.25 and 4.26) indicated that :

- the algal extracts used in this project remain stable as spikes in natural water for a period considerably longer than experimentation and subsequent analysis ;
- the microcystins toxins are not decomposed naturally as a result of the water matrix used ;
- the removal of microcystins from water treated in the experimental reactors (1 and 2A) is primarily realized by PCO.

Based on the results obtained above, it was decided to conduct more parametric studies in order to assess the performance of Reactor 2A as immobilized-bed (IMM) and slurry-immobilized (SLIMM) reactor for the PCO of microcystins in natural water. System parameters were mainly evaluated at their standard reference levels (unless stated otherwise). Sheet modules were prepared using the standard coating procedure as before.

(g) Water Matrix Effects (Immobilized-Bed Reactor)

Introduction and Objectives:

Water matrix effects were examined by operating Reactor 2A as IMM reactor and comparing results for the treatment of microcystins LR and RR in deionized water and natural lake water. Lake water from Zeekoevlei was used in this study. All system parameters were evaluated at standard reference levels (Table 4.20). The objectives of this study were to (1) compare PCO efficiency as a function of water matrix and microcystin variant (in 2^2 factorial format) and (2) assess the impeding effect of inorganic ions on PCO.

Results and Discussion:

Table 4.27: Microcystin concentration data (in ug/L) as a function of time, water matrix and variant.

Irradiation Time (mins)	Microcystins (ug/L)			
	LR		RR	
	Deionized Water	Lake Water	Deionized Water	Lake Water
0	48	59	55	66
2	25	43	32	53
4	17	35	23	43
6	10	34	18	36
8		32	10	35
10		23	ND	31
12		13		23
14		10		16
16		ND*		ND
18				
20	ND			
10^2 k_{obs} (mins^{-1})	25.46	11.74	19.92	8.99
Half-life (mins)	2.7	5.9	3.5	7.7
R^2	0.99	0.92	0.98	0.96

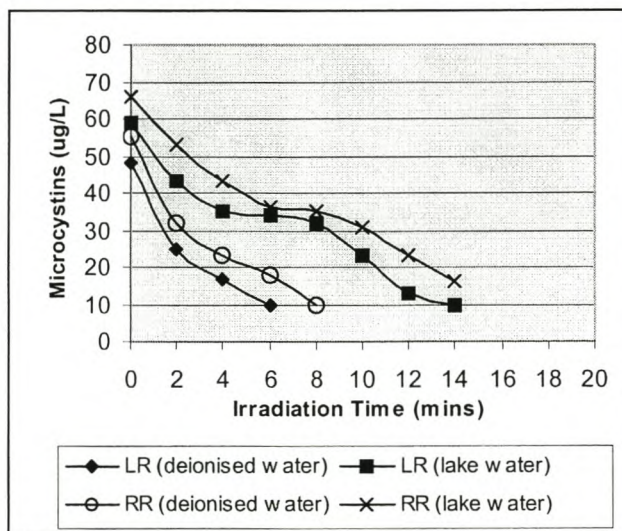**ND* = Not detected; LOD = 10 ug/L**

Figure 4.26: Microcystin oxidation as a function of time, variant and water matrix.
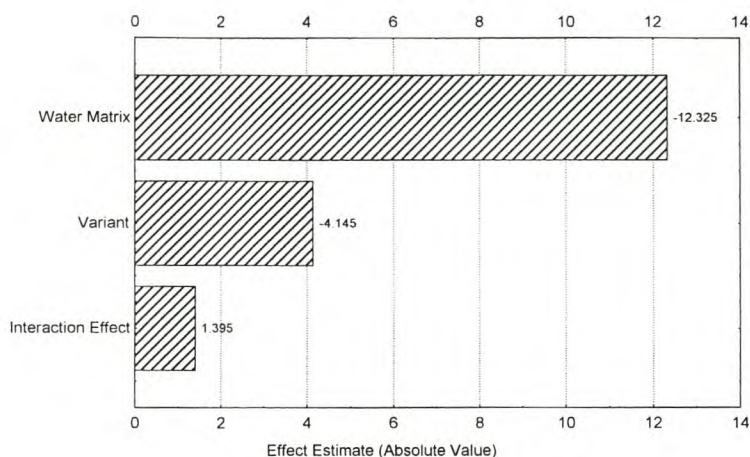
177

Figure 4.27: Pareto chart illustrating parameter main effects and second order interaction effect for water matrix and microcystin variant.

The results obtained from this experiment (Table 4.27 and Figures 4.26 to 4.27) indicated that:

- the PCO rate constants for both microcystin variants decrease markedly when switching from deionized water to natural lake water. This result is anticipated in view of (1) pronounced scavenging of hydroxyl radicals by NOM and inorganic ions (such as phosphate) in natural water and (2) inference effects caused by inorganic ions in terms of the blocking of active surface sites on TiO_2 ;
- the PCO rate constant for microcystin RR is marginally lower than for LR for both water matrices (at comparative initial concentration). Hence, RR and LR exhibit similar susceptibility for PCO ;
- the interaction effect between the 2 parameters is negligible compared to individual main effects. This observation implies that the inherent PCO susceptibility of a microcystin variant could be linked to organic structure and water quality on a *separate* basis. The application of (1) quantum mechanical modeling (2) neural network simulation (3) multivariate experimental design and (4) QSAR, is envisaged as part of this exercise.

Based on the results obtained above, it is evident that by using deionized water as spiking matrix for microcystins, it is possible to conduct an absolute comparison of PCO susceptibility as a function of variant.

(h)   Solution pH   (Immobilized-Bed Reactor)

Introduction and Objectives:

The effect of pH was examined by operating Reactor 2A as IMM reactor and comparing results for 2 different initial solution pH conditions against the standard (neutral) pH of 8. 1M NaOH, 1M HCl and 1M H_2SO_4 (and dilutions thereof) were used as additives to adjust pH. Microcystins LR and RR were spiked in lake water from Zeekoevlei (pH 8) prior to PCO treatment. All system parameters were evaluated at standard reference levels (Table 4.20) and the standard coating procedure applied for the sheet module. The objectives of this study were to (1) compare PCO efficiency as a function of initial solution pH and microcystin variant and (2) assess the impeding effect of inorganic ions on PCO.

Results and Discussion:

Table 4.28: Microcystin concentration data (in ug/L) as a function of time, solution pH and variant.

Irradiation Time (mins)	Microcystins (ug/L)							
	LR				RR			
	pH 3 (HCl)	pH 3 (H_2SO_4)	pH 8 (neutral)	pH 11 (NaOH)	pH 3 (HCl)	pH 3 (H_2SO_4)	pH 8 (neutral)	pH 11 (NaOH)
0	49	32	59	45	54	44	66	57
2	NA	31	43	32	28	33	53	42
4	32	20	35	26	19	23	43	35
6	20	19	34	24	12	19	36	35
8	19	NA	32	21	ND	17	35	26
10	14	NA**	23	NA		15	31	26
12	ND*	11	13	13		ND	23	16
14		ND	10	ND			16	ND
16			ND				ND	
18								
20								
$10^2 k_{obs}$ (mins^{-1})	12.61	9.26	11.74	9.49	24.50	10.80	8.99	9.05
Half-life (mins)	5.5	7.5	5.9	7.3	2.8	6.4	7.7	7.7
R^2	0.97	0.96	0.92	0.97	0.99	0.95	0.96	0.93

ND* = Not detected; LOD = 10 ug/L
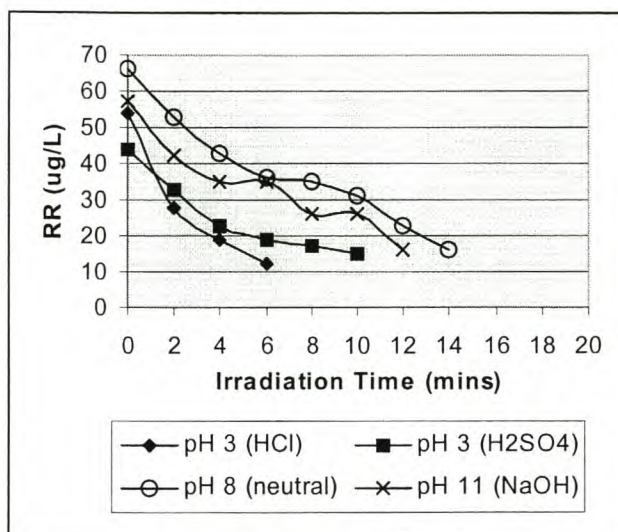**NA** = Not analyzed**

Figure 4.28: Microcystin RR oxidation as a function of time and initial solution pH.

The results obtained from this experiment (Table 4.28 and Figure 4.28) indicated that:

- the PCO rate constant for microcystin LR increases marginally when adjusting the initial pH to 3 using HCl as additive. This result is ascribed to favorable adsorptive interaction between negatively charged microcystin molecules and positively charged TiO_2 species (existing as $TiOH_2^+$) at pH 3. The effect is markedly amplified for the PCO of RR under the same conditions ;

- when using H_2SO_4 as acidic additive, the PCO rate constant for LR drops marginally compared to HCl. This result is ascribed to the inhibiting effect of sulphate ions acting as hydroxyl radical scavengers. The effect is markedly amplified for RR with more than 50 % reduction in PCO rate constant during H_2SO_4 addition ;

- the PCO rate constant remains relatively unchanged when adjusting the initial pH to 11. This result is unexpected in view of pronounced electrostatic repulsion existing between TiO^- species and negatively charged microcystin molecules in this pH range. The utility of the reactor for microcystin oxidation in waters of high pH is therefore demonstrated ;

- the PCO rate constant for microcystin LR is relatively insensitive to pH variation, whereas the PCO of RR reveals a marked dependence on pH ;

- the treatment of LR in an IMM reactor configuration is of practical importance.

Based on the results obtained above, it is evident that the PCO of microcystins is a complex process that depends on the (1) organic structure (2) relative pH sensitivity (3) adsorption kinetics as a function of pH and (4) oxidation susceptibility, of the variant under investigation.

(i)   Slurry pH   (Combined Slurry-Immobilized Reactor)

Introduction and Objectives:

The effect of slurry pH was examined by operating Reactor 2A as SLIMM reactor and comparing results for 2 different initial slurry pH conditions against the standard (neutral) pH of 7 (for a 5 g/L TiO_2 suspension in lake water). 1M H_2SO_4 (and dilutions thereof) were used as additive to adjust pH. Algal extract (containing microcystin LR) was added to 5 L lake water (Zeekoevlei) with the addition of a catalyst suspension loading of 5 g/L TiO_2 prior to photocatalytic treatment. All system parameters were evaluated at standard reference levels (Table 4.20) and the standard coating procedure applied for the sheet module.

The objectives of this study were to (1) assess the PCO efficiency for microcystin LR as a function of initial slurry pH (2) monitor the inhibiting effect of sulphate ions and (3) compare PCO results as a function of reactor configuration (i.e. SLIMM versus IMM reactor).

Results and Discussion:

Table 4.29: Microcystin concentration data (in ug/L) as a function of time, slurry pH and variant.

Irradiation Time (mins)	Microcystin LR (ug/L)	
	Slurry pH 7 (neutral)	Slurry pH 3
0	30	42
2	27	36
4	23	28
6	19	23
8	15	18
10	14	15
12	11	ND
14	ND*	
16		
18		
20		
10^2 k_{obs} (mins^{-1})	8.48	10.61
Half-life (mins)	8.2	6.5
R^2	0.99	0.99

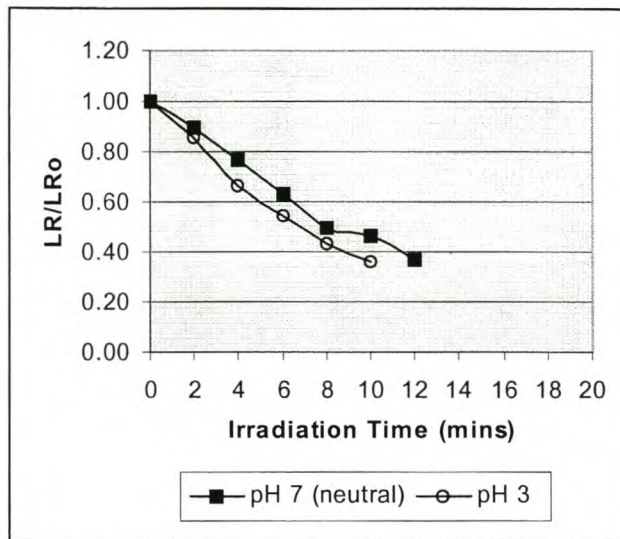**ND* = Not detected; LOD = 10 ug/L**

Figure 4.29: Microcystin LR oxidation as a function of time and initial slurry pH. (Concentrations are normalized as LR/LR_o)

The results obtained from this experiment (Table 4.29 and Figure 4.29) indicated that :

- the first order PCO rate constant increases with approximately 10% when adjusting the initial pH of the 5g/L TiO_2 slurry from 7 to 3 with H_2SO_4. This result indicates the utility of the SLIMM reactor to enhance the PCO of microcystin LR, which is otherwise relatively insensitive to pH variation in IMM reactor configuration ;
- the detrimental effect of sulphate ions is countered when operating the SLIMM reactor ;
- the first order PCO rate constant for LR is fairly independent of reactor configuration (i.e. SLIMM rates are similar to IMM rates). This result is also obtained for RR using identical conditions and demonstrates the utility of the IMM reactor configuration for treating microcystins such as LR and RR.

Based on the results obtained above, it is concluded that Reactor 2A can be successfully operated as an immobilized-bed system for the treatment of microcystins in natural waters. The operation of slurry-phase reactors does not present a significant improvement on the former configuration.

(j)   Gas Flow Rate   (Immobilized-Bed Reactor)

Introduction and Objectives:

The effect of oxygen gas flow rate was examined by operating Reactor 2A as IMM reactor and comparing results for an elevated rate of 20 L/minute against the standard rate applied (5 L/minute O_2). Algal extract (containing microcystins LR and RR) was spiked in lake water from Zeekoevlei (natural pH 8) prior to photocatalytic treatment. All system parameters were evaluated at standard reference levels (Table 4.20) and the standard coating procedure applied for the sheet module. The objectives of this study were to (1) compare PCO efficiency as a function of oxygen flow rate and (2) assess the change in PCO susceptibility for each variant.

Results and Discussion:

Table 4.30: Microcystin concentration data (in ug/L) as a function of time, O_2 flow rate and variant.

Irradiation Time (mins)	Microcystins (ug/L)			
	LR		RR	
	Gas Flow Rate (L/min O_2)		Gas Flow Rate (L/min O_2)	
	5	20	5	20
0	59	60	66	145
2	43	40	53	109
4	35	NA**	43	86
6	34	30	36	68
8	32	15	35	40
10	23	NA	31	41
12	13	ND	23	21
14	10		16	11
16	ND*		ND	ND
18				
20				
$10^2 k_{obs}$ (mins^{-1})	11.74	15.30	8.99	17.29
Half-life (mins)	5.9	4.5	7.7	4.0
R^2	0.92	0.92	0.96	0.95

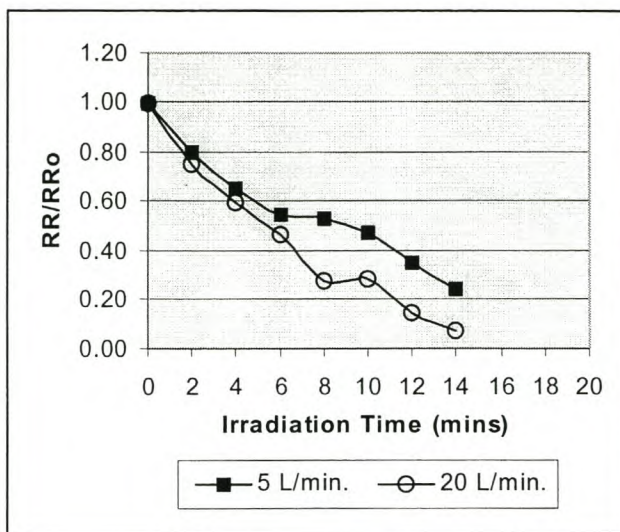ND* = Not detected; LOD = 10 ug/L
NA** = Not analyzed

Figure 4.30: Microcystin RR oxidation as a function of time and oxygen flow rate (in L/min.). (Concentrations are normalized as RR/RR$_o$)
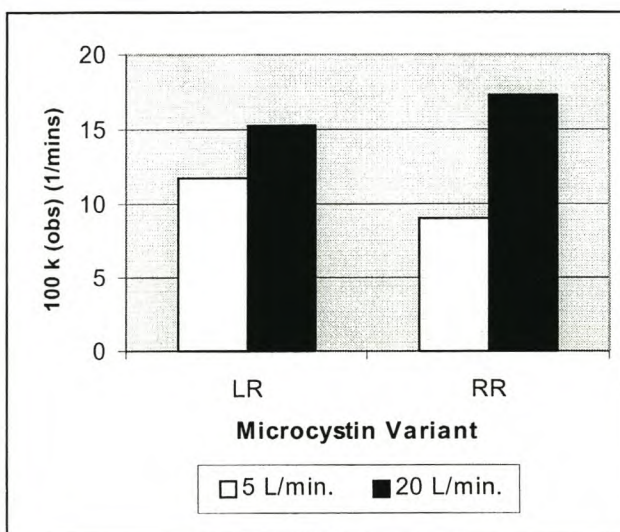

Figure 4.31: Observed first order rate constant as a function of microcystin variant and oxygen flow rate (in L/min.)

The results obtained from this experiment (Table 4.30 and Figures 4.30 to 4.31) indicated that :

- the first order rate constants for PCO of both variants (LR and RR) increase substantially when increasing the oxygen flow rate from 5 to 20 L/minute. This result confirms the importance of oxygen for efficient PCO ;

- the observed increase is non-linear which indicates that the aqueous solution becomes saturated with oxygen during prolonged recirculation time. This result motivates the use of a convenient lower O_2 flow rate for PCO when reaction times are longer ;
- the PCO rate constant for LR increases with approximately 30%, while the corresponding RR constant is almost doubled. This observation indicates that RR may be more susceptible to PCO than LR. However, the result should be verified by other means because the higher initial concentration for the second RR run distorts the comparison of rate constants ;
- the discrepancy in initial concentration of RR is due to underlying interferences experienced during the HPLC analytical procedure ;
- the normalization of concentration data facilitates comparison of experimental runs using identical theoretical starting concentrations, but with variable observed starting concentration (see Figure 4.30).

Based on the results obtained above, it is evident that variation in the oxygen gas purge rate presents another useful parameter for comparing PCO susceptibility of different microcystin variants.

(k)   Catalyst Impregnation Loading   (Immobilized-Bed Reactor)

Introduction and Objectives:

The effect of catalyst impregnation loading was examined by operating Reactor 2A as IMM reactor and comparing results for an elevated impregnation loading against the standard loading of the fiber glass sheet module. The conditions for enhanced coating were similar to the standard coating procedure with the exception of a 20 g/L TiO_2 suspension used in stead of the standard 5 g/L. This alteration resulted in a net mass loading of 21.6 g TiO_2 on the sheet module (i.e. 24.5 g/m^2) compared to the original loading of 7.5 g/sheet (i.e. 8.5 g/m^2). Algal extract (containing microcystins LR and RR) was spiked in lake water from Zeekoevlei (natural pH 8) prior to photocatalytic treatment. The remainder of the system parameters was evaluated at standard reference levels (Table 4.20). The objectives of this study were to (1) compare PCO efficiency as a function catalyst impregnation loading and (2) assess the change in PCO susceptibility for each variant.

Results and Discussion:

Table 4.31: Microcystin concentration data (in ug/L) as a function of time, catalyst impregnation loading and variant.

Irradiation Time (mins)	Microcystins (ug/L)			
	LR		RR	
	Catalyst Impregnation Loading (g/m^2)		Catalyst Impregnation Loading (g/m^2)	
	8.5*	24.5**	8.5	24.5
0	59	60	66	127
2	43	43	53	90
4	35	34	43	70
6	34	32	36	65
8	32	24	35	56
10	23	19	31	41
12	13	ND	23	21
14	10		16	ND
16	ND***		ND	
18				
20				
10^2 k$_{obs}$ (mins^{-1})	11.74	10.80	8.99	12.85
Half-life (mins)	5.9	6.4	7.7	5.4
R^2	0.92	0.98	0.96	0.92

* Catalyst suspension loading = 5 g/L TiO$_2$
** Catalyst suspension loading = 20 g/L TiO$_2$
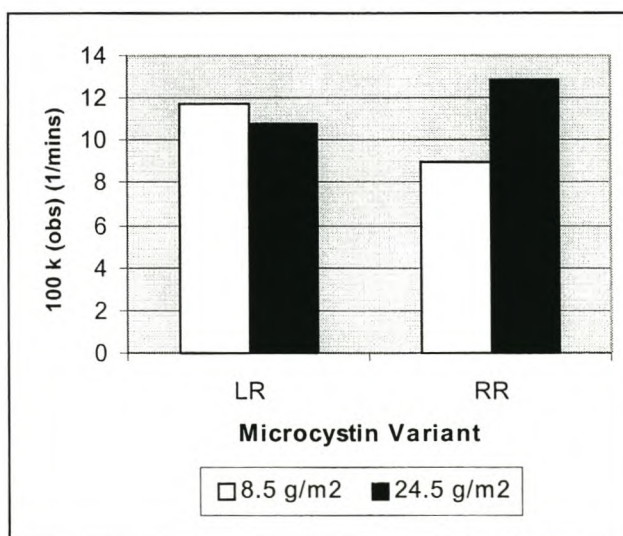***ND = Not detected ; LOD = 10 ug/L

Figure 4.32: Observed first order rate constant as a function microcystin variant and catalyst impregnation loading (in g TiO$_2$/m^2).

186

The results obtained from this experiment (Table 4.31 and Figure 4.32) indicated that :

- the rate constants for PCO of microcystins LR and RR do not change appreciably with a threefold increase in catalyst impregnation loading of the sheet module. This result demonstrates the utility of Reactor 2A to be operated as an IMM reactor with economical (low) impregnation loadings of TiO_2 .

Based on the results obtained above, it is evident that the degree of interaction between microcystin molecules and TiO_2 on a stationary support is an important factor for scaling-up of immobilized-bed reactor configurations. The attainment of sufficient interaction at the lowest practical impregnation loading should yield high PCO conversion rates when the reactor is optimized for microcystin removal via statistical techniques and comprehensive reactor modeling.

4.2.2 Sequential Single Pass Mode

(a) System Parameters

The PCO treatment of three variants of microcystins in water was investigated by operating Reactor 2A as an immobilized-bed (IMM) reactor. The following system parameters were evaluated at discrete levels in terms of the defined kinetic response functions for this mode of operation (see Section 2.4 and Table 4.32):

Table 4.32: System parameters for microcystin study (Reactor 2A; Sequential Single Pass Mode)

Parameter	Assigned Levels
Catalyst Loading for Impregnation (g/L)	5
Volumetric Flow Rate (L/min.)	2.0[a]
Horizontal Irradiation Distance (cm)	15
Microcystin Variants	YA, YR and LR
Reaction Volume (L)	5
Water Matrix	Lake water
Gas Purge	Oxygen
Gas Flow Rate (L/min. O_2)	5
Number of UV-C lamps for Irradiation	12[b]
Average UV Contact Time (sec)	4.1

* Denotes standard reference level of parameters
a Surface flow rate = 136 L/hr/m^2
b UV Irradiance   = 204.5 W/m^2 (= 20.45 mW/cm^2)